Properties of the Free Energy Barriers for Folding of the α-Amylase Inhibitor Tendamistat

INAUGURALDISSERTATION

zur
Erlangung der Würde eines Doktors der Philosophie
vorgelegt der
Philosophisch-Naturwissenschaftlichen Fakultät
der Universität Basel

von
Manuela Schätzle
aus
Freiburg im Breisgau, Deutschland

Basel, 2005

Genehmigt von der Philosophisch-Naturwissenschaftlichen Fakultät auf Antrag von

Prof. Dr. Thomas Kiefhaber
Prof. Dr. Rudolf Glockshuber

Basel, den 20.09.2005

Prof. Dr. Hans-Jakob Wirz
(Dekan)

Contents

1. INTRODUCTION 1

1.1 The Protein Folding Problem 1

1.2 Protein Stability 2

1.3 Kinetic Mechanism of Protein Folding 5

1.3.1 Properties of the Unfolded State 6

1.3.2 Kinetic Models 8

1.3.3 Kinetic Mechanism 9

1.3.4 Characterization of the Free Energy Barriers 14

1.4 The Model Protein: Tendamistat 21

2. AIMS OF RESEARCH 25

3. SUMMARY OF MANUSCRIPTS READY FOR SUBMISSION 26

3.1 Shape of the Free Energy Barriers in Tendamistat Folding 26

3.1.1 Multiple Perturbation Analysis 26

3.1.2 Thermodynamic Properties of the Free Energy Barriers 28

3.1.3 Evidence for Parallel Pathways 29

4. SUMMARY OF UNPUBLISHED WORK 31

4.1 Studies on Tendamistat Fragments 31

4.1.1 Stability of the N-terminal β-hairpin of Tendamistat and the C-terminal β–hairpin from the B1 domain of streptococcal protein G 32

4.1.2 Structural Property, Stability and Assembly of the Tendamistat Fragments T(1-34) and T(35-74) 44

4.1.3 Structural Property and Stability of the Tendamistat Fragment T(11-74): Contributions of the first ten N-terminal Amino Acids to Protein Stability 51

4.2 Studies on Tendamistat Variants 58

4.2.1 Spectroscopic Characterization of Tendamistat Variants 61

4.2.2 Stability and Folding Kinetics of Tendamistat Variants 64

4.2.2.1 Tendamistat Variants with Apparent Two-State Folding 64

4.2.2.2 Tendamistat Variants with Complex Unfolding Kinetics 77

4.2.2.3 Influence of Surface-Exposed Charges on the Stability of Tendamistat 92

4.2.3 Effect of Sodium Sulfate on the Folding Reaction of the Tendamistat Variants L14A and N25A 99

5. SUMMARY 112

6. ACKNOWLEDGEMENTS 115

7. REFERENCES 116

8. MANUSCRIPTS READY FOR SUBMISSION 131

8.1 Shape of Free Energy Barrier for Tendamistat Folding Measured by Multiple Perturbation Analysis 131

8.2 Thermodynamic Properties of the Transition States in Tendamistat Folding 160

8.3 Evidence for Parallel Pathways at the Early Stage of Tendamistat Folding 189

9. APPENDIX 219

9.1 Temperature-dependence of Tendamistat wild type at pH 2 220

9.2 Temperature-dependence of the tendamistat disulfide variant C11A/C27S at pH 7 230

9.3 Variants with the early transition state rate-limiting 237

9.4 Variants with the late transition state rate-limiting 258

9.5 Variants with complex unfolding kinetics 269

10. CURRICULUM VITAE 277

1. Introduction

1.1 The Protein Folding Problem

Proteins are involved in nearly every biological process in a living organism. They are synthesized as linear chains in a specific order on ribosomes. To fulfill their function it is necessary for them to fold into unique, native, three-dimensional structures that are characteristic for each individual protein. The molecular structures of native proteins consist of secondary structures such as α-helices, β-sheets, loops and turns, which represent the basic structural elements. The arrangement in space of all the atoms in a single polypeptide chain is termed the tertiary structure. The overall organization of proteins to not covalently linked oligomers is known as the quaternary structure.

Within the cell, protein folding takes place in a complex, highly crowded molecular environment. To enable folding and to prevent aggregation a whole range of helper proteins exists in the cell, collectively termed molecular chaperones.[1] A wide spectrum of chaperone proteins interacts with and stabilizes non-native states of polypeptides. There are also several classes of proteins that speed up specific steps in the folding process which might otherwise be slow.[2] These folding catalysts include proteins involved in increasing the rates of isomerization of peptidyl-prolyl bonds[3] and of non-prolyl bonds[4], and accelerating the formation and rearrangement of disulphide bonds[5,6].

In vitro, it has been shown that chemically denatured proteins refold spontaneously to their fully native states when removed from denaturing conditions in the absence of any additional molecular species.[7,8] In 1961, Anfinsen and co-workers could show in their famous experiment that the amino acid sequence of RNase A contains the information needed to form the correct four disulfide bonds of the native protein.[9] The information needed for a protein to form the native fold is therefore defined in the genetically encoded sequence. Thus, *in vitro* studies of proteins should suffice to understand protein folding.

Despite of enormous progress in the field the protein folding problem is still not solved. It can be divided into two major questions: (i) How is the native structure encoded in the amino acid sequence? The folding code is non-linear and of discontinuous nature since residues far apart in sequence come close together in the native structure. The folding code is degenerated: the same sequence can adopt

different structures and different sequences can encode a similar structure. (ii) What is the mechanism to reach this state? Polypeptide chains can adopt an astronomical number of conformations and it would take an unrealistic amount of time to find the native structure by random chain fluctuations. Therefore, there must be an effective mechanism to restrict conformational space.

1.2 Protein Stability

It is essential for the understanding of protein structure and function to know the origins of protein stability. One of the most peculiar features of proteins is their marginal stability within a narrow range of thermodynamic conditions.[10] This, however, allows for the flexibility of the polypeptide chain, which is known to be significant for enzyme catalysis and protein-protein and protein-nucleic acid interactions.[10-12] The native state can be disrupted by increasing or decreasing the temperature, the pressure, pH or by adding denaturants. By disrupting a structure one can study its architecture and energetics.

The temperature dependence of enthalpy, $\Delta H^0(T)$, and entropy, $\Delta S^0(T)$, is defined by the heat capacity changes, ΔC_p. Assuming that ΔC_p is independent of temperature we can write:

$$\Delta H^0(T) = \Delta H^0(T_0) + \Delta C_p(T - T_0) \tag{1.1}$$

$$\Delta S^0(T) = \Delta S^0(T_0) + \Delta C_p T \ln\left(T/T_0\right) \tag{1.2}$$

where T_o is the reference temperature, and $\Delta H^0(T_0)$ and $\Delta S^0(T_0)$ are the enthalpy and entropy changes, respectively, at the reference temperature.

Thus, the Gibbs energy, $\Delta G^0(T)$, is defined as

$$\Delta G^0(T) = \Delta H^0(T_0) - T\Delta S^0(T_0) + \Delta C_p\left[T - T_0 - T\ln\left(T/T_0\right)\right] \tag{1.3}$$

The large ΔC_p of protein unfolding causes a temperature at which stability of the folded state is at a maximum and a temperature at which the entropy is zero (T_s) (equation (1.3); Figure 1-1). The net stability decreases at both higher and lower temperatures. Proteins therefore unfold at both high (heat denaturation, T_m) and low (cold denaturation, $T_{m'}$) temperatures (Figure 1-1).[10,13,14]

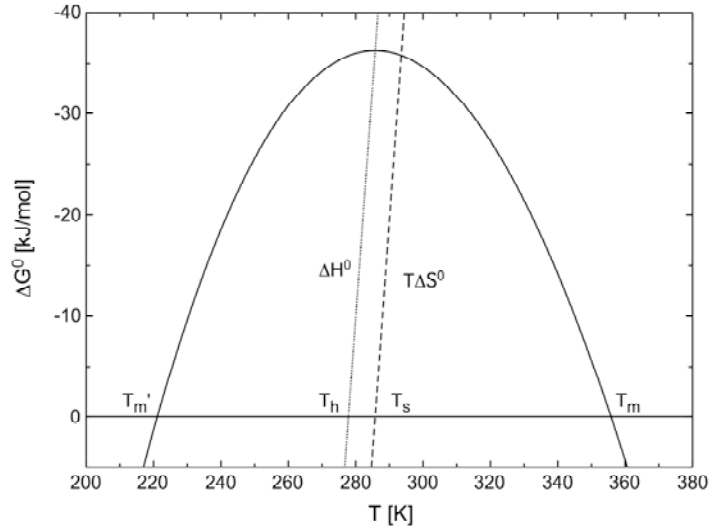

Figure 1-1: Temperature dependence of Gibbs energy, ΔG^0 (—), enthalpy, ΔH^0 (····), and entropic contribution, $T{\cdot}\Delta S^0$ (---), for tendamistat wild type at pH 7. Thermodynamic functions were calculated according to equations (1.1), (1.2) and (1.3) using the following parameters: ΔC_p = -4.56 kJ/(mol·K), ΔH^0 = -92.61 kJ/mol, ΔS^0 = -0.193 kJ/(mol·K) and a reference temperature T_0 = 298.15 K. Data were taken from ref.[15]. Other abbreviations: T_m temperature of heat denaturation, $T_{m'}$ temperature of cold denaturation, T_h temperature at which enthalpy is zero, T_s temperature at which entropy is zero.

The very strong temperature dependence of both $\Delta H°$ and $T{\cdot}\Delta S°$ compensate the relative small changes in $\Delta G°$. This is due to the widely reported phenomenon of entropy-enthalpy compensation, a natural consequence of a weakly interacting system itself.[16,17] It is known that even small perturbations in the properties of solvents produce dramatic changes in the enthalpy and entropy of unfolding.[18] To analyze the factors important for protein stability it is thus necessary to consider not only the interactions between protein groups but also interactions between protein groups and the solvent. The goal of studies concerning the thermodynamics of protein unfolding is to be able to understand the contribution of different types of interactions to the heat capacity, enthalpy and entropy changes.

The stability of folded structures has been found to exhibit an unusual temperature dependence caused by large ΔC_p.[19-22] The change in heat capacity upon unfolding is large and positive and, within experimental error, it can be taken as a constant for a given protein[20], leading to a curvature in plots of the free energy of unfolding as a function of temperature[10] (Figure 1-1 and equation (1.3)). A number of special properties of proteins result form this curvature: a maximum in stability and denaturation at both high and low temperatures. It was found that the ΔC_p between native and unfolded proteins correlates well with changes in accessible surface area

(ASA).[23] Heat capacity changes upon unfolding are entirely defined by the interactions with the solvent of the protein groups that were buried in the native state but become exposed upon unfolding. Non-polar groups have a large positive contribution while the polar groups have a smaller and negative contribution to ΔC_p.[21-29] There is evidence that the dynamic properties of the native state also contribute to ΔC_p.[30]

There are two major types of interactions, which can be considered as a possible source of enthalpy: interactions with the solvent and internal interactions between protein groups in the native state.[29] The enthalpies of the internal interactions between protein groups in the native state are enthalpically stabilizing. The internal interactions are the hydrogen bonding and packing interactions between groups in the protein interior. Direct evidence that disruption of packing interactions in the protein interior leads to large positive enthalpy upon unfolding, was obtained by measuring the effects of substitutions.[31] Measuring the effect of hydrogen bonding is complicated because the enthalpy of disruption of hydrogen bonds in the protein interior is difficult to separate from the effect of exposure (hydration) of hydrogen bonding groups to the solvent.[29] The enthalpy of transfer of polar groups from the protein interior into water is positive at lower and negative at higher temperatures.[22,26,29,31-34] In contrast, the transfer of non-polar groups is negative at low and positive at high temperatures.[22,26,29,31-34] Both effects are due to the more ordered water molecules at low temperature. The polar groups form their "own" ordered water, which generates a negative enthalpy due to the increased molecular interactions, but the breakdown of water structure makes a positive contribution to the overall enthalpy, which is greater at low temperatures. In contrast, non-polar groups enhance pre-existing order, which is lost with increasing temperatures. Thus, at high temperatures, the creation of ordered clathrate structures is accompanied with positive enthalpy.

The effect of ordered water molecule at low temperature is also responsible for cold denaturation since the entropic cost of denaturation is reduced due to the structuring of the water molecules around the exposed groups. Due to the increase in the order of water molecules around the solute relative to the bulk water, interactions with the solvent by both polar and non-polar groups occur with negative entropy at higher temperatures.[22,26,32,35] However, the entropy of hydration of non-polar groups decreases through zero with decreasing temperature. This hydration of protein groups is

overcompensated at higher temperature by the increase in the configurational freedom of the polypeptide chain in the unfolded state relative to the native state.[36-40]

Disulfide bridges

A single cross-link can affect the thermodynamic parameters of a particular protein in different ways. Pace and coworkers showed that disulfide bond removal decreases the stability of a protein by increasing the flexibility and conformational entropy of the unfolded state.[41] Doig and Williams, on the other hand, come to the opposite conclusion: cross-links destabilize folded structures entropically but stabilize them enthalpically to a greater extend.[42] To fully understand the entropic and enthalpic effect of disulfide bridges on protein stability, the native state must be considered as well.[43] Disulfide bonds are able to stabilize or destabilize local structures and therefore influence the global stability of proteins.[44-47] Thus disulfide bonds can introduce various compensating effects, making it impossible to predict the consequences of a natural or engineered covalent crosslink on the stability of a protein.

1.3 Kinetic Mechanism of Protein Folding

The folding kinetics are usually treated as a conformational change of two ground states, the unfolded and the native one, and a number of intermediates. This approximation is valid because the energy barriers of the intrachain diffusion in the unfolded state is significantly smaller (10 to 100 ns time scale)[48,49] than the fastest protein folding reaction (μs to ms time scale)[50,51]. Thus, the transition between the large ensembles of states can be analyzed using concepts from classical reaction kinetics and from physical organic chemistry. With this simplified approximation questions can be answered concerning the folding mechanism and the transition state regions: What is the number of reaction pathways and intermediates between the unfolded and the native state of a protein? What is the shape of the transition barrier, and what is the structure of the protein at the top of the barrier?

1.3.1 Properties of the Unfolded State

The extreme case of an unfolded state of a protein is known as a 'random coil'. This leads to one of the key questions in protein folding: How does a protein find its lowest energy structure in a reasonable time? In 1969, Levinthal pointed out that a polypeptide chain would require an astronomical time to explore at random all possible conformations in order to finally reach the native state.[52] When Levinthal´s calculation was repeated in 1992, with the addition of a small free energy bias as the driving force for folding, the time needed to search all conformations by a random search process was reduced to a few seconds.[53] Several NMR studies revealed local residual structures under high denaturing conditions. [54-58] Recent analysis of the effect of mutation and denaturants on folding has shown that these interactions in the unfolded state increase the speed of folding.[59] Tiffany and Krimm hypothesized that proteins unfolded in chemical denaturants possess significant polyproline II helical content.[60] In recent years, several measurements seem to confirm this hypothesis.[61-69]

The results from studies of peptide dynamics show that the amino acid sequence has only little effect on local dynamics of polypeptide chains.[49] To form secondary structure elements a first intramolecular contact on the linear polypeptide chain is essential. The discovery of very fast folding proteins sparked the interest in finding the speed limit for protein folding, which is closely related to the speed limit of the fundamental steps of protein folding.[51] These fast folding proteins are small single domain proteins and include α-helical proteins[70-72], β-proteins[73,74] and α,β-proteins[75]. Some of them even fold on the 10 to 100 μs timescale. Due to the limitations set by chain dynamics, proteins will not be able to fold faster than on the 10–20 ns timescale.[76]

The unfolded state of a protein can be treated as a single kinetic species as long as the interconversion is faster than the kinetic reactions leading to the native state (chapter 1.1). Slow interconversion reactions between the different unfolded conformations lead to kinetic heterogeneity. This was first observed by Garel and Baldwin who showed that both fast and slow refolding molecules exist in unfolded ribonuclease A (RNase A).[77] Brandts and co-workers suggested that slow and fast folding forms of RNase A are caused by a slow equilibration process in the unfolded state and proposed *cis-trans* isomerization at Xaa-Pro peptide bonds ("prolyl isomerization") as the molecular origin.[78] This was confirmed later with proline mutations[79] and catalysis of the slow

reactions by peptidyl-prolyl *cis-trans* isomerases[3]. The partial double bond character of the peptide bond demands a planar geometry, which can be achieved in either *cis* or *trans* orientation of the substituents (Figure 1-2). The partial double bond character is also responsible for a high energy barrier for the *cis-trans* isomerization[78] which gives rise to relaxation times of about 10 to 60 s at 25°C[80]. This isomerization usually limits the folding reaction of the unfolded molecules with non-native prolyl isomers. The equilibrium population of the *cis* isomer in Xaa-Pro peptide bonds is between 7 and 36 %, depending on the preceding residue[81]. This mechanism has meanwhile been shown for many protein folding reactions[80,82].

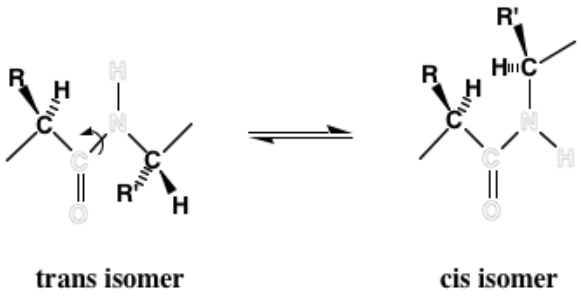

Figure 1-2: Schematic representation of the trans and cis conformations of a peptide bond in a protein. R and R' denote the side chains of the residues.

Another cause of heterogeneity in the unfolded state is the *cis-trans* isomerization of non-prolyl peptide bonds (Figure 1-2).[83,84] The rate constant of non-prolyl isomerization is around 1 s^{-1},[84,85] which is significantly faster than prolyl peptide bond isomerization. Fast non-prolyl isomerization will mainly effect the early stages of folding as well as folding of fast folding proteins.[84] The population of the *cis* isomer in equilibrium in the unfolded state is only about 0.15 % [85] but the large number of peptide bonds in a protein leads to a significant amount of unfolded molecules with at least one non-native peptide bond. Thus the non-prolyl isomerization will dramatically effect protein folding of large proteins.[86]

Religation of the heme group in the unfolded state has been shown to cause parallel pathways in the folding of cytochrome c and is a source for kinetic heterogeneity in the unfolded state other than prolyl and non-prolyl isomerization.[87-89]

1.3.2 Kinetic Models

Since the formation of the native structure cannot be achieved by random exploration of the conformational space ("Levinthal paradox", chapter 1.3.1), several models were developed to explain the phenomenon of protein folding. The observations of transient populations of intermediates in protein folding led to two alternative folding models. The first model was the "hydrophobic collapse model" which describes the rearrangement of a compact collapsed structure to form the native protein conformation.[90-93] The early step in the folding pathway for this model is the formation of a hydrophobic collapse, which reduces the entropy of the system and narrows the conformational search to the native state. However, a nonspecific hydrophobic globule may hinder reorganization of both the polypeptide chain and the side chains.

Based on the rapid formation of isolated α-helices[94], a step-wise mechanism to reduce the conformational search was proposed. In such a "framework model" it is assumed that the secondary structure is formed early and the tertiary structure rather late in the folding process.[95-98] However, very strong conformational preferences are rare and most sequences that form regular secondary structures in proteins are disordered in small peptides.

Both models involve the formation of partially folded kinetic intermediates and increased the interest in those. Partially folded equilibrium states of proteins were of special interest due to the difficulty to study the structure and energetics of transiently populated intermediates.[99,100] Correlations of the partially folded equilibrium species to the corresponding kinetic intermediates were successful in some cases.[100,101] The framework model led, additionally, to an increased interest in structural studies of peptide fragments as models for early events in folding.[49,102]

For many years it was assumed that intermediates were an essential part of the folding process.[97] The characterization of several small single-domain proteins that fold and unfold in two-state reactions changed this view of stepwise folding and argued against the importance of intermediates.[103,104] This changed the view of populated intermediates that slow down folding[105] or as a result of independent folding of structural fragments in multidomain proteins[106].

The "nucleation-condensation model" was suggested to explain rapid folding of a number of small proteins, which fold without detectable intermediates.[103,104] Folding is limited by the formation of some critical side chain contacts and structure propagates

cooperatively from this nucleus.[107,108] This leads to the conclusion that small proteins fold over one single broad and structural less-defined free energy barrier.[109]

Apparent two-state behavior, however, does not exclude the presence of obligatory intermediates on defined folding pathways.[110,111] In the last years, it could be shown that many small proteins fold via sequential pathways with consecutive distinct barriers and a few obligatory high-energy intermediates[59,110-113], which can speed up folding as long as they are not significantly populated[114]. These findings suggest that apparent two-state or multi-state folding may be governed by a unified mechanistic scheme, namely that folding takes place over linear pathways with obligatory intermediates that become populated only under certain conditions.[110,111]

1.3.3 Kinetic Mechanism

General treatment of kinetic data

To identify the kinetic mechanism the determination of the number of species during folding is essential. This number can be easily determined for a monomeric protein. Measurements of monomeric proteins have the major advantage that the folding kinetics follow a simple exponential time course. With A as measured signal (e.g. fluorescence) and A_∞ as signal after infinitely long time, the time dependent change can be represented as the sum of n exponentials with observable rate constants (λ_i) and corresponding amplitudes (A_i):[115,116]

$$A = \left(\sum_{i=1}^{n} A_i \cdot e^{-\lambda_i t} \right) + A_\infty \qquad (1.4)$$

The apparent rate constants, λ_i, are functions of the microscopic rate constants, which depend on external parameters like temperature, pressure and denaturant concentrations. Generally, kinetics with the sum of n exponential functions have n+1 different species significantly populated during the process and n-1 apparent rate constants.[115,116]

Heterogeneity in the unfolded state

The refolding of most monomeric proteins shows no simple kinetics. In many cases this is caused by the coupling of slow processes to the folding kinetics such as in the case of disulfide bond formation[117,118], proline[78,80,86] and non-proline isomerization[84,86], or heme-religation[119] (chapter 1.3.1). The most common cause for complex folding kinetics are slow proline[78,80,86] and non-proline isomerization[84,86] reactions. A way to test for slow *cis-trans* equilibration reactions are double-jump experiments, which monitor slow spectroscopically silent equilibration processes in unfolded proteins.[78] In these experiments, native protein is unfolded under conditions where the unfolding reaction is fast. After various times, unfolding is stopped by transfer the solution to refolding conditions. Slow folding molecules, which are produced by slow isomerization reactions in the unfolded state, will be formed slowly after unfolding has occured.

Apart from these complications, two main classes of proteins can be described according to the folding mechanism: multi-state and two-state systems.

Two-state folding

The simplest case in protein folding with single exponential kinetics (n=1) can be described by a two-state mechanism (equation (1.5)) with k_f and k_u as the microscopic rate constants for the folding and unfolding reaction, respectively:

$$U \underset{k_u}{\overset{k_f}{\rightleftharpoons}} N \tag{1.5}$$

The apparent rate constant λ is defined as

$$\lambda = k_f + k_u \tag{1.6}$$

The ratio of native and unfolded molecules in equilibrium gives the equilibrium constant K:

$$K = \frac{[N]_{eq}}{[U]_{eq}} = \frac{k_f}{k_u} \tag{1.7}$$

The equilibrium constant K is connected with the Gibbs free energy by the van't Hoff relation:

$$\Delta G^0 = -RT \cdot \ln(K) = -RT \cdot \ln\left(\frac{k_f}{k_u}\right) \tag{1.8}$$

Thus, in a two-state system, the free energy value obtained from kinetic measurements must be identical to the free energy value received by equilibrium methods.

Using extra thermodynamic relationships allows to obtain information on the free energy of activation, $\Delta G^{0\ddagger}$, for a given reaction (equation (1.9) and Figure 1-3).

$$k = k_0 \cdot e^{-\Delta G^{0\ddagger}/RT} \tag{1.9}$$

The absolute value of $\Delta G^{0\ddagger}$ depends strongly on the correct pre-exponential factor k_o, which reflects the maximum rate of the reaction in the absence of free-energy barriers. The pre-exponential factor is strongly influenced by intrachain diffusion processes and is in the range of 10^7-10^8 s^{-1}.[49] It probably also depends on the protein and on the location of the transition state along the reaction coordinate, which may change with solvent conditions or mutation.[49,59,110,111]

Combination of equation (1.8) and (1.9) provides us with information on the free energy changes along the reaction coordinate (Figure 1-3).

$$\Delta G^0 = \Delta G_f^{0\ddagger} - \Delta G_u^{0\ddagger} \tag{1.10}$$

If the two-state assumption used for the transition state analysis is valid, then the difference of the activation free energy for refolding and unfolding reactions will agree with the free energy of stabilization from equilibrium data.

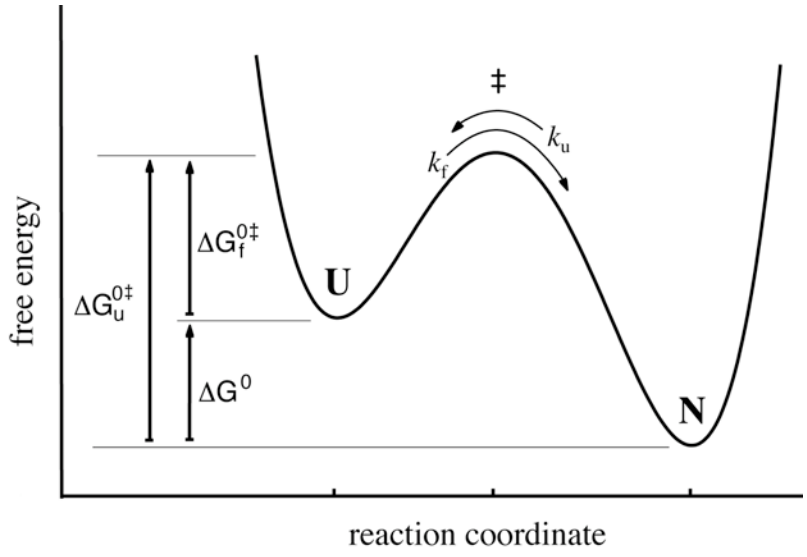

Figure 1-3: Free energy profile for a two-state folding reaction. (from ref.[59])

Folding through intermediates

For a single folding intermediate (n=2) three possible pathways exist: with an on-pathway intermediate (equation (1.11)), an off-pathway intermediate (equation (1.12)) and the triangular mechanism (equation (1.13)). The on- and off-pathway are special cases of the triangular mechanism.

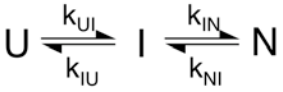

(1.11)

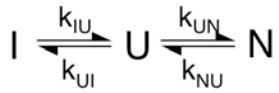

(1.12)

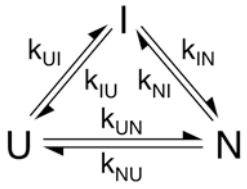

(1.13)

The population of an intermediate can be detected by observation of two apparent rate constants. Frequently, the formation of the intermediate is rapid and occurs in the deadtime. In this case, a deadtime reaction can be observed by analysis of the initial values of the measured kinetic trace and its amplitudes if there are deviations from the expected values.[86,120] The distinction between the different pathways can be done by interrupted refolding experiments[121,122] and kinetic modeling[86].

Interrupted refolding experiments, which are able to specifically monitor the formation of native molecules during folding, can be used to discriminate between the triangular (equation (1.13) and the on-pathway mechanism (equation (1.11).[86,121,122] In the on-pathway mechanism (equation (1.11) the native state is formed with a lag phase, in contrast to the triangular mechanism (equation (1.13), where the native molecules are produced in both kinetic phases. In interrupted refolding experiments the protein is allowed to refold for a certain time ("age time") and is then transferred to unfolding conditions to monitor the resulting kinetics (Figure 1-4). Unfolding of all native molecules (N) and partially folded intermediates (I) is monitored (Figure 1-4). Each state (N and I) has its characteristic rate constant for the unfolding reaction. The observed amplitudes of the unfolding reaction reflect the amounts of the respective species present at the age time. Varying the age time gives the time course of the formation of native protein and of population of the intermediate during the folding process.

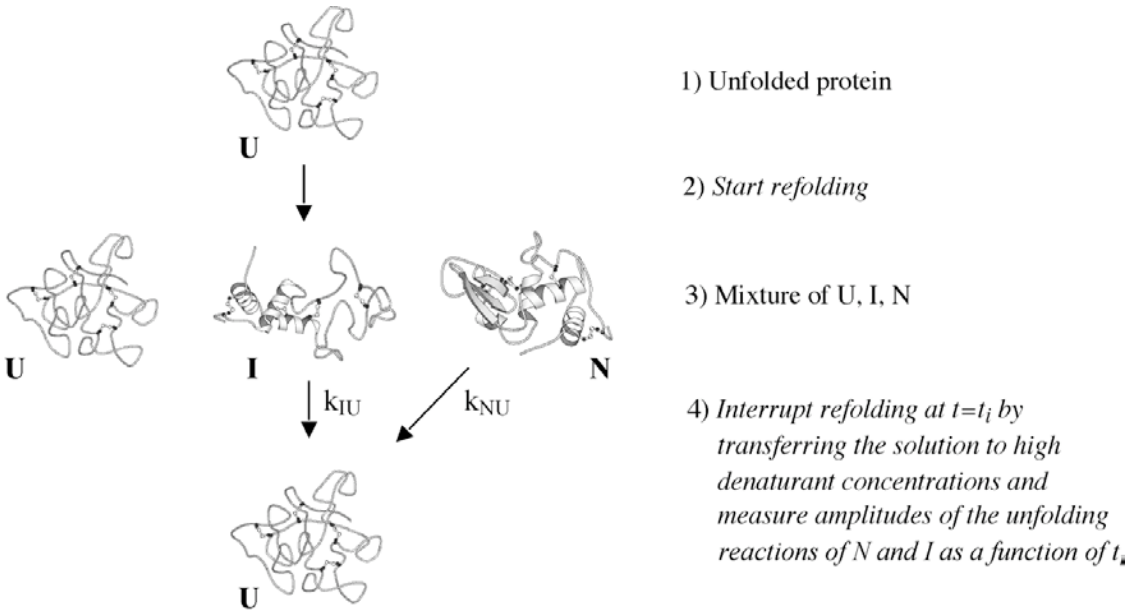

Figure 1-4: Principle of interrupted refolding experiments to measure the time course of the population of a folding intermediate (I) and of native proteins (N) starting from completely unfolded protein (U). (from ref.[86])

However, interrupted refolding experiments do not allow to discriminate between the off-pathway mechanism (equation (1.12)) and the triangular mechanism (equation (1.13)). Therefore, the analysis of the denaturant dependence of all folding and unfolding rate constants is required.[86]

As discussed in chapter 1.3.2, it was shown that many apparent two-state folders fold through an sequential pathway with high energy intermediates.[111] Due to their lower stability compared to N and U, the existence of high energy intermediates can not be detected directly with spectroscopic methods.[110,111,123] The kinetics at a single denaturant concentration cannot be distinguished from two-state folding. However, the chevron plots in this case, shows a clear downward curvature.[86,110,111,123] The stability of the high-energy intermediate cannot be determined, since it does not become populated, but the difference in free energy between both transition states ($\Delta G^0_{TS2/TS1}$) can be obtained.[86,110,123]

The analysis of more complex mechanisms lead to less obvious dependencies of the macroscopic rate constant on the microscopic ones. Therefore, the determination of all constants need to combine the results from interrupted refolding[121] and double-jump[78] experiments and from the denaturant dependences of all observable folding and unfolding reactions.[86]

1.3.4 Characterization of the Free Energy Barriers

The structural and thermodynamic characterization of the energy barriers between unfolded and native proteins is one of the major goals of protein folding studies and has been targeted by several experimental approaches. With the knowledge of the pathways and the numbers of intermediates one can analyze the shape and nature of the rate-limiting transition state region.

Linear rate equilibrium free energy relationship in protein folding

A common approach to characterize the energy barriers is the analysis of the rate-equilibrium free energy relationships (REFERs).[59,111,123-126] It was observed in many reactions that the changes in activation free energy ($\Delta G^{0\ddagger}$) induced by changes in the solvent or in structure are linearly related to the corresponding changes in equilibrium free energy (ΔG^{0}) between reactants and products.[123,124] To quantify the energetic sensitivity of the transition states in respect to a perturbation, ∂x, a proportionality constant can be defined:[124]

$$\alpha_x = \frac{\partial \Delta G^{0\ddagger} / \partial x}{\partial \Delta G^{0} / \partial x} \tag{1.14}$$

α_x is commonly used to obtain information on the structural properties of the transition state and it is a measure for the position of the transition state along the reaction coordinate investigated by ∂x. The range of α_x is normally from 0 for an unfolded-like transition state to 1 for a native-like transition state.

To gain information on different properties of the transition state in protein folding different perturbations can be applied. The Gibbs fundamental equation of chemical thermodynamics

$$d\Delta G^{0} = \Delta V^{0} dp - \Delta S^{0} dT + \sum \Delta \mu_i^{0} dn_i \tag{1.15}$$

where ΔG^{0}, ΔV^{0}, ΔS^{0} and $\sum \Delta \mu_i^{0}$ are the differences in Gibbs free energy, volume, entropy and chemical potential, respectively, can be adapted for protein folding transitions. Assuming a free energy barrier between the unfolded and the native protein, the Gibbs equation can be applied to the activation free energy:

$$d\Delta G^{0\ddagger} = \Delta V^{0\ddagger} dp - \Delta S^{0\ddagger} dT + \sum \Delta \mu_i^{0\ddagger} dn_i \tag{1.16}$$

In protein folding the most common perturbation of chemical potential is the addition of chemical denaturants like urea and guanidinium chloride (GdmCl). Denaturation of proteins with urea is known since 1900[127], when also denaturation of complex systems were known ("A dead frog placed in saturated urea solution becomes translucent and falls to pieces in a few hours.")[128]. GdmCl is known since 1938[129] and has an even greater effectiveness than urea[130]. Generally, the equilibrium free energy (ΔG^0) [131,132] and the activation free energy for folding ($\Delta G_f^{0\ddagger}$) and unfolding ($\Delta G_u^{0\ddagger}$) [133] depend linearly on both denaturant compounds:

$$\Delta G^0(D) = \Delta G^0(H_2O) + m \cdot [Denaturant] \tag{1.17}$$

$$\Delta G_{f,u}^{0\ddagger}(D) = \Delta G_{f,u}^{0\ddagger}(H_2O) + m_{f,u} \cdot [Denaturant] \tag{1.18}$$

The linear denaturant dependence of the activation free energies ($\Delta G^{0\ddagger}$) for refolding and unfolding for a two state mechanism leads to a V-shaped plot of $ln\lambda$ ($\lambda=k_f+k_u$) *versus* chemical denaturant concentration, commonly called chevron plots (Figure 1-5).[134,135] It was shown that the m_{eq}-values are proportional to the change in solvent accessible surface area (ASA) upon unfolding of the protein.[23] Thus, the kinetic *m*-values are interpreted as the changes in ASA with formation of the transition state in the refolding (m_f) or unfolding (m_u) reaction. One can define a denaturant-induced free energy relationship:

$$\alpha_D = \frac{\partial \Delta G_f^{0\ddagger} / \partial [Denaturant]}{\partial \Delta G^0 / \partial [Denaturant]} = \frac{m_f}{m_{eq}} \tag{1.19}$$

α_D is a measure for the relative change in solvent accessible surface area between the unfolded state and the transition state.

A practical way to determine α_x and to test for linearity is to plot the activation free energy for folding $\Delta G_f^{0\ddagger}$ *vs*. the Gibbs free energy ΔG_{eq}^0 and the rate constant for folding (k_f) *vs*. the equilibrium constant (K_{eq}), respectively, determined under the same conditions.

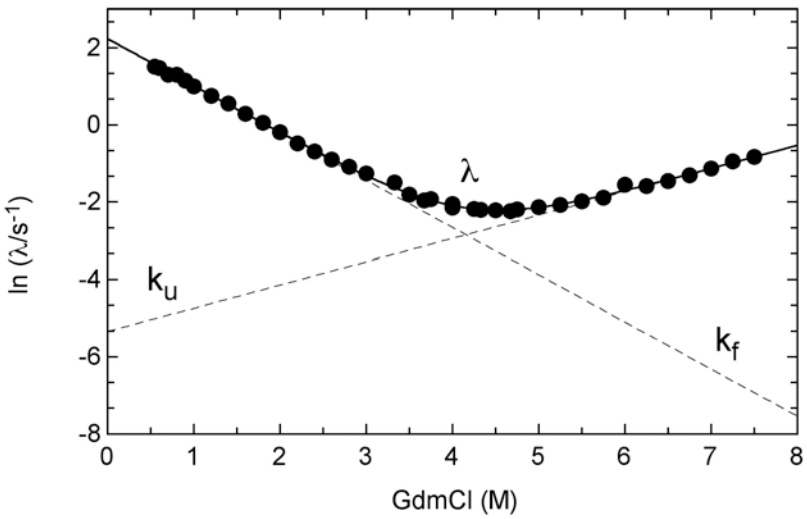

Figure 1-5: Kinetic data for two-state tendamistat folding and unfolding at pH 2.0. GdmCl-dependence of the logarithm of the apparent rate constant ($\lambda=k_f+k_u$) gives a V-shaped profile commonly termed Chevron plot. This reveals a linear dependence between GdmCl concentration and the ln($k_{f,u}$) as indicated by the dashed lines. (from ref.[136])

Less data are available on the effect of temperature to determine REFERs in protein folding. With variation of temperature one receives the equilibrium parameters as well as the activation parameters of enthalpy, entropy and heat capacity (chapter 1.2), which allow the definition of α_T, α_H and α_C :

$$\alpha_T = \frac{\partial \Delta G_f^{0\ddagger} / \partial T}{\partial \Delta G^0 / \partial T} = \frac{\Delta S_f^{0\ddagger}}{\Delta S^0};\ \alpha_H = \frac{\Delta H_f^{0\ddagger}}{\Delta H^0};\ \alpha_C = \frac{\Delta C_{p\,f}^{0\ddagger}}{\Delta C_p^{\,0}} \tag{1.20}$$

α_T and α_H give information on the entropy and on the enthalpy of the transition state, respectively. $\Delta C_p^{\,0}$ like the m-values correlates with changes in accessible surface area.[23] Thus α_C allows the characterization of the transition state in terms of its relative solvent exposure in the same way as α_D. It is commonly observed that the α_D-values are higher compared to α_C-values.[123]

For equilibrium and kinetic measurements at constant temperature and different pressures equation (1.14) can be rewritten as:

$$\alpha_p = \frac{\partial \Delta G_f^{0\ddagger} / \partial p}{\partial \Delta G^0 / \partial p} = \frac{\Delta V^{0\ddagger}}{\Delta V^0} \tag{1.21}$$

Equations (1.19), (1.20) and (1.21) can be considered as medium- or solvent-induced REFERs. Kinetic analysis of engineered proteins has often been used as a tool to provide energetic and structural information about the transition state between folded

and denatured states.[137,138] Therefore the structure-induced REFER is defined as:[135,137,139,140]

$$\alpha_S = \phi_f = \frac{\partial \Delta G_f^{0\ddagger} / \partial Structure}{\partial \Delta G^0 / \partial Structure} \tag{1.22}$$

α_S, commonly called ϕ_f,[137] measures the degree of formation of all interactions formed by a side chain with the rest of the protein in the transition state relative to the native state with the unfolded state as a reference. If interactions are completely formed in the transition state the ϕ_f -value will be 1. The other limiting case, ϕ_f =0, means that the interactions are completely absent in the transition state.

Many proteins were analyzed using this method.[138] The interpretation of the results is often focused on a few residues with higher ϕ_f –values than the other values or even higher than 1. It was proposed that these residues belong to the "folding nucleus" of the protein.[141] However, it was recently shown that the ϕ_f -values are highly inaccurate if the stability change of a mutation is smaller than 6-7 kJ mol^{-1}.[140] Re-analysis of the ϕ_f–values of eleven proteins taking into account all the values obtained contradict a nucleation-condensation mechanism and revealed that transition states are best described as diffused or polarized.[140]

Nonlinear rate equilibrium free energy relationships in protein folding

The linearity of the REFERs over a long range of experimental conditions in many cases in protein folding indicates that the transition states are narrow and robust maxima in the free energy landscape.[59,123] However, deviations from linearity in the REFERs upon mutation or changes in solvent conditions are frequently observed in protein folding.[110,112,113,142,143] They were shown to be caused by different effects: (i) a change in the rate limiting step (Figure 1-6C)[110-113], (ii) a change in the mechanism of the reaction such as a switch to a parallel pathway[59,144], (iii) a change from two-state folding to folding through a populated intermediate [143,145,146], (iv) a movement of the transition state along the reaction coordinate (Hammond behavior; Figure 1-6A and B)[147] and (v) structural changes in the ground states[59]. Thus, nonlinearities in REFERs can give information on various properties of the transition states.

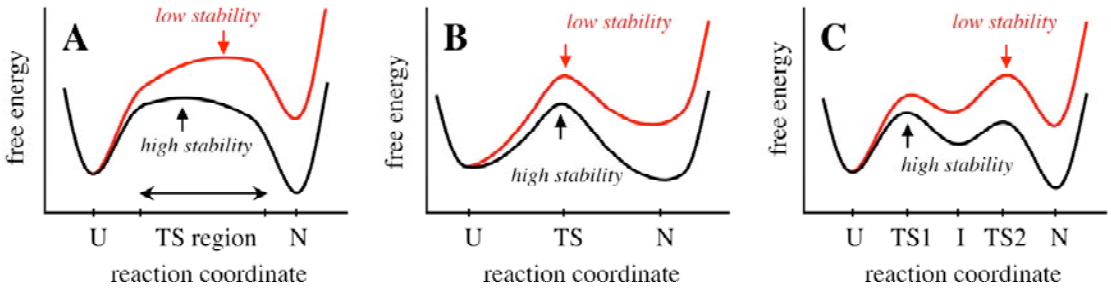

Figure 1-6: Schematic representation of the response of different types of free energy barriers to the same perturbation. The position of the transition state along the reaction coordinate is more sensitive to the perturbation if the free energy shows a broader maximum (A) than if the maximum is narrow (B). An apparent movement of the position of the transition state can also be due to a switch between consecutive transition states on a linear pathway (C). An arrow indicates the position of the highest point along the barrier region. (from ref.[59])

A practical and systematic way to detect and analyze non-linearities was proposed by Jencks and coworkers by applying self-interaction (p_x) and cross-interaction (p_{xy}) parameters.[148] A self-interaction parameter p_x measures the shift in the position of the transition state along the reaction coordinate due to changes in equilibrium free energy upon perturbation:

$$p_x = \frac{\partial \alpha_x}{\partial \Delta G_x^0} = \frac{\partial^2 \Delta G_f^{0\ddagger}}{\left(\partial \Delta G_x^0\right)^2} \tag{1.23}$$

A positive p_D-value indicates a movement of the transition state to the destabilized state according to Hammond postulate (Figure 1-6A and B), or a change in the rate-limiting step (Figure 1-6C). In contrast, parallel pathways could cause negative values. Self-interaction parameters are often not sensitive enough, because the energy range of the measurements is too narrow or the curvature is too small. The sensitivity can be improved by measuring the position of the transition state under different ΔG^0 caused by a second perturbations ∂y:

$$p_{xy} = \frac{\partial \alpha_x}{\partial \Delta G_y^0} = \frac{\partial^2 \Delta G_f^{0\ddagger}}{\left(\partial \Delta G_x^0\right)\left(\partial \Delta G_y^0\right)} = \frac{\partial \alpha_y}{\partial \Delta G_x^0} = p_{yx} \tag{1.24}$$

For nonlinear REFERs the value of the self-interaction as well as of the cross-interaction parameters will be unequal zero. By definition, Hammond behavior and ground state effects will yield positive p_{xy}-values; whereas negative values indicate parallel pathways.

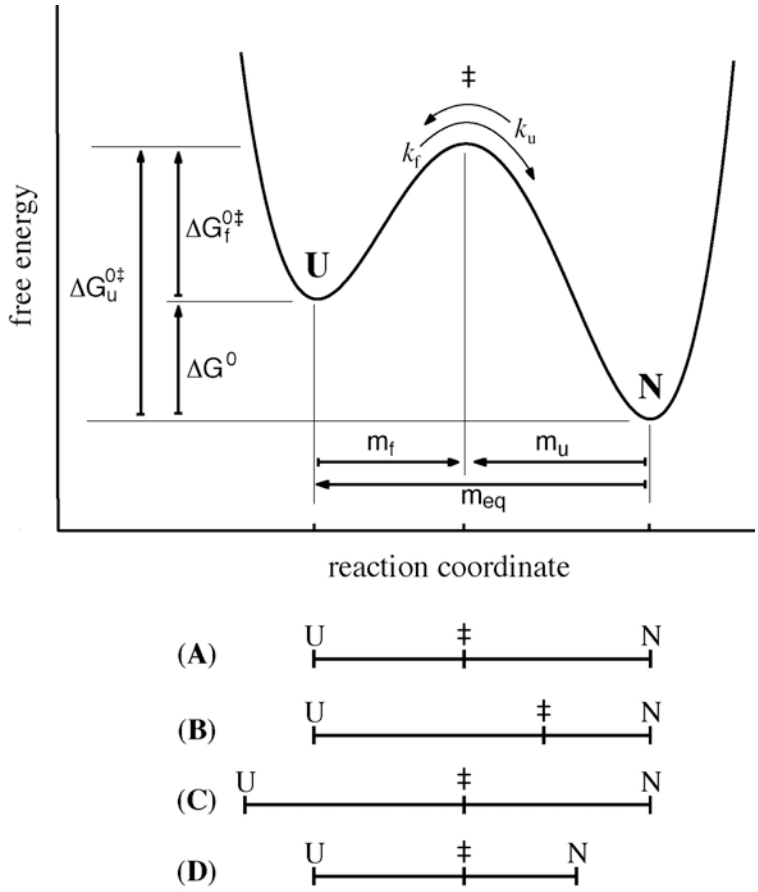

Figure 1-7: Schematic representation of the possible effect of a perturbation on the position of the ground states and on the transition states along a reaction coordinate probed by the change in denaturant concentrations. The reference condition (A) is compared to real Hammond behavior (B) and to apparent transition state movements caused by ground state effects due to change in the structure of the unfolded (C) and native state (D). In all three cases (B-D) the position of the transition state will change by the same amount relative to the ground states. (from ref.[59])

According to the Hammond postulate the position of a transition state is shifted towards the ground state that is destabilized by the perturbation relative to the unfolded state, leading to an increase in α_x and curvatures in REFERs (Figure 1-6A and B, Figure 1-7(B)).[147] Any transition state should show Hammond behavior but if the transition state is a rather narrow free energy barrier, the changes in α_x will be too small to be detected experimentally (Figure 1-6B).[149] By contrast, Hammond behavior should be observed experimentally for a broad and smoothly curved transition state (Figure 1-6A).[149] The structural changes in the native (Figure 1-7 (C)) or unfolded (Figure 1-7 (D)) protein caused by a perturbation can change the length of the reaction coordinate. These ground state effects can easily be mistaken for genuine transition state movement.[59,123,150] The combined analysis of denaturant and structure-induced rate-equilibrium free energy relationships revealed that Hammond behavior is rare in

protein folding transition states and that most apparent transition state movements are due to ground state effects.[59]

In contrast to Hammond behavior, a decrease in α_x with destabilization of the ground state relative to the unfolded state by the perturbation indicates anti-Hammond or parallel pathways. This effect was observed for the first helix of barnase[151,152] and for protein G[153]. For both proteins, parallel pathways could explain the effect and no clear example for anti-Hammond exists so far. Theoretical studies suggested the presence of a manifold of parallel routes to the native state.[154,155] Interrupted refolding experiments[121] and kinetic modeling[86] can directly test the presence of parallel pathways with populated intermediate (chapter 1.3.3). For lysozyme folding at least three parallel pathways were described, some of which are detectable only under certain conditions.[145,156-158] However, evidence for parallel pathways in the absence of intermediates is rare. A clear upward curvature in the chevron plot was reported for a titin domain, which is the clearest example for parallel pathways in two-state folding.[144] The existence of parallel pathways was also proposed for GCN4[159], the formation of the first helix of barnase[151,152], and for protein G[153].

Compared to the amount of data in protein folding by changing the denaturant concentration in combination with mutations, only little is known about transition state movements induced by changes in pressure and temperature. One of the few examples is tendamistat, where the destabilization of the protein with increasing pressure leads to a movement of the transition state to a less solvent-exposed structure, in accordance with Hammond behavior.[123,160]

1.4 The Model Protein: Tendamistat

Tendamistat is an α-amylase inhibitor from the soil bacterium *Streptomyces tendae*, which secrets the protein into the media. It contains 74 amino acids with a total molecular mass of 7952 Da and two disulfide bonds between residues 11 and 27 and residues 45 and 73 (Figure 1-8). It exhibits a high degree of homology with other α-amylase inhibitors from *Streptomyces* species.[161] Its initial biochemical characterization[162] showed that it is highly soluble in aqueous solvents with an isoelectric point of 4.35. It is a highly stable protein and resistant against acidic pH, high temperature and proteases. Calorimetric studies on the wild type confirmed the high thermostability and gave a pH optimum of stability around pH 5 for wild type.[163] The absorbance spectrum has a maximum at 276 nm ($A_{276}^{1\%}$ = 16.1 cm^{-1}) and a shoulder at 281 nm. Tendamistat binds and inhibits mammalian α-amylases with an inhibition constant K_i of $2 \cdot 10^{-10}$ M - $9 \cdot 10^{-12}$ M.[162]

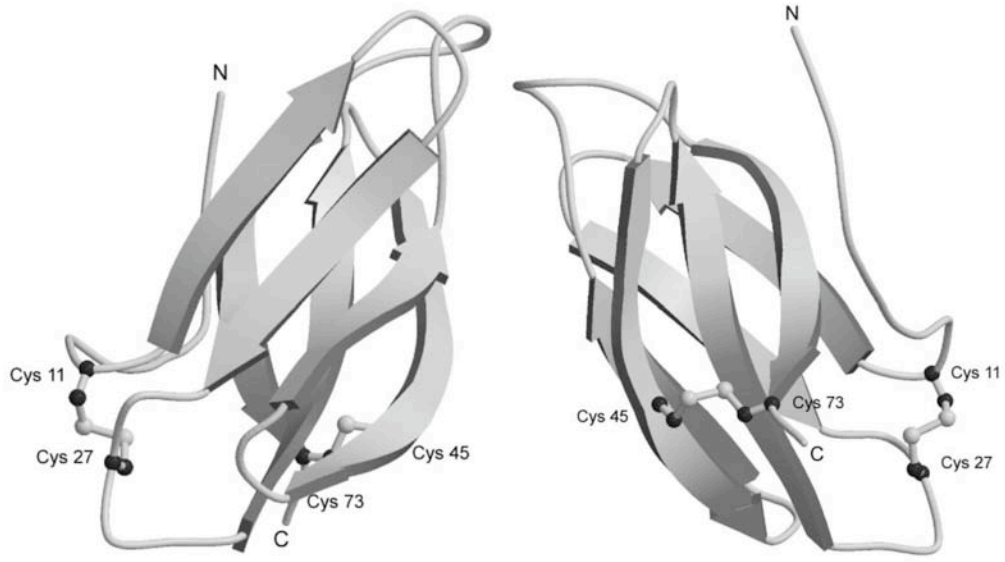

Figure 1-8: Schematic drawing of the structure of tendamistat. The disulfide bonds between Cys11-Cys27 and Cys45-Cys73 are shown as ball-and-stick models. The figure was generated using MOLSCRIPT[164] and Raster3D[165].

The three dimensional structure of tendamistat was solved independently in parallel by both NMR spectroscopy[166,167] and X-ray crystallographic methods[168]. Both approaches gave very similar results.[169] The structure of the inhibitor/α-amylase complex was also solved by X-ray crystallocraphy.[170] Tendamistat is comprised of β-sheets and loops only (Figure 1-8). The strands are ordered in two twisted antiparallel β-sheets that form a β-barrel structure. The topology of the β-strands is homologous to the immunoglobulin fold, but the seventh strand and the inter-sheet disulfide bond are missing in tendamistat.[171] The first disulfide bond is located at the base of the hairpin in the first sheet, whereas the second one is between the two outer strands of the second sheet (Figure 1-8). The structure of the disulfide variant C45A/C73A, which was solved by NMR, has only very local changes at the mutation site but is otherwise virtually identical with the wild type structure.[46] The solvent exposed triplet Trp18-Arg19-Tyr20 at the first hairpin turn is necessary for the inhibitory activity of tendamistat and is conserved in all inhibitors of this class.[161,170,172] The tryptophan residue presents a rare case of a solvent exposed tryptophan in a native structure. A Cl-binding site is located at Arg19.[168]

The folding kinetics of tendamistat with intact disulfide bonds are well characterized.[15,84,110,160,173,174] About 85 % of the fluorescence change upon folding occur in a rapid reaction with an observable rate constant λ of about 100 s^{-1} in the absence of denaturants at pH 7 and 25°C.[173] No hydrophobic collapse could be observed and the folding kinetics fulfill the criterion for a two-state reaction.[173] The remaining 15 % of the unfolded molecules fold in two slower reactions, which were shown to be caused by *cis-trans* isomerization of non-prolyl[84] and prolyl peptide bonds[81,173] (Figure 1-9). With the help of interrupted refolding experiments, an additional very slow folding reaction could be detected with an amplitude of about 12 %, which is caused by the interconversion of a highly structured intermediate to native tendamistat.[174] About 2 % of this native like intermediate (N*, Figure 1-9) remain populated in equilibrium after folding is complete. This very slow reaction reflects prolyl isomerization of the Glu6-Pro7 and Ala8-Pro9 peptide bonds, located in a region that makes strong backbone and side-chain interactions to both β-sheets (Figure 1-9).[174]

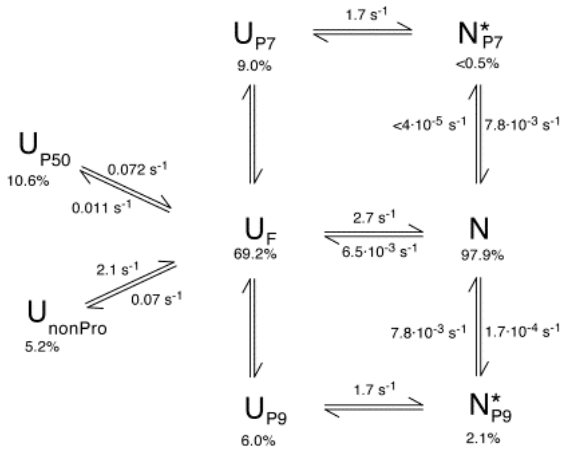

Figure 1-9: Kinetic scheme of tendamistat wild type folding at pH 2.0 and 1.0 M GdmCl including all detectable native (N), native-like (N) and unfolded (U) conformations. The subscripts indicate peptide bonds in the cis conformation. The subscript F indicates fast folding molecules with all prolyl and non-prolyl peptide bonds in the native isomerization state. The numbers below the unfolded and native states give the relative equilibrium populations under strongly denaturing conditions and native conditions, respectively. (from ref.[174])*

Early thermodynamic characterization of the transition state of tendamistat wild type were done varying of pressure at pH 2[160] and temperature at pH 7[15]. The pressure dependence of the kinetic data shows that the volume of the transition state is 60 % native-like, indicating partial solvent accessibility of the core residues.[160] Also Hammond behavior could be observed for tendamistat at pH 2 due to the destabilization of tendamistat with increasing pressure.[123,160] No transition state movements could be observed for the temperature dependence at pH 7.[15] However, the transition state movement could easily elude due to the high stability at pH 7 and the uncertainty of the unfolded branch resulting in relative large errors of the m_u-values. A careful analysis of the temperature dependence of the folding kinetic at slightly destabilizing conditions like pH 2 and/or of a destabilizing amino acid replacement could, therefore, provide a better inside into the effect of temperature to the transition state.

The disulfide topology is conserved among the α-amylase inhibitors from different *Streptomyces* species.[161] The disulfide bridges in tendamistat were shown to be important for maintaining proper folding and stability.[47,175] Calorimetric studies on single disulfide variants of tendamistat showed that the destabilization occurring upon removal of the 45-73 disulfide bridge is purely entropic whereas the stability decrease of the replacement of the 11-27 disulfide bridge is caused by changes in both enthalpic and entropic terms.[47] In addition, kinetic measurements of the effect of the C11/C27 disulfide bond replacements suggest the importance of the 12-26 β-hairpin for the

initiation of β-sheet formation.[15] The equilibrium *m*-values are significantly increased compared to the wild type reflecting an increase in solvent accessibility of the unfolded state upon removal of the disulfide bond. Initial analysis of the temperature dependence of the kinetic data reveals no significant change of the kinetic *m*-values.[15] However, small changes in *m*-values can easily elude detection, therefore a more careful analysis is necessary. Elimination of the C45/C73 disulfide bond results in a pronounced non-linearity of the rate-equilibrium free energy relationship, albeit the lack of detectable populated intermediates.[110] The result argues for a denaturant-dependent switch between two distinct rate-limiting steps of folding with a metastable obligatory intermediate (Figure 1-10).[110,111,123]

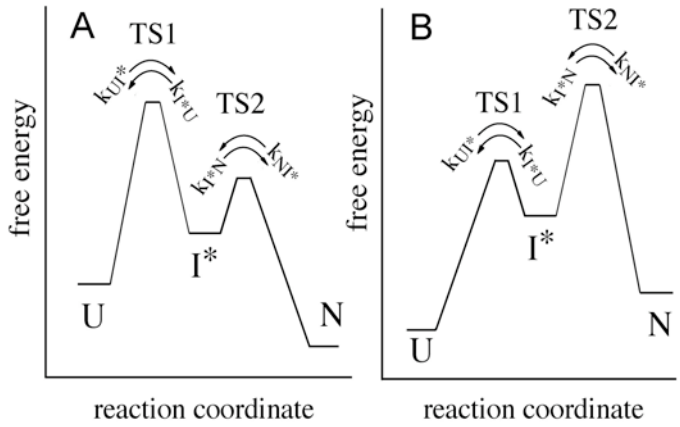

Figure 1-10: Free energy reaction coordinate for the folding of tendamistat C45A/C73A at low (A) and high (B) denaturant concentrations. Upon addition of denaturant a change in the rate-limiting step occurs between two barriers separated by a high-energy intermediate. (from ref.[110])

Less is known so far about the structural properties of both transition states. It will therefore be of great interest to elucidate their structure and to verify the folding mechanism by amino acid replacements and fragmentation. The difference of the effect of temperature on both of the two transition states is also of great interest because it would provide more information about the shape elucidate the shape of the two rate-limiting steps in tendamistat folding.

2. Aims of Research

Tendamistat is a small disulfide bonded all β-sheet protein. It is a good model system to study the structural and thermodynamic properties of the rate-limiting steps of folding of a small all-β-sheet protein due to the wealth of structural information and the well-characterized folding pathway. The known structure allows a molecular interpretation of the results. Tendamistat wild type folds and unfolds in an apparent two-state reaction. Folding kinetics of a disulfide variant have been shown to include at least two distinct consecutive transition states with a high-energy intermediate. Thus, tendamistat is an ideal system to characterize the structural and thermodynamic properties of the barriers in folding of an apparent two state folder. By investigations the stability and folding kinetics of different tendamistat variants and of various fragments we hoped to receive an answer to the following specific questions on the properties of the free energy barriers:

1) **What are the properties of the two consecutive transition states in tendamistat folding? Can we populate and characterize folding intermediates?** To obtain a more detail insight into the structural and thermodynamic properties of the shape of the free energy barriers we analyzed the combined influence of mutation, temperature, denaturant and sodium sulfate on tendamistat stability and folding.
2) **Are fragments of tendamistat able to form specific structures? Is folding initiated by the formation of secondary structures and are there initiation sites?** In order to examine these questions we studied spectroscopic properties and the stability of different fragments of tendamistat.

3. Summary of Manuscripts Ready for Submission

3.1 Shape of the Free Energy Barriers in Tendamistat Folding

These results are described in detail in the following manuscripts:

"Shape of Free Energy Barrier for Tendamistat Folding Measured by Multiple Perturbation Analysis" Manuela Schätzle and Thomas Kiefhaber (2005). *To be submitted.*

"Thermodynamic Properties of the Transition States in Tendamistat Folding" Manuela Schätzle and Thomas Kiefhaber (2005). *To be submitted.*

"Evidence for Parallel Pathways at the Early Stage of Tendamistat Folding" Manuela Schätzle and Thomas Kiefhaber (2005). *To be submitted.*

3.1.1 Multiple Perturbation Analysis

A common approach to characterize transition barriers in protein folding is the analysis of the rate-equilibrium free energy relationships (REFERs), which test the effect of a perturbation on the kinetics and the equilibrium of a reaction.[123-126] The most common perturbation in protein folding is the addition of denaturants often combined with mutations.[59,123,133,135,137,176] Less is known, however, of pressure and temperature induced transition state movement.[15,59,110,123,160,177-179] Analysis of non-linear REFERs yields information on the shape of the transition barriers and on the mechanism in protein folding. A detailed analysis of data from several proteins suggested that the transition states represent structurally well-defined barriers on the folding free energy landscape and showed that Hammond behavior is rare.[59,111] One of the clearest examples, where Hammond behavior was described, was reported for the all-β-sheet protein tendamistat.[160] Tendamistat folding involves two sequential transition states. Linear Leffler plots induced by GdmCl are observed for tendamistat folding. However, Hammond behavior could be detected by applying both pressure and denaturant as perturbations. The results suggest that using multiple perturbation analysis may reveal Hammond behavior in protein folding.

Here, we used multiple perturbation analysis to test if transition state movement could also be observed applying denaturant and temperature as perturbations and to test the broadness of the different barriers during tendamistat folding. We measured the effect of temperature and denaturant on tendamistat folding and stability. Perfectly linear Leffler plots were obtained from Chevron plots at all measured temperatures indicating that single perturbations are not sufficient to detect Hammond behavior. We used the denaturant temperature cross-interaction parameter p_{DT} to probe for transition state movements.

$$p_{DT} = \frac{\partial^2 \Delta G^{0\ddagger}}{\partial \Delta G_D^0 \partial \Delta G_T^0} = \frac{\partial \alpha_D}{\partial \Delta G_T^0} = \frac{\partial \alpha_T}{\partial \Delta G_D^0} \tag{3.1}$$

p_{DT} can be determined in two different ways: analysis of the effect of temperature on α_D or analysis of the effect of denaturant concentration on α_T. Determination of p_{DT} with both methods gave identical values within errors. The results revealed Hammond behavior for tendamistat folding. Multiple perturbation analysis for tendamistat variants, which have different rate-limiting transition states, revealed that ground state effects for the late transition state accompany Hammond behavior, whereas for the early transition state no ground state effect could be observed. The early transition state exhibits significantly stronger Hammond behavior than the late barrier. Comparison of our results with previous findings of the effect of pressure and denaturant on tendamistat folding[160] shows that the transition barriers become increasingly narrow and structurally more defined as the folding polypeptide chain approaches the native state (Figure 3-1).

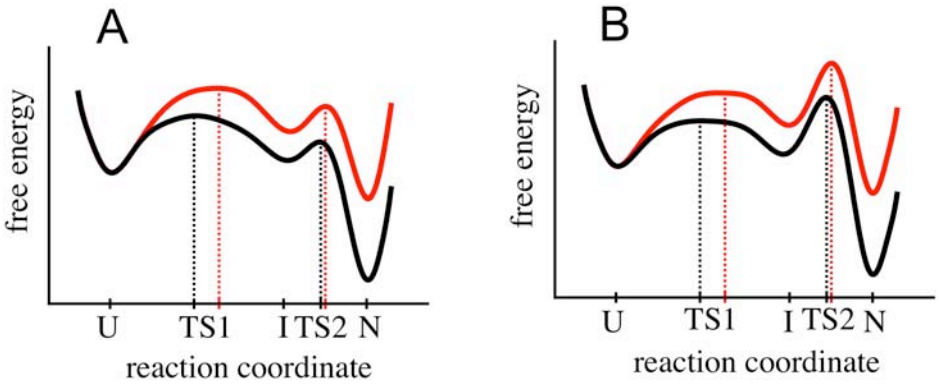

Figure 3-1: Schematic drawing of the free energy barriers for folding of tendamistat with (A) the early and (B) the late transition state rate limiting. The response of variation in temperature on the early transition state (TS1) is more sensitive than on the late one (TS2) due to the different broadness of the barriers.

We have also examined data for 6 different monomeric proteins for which temperature dependence of the kinetic data exists are published. 4 proteins show clearly Hammond behavior and one has negative cross-interaction parameters suggesting parallel pathways. Nearly all proteins show linear Leffler plots. Our results show that temperature-induced Hammond behavior in protein folding is common.

Comparison of our results on the effect of mutations and denaturants of proteins on the transition state suggests that the transition barriers in protein folding exhibit different sensitivity to various perturbations. Hammond behavior was only observed in tendamistat folding when multiple perturbations are applied. The use of multiple perturbation analysis reveals important features on the shape of the free energy barrier in tendamistat folding and, in addition, reveals the underlying complexity of apparent two-state folding.

Another important consequence of our work is that we could show the need for identical conditions in the experiments and simulations. Simulations are commonly performed at high temperature. However, as we were able to show with our work, the ASA of the transition state is temperature dependent.

3.1.2 Thermodynamic Properties of the Free Energy Barriers

We further studied the effect of temperature and denaturant concentration on tendamistat folding and stability to gain information on the other thermodynamic properties of the free energy landscape. The addition of denaturant leads to linear changes of the activation parameters according to the linear free energy model.[180] Due to the linear denaturant dependence of the activation parameters we globally analyzed the data. Comparison of the results reveals good agreement except for the denaturant dependence of the heat capacity of transition states, which is, however, accompanied with large uncertainties.

The activation parameters of both transition states show only less difference. The transition states are both enthalpic and entropic barriers. However, they differ significantly in their denaturant dependences. As discussed in chapter 3.1.1, the denaturant dependence of the activation entropy of transition states correlates with the temperature dependence of the m-values.

Analysis of $\Delta H^{0‡}$ of the early transition state reveals that addition of denaturant has the same pH-independent enthalpic effect on the unfolded and the transition state. In contrast to the early transition state, only small changes of the activation enthalpy with variation in denaturant concentration was observed for the late transition state indicating that the late barrier is more robust against perturbations.

The m and ΔC_p^0-values correlate well with each other because both depend on the amount of protein surface which becomes exposed to solvent upon unfolding.[23] However, analyses of the denaturant dependence of $\Delta C_p^{0‡}$ of the early transition state of tendamistat wild type and tendamistat variants, reveals transition state movement and ground state effects. This is in contrast to our previous observations. In contrast to the m-values which have mainly contributions of the backbone, ΔC_p^0 have contribution of the side chains and nearly none backbone contributions, which could explain the differences. The denaturant dependence of $\Delta C_p^{0‡}$ of the early transition state is in contrast to the denaturant dependence of $\Delta H^{0‡}$ and $\Delta S^{0‡}$. The denaturant dependence of $\Delta C_p^{0‡}$ of the late transition state observed from measurements of two tendamistat variants, revealed only ground state effect and no transition state movement.

Analysis of the denaturant dependencies of the activation parameters confirm our previous results that the transition barriers become increasingly narrow and structurally more defined upon folding of tendamistat (Figure 3-1). It further reveals the importance of multiple perturbation analysis to test the properties of the free energy barriers.

3.1.3 Evidence for Parallel Pathways

Theoretical studies suggested the presence of a manifold of parallel routes to the native state.[154,155] Although predicted, parallel pathways are not often observed in protein folding. For lysozyme folding at least three parallel pathways were described.[145,156-158] Parallel pathways in two-state folding was described for folding of the 27th immunoglobulin domain of the human giant muscle protein titin (TI I27).[144] The existence of parallel pathways was also suggested for the formation of the first helix of barnase[151,152], and for protein G[153].

A destabilization of the native state will more affect the free energy of native-like transition states. Therefore, a destabilization of the native state leads to a shift of the rate-limiting step to a less native-like transition state. This leads to a decrease in α_x with decreasing protein stability, which is also sometimes referred to as anti-Hammond behavior.[59,152,181]

In chapter 3.1.1 we could show the importance of multiple perturbation analysis to improve the sensitivity to test the properties of the free energy barriers. To test for parallel pathways, we therefore measured the effect of denaturant and temperature on the folding kinetics of a tendamistat variant lacking one of the two disulfide bonds. Removal of the disulfide bond results in a strong destabilization[15,110] and leads to a change of the rate-limiting step at high denaturant concentrations. Assuming linear denaturant-dependence of the activation parameters we are also able to fit the kinetic data globally. The results of the single and global fits are in good agreement.

Determination of the temperature-denaturant cross-interaction parameters p_{DT} (equation (3.1)) reveals switches between parallel pathways at the early stage in folding upon destabilization of the protein. In contrast, the apparent transition state movement observed for the late transition state is caused by an increase in the average solvent exposure of the unfolded state when temperature is increased, while the structure of the transition state seems to be robust against this perturbation.

Analysis of the changes of the activation parameters with increasing denaturant concentration reveals that the late transition state is rather insensitive to the addition of perturbations compared to the early transition stages in tendamistat folding. These are in accordance with our previous observation that the barriers become increasingly narrow and transition state structures become more defined upon folding of the protein. Parallel pathways are not observed in tendamistat folding when single perturbation was applied. The results confirm our previous finding that multiple perturbation analysis are important to test the shape of the free energy barrier in protein folding. and to reveal underlying complexities of apparent two-state protein folding.

4. Summary of Unpublished Work

4.1 Studies on Tendamistat Fragments

Analysis of folding and association of fragments derived from proteins provides insight into the mechanism of protein folding. The association of peptide fragments to form a fully reconstituted native-like protein structure has been described in detail for a few small proteins like RNaseS[182], barnase[183,184], CI-2[185,186], GB1[187], thioredoxin[188,189], ubiquitin[190] and cytochrome c[191]. The analysis of individual fragments and of their assembly to form native-like structures can give information on the existence of initiation sites for the folding of a protein. Some fragments show evidence for a native-like structural propensity,[184,185,190,192] whereas other fragments associate into native-like protein structures without any evidence for well-defined initiation sites[183,189,191]. The tendency of fragments to form structure similar to the one adopted in the full protein supports the idea that local interactions play an important role in the early steps of the folding process.[184,186,188,190,192,193]

We studied four different fragments of tendamistat (Figure 4-1). One of the fragments, T(10-28)-A28G was chemically synthesized and corresponds to the N-terminal β–hairpin of tendamistat. Two of the fragments, T(1-34) and T(35-74), are products from the cleavage of native tendamistat with lysylendopeptidase. We introduced a methionine to be able to chemically cleave the protein using cyanogen bromide and to subsequently isolate the fourth fragment, T(11-74). The goal of these investigations was to elucidate the capability of the fragments to fold autonomously as well as to analyze their stability. A second aim was to find out where the two fragments T(1–34) and T(35-74) are able to assemble into a native-like structure.

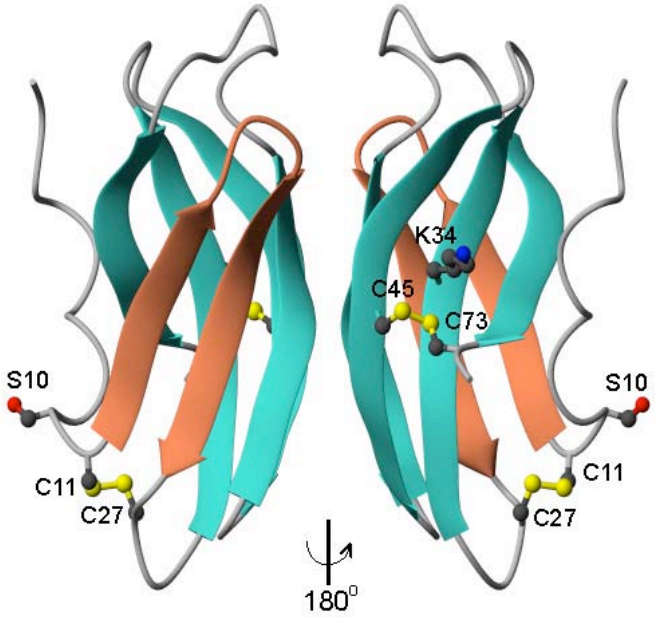

Figure 4-1: Schematic drawing of the structure of tendamistat. The N-terminal β-hairpin is coloured in red. The disulfide bonds between Cys11-Cys27 and Cys45-Cys73 and the residues Ser10 and Lys34 at the cleavage sites are shown as ball-and-stick models. The figure was generated using MOLMOL[194].

4.1.1 Stability of the N-terminal β-hairpin of Tendamistat and the C-terminal β–hairpin from the B1 domain of streptococcal protein G

Designed short peptides that fold autonomously in water like α-helices and β-sheets, have proven extremely valuable in probing the relationship between local sequence information and folded conformation in the absence of the tertiary interactions found in the native state of proteins. Studies on water-soluble, non-aggregating monomeric β-sheets have emerged only recently,[195] while the literature is rich in studies of α-helical peptides.[196] Autonomously folding β-hairpin motifs, consisting of two anti-parallel β–strands linked by a reverse β-turn, represent the simplest systems for probing weak interactions in β-sheet folding and assembly. The first peptides, which could be investigated in the monomeric soluble form, were derived from tendamistat,[197] B1 domain of protein G,[198,199] ubiquitin[200] and ferredoxin[201]. In most cases, however, they showed a very weak tendency to fold in the absence of tertiary contacts.

The first example of a natural β-hairpin sequence that folded autonomously in water was the C-terminal fragment of the B1 domain of streptococcal protein G, termed

β–hairpin Gb1p.[198] Around 42 % β-hairpin structure population in water was estimated from NMR measurements.[198] It was proposed that this β-hairpin is the initiation site of folding of protein G.[192] Calorimetric and NMR studies of the peptide gave values of the free energy of folding, ΔG_f, of 0.9 and 0.5 kJ/mol, respectively.[202] Kinetic analysis of this peptide was studied by laser-induced temperature-jump, which reveals a single exponential relaxation process with a time constant of 3.7 μs.[203]

Several peptides have been synthesized based on the amino acid sequence of the N-terminal β-hairpin of tendamistat located between the residues V12 and V26, termed β-hairpin 12-26. Some of these have been examined for protein structure and folding,[175,204] whereas others were made in attempts to generate enzyme inhibitors[205]. A 9 residue fragment of the β-hairpin region has been shown to form transient β–turn-like structures in the same region where the native β-turn exists, although no β-hairpin structure was detected.[204] A disulfide bond is located at the base of this β–hairpin in tendamistat (C11-C27), which is important for folding and stability.[15,47,110] Folding studies on disulfide variants gave evidence for late formation during folding of the β-hairpin 12-26.[110]

We studied the stability of a 19 residue peptide, T(10-28)-A28G, of the β-hairpin 12–26 of tendamistat. In order to investigate the tendency of this peptide to form a β–hairpin we used the concept of the effective concentrations, C_{eff}, for disulfide bond formation. [206] To compare our results with other β-hairpins, we measured the stability of the β-hairpin Gb1p, where folding and stability are well described in literature.[192,198,199,202,203]

Theory

The linkage relationship between disulfide bond formation and protein stability were first described by Creighton[207] and further developed by Lin and Kim.[206,208] For proteins or peptides that contain a disulfide bond, unfolding free energies can be obtained using the following thermodynamic cycle:

$$\begin{array}{ccc} N_{SH}^{SH} & \overset{K_1}{\rightleftharpoons} & N_S^S \\ K_3 \uparrow\downarrow & & \uparrow\downarrow K_4 \\ U_{SH}^{SH} & \underset{K_2}{\rightleftharpoons} & U_S^S \end{array} \qquad (4.1)$$

where N_S^S, N_{SH}^{SH}, U_S^S and U_{SH}^{SH} represent the native oxidized, native reduced, unfolded oxidized, and unfolded reduced states, respectively. With the unfolding equilibrium constants for the reduced, K_3, and oxidized form, K_4, and the pseudo equilibrium constants for the half reactions of disulfide formation in the native, K_1, and denatured states, K_2, the linkage between conformational stability and disulfide stability is

$$\frac{K_1}{K_2} = \frac{K_3}{K_4} \tag{4.2}$$

For the analysis of linkage relationships in protein stability the concept of effective concentration (C_{eff}) was introduced.[207] C_{eff} represents the ratio of rate or equilibrium constants of otherwise identical intra- and intermolecular reactions and is a useful concept in enzymology.[209] It is an empirical parameter, measured relative to a standard species at a given set of conditions. C_{eff} can be experimentally measured in a redox equilibrium mixture for a polypeptide with two cysteines that can form a disulfide bond, and glutathione:

$$P_{SH}^{SH} + GSSG \overset{K}{\rightleftharpoons} P_S^S + 2GSH \tag{4.3}$$

where P_{SH}^{SH} and P_S^S refer to the reduced and oxidized forms of the polypeptide and GSH and GSSG refer to reduced and oxidized glutathione. C_{eff} can be obtained by comparing the pseudo equilibrium constant for disulfide formation in the peptide or protein (K_{intra}) to that for intermolecular disulfide bond formation (K_{inter}) in glutathione:

$$C_{eff} = K = \frac{K_{intra}}{K_{inter}} = \frac{\left[P_S^S\right]\left[GSH\right]^2}{\left[P_{SH}^{SH}\right]\left[GSSG\right]} \tag{4.4}$$

To fix the redox potential of the solution, the concentrations of GSH and GSSG are much larger than those of the protein or peptide. Thus, C_{eff} can be calculated by measuring the ratio of oxidized and reduced polypeptide. The ratio between K_1 and K_2 can be obtained by measuring C_{eff} of the thiols in the native (N) and unfolded (U) states with:

$$\begin{aligned} C_{eff}^N &= K_1 \cdot \frac{\left[GSH\right]^2}{\left[GSSG\right]} \\ C_{eff}^U &= K_2 \cdot \frac{\left[GSH\right]^2}{\left[GSSG\right]} \end{aligned} \tag{4.5}$$

It could be shown that urea does not affect the measurements, thus C_{eff}^U can also be measured in concentrated urea solutions.[206] Empirically, glutathione was shown to be

an excellent reference thiol since formation of its disulfide bond does not depend on urea concentration.[210] Observation of a high C_{eff} usually indicates that the molecule adopts a conformation that brings the two reactive cysteine residues into an optimal proximity and orientation for interaction, whereas a low C_{eff} may indicate that either the molecule lacks a defined structure or the two cysteine residues are even being held apart from each other.[207]

Assuming a two-state mechanism for the denaturant-induced unfolding and using equations (4.5) and (4.2), the equilibrium constant for unfolding of reduced polypeptide is therefore

$$K_3 = \frac{C_{eff}^N - C_{eff}}{C_{eff} - C_{eff}^U} \tag{4.6}$$

This method can therefore be used to provide a sensitive probe for folded structure in peptides and proteins as well as to obtain unfolding free energies for both the reduced and the oxidized form by measuring the effective concentrations of thiols.[206]

In our case, we used the method as a probe for folding and stability of the β-hairpin 12–26 of tendamistat with the β-hairpin Gb1p, as a reference peptide.

Results and Discussion

NMR measurements of the 12-26 and the 15-23 fragment of tendamistat gave evidence that the peptides are not random but adopt turn-like structures around their central region, the same region where the native β-turn is formed in the protein.[204] Therefore, we synthesized the peptide **T(10-28)-A28G** based on the sequence of the β–hairpin 12-26 of tendamistat:

Ac-^{10}SCVTLYQ**SWRY**SQADNGCG^{28}-NH_2.

The turn sequence is highlighted in bold. A glycine residue replaced the alanine residue at the position 28 to raise the yield of synthesized peptide. To prevent the influence of the charged termini, the C-terminus was amidated and the N-terminus was acetylated.

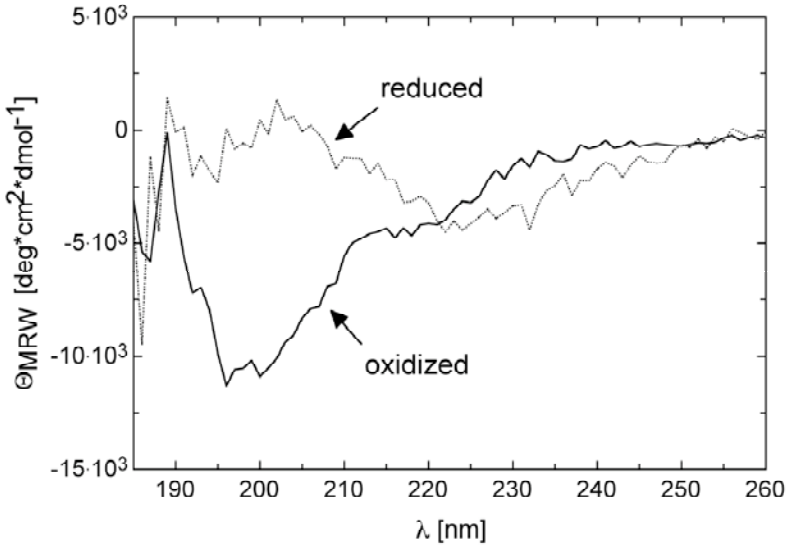

Figure 4-2: CD spectra in the far-UV region of the peptide T(10-28)-A28G with reduced (dotted line) disulfide bond and with disulfide bond oxidized (solid line) of about 21 %. Condition were 18 µM peptide in 50 mM KP_i, pH 8.0, 4°C. 35 µM DTT were added to the solution to reduce the peptide.

At pH 8 and 4°C the far-UV CD spectrum of T(10-28)-A28G in its reduced form after treadment with dithiothreitol (DTT) shows a negative band between 220 nm and 230 nm and a positive band around 200 nm (Figure 4-2). The peptide was analyzed by HPLC after air oxidation and the relative amount of oxidized peptide was calculated. Only about 21 % of the peptide was oxidized. The far-UV CD spectrum of the air oxidized peptide (Figure 4-2) shows the same shape as the fully oxidized tendamistat fragment T(1-34) (chapter 4.1.2, Figure 4-6) but with less signal intensity. In contrast to the spectrum of the reduced peptide, the far-UV CD spectrum of the oxidized peptide shows a negative band around 200 nm and a small shoulder at 210 nm, whereas the negative band between 220 and 230 nm has disappeared (Figure 4-2). These bands are typical for unordered peptides. The positive band around 190 nm, on the other hand, is typical for β-sheet structure. However, the contribution of β-sheets to the far-UV CD spectra is weak and diverse. The shape depends on the length and orientation of the strands and on the twist of the sheet. Also, the aromatic side chains contribute strongly to the far-UV CD spectrum. Thus, the CD data give little information on the possible folded structure of the peptide. Interestingly, the far-UV CD spectrum of Gb1p in water shows a similar shape as the far-UV CD spectrum of oxidized T(10–28)-A28G with a negative band at 200 nm and a positive band around 190 nm.[192]

As described above, the effective concentration C_{eff} can be used as a measure of intramolecular interactions that specifically stabilize the disulfide-bonded form. Thus, if there were hairpin formations in our peptides, we would expect to detect them by measuring the stability of the disulfide bond. Measurements were performed at varying conditions in order to stabilize the secondary structure to different extends. Thus, a change in C_{eff} as the structure is destabilized by chemical means would be a strong indication that there is hairpin formation in water. The results of the measurements are shown in Figure 4-3 and in Table 1 and Table 2.

The measurements of C_{eff} of the peptide T(10-28)-A28G at different urea concentrations reveal, that the thiol-disulfide equilibrium is denaturant-independent with a low C_{eff} = (27.0 ±1.4) mM (Figure 4-3).

Due to the well described folding and stability of the C-terminal fragment of the B1 domain of streptococcal protein G[192,198,199,202,203] we synthesizes the peptide **SSGB1** based on the sequence of this β-hairpin with the following sequence:

Ac-[40]CGEWTYD**DATK**TFTVTECSG[59]-NH_2

The turn sequence is highlighted in bold. We introduced a cysteine residue at both ends, as well as a serine and glycine at the C-terminus because of synthetic reasons. As in T(10-28)-A28G, we amidated the C-terminus and the N-terminus was acetylated.

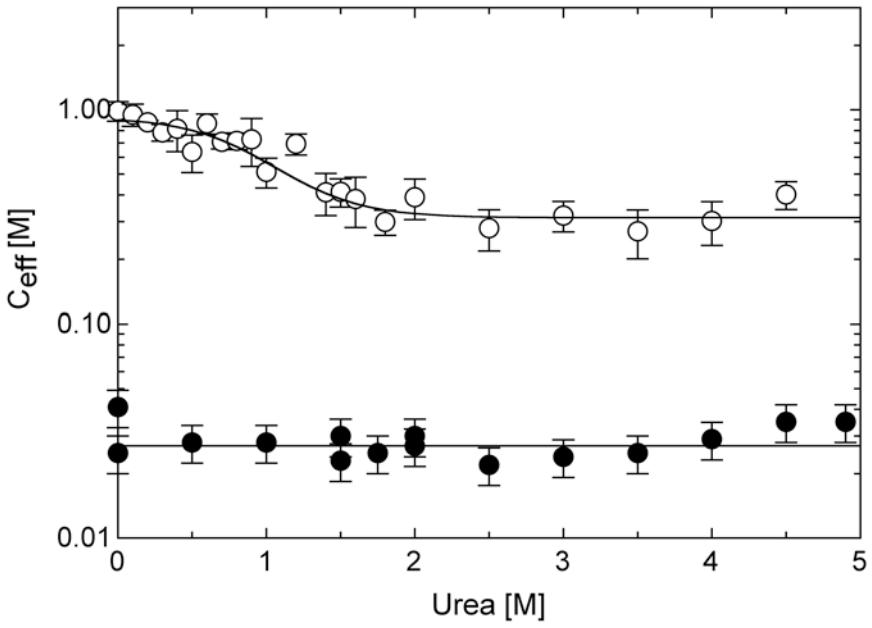

Figure 4-3: Urea dependence of C_{eff} in the peptides T(10-28)-A28G (●) and SSGb1 (○). C_{eff} was measured under the conditions as described in methods. The results for SSGB1 were analyzed using equation (4.6). Results of the fits are given in Table 1 and Table 2.

In contrast to T(10-28)-A28G, the values of the effective concentration of the peptide SSGB1 decrease between 0 and 2 M urea (Figure 4-3). An effective concentration of C_{eff}^{N} = (923 ±54) mM in absence of denaturant and of C_{eff}^{U} = (313 ±26) mM above 2 M urea were received by fitting the data using equation (4.6). Both, C_{eff}^{N} and C_{eff}^{U}, are significantly larger than C_{eff} for T(10-28)-A28G (Figure 4-3 and Table 1). To fit the data we assumed a two-state mechanism for the unfolding of the β-hairpin, although this has not been proven yet. However, all data of earlier measurements of Gb1p found in literature were analyzed using a two-state mechanism.[202,203,211]

Table 1: Effective concentrations of disulfide formation in different peptides and proteins.

		C_{eff} [mM]	T [K]
peptides	*random coil*		
	Ac-Cys(Gly)$_6$Cys-NH$_2$[206] 0-7 M urea	60	296
	α-helix		
	Apamin variants[212]	18; 33	298
	>6M urea	10; 15	
	β-hairpin		
	T(10-28)-A28G[a]	27	288
	SSGB1[a]	923	288
	>2M urea	313	
	bhpW[213,214]	210	293
	bhpW variants[213-216]	51 – 710[b]	293
		141 – 1181[c]	
		38 – 167[d]	
	ω–Conotoxin[217]	9 – 390	298
	8M urea	3 – 330	
proteins	BPTI[218]	$2 \cdot 10^5$ – 10^8	298
	Thioredoxin[206,208]	10^4	296
	>6M urea	24	
	Thioredoxin variant P34S[208]	380	296
	>6M urea	77	
	PDI[219,220]	0.04; 0.06	
	DsbA[221]	0.081	298
	8M urea	170	
	four-helix bundle protein[222]	246	298
	α-lactalbumin disulfide variants[223]	29 – 10^3	298
	6M GdmCl	0.5 – 23	
	hen lysozyme disulfide variants[224]	21 – 72	298
	>6M urea	0.7 – 13	
	barnase disulfide variant[225] >3M GdmCl	~ 5	298
	sc-Arc-NC11[226]	$71 \cdot 10^3$	298
	denatured with GdmCl	0.04	

[a] this work
[b] amino acid replacements at non-hydrogen-bonded strand positions
[c] amino acid replacements at the hydrogen-bonding strand positions
[d] amino acid replacements at turn positions

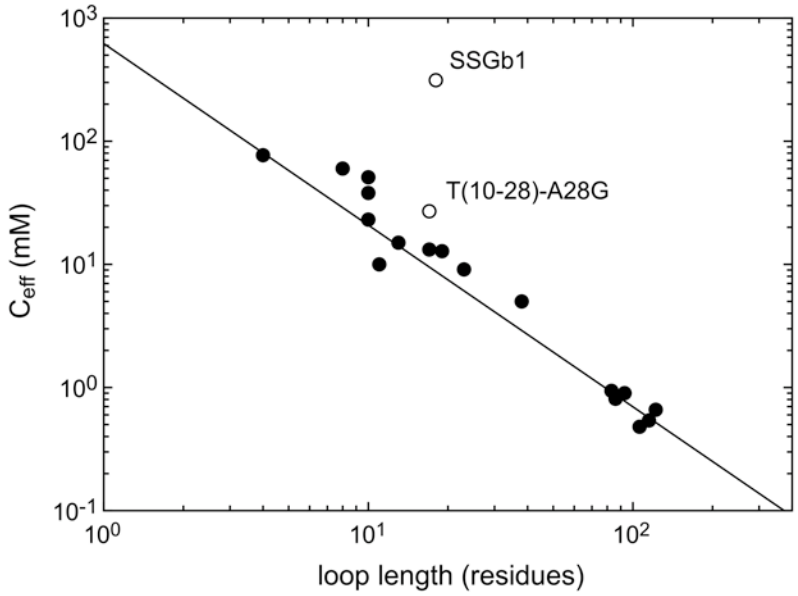

Figure 4-4: Effective concentrations of the formation of an intramolecular disulfide bond in different peptides and proteins under denaturing conditions (●), plotted as a function of the number of amino acid residues in the intervening loop. The line represent a single parameter fit to the random walk model of an unfolded polypeptide chain using equation (4.7).[91,227] *C_{eff} of T(10–28)-A28G and C_{eff}^{U} of SSGB1 are plotted for comparison.*

In Table 1 we compare our results with effective concentrations of different peptides and proteins found in literature. The values of the effective concentrations in peptides varied from 3 mM to 1181 mM, whereas in native proteins C_{eff} ranged from 40 μM for PDI to 10^5 M for BPTI (Table 1). Very low C_{eff}-values were found for DsbA and PDI, which are involved in the formation of the correct disulfide bridges in protein folding.[219,221] The formation of the disulfide bonds are structurally not favored in both proteins, which makes them ideally suited as a potent oxidant.[221] This also explains the increase of C_{eff} for DsbA when adding denaturant.[221] In general, the C_{eff}-values are significantly smaller for unfolded proteins compared to the native forms due to an increase in chain flexibility. C_{eff}–values typically lie in the range of 0.5 mM to 100 mM depending on the loop length (Table 1, Figure 4-4). The significant deviation for sc–Arc-NC11 could be explained by a non-native residual structure in the unfolded state.[226]

C_{eff} strongly depends on the loop length of the polypeptide chain in the absence of residual structures. In Figure 4-4 the effective concentrations C_{eff} of different peptides and proteins under denaturing conditions are plotted as a function of the loop length (N) for the individual disulfides. They show the expected inverse relationship. C_{eff}-values for peptides and C_{eff}^{U}–values for proteins were only used where no residual

structure was found and no proline residue is located in the loop. The data were fit to a function of the form:

$$C_{eff}^{U} = aN^{b} \tag{4.7}$$

as predicted for a random-walk polymer,[227] where *a* and *b* are empirical constants and N is the number of residues in the loop. The obtained value for the exponent b = -1.47 ±0.02 is in good agreement with the value $-3/2$ predicted by simple random-walk models of disordered chains.[227] However, this is lower than the value of –1.8 expected from the excluded volume effect. For the constant *a* a value of (621 ±49) mM was obtained, similar to what was observed previously by Kim & co-workers.[223]

As shown in Figure 4-4, the C_{eff}-value of T(10-28)-A28G is in the range expected for a disordered chain revealing that no structure is formed. In contrast, the C_{eff}^{U}–value found for SSGB1 is significantly higher than expected for a random-walk polymer (Figure 4-4). This could be explained by residual structure under denaturing conditions. This is consistent with the results observed by Blanco & Serrano.[192] They found some folded structure even in the presence of 6 M urea for the β-hairpin.

From the urea dependence of the C_{eff} the unfolding equilibrium constant for the reduced form K_3 was also obtained from the fit with a value of $K_3 = (4.4 \pm 5.2)\cdot 10^{-2}$ (Figure 4-3) as well as the equilibrium *m*-value with m = -(8.3 ±2.7) kJ/(molM). Using equation (4.2) the unfolding equilibrium constant for the oxidized form, $K_4 = (1.5 \pm 2.0)\cdot 10^{-2}$, was calculated. Thus, we received the free energies of unfolding for the reduced and oxidized form with ΔG_u^{red} = (7.5 ±2.8) kJ/mol and ΔG_u^{ox} = (10.1 ±3.2) kJ/mol, respectively.

In Table 2 the Gibbs free energies of folding of different β-hairpins are compared. The measured free energies for the reduced and oxidized form for SSGB1 are significantly larger compared to previous measurements of the peptide Gb1p using NMR[202], DSC[202] and Temperature-jump[203] methods (Table 2). All three methods gave values for ΔG_f in the range from 0.09 to 0.9 kJ/mol (Table 2). However, the difference of C_{eff} in the absence of denaturant and at high urea concentrations (>2M) is small relative to the errors (Figure 4-3). Thus, the results must be considered with caution. In addition, the contribution of the cysteine groups to the β–hairpin stability is not known.

Table 2: Stability of β-hairpin peptides at 298 K including only natural amino acids.

Method	**β-hairpin**	**ΔG_f [kJ/mol]**
CD melting curves	trpzip 1-3 [228]	-2.5 – -5.6
	trpzip 4-6[a] [228]	-2.0 – -7.1
	trpzip 3 & 4[229]	-4.8; -6.3
	Chignolin[230]	-1.6
	β4[231]	0.6
NMR	β-hairpin mimic of *met* Repressor[232]	0.3
	β-hairpin 1&2[233]	0.7 – 2.8
	YTV[234]	0.01; 1.0
	β1-4[231]	2.4 – -1.2
	peptide 1-6 [235]	1.4 – -2.9
	Gb1p[b] [202]	0.9
FTIR melting curve	peptide 1[236]	-0.4
	trpzip 4[229]	-6.7
DSC	Gb1p[b] [202]	0.5
Temperature-jump	Gb1p[b] [203]	0.09
	peptide 1[c] [236]	-0.6
	BH8[b,c] [237]	-0.02
	MrH3a[b,c] [237]	-5.8
	tripzip 1-4[d] [229]	-2.6 – -6.8
C_{eff} measurements	SSGB1 oxidized[e]	-7.5
	reduced[e]	-10.1

[a] sequence derived from Gb1p
[b] with ΔC_p=0
[c] peptides are dissolved in 21% hexafluoro-2-propanol
[d] at 23°C
[e] at 15°C, this work

Gb1p is the first example of a natural β-hairpin sequence which shows folded structure in water.[198] The stability of the hairpin state of Gb1p is attributed to hydrophobic cluster formation between a valine side chain and the rings of three aromatic residues (Trp, Tyr, Phe). These four residues are arranged in pairs, located in opposing non-H-bonded strand positions. Cochran and co-workers have demonstrated significant hairpin stabilization for the Gb1p sequence when all four side chains in the cluster are indole rings (trpzip 4-6), with trpzip 4 displaying a melting point of 70°C and Gibbs free energy of folding of –7.1 kJ/mol (Table 2).[228]

In contrast to SSGB1, T(10-28)-A28G shows no structural formation in water under the conditions used in our measurements. The stability of the folded state of β–hairpins has been attributed to interstrand hydrogen bonding and hydrophobic interactions.[195] However, the origin of specificity of β-hairpin folding is largely dictated by the

conformational preferences of the turn sequence.[238] The sequence at the turn for the N-terminal β-hairpin of tendamistat is very well conserved in microbial α-amylase inhibitors and when modified the biological function is lost.[161,170,172] The apparent lack of evidence for folding of the peptide derived from residues 15-23 of tendamistat led do a partial redesign of the sequence to enhance folding through modification to the β-turn sequence by replacing the SWRY by an NPDG type I turn.[197] The replacements stabilised the β-hairpin but the peptide folded into non-native conformations with a three-residue G-bulged type I turn (PDG).[197] Thus, the lack of hairpin formation could be explained by the non-ideal β-turn sequence, which is however important for the biological function of tendamistat.

In summary, we have shown that the formation of the N-terminal β-hairpin in tendamistat is not favoured implying that the disulfide bond at the base of the β-hairpin plays an important role for formation of the hairpin during protein folding. This is agrees with the observation that cyclisation through a disulfide bridge increases β–hairpin conformational stability.[239] Measurements of a tendamistat variant lacking the disulfide bond C11-C27 revealed a dramatically decrease of stability,[15] which also confirms our result.

Materials and Methods

Peptide synthesis and purification

Both peptides were synthesized chemically with an ABIMED economy peptide synthesizer EPS 221 (Abimed, Germany) using standard fluorenylmethoxycarbonyl (F-moc) chemistry on preloaded NovaSyn TGK resin (Novabiochem, Switzerland).[49] The peptides were purified using HPLC with a C-8 reverse-phase preparative column. Amino acids were from Alexis Biochemicals, USA or from Iris Biotech, Marktredwitz, Germany. Solvents and other chemicals were from Fluka (Buchs, Switzerland). Peptide purity was checked by mass spectroscopy and analytical HPLC. The mass was confirmed by electrospray ionization mass spectroscopy. Peptide concentrations were determined using the method of Gill & von Hippel[240] with an extinction coefficient at 280 nm of 7980 $M^{-1}cm^{-1}$ (reduced form) and 8105 $M^{-1}cm^{-1}$ (oxidized form) for T(10-28)-A28G, respectively, and 6970 $M^{-1}cm^{-1}$ (reduced form) and 7090 $M^{-1}cm^{-1}$ (oxidized form) for SSGb1, respectively.

Spectroscopic Techniques

CD spectra were recorded in an Aviv 62A DS spectropolarimeter. Peptide concentrations were 18 μM in 50 mM KP_i at pH 8.0. The solution was incubated over night to oxidize the disulfide bond by air. The amount of oxidized peptides was analyzed using analytical HPLC. To measure the reduced peptide, 35 μM DTT was added to the solution and the reaction mixture was also incubated over night. The ellipticity was measured in a thermostatted 1 cm cell.

Thiol-disulfide equilibrium measurements

Lin and Kim have first described a HPLC assay to determine C_{eff} in peptides or proteins.[206,208] The reaction is performed under argon to prevent air oxidation and all solutions are degassed before use. Peptides were incubated with a mixture of GSH and GSSG in 0.1 M Tris, 1 mM EDTA and 0.2 M KCl, at pH 8.7. For measurements of C_{eff} in urea solutions, the same conditions were used. To fix the redox potential of the solution, the concentrations of GSH and GSSG in the reaction mixture were at least 100-fold higher than those of the peptide. The GSSG concentrations were 0.5 and 1 mM, respectively, and the GSH concentrations ranged from 3 to 35 mM. To prevent dimer formation a low concentration of peptide was used (30 μM T(10-28)-A28G and 10 μM SSGb1, respectively). The reaction mixture was incubated for at least 3 h at 15°C to allow equilibration. The reaction mixture was then quenched with HCl to pH 2 and loaded onto a C8 reverse-phase column. GSH, GSSG, reduced and oxidized peptides were then separated with a shallow gradient of acetonitrile in the presence of 0.1 % trifluoric acid. The reduced and oxidized forms of the peptides were detected by simultaneous absorbance s at 230 nm and 280 nm for T(10-28)-A28G and by fluorescence with an excitation wavelength of 280 nm and an emission wavelength of 345 nm for SSGb1. The peaks were quantitated by integration to receive the ratio of oxidized and reduced peptides. C_{eff} was calculated as described above.

4.1.2 Structural Property, Stability and Assembly of the Tendamistat Fragments T(1-34) and T(35-74)

Lysylendopeptidase C cleaves tendamistat selectively after Lys34. The products of the cleavage are the two fragments of similar size: T(1-34) and T(35-74). Figure 4-5 shows the cleavage site and two resulting fragments highlighted in different colours. The fragment T(1-34) consists of the N-terminal β-hairpin, which is held together by the disulfide bond C11-C27 (Figure 4-5). It contains a tryptophan residue and two tyrosine residues. All three aromatic residues are located in the hairpin. In contrast, the fragment T(35-74) contains four tyrosine residues and no tryptophan. It consists of one triple stranded β-sheet, one strand of the second triple stranded β–sheet and the disulfide bond C45-C73 (Figure 4-5).

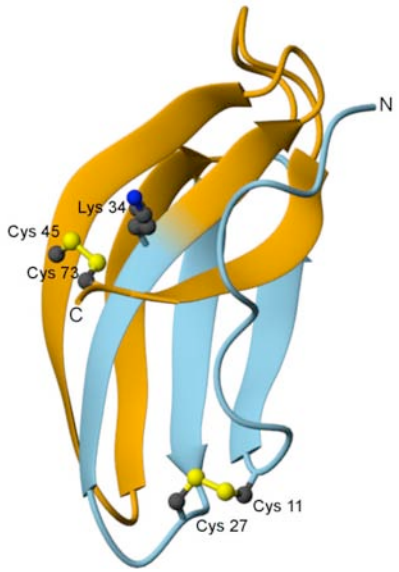

Figure 4-5: *Schematic drawing of the structure of tendamistat. The two fragments are coloured in blue (T(1-34)) and orange (T(35-74)). The disulfide bonds between Cys11-Cys27 and Cys45-Cys73 and the residue Lys34 at the cleavage site are shown as ball-and-stick models. The figure was generated using MOLMOL*[194].

Recent studies of both fragments gave evidence for structure formation of the N–terminal β-hairpin, suggesting that this region of the protein can serve as an initiation site for the folding process of tendamistat.[241] We used fluorescence and CD measurements under different conditions to study the structure of both separated fragments. To test whether the fragments can assemble to fold into a native-like structure, equilibrium studies were performed.

Results and Discussion

N-terminal fragment T(1-34)

Fluorescence measurements of T(1-34) at pH 5.5 showed an emission maximum at 347 nm which is typical for tryptophan fluorescence (Figure 4-6A). With the addition of 6 M GdmCl, the signal intensity increases. This is in contrast to tendamistat where the intensity of the signal decreases upon denaturation by GdmCl. The decrease of the pH to 2 also induces an increase of the signal intensity. The maximum of the signal shifts to 343 nm at pH 2. The increase of the signal intensity suggests a change in the solvent environment of the fluorophores.

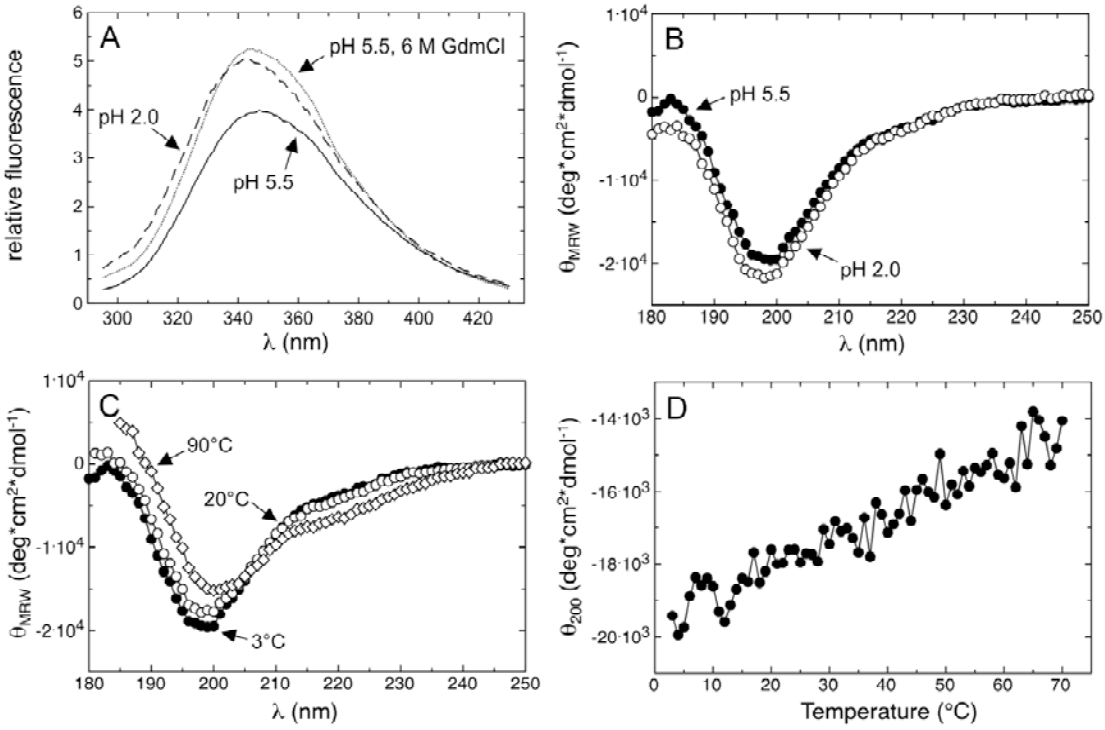

Figure 4-6: Spectroscopic properties of the tendamistat fragment T(1-34). (A) Fluorescence spectra at pH 2.0 and pH 5.5, respectively and at pH 5.5 and 6 M GdmCl. Fragment concentration was 5 µM in 10 mM KP_i at 3°C. (B) Far-UV CD spectra at pH 5.5 and pH 2.0, respectively at 3°C and (C) far-UV CD spectra at pH 5.5 and at 3°C, 20°C and 90°C. (D) Temperature dependence of the far-UV CD signal at 200 nm. (B)-(D) Fragment concentration was 20 µM in 10 mM KP_i.

Comparison of the far-UV CD spectra at pH 5.5 and pH 2.0 reveals only a small increase of the signal intensity with decreasing pH (Figure 4-6B). However, no change in the shape of the spectrum could be observed, suggesting that variation of pH does not induce structure. Both spectra show a small shoulder between 210 nm and 220 nm and a negative band around 198 nm. The shape of the far-UV CD spectra is similar to that of the oxidized peptide derived from the N–terminal β-hairpin of tendamistat (Figure 4-2), suggesting that the signal is mainly originating from the β-hairpin.

The negative band in the far-UV CD at pH 5.5 increases with increasing temperature and shows a slight red shift (Figure 4-6C). At higher temperature the signal intensity of the shoulder between 210 nm and 220 nm increases. The spectrum of the fragment at 90°C has the same shape as that of tendamistat (Figure 4-8A). The fragment exhibits reversible linear temperature dependence of the CD signal (Figure 4-6D).

Comparison of T(1-34) with the far-UV CD spectra of the N-terminal β-hairpin provides evidence for the formation of the hairpin. However, in contrast to α-helices, the contribution of β-sheets to the far-UV CD spectra is weak and diverse. Taking into account that the aromatic side chains also strongly contribute to the far-UV CD spectrum, the far-UV CD data give little information on the possible folded structure of the fragments. Even the CD spectrum of native tendamistat lacks the typical bands of β-sheet structures (Figure 4-8A), a positive band between 190 nm and 200 nm and a negative band around 220 nm.

C-terminal fragment T(35-74)

The fluorescence spectrum of T(35-74) shows a maximum around 300 nm which is typical for a random coil peptide containing only tyrosines (Figure 4-7A). The signal intensity at this maximum increases upon addition of denaturant and at lower pH suggesting a change in the solvent environment of the tyrosine residues. The fluorescence spectra show a shoulder around 340 nm under all conditions but with different intensities.

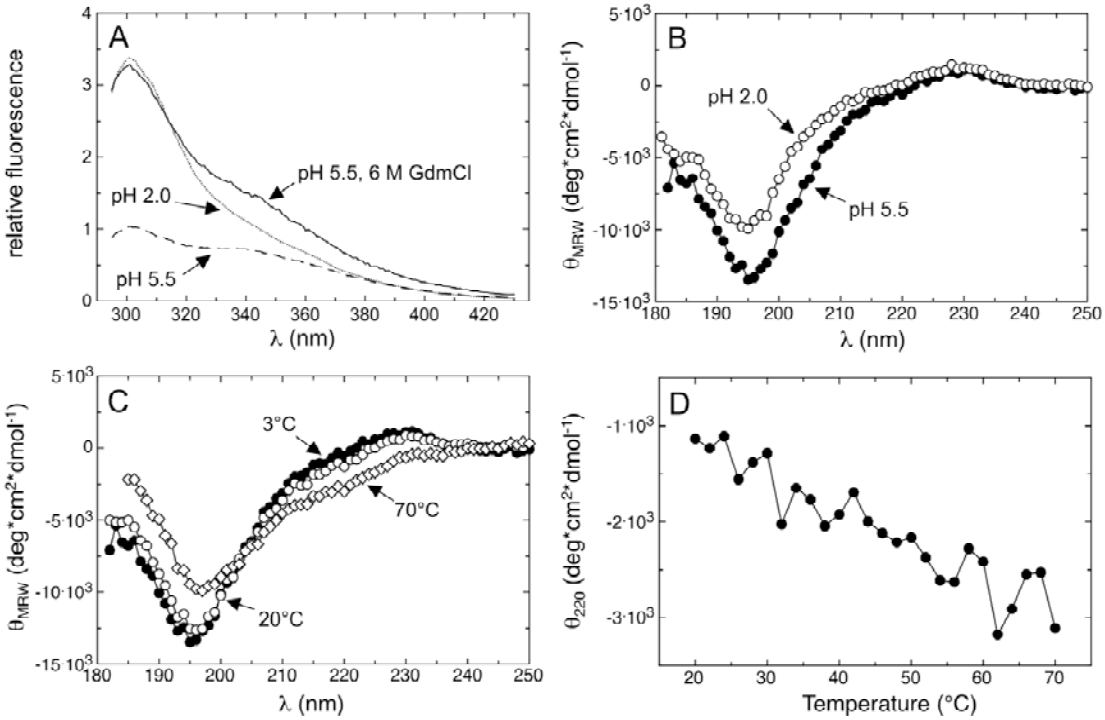

Figure 4-7: Spectroscopic properties of the tendamistat fragment T(34-74). (A) Fluorescence spectra at pH 2.0 and pH 5.5, respectively and at pH 5.5 and 6 M GdmCl. Fragment concentration was 5 µM in 10 mM KP_i, at 3°C. (B) Far-UV CD spectra at pH 5.5 and pH 2.0, respectively at 3°C and (C) far-UV CD spectra at pH 5.5 and at 3°C, 20°C and 70°C. (D) Temperature dependence of the far-UV CD signal at 220 nm at pH 5.5. (B)-(D) Fragment concentration was 20 µM in 10 mM KP_i.

The signal intensity of the T(35–74) far-UV CD spectra between 180 nm and 220 nm decreases upon decreasing of the pH from 5.5 to 2.0. In contrast, the spectra at both pH are nearly identical between 220 and 250 nm, with a positive band at 231 nm (Figure 4-7B). The far-UV CD spectrum of native tendamistat also shows a positive band at 227 nm, suggesting a native-like β-sheet formation of T(35-74). Both spectra have their minimum at 195 nm. Between 205 and 210 nm a small shoulder is visible which significantly increases at higher temperature (Figure 4-7C). With rising temperature the positive band at 231 nm disappears and a shift in the minimum from 195 nm to 198 nm occurs. The far-UV CD spectra of the temperature-denatured fragment has a shape similar to the temperature-denatured tendamistat and the fragment T(1-34) (Figure 4-6C and Figure 4-8A). The far-UV CD spectra of all three denatured polypeptides show a shoulder between 210 and 220 nm, which could be explained with the increasing amount of polyproline II helical structure in the unfolded state. This is in accordance with other proteins, where an increase of signal intensity at around 220 nm

in the far-UV CD spectra could be observed with increasing denaturant concentrations.[69]

Similar to the fragment T(1-34), the far-UV CD signal of the fragment T(35–74) at 220 nm shows a linear temperature dependence (Figure 4-7D).

Interaction of T(1-34) and T(35-74)

To find out if the two fragments associate, a solution of equal amount of both peptides was incubated at pH 5.5, where native tendamistat has the highest stability. Different far-UV CD spectra of this solution were recorded after incubation time from 2 h to 2 days. The spectra are identical at all incubation times. Comparison of the spectra with the far-UV CD spectrum of native and unfolded tendamistat revealed, that no native-like structure was formed (Figure 4-8A).

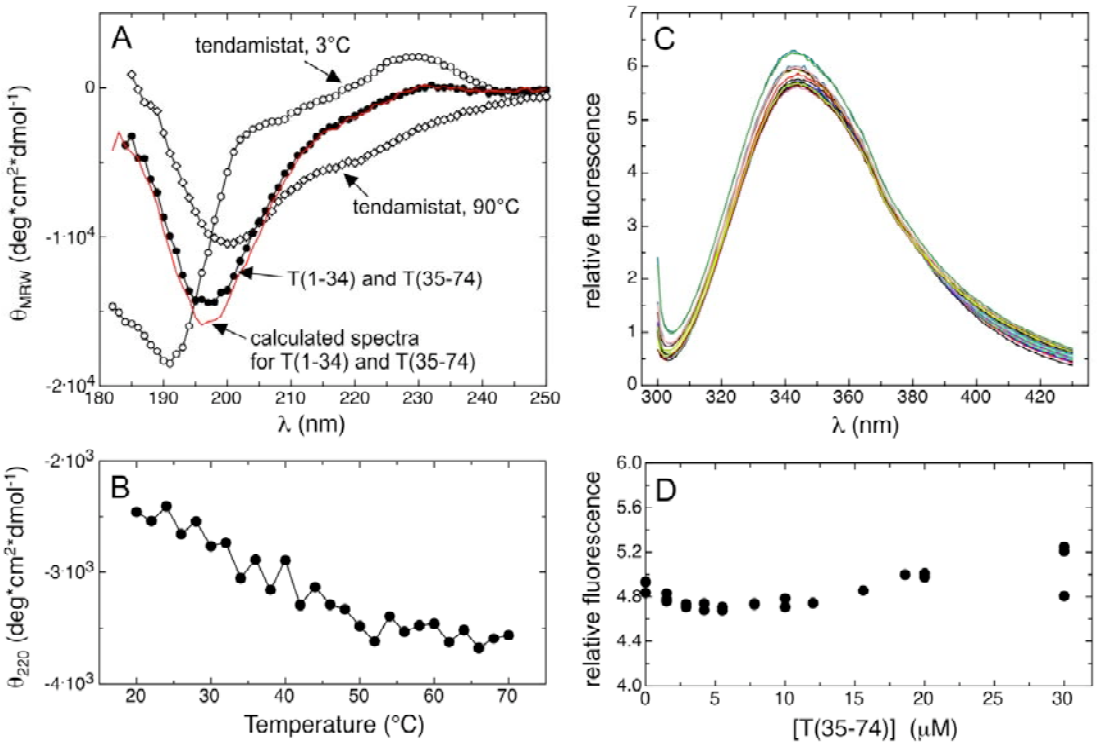

Figure 4-8: Association studies. (A) CD spectra in the far-UV region of both fragments T(1-34) and T(35-74) at 3°C, and tendamistat. Fragment concentrations were 20 µM in 10 mM KP_i, pH 5.5. The red line is the calculated spectra assuming that no interaction takes place. (B) Temperature dependence of the far-UV CD signal at 220 nm at pH 5.5 for the solution containing both fragments. Conditions as in (A). (C) Change in the fluorescence spectrum of T(1-34) (5 µM) upon addition of 1.5-30 µM T(35–74). Excitation wavelength was at 295 nm, and the buffer was 10 mM KP_i, pH 5.5. (D) Change in fluorescence at 345 nm upon addition of T(35-74). Conditions as in (C).

The CD spectrum of two different peptides in solution without intermolecular interactions should be additive. Thus, with the assumption that both fragments do not associate, we could calculate the spectrum using the following equation:

$$\Theta_{MRW}^{calc} = \frac{1}{\sum_i n_i^{aa}} \cdot \sum_i \left(n_i^{aa} \cdot \Theta_{MRW}^{i} \right) \tag{4.8}$$

Where n_i^{aa} is the number of amino acids of protein *i* and Θ_{MRW}^{i} the corresponding CD signal. The calculated spectrum of both fragments is virtually identical with the measured far-UV CD spectrum. The far-UV CD spectrum (Figure 4-8A) and the linear temperature dependence (Figure 4-8B) of the reaction solution confirm that the fragments do not associate.

We further analyzed the change of the fluorescence spectrum of T(1-34) upon addition of different concentrations of T(35-74). T(1-34) contains one tryptophan residue, whereas T(35-74) has none. We chose an excitation wavelength of 295 nm to excite only the tryptophan residue. This allowed us to analyse the structural changes of T(1-34) upon addition of T(35-74). Figure 4-8C and Figure 4-8D show the different fluorescence spectra of 5 µM T(1-34) and varying concentration of T(35-74). The spectra were recorded after different incubation times. No change in fluorescence spectra with varying concentrations and at different incubation time could be observed indicating that no association takes place.

Why do the two fragments not associate? One explanation could be that the cleavage site is in the centre of the second β-sheet. Thus, the cleavage seems to interrupt structural properties, which are important to form native like structures. Analysis of both fragments revealed only little evidence for structure formation. Some non-native residual structure of the fragments may also inhibit the association of both fragments.

Materials and Methods

Cleavage and purification

Wildtype tendamistat and lysylendopeptidase C (LEP) were mixed in a mass ratio of 25:1 in 8 M urea buffered with 50 mM Tris pH 8.5. The mixture was left to react for 14 h at 16°C. In a first step, more LEP was added to tendamistat to a final mass ratio of 1:100 and the reaction temperature was raised to 25°C for a further 6h. In a second step, more LEP was added to the mixture (again in a mass ratio of enzyme to substrate 1:100) buth the urea concentration was simultaneously lowered from 8 M to 5 M by addition of 50 mM Tris pH 8.5. The mixture was incubated for no more than 45 minutes at 37°C. Finally, the enzymatic cleavage was stopped by adjusting the activity of the solution to pH 2.0 with trifluoric acid.

The fragments were purified using HPLC with a C-8 reverse-phase preparative column. The purity and the mass were checked by mass spectrometry and analytical HPLC. Protein concentrations were determined using the method of Gill & von Hippel[240] with an extinction coefficient at 280 nm of 8105 $M^{-1}cm^{-1}$ for T(1-34) and 5185 $M^{-1}cm^{-1}$ for T(35-74).

Spectroscopic Techniques

Corrected fluorescence spectra were recorded on an Aminco-Bowman fluorimeter with a thermostated cell holder and magnetic stirrer. Excitation wavelengths were 276 nm and 295 nm, respectively. Protein concentration was 5 μM in 10 mM KP_i at pH 5.5 and pH 2.0, respectively. For spectra with both fragments, the protein concentration of T(1-34) was 5 μM in 10 mM KP_i at pH 5.5 whereas different concentrations of T(35-74) from 1.5-30 μM were used.

CD spectra were recorded in an Aviv 62A DS spectropolarimeter. Fragment concentrations were 20 μM in 10 mM KP_i at pH 5.5 and pH 2.0. The ellipticity was measured in a thermostatted 1 mm cell at the indicated temperature.

Thermally Induced Denaturation

Far-UV CD at 200 and 220 nm, respectively, was used to monitor the thermal unfolding using an Aviv 62A DS spectropolarimeter with a temperature control system and cuvettes with 1 mm pathlength. The thermal unfolding curves were recorded using a heating rate of 0.5°C/min. The fragment concentrations were 20 μM in 10 mM KP_i at pH 5.5.

4.1.3 Structural Property and Stability of the Tendamistat Fragment T(11-74): Contributions of the first ten N-terminal Amino Acids to Protein Stability

Tendamistat contains two β-sheets and a N-terminal region consisting of 10 amino acids. Although no regular secondary structure could be observed, the residues between Ser5 and Ser10 are highly ordered.[166,168] This region is part of the hydrophobic core and makes strong backbone and side-chain interactions to both β-sheets. Pro7 and Pro9 are found to be responsible for the formation of a highly structured intermediate.[174] To elucidate if the protein is still stable without this N-terminal region and if the structure formed similar to the native-like intermediate we designed the tendamistat variant S10M to specific cleave of the 10 N-terminal amino acids with cyanogen bromide. Only one proline, Pro50, still remains in the protein. In Figure 4-9 the missing N–terminal region between Asp1 and Ser10 is highlighted in red.

Analysis of this fragment T(11-74) should give valuable information of the contribution of the N–terminal region between Asp1 and Ser10 to the stability and structural formation of tendamistat. To elucidate the capability of the fragment T(11-74) to form a structure and to analyze the possible fold we used fluorescence and CD measurements. To investigate the stability of this fragment, thermal and denaturant-induced transitions were performed.

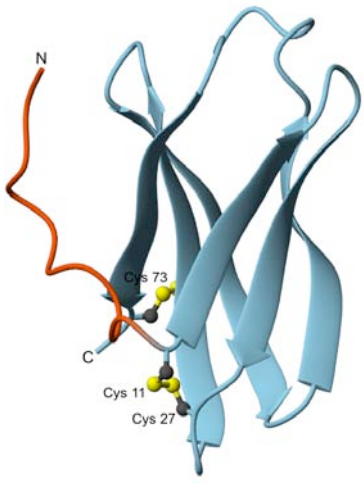

Figure 4-9: Schematic drawing of the structure of tendamistat. The first N–terminal residues are highlighted in red. The disulfide bonds between Cys11-Cys27 and Cys45-Cys73 are shown as ball-and-stick models. The figure was generated using MOLMOL[194].

Results and Discussion

Cyanogen bromide selectively cleaves polypeptide chains after methionine residues. Because of the lack of methionine in the sequence of tendamistat wild type, we produced the S10M variant. The cyanogen bromide cleavage reaction of the variant S10M produces two fragments: one fragment with the 10 N-terminal amino acids of tendamistat with a homoserine as the C-terminal amino acid and a second fragment, T(11-74), containing the residues 11 until 74 (Figure 4-9). We used spectroscopic techniques to elucidate how the removal of the ten N–terminal amino acids affects the protein and if it still folds into a native-like structure.

Fluorescence spectra were measured at pH 7 and pH 2 at 25°C (Figure 4-10). The spectra of the fragment at both pH values show a maximum at 339 nm and have the same shape as native tendamistat but with less signal intensity. Addition of 6 M GdmCl results in a strong decrease in tryptophan fluorescence. The tyrosine band at 301 nm becomes visible as a consequence of the increase in distances and a less efficient energy transfer between tyrosine and tryptophan. Comparison of the spectra of the unfolded proteins, tendamistat and T(11-74), reveals nearly identical shapes and similar intensity of the signal. These are strong indications for native-like structure formation of the tendamistat fragment T(11-74).

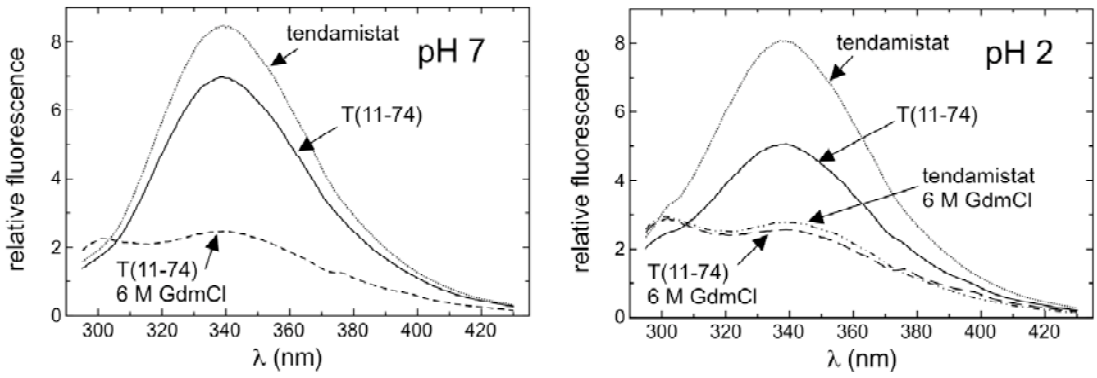

Figure 4-10: Fluorescence spectra at pH 7 and pH 2 of tendamistat and the tendamistat fragment T(11-74). Conditions were 5 μM protein in 10 mM KP_i at 25°C.

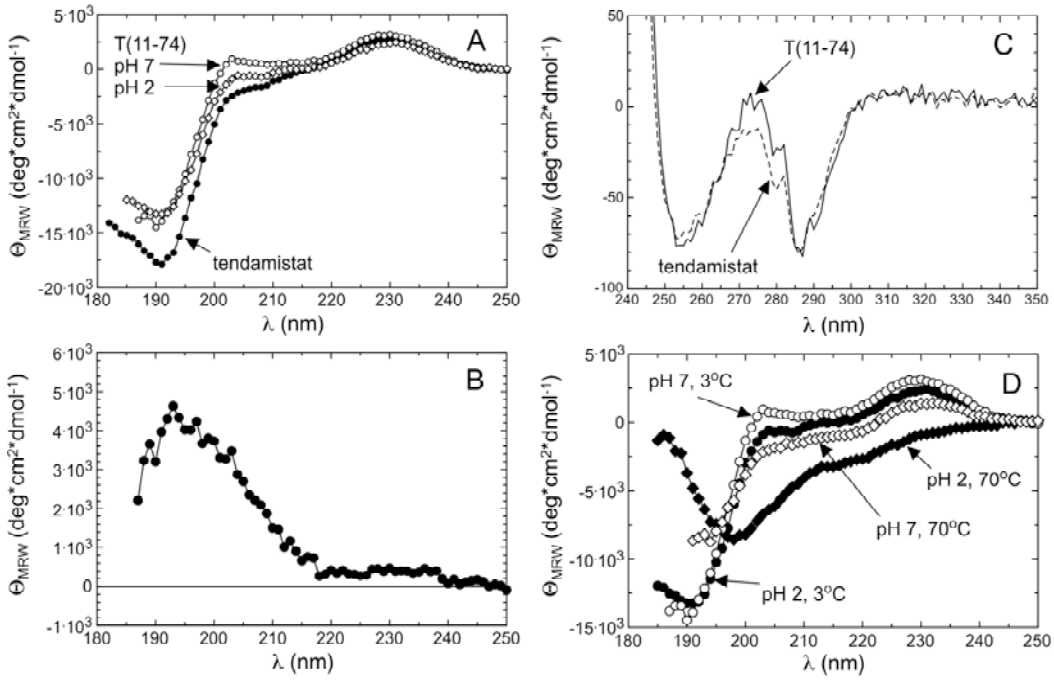

Figure 4-11: CD spectra of tendamistat and the fragment T(11-74). (A) Far-UV CD spectra at 3°C. Fragment concentration was 20 µM in 10 mM KP_i. (B) Difference spectra of the far-UV CD spectra of tendamistat and T(11-74) at pH 7 and 3°C shown in (A). (C) Near-UV CD spectra at pH 7 and pH 2, respectively. Conditions were 40 µM in 10 mM KP_i at 3°C. (D) Far-UV CD spectra of T(11-74). Fragment concentration was 20 µM in 10 mM KP_i.

The far-UV CD spectrum of T(11-74) shows a minimum at 191 nm and two maxima at 230 nm and 203 nm, respectively (Figure 4-11A). The signal intensity at both maxima decreases when decreasing the pH from 7 to 2, whereas the signal intensity at the minimum is pH-independent. Compared to T(11-74), the far-UV CD spectrum of tendamistat shows only a small shoulder around 205 nm and more signal intensity at the minimum at 190 nm. Analysis of the difference of the far-UV CD spectra of the two proteins (Figure 4-11B) reveals a maximum around 193 nm, where the spectra of both proteins have their minimum. Comparison of both spectra displays strong evidence for a native-like structure formation of T(11-74).

The near-UV CD spectra of T(11-74) and tendamistat show the same shape but have small differences in the magnitudes (Figure 4-11C). Both spectra have two minima at 254 and 286 nm, respectively, a maximum between 270 nm and 275 nm and a shoulder around 281 nm. Bands in the near-UV CD spectrum originate from the aromatic amino acids and from small contributions of disulfide bonds. It is almost zero when the aromatic residues are mobile, such as in unfolded proteins, due to their intrinsically symmetric chromophores. In the presence of ordered structures, the environment of the aromatic side chains becomes asymmetric, and therefore they show CD bands in the

near UV. Thus, the near-UV CD spectrum represents a highly sensitive criterion for the native state of a protein. The signs and the magnitudes of the aromatic CD bands depend on the immediate structural and electronic environment of the immobilized chromophores. Therefore, comparison of the near-UV spectra of tendamistat and T(11-74) reveals that the aromatic residues have a similar structural environment and thus, we can conclude that T(11-74) folds into a native-like structure.

Comparison of the far-UV CD spectrum of T(11-74) at different temperatures (Figure 4-11D) reveals that at pH 7 the protein still shows some folded structure at 70°C. In contrast, the spectrum at pH 2 and 70°C has the same appearance as unfolded tendamistat at high temperatures (Figure 4-8A). Both spectra have a minimum between 195 and 200 nm and a weak positive CD signal around 210 nm, which is characteristic for unordered proteins and peptides.

Thermal unfolding and refolding experiments were monitored by the change in ellipticity at 230 nm and are shown in Figure 4-12. The temperature transition at pH 2 is fully reversible and shows a linear dependence. In contrast, cooperative temperature dependence could be observed for the thermal unfolding curve at pH 7 with a transition midpoint at 68°C. In comparison, the calorimetrically determined transition temperature for tendamistat wild type at pH 7 is 81.6°C.[163] However, the thermal unfolding transition of T(11-74) is not fully reversible. The far-UV CD spectrum after cooling shows the same spectrum as before heating but with ~25 % less signal magnitude. Also, the thermal refolding curves show only a small cooperative and otherwise linear temperature dependence.

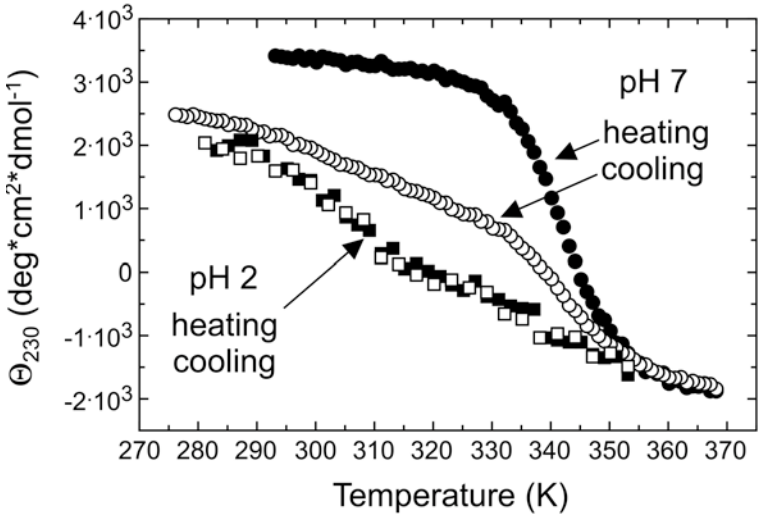

Figure 4-12: Temperature dependence of the far-UV CD signal of the tendamistat fragment T(11-74) at 230 nm at pH 7 and pH 2, respectively. Fragment concentrations were 20 µM in 10 mM KP_i

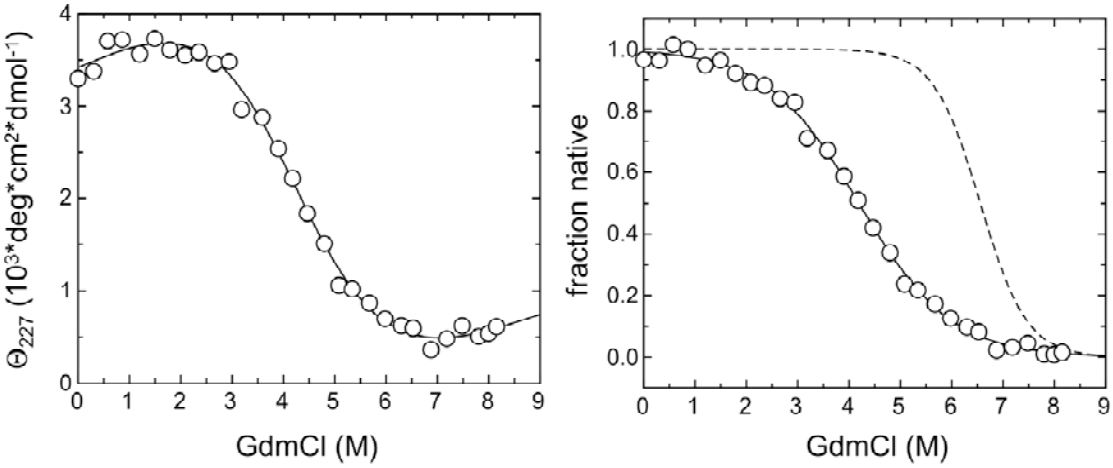

Figure 4-13: GdmCl-induced unfolding transition of the tendamistat fragment T(11-74) at pH 7 and 25°C monitored by ellipticity at 227 nm. Concentration was 10 µM in 100 mM cacodylic acid. The solid line represents the analysis assuming the two-state model. The results are given in Table 3. The fit of the wild type (dotted line) was taken from Schönbrunner et al. [173].

To compare the stability of the fragment with tendamistat we further analyzed the chemical denaturation of T(11-74). The GdmCl-induced unfolding transition of T(11-74) shows a broad transition between 2 M and 7 M GdmCl (Figure 4-13). In contrast, tendamistat has its cooperative unfolding transition between 5 M and 8 M GdmCl.
The GdmCl-induced unfolding transition was fitted and the result is given in Table 3. Comparison with tendamistat revealed a dramatical decrease of the Gibbs free energy, ΔG^0, and the *m*-value after the removal of the ten N-terminal amino acids. The ΔG^0-value of T(11-74) is only $^1/_3$ of the ΔG^0-value for tendamistat, whereas the *m*-value of T(11-74) is only half of that of tendamistat.

Table 3: Comparison of the Gibbs free energy and the m-value of tendamistat and the tendamistat fragment T(11-74) at pH 7 and 25°C. The data are results from GdmCl-induced unfolding transition states.

	ΔG^0 [kJ/mol]	**m [kJ/(mol·M)]**
Tendamistat[173]	-(34.0 ±0.7)	5.32 ±0.06
T(11-74)	-(11.5 ±1.8)	2.75 ±0.44

It was shown that the *m*-values are proportional to the change in solvent accessible surface area (ASA) upon unfolding of the protein.[23] Thus, as a rule, the larger the protein the bigger the ASA and therefore the larger the *m*-value. However, the *m*-value is smaller than expected from ΔASA upon unfolding of tendamistat.[173] This might be due to the presence of two disulfide bonds, which probably restrict the GdmCl

accessibility of the unfolded state,[173] and could be also originating from residual structure in the unfolded state.

The removal of the ten N-terminal amino acids leads to a decrease in ΔASA of about 2200 Å, which is significantly larger than expected from the calculated differences in ΔASA between tendamistat and T(11-74) (≈ 530 Å).[23] Although the N-terminal region between Asp1 and Ser10 shows no regular secondary structure, the residues between Ser5 and Ser10 are highly ordered and form strong hydrophobic interactions and hydrogen bonds with the rest of the protein. The side-chain of Ala8, which is located between the two prolyl residues, is part of the hydrophobic core and makes contact with side-chains from both β-sheets. Glu6, Ala8 and Pro9 participate in backbone hydrogen bonds with Arg72, Leu70 and Val12, respectively. Removal of these amino acids leads to a significant destabilization and more compact state of the core.

To obtain information of the influence of the N-terminal region on folding and on formation of intermediates, studies on folding kinetics at various denaturant conditions would be of great use. Another interesting question to answer is whether the re-association of a peptide consisting of the 10 N-terminal amino acids leads to a native-like structure and what would than be the association constant and rate. Variation of the amino acid sequence of the N-terminal peptide could also help to find out about the influence of the N-terminal amino acids on tendamistat folding and stability.

Materials and Methods

Cleavage and purification

The tendamistat variant S10M was expressed in *Streptomyces lividans* and purified as described by Haas-Lauterbach *et al.*[242] The molecular mass is 8005 Da and was confirmed by electrospray ionization mass spectrometry. Protein concentration was determined by UV absorption measurements using an absorption coefficient $A_{276}^{0.1\%} = 1.61$ like for wild-type.[162]

S10M was dissolved in 0.1 M HCl. The sample was mixed with BrCN in 0.1 M HCl to a final ratio of BrCN/methionine ≈ 200. The solution was incubated for 4 h at 30°C in the dark. The sample was lyophilized and redissolved for separation in 20 % acetonitrile and 0.1 % TFA. The solution was analyzed using analytical HPLC.

The fragment was purified using HPLC on a C-8 reverse-phase preparative column. The purity and the mass were checked by mass spectrometry and analytical HPLC. The mass of T(11-74) is 6976 Da. Protein concentration was determined by UV absorption measurements using the same absorption coefficient $A_{276}^{0.1\%} = 1.61$ like for wild-type.[162]

Spectroscopic Techniques

Fluorescence spectra were recorded on an Aminco-Bowman fluorimeter with a thermostated cell holder and magnetic stirrer. The excitation wavelength was 276 nm. Protein concentration was 5 μM in 10 mM KP_i at pH 7 and pH 2, respectively.

CD spectra were recorded in an Aviv 62A DS spectropolarimeter. Fragment concentrations were 20 μM in 10 mM KP_i at pH 7 and pH 2, respectively. The ellipticity was measured in a thermostatted 1 mm cell.

Thermally induced denaturation

Far-UV CD at 230 nm was used to monitor the thermal unfolding and refolding using an Aviv 62A DS spectropolarimeter with a temperature control system and cuvettes with 1 mm pathlengths. The thermal unfolding curves were recorded using a heating rate of 0.5°C/min. The protein concentration was 20 μM in 10 mM KP_i at pH 7 and pH 2, respectively.

Equilibrium unfolding transitions

The GdmCl-induced equilibrium transitions were monitored by the change in ellipticity at 227 nm in an Aviv 62A DS spectropolarimeter. Protein concentrations were 10 μM in 100 mM cacodylic acid, pH 7. Samples were incubated for at least two hours before measurements. The ellipticity was measured in a thermostatted 1 cm cell.

The data were fit based on the two-state model and a linear dependence of the free energy of folding on the GdmCl concentration following the procedure described by Santoro & Bolen[131]. This yields the free energy in the absence of denaturant ($\Delta G_{H_2O}^0$) and the associated *m*-value.

4.2 Studies on Tendamistat Variants

One of the major goals in protein folding is to understand the structural properties of the energy barriers. Studies of the effect of amino acid replacements on folding kinetics and stability give valuable information on the structural formation of the protein during the folding pathways. The aim of these studies is to identify interactions, which are formed in the rate-limiting step in folding. Mutational studies of different proteins revealed that some proteins show a "diffuse" or "delocalized" transition state whereas others have a "polarized" transition state structure.[59] Diffuse transition states have low ϕ_f-values (chapter 1.3.4) throughout the structured regions of the protein, indicating partial formation of the native set of interactions. In contrast, polarized transition states ϕ_f-values are significantly higher in a large substructure but are close to zero in other parts of a protein.

Analysis of the effect of mutations on the transition state structure revealed that transition state movements according to Hammond are rare in protein folding indicating structurally well-defined transition states.[59,123] Many proteins have significantly structured unfolded states, which are sensitive to mutation.[59] Thus, studies on the effect of amino acid replacements provide not only information on the structural formation of the transition state but also on residual structures in the unfolded states. In some cases, the replacement of amino acids revealed further information on the folding pathway due to the population of transient intermediates or changes in the rate-limiting steps during folding.[110,111,243]

In order to gain further information on the folding mechanism of tendamistat and the structural properties of the transition states, we have studied the consequences of the amino acid replacements on stability and folding kinetics. We chose 14 different sites mainly in the two β-hairpins of tendamistat: 4 are located in the N-terminal β–hairpin (**Leu14**, **Arg19**, **Ser21**, **Asn25**), whereas 8 sites are located in the C-terminal β-hairpin (**Val31**, **Thr32**, **Val36**, **Glu38**, **Asp39**, **Asp40**, **Glu42**, **Leu44**) (Figure 4-14 and Figure 4-15). In four positions the original amino acids were replaced by two different amino acids: **Leu14** was replaced by alanine and valine, **Ser21** by alanine and glycine, **Val36** by alanine and glycine, and **Asp39** by asparagine and alanine (Figure 4-14 and Figure 4-15). Two of the sites are not located in either of the hairpins: **Ser10** and **Ile61** (Figure 4-14 and Figure 4-15).

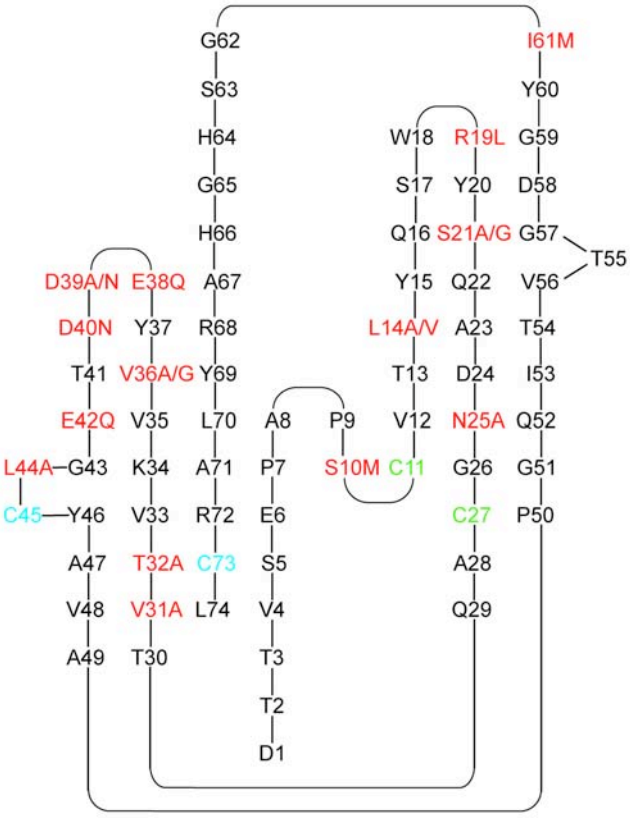

Figure 4-14: Schematic representation of the backbone structure of tendamistat. The four cysteine residues, which are connected via a disulfide bridge, are indicated in blue and green. The amino acid residues, which are replaced, are indicated in red.

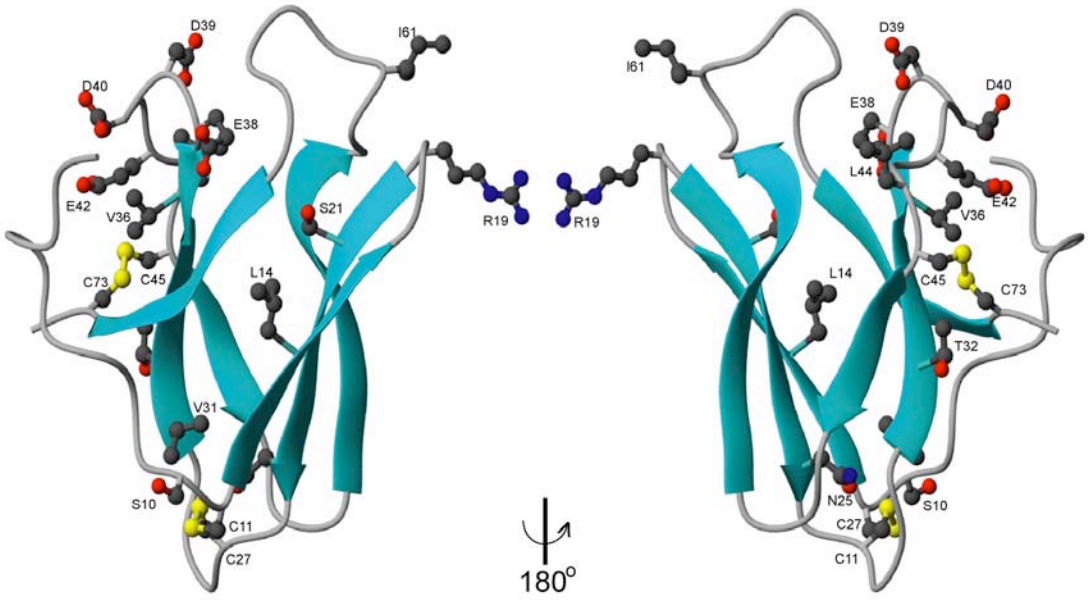

Figure 4-15: Schematic drawing of the structure of tendamistat. The disulfide bonds between Cys11-Cys27 and Cys45-Cys73 and the residues Ser10, Leu14, Arg19, Ser21, Asn25, Val31, Thr32, Val36, Glu38, Asp39, Asp40, Glu42, Leu44 and Ile 61 are shown as ball-and-stick models. The figure was generated using MOLMOL[194].

Tendamistat wild type folds and unfolds in an apparent two-state behavior and shows a perfectly linear Leffler plot indicating that the change in accessible surface area (ASA) between unfolded state and the transition state is insensitive to denaturant concentrations (chapter 3).[123,160,173] In previous studies it could be shown that folding of tendamistat involves two sequential transition states.[110] A change in the rate-limiting step can be induced by mutation or changes in solvent conditions upon addition of denaturant (chapter 3).[110] The effect of temperature on folding and stability as a function of denaturant concentration was measured for tendamistat wild type and some variants (chapter 3). Analysis of the temperature and denaturant dependence of the early transition state revealed transition state movements. In contrast, ground state effect and only small Hammond behavior could be observed in tendamistat variants for the late transition state rate limiting. This indicates that the early transition state is a broad and diffuse maximum, whereas the late transition state is rather narrow and well defined.

We first analyzed the spectroscopic properties of the tendamistat variant to elucidate if they form native structure (chapter 4.2.1). Furthermore, we analyzed the combined influence of mutation and denaturant on the stability and folding of tendamistat (chapter 4.2.2). To analyze the structural properties of the transition states, we determined ϕ_f-values of the tendamistat variants, which fold with an apparent two-state behavior (chapter 4.2.2.1). For the tendamistat variants with unknown folding mechanism, we measured the effect of pH and temperature on stability and folding and performed interrupted refolding and double-jumps measurements to elucidate the folding mechanism (chapter 4.2.2.2). We further wanted to determine the influence of surface-exposed charges on tendamistat stability and folding by measuring loaded variants (chapter 4.2.2.3). To measure the effect of sodium sulfate on tendamistat stability and folding, we chose variants with the late transition state rate limiting (chapter 4.2.3).

4.2.1 Spectroscopic Characterization of Tendamistat Variants

To study the formation of the native structure we performed far-UV CD measurements for all tendamistat variants except for the variant R19L. Only the structure of the variant R19L was investigated so far and was determined by NMR spectroscopy.[244] Comparison of R19L with the tendamistat structures in solution and as crystals revealed that the structure of R19L is nearly identical to tendamistat wild type.[244] However, structural and spectroscopic properties of tendamistat variants other than R19L are not determined in such detail. Figure 4-16 shows the far-UV CD spectra of tendamistat wild type and the different tendamistat variants at pH 7.0 and 25°C.

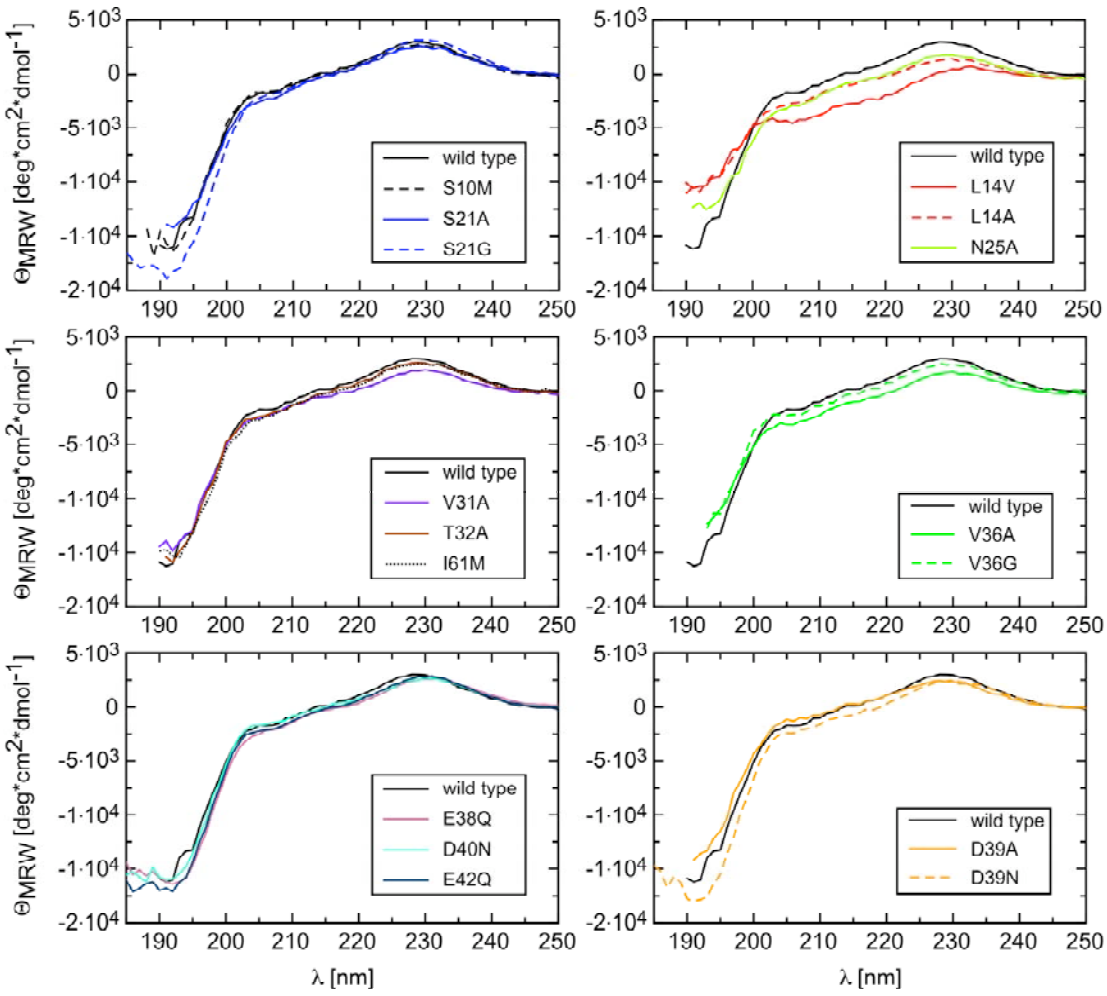

Figure 4-16: Far-UV CD spectra of tendamistat wild type and variants at 25°C and pH 7.0. Protein concentration was 20 µM in 10 mM KP_i.

The far-UV CD spectrum of tendamistat wild type at pH 7 and 25°C shows a positive band at 227 nm, a small shoulder around 205 nm and a minimum at 190 nm (Figure 4-16). It lacks the typical bands of β-sheet structures: a positive band between 190 nm and 200 nm and a negative band around 220 nm. Interestingly, the far-UV CD spectrum of tendamistat wild type shows more similarity to an unordered polypeptide chain, with a pronounced minimum between 195 and 200 nm. However, in contrast to α-helices, the contribution of β-sheets to the far-UV CD spectra is weak and diverse. The shape of the CD spectrum of a β protein depends, among other factors, on the length and orientation of the strands and on the twist of the sheet. Tendamistat has a high content of aromatic amino acids (9.5%). Taking into account that aromatic side chains strongly contribute to the far-UV CD spectrum, the far-UV CD data give little information on the possible folded structure of the variants. However, comparison of the far-UV CD spectra of tendamistat wild type and tendamistat variants gives information about the influence of the amino acid replacements on structure formation.

Comparison of the far-UV CD spectra of tendamistat wild type and its different variants reveals that the spectra of the tendamistat variants S10M, S21A, S21G, T32A, V36G and I61M show virtually identical shapes to the wild type (Figure 4-16). The far-UV CD spectra of the tendamistat variants V31A, V36A and D39A have the same shape as the wild type but with small differences in signal intensities (Figure 4-16).

Replacement of the carboxyl group of the acidic amino acids in the C-terminal β–hairpin by an amide group leads to a shift of the maximum from 227 to 230 nm (Figure 4-16). The four variants E38Q, D39N, D40N and E42Q are located in the turn of the C-terminal β-sheet (Figure 4-15). Changes of the overall charges in the protein may lead to small changes of the orientation of the strands or the twist of the sheet leading to a shift of the maximum in the far-UV CD spectra. Interestingly, the variant D39A does not show a shift of the maximum as the variant D39N do.

The two variants L14A and N25A, both located at the N-terminal β-hairpin, show less signal amplitude in the far-UV CD spectra than the wild type (Figure 4-16). Both, Leu14 and Asn25 are involved in the hydrophobic core and make strong interactions with the other β-sheet. Amino acid replacements at these positions could cause changes in the orientation of the strands and on the twist of the sheets and thus could lead to differences in the far-UV CD spectra.

The changes in the β-sheet structure induced by the amino acid replacement at Leu14 could also explain the far-UV spectrum of L14V. It shows a pronounced smaller signal magnitude than found for the wild type and the other variants (Figure 4-16). The positive band is shifted from 227 to 233 nm and the shoulder is around 200 nm. Due to the shift of the maximum and the significantly reduced stability, the equilibrium measurements were performed at 233 nm (appendix 9.3). A tyrosine is located at position 15, which also influences the far-UV CD spectrum.

L14V has the same absorption spectrum as the wild type and all other tendamistat variants with a maximum at 276 nm and a shoulder around 282 nm (data not shown). Measuring the refolding kinetics by change in fluorescence signal above 230 nm after excitation at 276 nm reveals, however, a different signal behavior from the wild type and the other variants. This will be discussed in chapter 4.2.2.1 (Figure 4-19). A detailed analysis of the GdmCl dependence and the temperature dependence of the kinetic data reveals a similar behavior of L14V and the tendamistat wild type (chapters 3.1 and 4.2.2.1). The unusual spectroscopic properties of tendamistat variant L14V seems therefore to be due to small structural changes in the folded state compared to the wild type. Interestingly, the replacement of the leucine residue by a valine residue has a more pronounced effect on the far-UV CD signal than the substitution with an alanine residue at the same position.

We can conclude from our far-UV CD measurements that all tendamistat variants fold into native like structure.

4.2.2 Stability and Folding Kinetics of Tendamistat Variants

To characterize the structural properties of the free energy barriers in tendamistat we studied the effect of amino acid replacements on stability and folding kinetics. To determine ϕ_f-values (chapter 1.3.4), we analyzed tendamistat variants, which fold in an apparent two-state behavior as the wild type (chapter 4.2.2.1). The effect of amino acid substitution of Val36, Glu38 and Asp40 revealed an additional unfolding phase indicating a change in mechanism (chapter 4.2.2.2). Further, we analyzed the effect of the loading variants on stability and folding (chapter 4.2.2.3).

4.2.2.1 Tendamistat Variants with Apparent Two-State Folding

The method of protein engineering is a very powerful tool and provides an indirect way of probing the interactions that are formed in the rate-limiting structure.[123,137,138,176] Comparison of the resulting effects of a point mutation on the folding kinetics and on equilibrium stability is used widely for the structural characterization of protein folding transition states.[138,140]

10 of the tendamistat variants at 8 different positions in the protein were found to fold in an apparent two state behaviour at 25°C and pH 7 (Figure 4-17). To analyze the structural properties of the transition state, we determined ϕ_f-values (chapter 1.3.4). Furthermore, we used self- and cross-interaction parameters (chapter 1.3.4) to study the effect of mutations on the transition state structure.

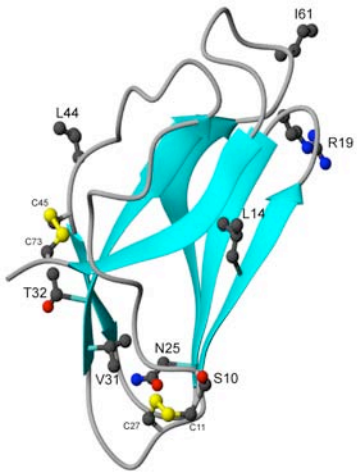

Figure 4-17: Schematic drawing of the structure of tendamistat. The disulfide bonds between Cys11-Cys27 and Cys45-Cys73 and the residues Ser10, Leu14, Arg19, Asn25, Val31, Thr32, Leu44 and Ile61 are shown as ball-and-stick models. The figure was generated using MOLMOL[194].

Effect of point mutation on the stability of tendamistat

All tendamistat variants are stable at native conditions (chapter 4.2.1). The GdmCl-induced equilibrium unfolding transitions of the variants were cooperative without any intermediate states (Figure 4-15).

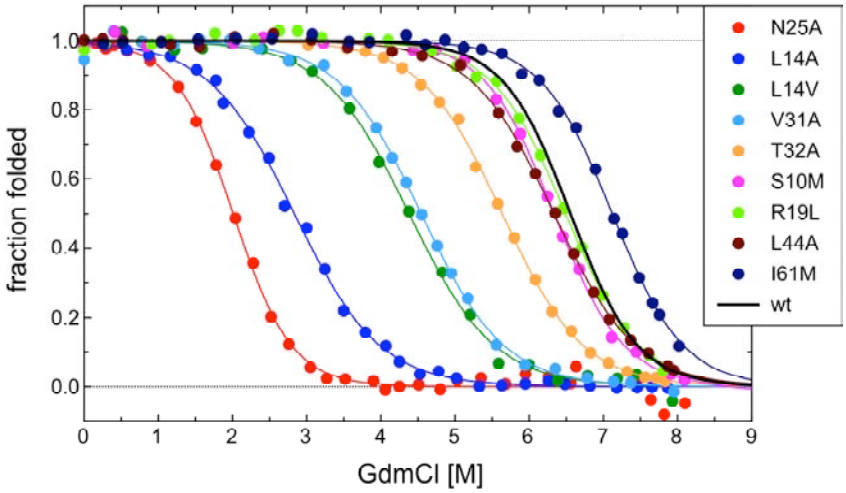

Figure 4-18: GdmCl-induced unfolding transitions at pH 7.0 and 25°C of tendamistat wild type and the tendamistat variants. The lines represent the least squares fit assuming the two-state model.[131]

All tendamistat variants are less stable compared to wild type except for I61M and S21A, which are about 2 kJ/mol more stable (Table 4). Amino acid replacements of Ser10, Arg19 and Leu61 have nearly no effect on protein stability, whereas substitutions of Thr32, Leu14, Val31 and Asn25 significantly destabilize tendamistat with a $\Delta\Delta G^0$ from 7 to 24 kJ/mol. The effect of amino acid replacement of Ser 21 on stability will be discussed later.

Table 4: Equilibrium parameters of tendamistat variants at pH 7 and 25°C. All data were result from global fit of equilibrium and kinetic data. Data for the wild type were taken from Schönbrunner et al.[173]

	ΔG^0 (kJ/mol)	m_{eq} (kJ/molM)
wt[173]	-35.93 ±0.03	5.48 ±0.01
S10M	-33.90 ±1.95	5.14 ±0.24
L14A	-14.41 ±0.11	4.85 ±0.03
L14V	-24.07 ±0.16	5.27 ±0.03
R19L	-33.62 ±1.54	5.18 ±0.19
S21G	-19.87 ±0.21	4.43 ±0.06
S21A	-38.76 ±2.49	4.98 ±0.30
N25A	-12.35 ±0.10	6.15 ±0.07
V31A	-23.24 ±0.49	5.10 ±0.08
T32A	-29.18 ±0.54	5.14 ±0.08
L44A	-33.67 ±0.59	5.38 ±0.08
I61M	-37.55 ±1.66	5.27 ±0.21

Effect of point mutation on the folding kinetics of tendamistat

Folding kinetics were measured following the change of fluorescence above 320 nm after excitation at 276 nm. The kinetic data for L44A, I61M, T32A and L14A were obtained by Daniel Poso. A sum of two and three exponential functions is needed to describe the unfolding and refolding kinetics, respectively (appendix 9.3 and 9.4). The two minor phases in refolding with amplitudes around 6 % and 8 % correspond to non-prolyl and prolyl-isomerization, respectively.[84,173,174] Interestingly, the apparent rate constants for refolding for prolyl ($\lambda_2 \approx 0.07$ s^{-1}) and non-prolyl ($\lambda_3 \approx 4$ s^{-1}) isomerization are insensitive to structural variations measured in this work.[173,174] The only exception is N25A, where the refolding traces could be fitted well to a sum of two exponentials due to a significant decrease of the fastest phase with the major amplitudes to a value of (5.0±0.1) s^{-1} at 0.4 M GdmCl.

The refolding traces of the tendamistat variant L14V show a different behaviour compared to the wild type and the other variants. The amplitudes for the non-prolyl isomerization have a different sign from the amplitudes for the other two phases in the refolding kinetics of L14V (Figure 4-19). The positive amplitudes decrease with increasing temperatures.

In what follows we will focus our analysis on the rate constants with the major amplitudes corresponding to the molecules with native prolyl and non-prolyl isomers (Figure 4-20). The kinetic and equilibrium data were fitted globally and the results are shown in Table 5. The kinetic and equilibrium data of the tendamistat variants S21A and S21G will be discussed later.

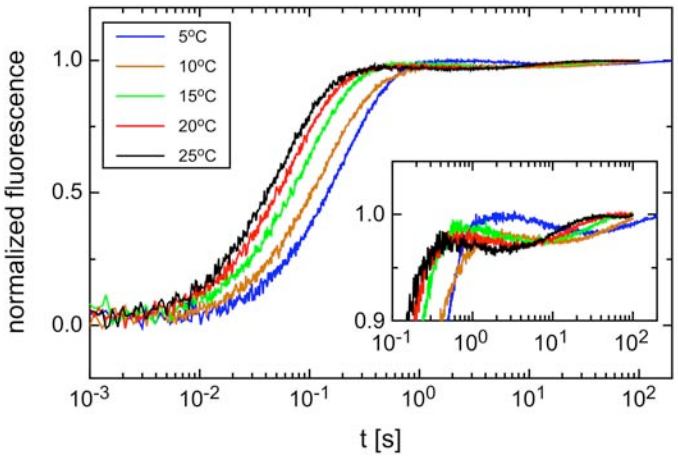

Figure 4-19: Kinetic traces of the refolding of tendamistat variant L14V at 0.65 M GdmCl, 100 mM cacodylic acid and pH 7.0 as monitored by fluorescence above 320 nm at different temperatures.

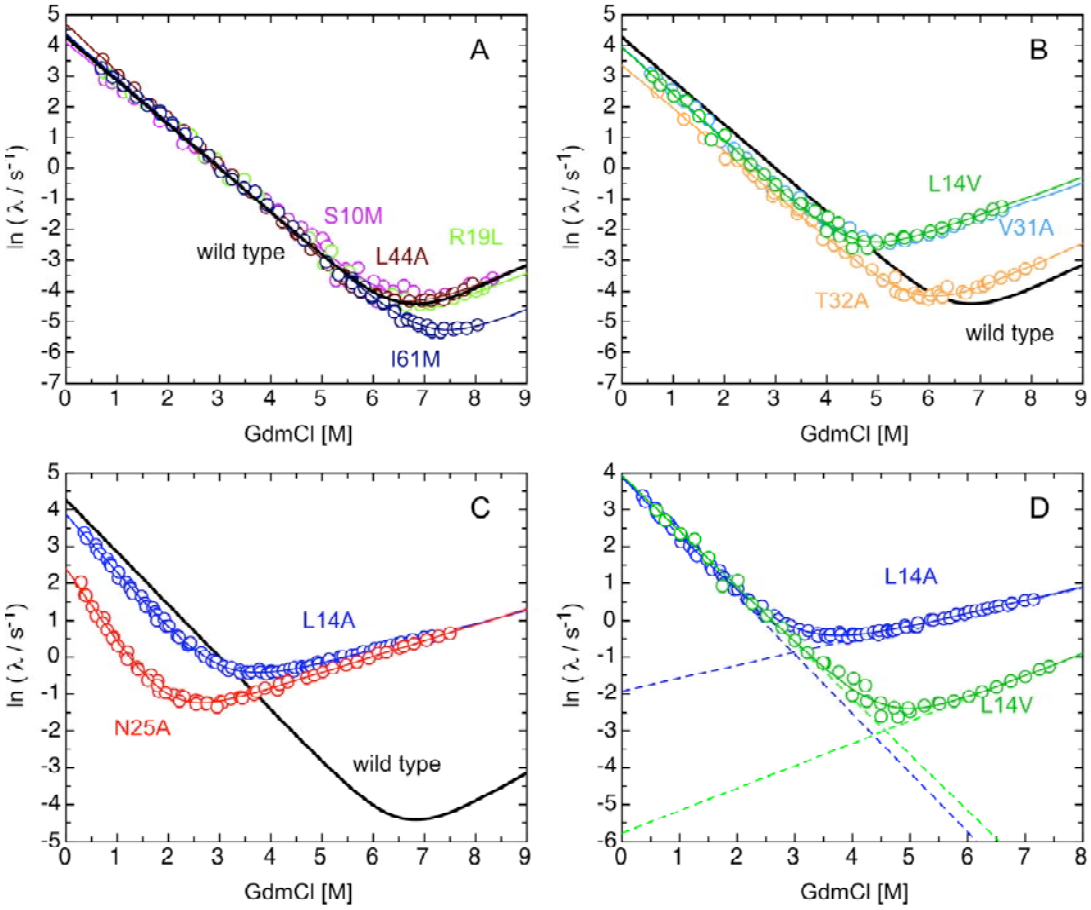

Figure 4-20: GdmCl-dependence of the apparent rate constants for folding of the tendamistat variants with similar α_D-value as wild type with a $\Delta\Delta G^0_{wt\text{-}variant}$ < 6 kJ/mol (A) and with a $\Delta\Delta G^0_{wt\text{-}variant}$ > 6 kJ/mol (B) as well as of tendamistat variants with significantly higher α_D-values (C) at pH 7 and 25°C. (D) Comparison of the apparent rate constants for folding of the tendamistat variants L14A and L14V at pH 7 and 25°C. (A-D) Only the rate constant with the major amplitude is plotted. The continuous lines represent the results of the global fits according to the two state model. The results of the global fits are given in Table 5. Data for the fit of tendamistat wild type (black line) were taken from Schönbrunner et al.[173].

The folding kinetics of S10M, L44A and R19L are virtually the same as for the wild type (Figure 4-20A). The tendamistat variant I61M folds with the same rate compared to wild type but unfolding is decelerated (Figure 4-20A and Table 5). Folding of L44A is 1.5-fold accelerated in the absence of denaturant (Table 5). In contrast, all other variants fold with similar or smaller rate constants compared to wild type (Figure 4-20B and C). Substitution of Val31, Leu14 and Asn25 significantly accelerate the unfolding rate constants of the protein (Figure 4-20B, C and Table 5). Substitution of Leu14 with alanine has little effect on refolding but the denaturant dependence of the folding and unfolding rates are different (Figure 4-20D). Except for N25A, where the rate constant is 6.5-fold decreased, variation of the structure has only little effect on the refolding rates of tendamistat (Figure 4-20 and Table 5).

Table 5: Kinetic and equilibrium parameters of tendamistat variants at pH 7 and 25°C. All data were resulted from global fit of equilibrium and kinetic data. The microscopic rate constants were extrapolated to 0 M GdmCl. Data for wild type were taken from Schönbrunner et al.[173]

	k_f (s^{-1})	k_u (s^{-1})	ΔG^0 (kJ/mol)	m_f (kJ/molM)	m_u (kJ/molM)	m_{eq} (kJ/molM)	$\alpha_D = m_f/m_{eq}$
wt[173]	71.6 ±1.6	$(3.6 \pm 0.1)\cdot 10^{-5}$	-35.93 ±0.03	3.53 ±0.01	1.95 ±0.02	5.48 ±0.01	0.64 ±0.01
S10M	60.4 ±5.0	$(7.0 \pm 3.8)\cdot 10^{-5}$	-33.90 ±1.95	3.37 ±0.05	1.77 ±0.30	5.14 ±0.24	0.66 ±0.04
β-hairpin V12-G26							
L14A	48.9 ±1.1	$(14.6 \pm 0.7)\cdot 10^{-2}$	-14.41 ±0.11	3.98 ±0.04	0.87 ±0.07	4.85 ±0.03	0.82 ±0.01
L14V	51.3 ±2.5	$(3.1 \pm 0.2)\cdot 10^{-3}$	-24.07 ±0.16	3.76 ±0.04	1.51 ±0.07	5.27 ±0.03	0.71 ±0.01
R19L	79.6 ±5.2	$(1.0 \pm 0.5)\cdot 10^{-4}$	-33.62 ±1.54	3.59 ±0.04	1.59 ±0.24	5.18 ±0.19	0.69 ±0.04
S21G	70.5 ±3.6	$(2.3 \pm 0.2)\cdot 10^{-2}$	-19.87 ±0.21	3.24 ±0.07	1.19 ±0.13	4.43 ±0.06	0.73 ±0.02
S21A	72.2 ±2.8	$(1.2 \pm 0.7)\cdot 10^{-5}$	-38.76 ±2.49	3.17 ±0.03	1.81 ±0.33	4.98 ±0.30	0.64 ±0.05
N25A	11.1 ±0.4	$(7.6 \pm 0.4)\cdot 10^{-2}$	-12.35 ±0.10	5.08 ±0.08	1.07 ±0.14	6.15 ±0.07	0.83 ±0.02
β-hairpin V31-V48							
V31A	53.9 ±3.0	$(4.6 \pm 0.9)\cdot 10^{-3}$	-23.24 ±0.49	3.77 ±0.05	1.33 ±0.13	5.10 ±0.08	0.74 ±0.02
T32A	30.8 ± 1.7	$(2.4 \pm 0.5)\cdot 10^{-4}$	-29.18 ±0.54	3.57 ±0.04	1.58 ±0.12	5.14 ±0.08	0.69 ±0.02
L44A	109.1 ± 4.0	$(1.4 \pm 0.3)\cdot 10^{-4}$	-33.67 ±0.59	3.82 ±0.02	1.56 ±0.10	5.38 ±0.08	0.71 ±0.01
I61M	79.5 ± 2.5	$(2.1 \pm 1.0)\cdot 10^{-5}$	-37.55 ±1.66	3.58 ±0.02	1.70 ±0.23	5.27 ±0.21	0.68 ±0.03

To characterize the transition states we determined α_D (chapter 1.3.4):

$$\alpha_D = \frac{\partial \Delta G^{0\ddagger} / \partial [Denaturant]}{\partial \Delta G^0 / \partial [Denaturant]} = \frac{m_f}{m_{eq}} \tag{4.9}$$

α_D is a measure for the relative change in ASA between the unfolded state and the transition state. Comparison of the α_D-values between tendamistat wild type and the variants reveals that α_D is in the range of 0.64 and 0.74 except for the two variants L14A and N25A, which have a significantly higher α_D-value of 0.82 and 0.83, respectively (Table 5). Tendamistat folding involves two sequential transition states.[110] Thus, we assume that L14A and N25A have the late transition state rate limiting, whereas the early transition state is the rate-limiting step for wild type and the other variants. However, the kinetic m-values and the α_D-values of the proteins with the early transition state as the rate-limiting step change with structural variations, which is an indication for transition state movement (Table 5).

Effect of amino acid substitution of Ser21 on tendamistat folding and stability

Serine was replaced by alanine and glycine, respectively. Figure 4-21A shows the GdmCl-induced unfolding transition of S21A. Due to the high stability no baseline of the unfolded state is measured and therefore, fits of the equilibrium unfolding transition are not reliable. Thus, we fitted the equilibrium data globally with the kinetic data (Figure 4-21).

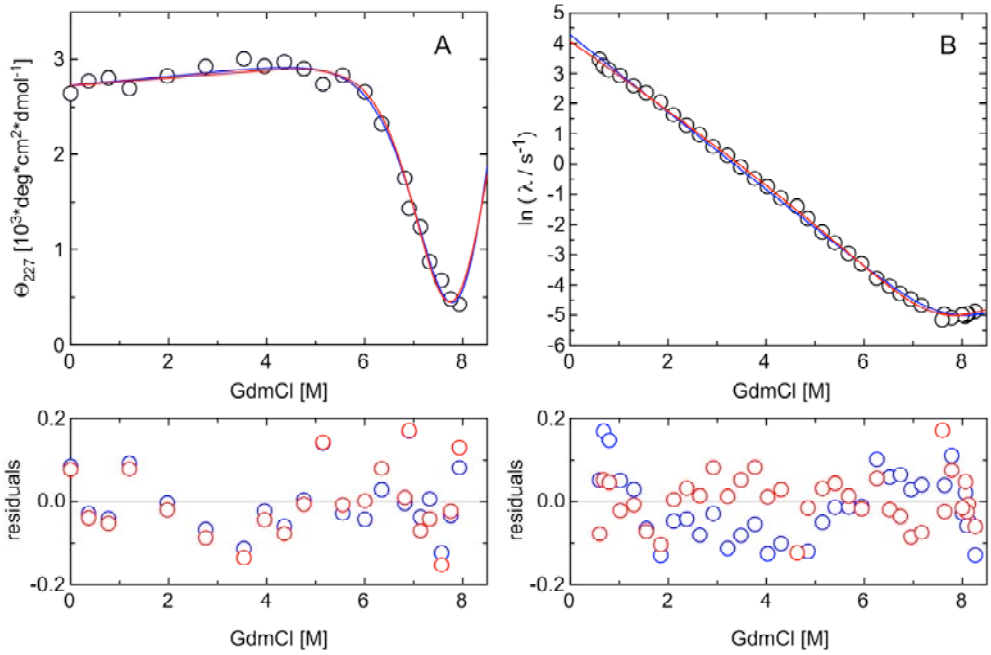

Figure 4-21: GdmCl-induced unfolding (A) and the GdmCl-dependence of the apparent rate constant of refolding and unfolding (B) and the residuals of the corresponding fit of the data at pH 7 and 25°C for S21A. Only the rate constant with the major amplitude is plotted. The solid lines represent the results of the global fit assuming a two-state model (blue) and a three-state model with a high-energy intermediate (red), respectively.

Analysis of the refolding rates of S21A reveals a small downward curvature. A population of intermediates in the deadtime of measurements will affect the amplitude of the refolding reaction. However, analysis of the amplitudes does not show any evidence for intermediates. However, deviation of linearity is hard to detect and it is not clear, if this non-linearity is due to a change in the rate-limiting step during folding or due to kinetic coupling of the prolyl-isomerization rates influencing the main refolding rates. Therefore, the data were analyzed globally assuming either a two-state model or a three-state model with high-energy intermediates. The results of both fitting models are given in Table 6.

Table 6: Kinetic and equilibrium parameters of the tendamistat variant S21A at pH 7 and 25 °C. The data are results from the global fit of equilibrium and kinetic data. The microscopic rate constants were extrapolated to 0 M GdmCl.

	k_f (s^{-1})	k_u (s^{-1})	ΔG^0 (kJ/mol)	m_f (kJ/molM)	$-m_u$ (kJ/molM)	m_{eq} (kJ/molM)	$\alpha_D = m_f/m_{eq}$
two-state model							
	72 ±3	$(1.2 \pm 0.7)\cdot 10^{-5}$	-38.8 ±2.5	3.17 ±0.03	1.81 ±0.33	4.98 ±0.30	0.64 ±0.05
three-state model							
TS1	63 ±2	$(23 \pm 2)\cdot 10^{-5}$	-42.4 ±0.29	2.65 ±0.04	2.89 ±0.06	5.53 ±0.11	0.48 ±0.02
TS2	801 ±61	$(3.0 \pm 0.1)\cdot 10^{-5}$		3.92 ±0.06	1.62 ±0.02		0.71 ±0.02

The substitution of serine with alanine stabilizes the protein compared to wild type of about 2.9 and 6.5 kJ/mol, depending on the fitting model, but seems not to have any influence on m_{eq} (Table 5 and Table 6). Assuming a two-state model, the α_D-value and the refolding rate k_f have the same values as wild type (Table 5 and Table 6). Comparison of the residuals of the kinetic data for both models reveals a better compliance with the three-state model with a high-energy intermediate (Figure 4-21). The α_D-value of the early transition state is significantly smaller compared to the other tendamistat variants (Table 5). However, the results of the fits are not very reliable due to the high stability of S21A.

To find out how the substitution of Ser21 influences the folding mechanism of tendamistat we determined the stability and folding kinetics of the more destabilized variant S21G (Figure 4-22). Interestingly, replacement of serine by glycine leads to a decrease in protein stability, whereas the substitution with alanine slightly increases the stability of tendamistat (Figure 4-21 and Table 6). The GdmCl-induced unfolding transition of S21G is cooperative without any apparent intermediate with a Gibbs free energy, ΔG^0, of –(17 ±3) kJ/mol and m_{eq} of (4.2 ±0.8) kJ/(mol·M) (Figure 4-22A). Folding of S21G is accompanied by a smaller change in accessible surface area (ΔASA) compared to wild type with a Δm_{eq} of 1.3 kJ/(mol·M) (Table 4). Figure 4-22B shows the rate constants for folding of the tendamistat variant S21G with the major amplitudes for refolding and unfolding. No curvature could be detect in the refolding limb and thus, we fitted the data globally assuming a two-state mechanism (Table 5).

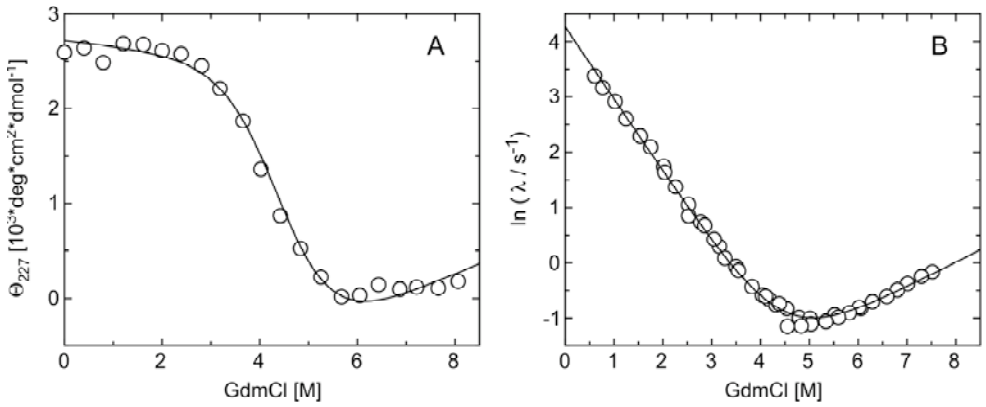

Figure 4-22: GdmCl-induced unfolding (A) and the GdmCl-dependence of the apparent rate constant (B) of refolding and unfolding of S21G at pH 7 and 25°C. Only the rate constant with the major amplitude is plotted. The solid lines represent the results of the global fit assuming a two-state model.

S21G is 16 kJ/mol less stable than the tendamistat wild type (Table 5, Table 7). The α_D-value of (0.73 ±0.02) indicates that folding occurs with the early transition state rate limiting. The refolding rate is essentially of the same value as the refolding rates of S21A and wild type (Table 5, Table 7).

To verify the folding mechanism of S21G we measured stability and folding kinetics at 5°C and 45°C. Figure 4-23 shows the GdmCl-induced equilibrium transition and the rate constants at both temperatures. No deviation from linearity was observed for the folding kinetics at 45°C and the data can well be fitted globally using a two-state model. In contrast, at 5°C a clear downward curvature appears in the refolding limb. Analysis of the amplitudes reveals no evidence for an intermediate. The data at 5°C was fitted using a sequential mechanism with a high-energy intermediate. The results of the fits are given in Table 7.

Table 7: Kinetic and equilibrium parameters of the tendamistat variant S21G at 5°C and 45°C. The data are results from the global fit of equilibrium and kinetic data. The microscopic rate constants were extrapolated to 0 M GdmCl.

	k_f (s^{-1})	k_u (s^{-1})	ΔG^0 (kJ/mol)	m_f (kJ/molM)	$-m_u$ (kJ/molM)	m_{eq} (kJ/molM)	$\alpha_D = m_f/m_{eq}$
45°C	105 ±5	0.73 ±0.05	-13.1 ±0.2	3.87 ±0.08	0.95 ±0.15	4.82 ±0.07	0.80 ±0.01
25°C	71 ±4	$(2.3 \pm 0.2)\cdot10^{-2}$	-19.9 ±0.2	3.24 ±0.07	1.19 ±0.13	4.43 ±0.06	0.73 ±0.02
5°C							
TS1	11.4 ±0.8	$(7 \pm 2)\cdot10^{-4}$	-22.3 ±0.7	1.38 ±0.17	3.22 ±0.20	4.59 ±0.37	0.30 ±0.06
TS2	66 ±15	$(42 \pm 5)\cdot10^{-4}$		3.61 ±0.21	0.98 ±0.04		0.78 ±0.11

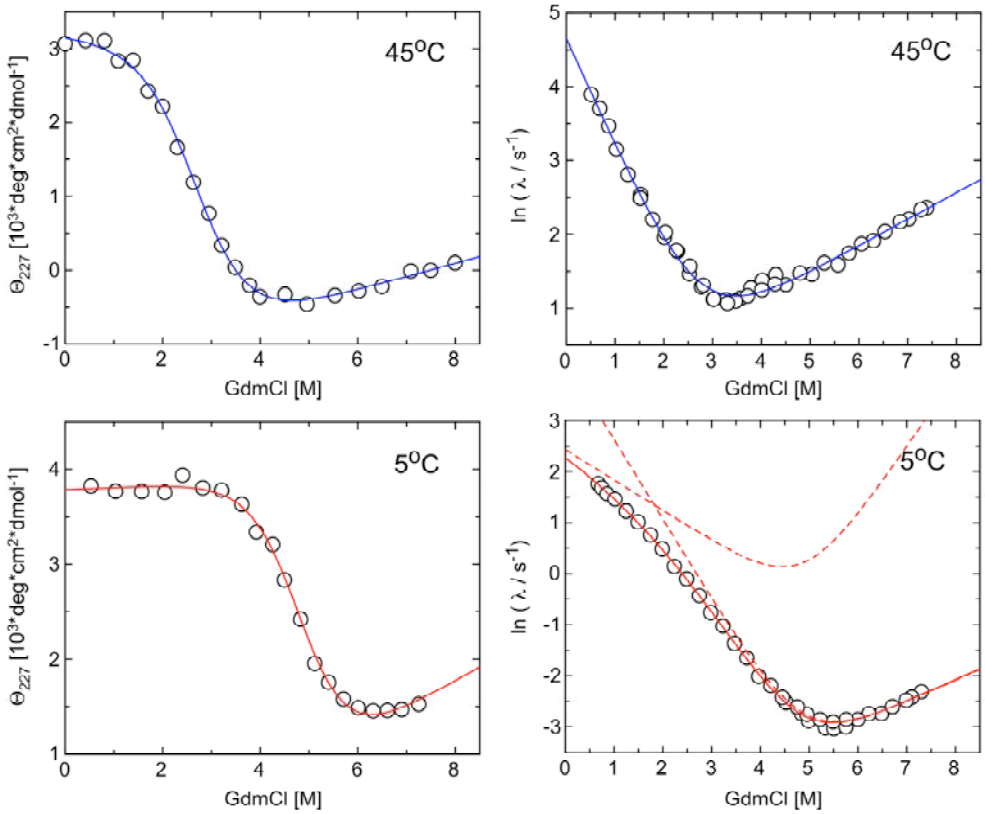

Figure 4-23: GdmCl-induced unfolding transition and the GdmCl-dependence of the apparent rate constant of refolding and unfolding 5°C and 45°C at pH 7. Only the rate constant with the major amplitude is plotted. The solid lines represent the results of the global fit assuming a two-state model (blue) and a three-state model with high-energy intermediate (red), respectively.

α_D at 5°C of the early transition state is significantly small with a value of (0.30 ±0.06) compared to wild type and the other tendamistat variants with the early transition state rate limiting. This indicates that maybe another mechanism causes the downward curvature at 5°C, which could be the same rate-limiting step as observed for tendamistat upon addition of sodium sulfate (chapter 4.2.3). To verify the origin of the downward curvature of S21G at low temperature further investigations are necessary.

ϕ_f-value analysis

The effect of point mutations are commonly used to obtain a structure-induced free energy relationship (chapter 1.3.4):[135,137-139]

$$\alpha_S = \phi_f = \frac{\partial \Delta G^{0\ddagger} / \partial Structure}{\partial \Delta G^{0} / \partial Structure} \qquad (4.10)$$

α_S, which is commonly called ϕ_f, measures the energetic of all interactions formed by a side chain with the rest of the protein in the transition state relative to the native state. ϕ_f-values of 0 indicate that the energetic of the interactions of the transition state are

the same as in the unfolded state. If the energetic of the interactions are the same as in the folded state, the ϕ_f-value is 1.

ϕ_f-values tends to be inaccurate if the difference in stability between the variant and wild type protein is less than about 7 kJ/mol.[140] Therefore, we determined ϕ_f only for variants with a $\Delta\Delta G^0$ of more than about 6 kJ/mol and for variants with the same transition state rate-limiting as wild type (Table 8).

Table 8: Changes in the Gibbs free energy and the activation free energy of folding upon mutation in tendamistat and the resulting ϕ_f-values. Only tendamistat variants with the early transition state as rate-limiting step were taken to calculate the ϕ_f-values.

Variant	$\Delta\Delta G^0$ (kJ/mol) $= \Delta G^0_{wt} - \Delta G^0_{mutant}$	$\Delta\Delta G_f^{0\ddagger}$ (kJ/mol) $= -RT\ln(k_{f,wt}/k_{f,mutant})$	ϕ_f $= \Delta\Delta G_f^0 / \Delta\Delta G^0$
S10M	-2.03 ±1.91	-0.42 ±0.14	n.d. [a]
L14V	-11.86 ±0.13	-0.83 ±0.06	0.07 ± 0.01
R19L	-2.31 ±1.51	0.26 ±0.10	n.d. [a]
S21A	2.84 ±2.46	0.02 ±0.04	n.d. [a]
S21G	-16.05 ±0.18	-0.04 ±0.07	0.002 ±0.004
V31A	-12.69 ±0.46	-0.70 ±0.08	0.06 ± 0.01
T32A	-6.75 ±0.50	-2.09 ±0.08	0.31 ± 0.03
L44A	-2.26 ±0.56	1.05 ±0.04	n.d. [a]
I61M	1.63 ±1.62	0.26 ±0.02	n.d. [a]

[a] Only variants with a $\Delta\Delta G^0 < 6$ kJ/mol were used to determine the ϕ_f-values

Due to this criterion only four of our variants were suitable for ϕ_f-value determination: L14V, S21G, V31A and T32A (Table 8). L14V, S21G and V31A have ϕ_f-values close to 0 indicating that the side chains have denatured-like interactions in the transition state. Leu14 and Ser21 are localized in the N-terminal β-hairpin (Figure 4-17). By contrast, Val31 is localized in the C-terminal β-hairpin but interacts with the N–terminal β-hairpin in the native state (Figure 4-17). Therefore, the ϕ_f-values argues for a late formation of the N-terminal β-hairpin. Also, destabilizing point mutations in this β-hairpin lead to a change of the rate-limiting step, i.e. the late transition state is more affected by mutations compared to the early transition state. However, ϕ_f-values only report on side chain interactions and do not say anything about backbone formation. It is possible to have a native-like topology without forming many or, indeed, any significant side chain interactions.

For the tendamistat variant T32A we obtain a fractional ϕ_f -value of 0.31 ±0.03. Interpretation of fractional ϕ_f values is more difficult. ϕ_f -value analysis of different proteins revealed a mean ϕ_f value of around 0.3.[140,245] The fractional ϕ_f -value could indicate partial formation of the interaction, revealing a possible early formation of the C-terminal β-hairpin.

The differences in stability of the two variants L14A and N25A are quite small ($\Delta\Delta G^0$= (2.1±0.2) kJ/mol). Therefore, a quantitative analysis of the ϕ_f values of the late transition state is not very reliable.[59] However, a qualitativ analysis of the kinetic data reveals similar rate constants at high denaturant concentration indicating ϕ_u (=1-ϕ_f)-values close to 0 (Figure 4-20 and Table 5). Therefore we conclude formation of the N–terminal β-hairpin in the late transition state.

Variation of the structure has only little effect on the refolding rates of tendamistat and thus, most of the variants have ϕ_f -values close to 0, indicating polarized transition states in tendamistat folding. The qualitativ analysis of the variants L14A and N25A confirms this observation.

Analysis of transition state movement

To determine transition state movements we used self- and cross-interaction parameters as proposed by Jencks and co-workers (chapter 1.3.4).[148,149] According to the Hammond postulate the position of a transition state is shifted towards the ground state destabilized by a perturbation, such as the addition of a denaturant (chapter 1.3.4).[147] A change in α_D due to different denaturant concentrations can be detected using the denaturant self-interaction parameter p_D:

$$p_D = \frac{\partial \alpha_D}{\partial \Delta G^0} = \frac{\partial^2 \Delta G^{0\ddagger}}{\left(\partial \Delta G^0\right)^2} \qquad (4.11)$$

Hammond behavior yields positive self-interaction parameters and in the case of the denaturant dependence of the folding and unfolding rates, that would result in a smooth downward curvature in the limbs of the Chevron plot. Figure 4-20 shows that p_D is 0 for nearly all tendamistat variants used for this analysis. The only exception is tendamistat variant S21A, already discussed above. However, in our previous work we showed that Hammond behavior is only observed in tendamistat when multiple perturbations are applied indicating that transition state movement is weak in protein folding (chapter 3.1).[59,123] Therefore, we analyzed the effect of denaturant and point

mutation on tendamistat folding and stability. Figure 4-24 shows the effect of ΔG^0 on the α_D-value and on the kinetic and equilibrium m-values.

The effect of denaturant and point mutations on folding and stability for the proteins with the late transition state as rate-limiting step is a positive structure-denaturant cross-interaction parameter

$$p_{DS} = \frac{\partial \alpha_D}{\partial \Delta G_S^0} = (3 \pm 1) \cdot 10^{-3} \text{ mol/kJ} \tag{4.12}$$

indicating transition state movement. Analysis of the m-values reveals Hammond behavior accompanied by a ground state effect (Figure 4-24). However, the m_f and m_{eq}-values of S21G are significantly smaller than expected from comparison with the other proteins. Analysis of the data without S21G reveals true Hammond behavior without ground state effect. This is due to the independence of the equilibrium m-values on point mutations and the changes of the kinetic m-values with changes in ΔG^0 with equal amount but different sign (Figure 4-24).

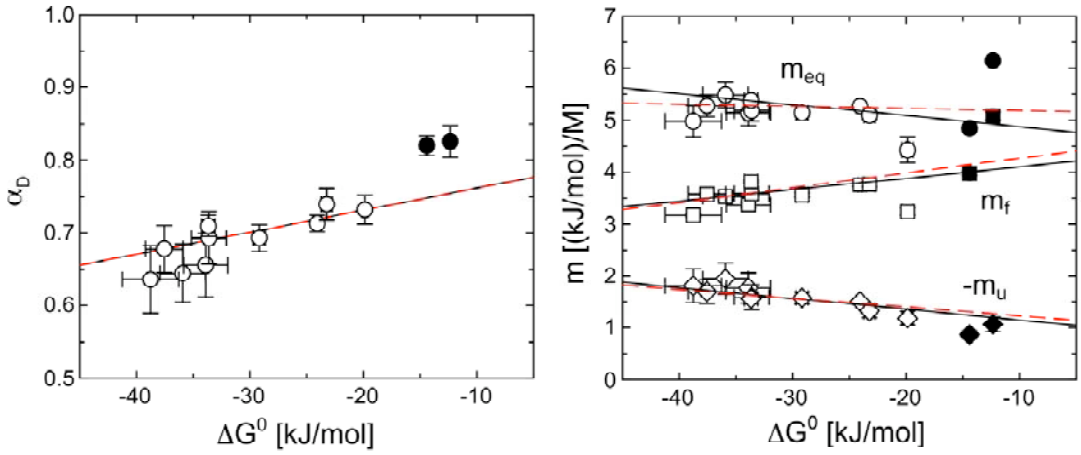

Figure 4-24: Effect of changes in ΔG^0 on α_D and on m_{eq}, m_f and $-m_u$ for the structure-denaturant perturbation of tendamistat at pH 7 and 25°C. The red lines indicate fits without the tendamistat variant S21G. The linear fits of all proteins with the early transition state rate limiting (open symbols; black line) give values of $p_{DS}=\partial\alpha_D/\partial\Delta G^0= (3\pm1)\cdot10^{-3}$ mol/kJ and $\partial m_{eq}/\partial\Delta G^0=-(2.1\pm0.6)\cdot10^{-2}$ M^{-1}, $\partial m_f/\partial\Delta G^0=(2.2\pm0.2)\cdot10^{-2}$ M^{-1} and $\partial(-m_u)/\partial\Delta G^0=-(2.1\pm0.8)\cdot10^{-2}$ M^{-1}. Linear fits without S21G (red line) give values of $p_{DS}=\partial\alpha_D/\partial\Delta G^0= (3\pm1)\cdot10^{-3}$ mol/kJ and $\partial m_{eq}/\partial\Delta G^0=-(0.4\pm0.6)\cdot10^{-2}$ M^{-1}, $\partial m_f/\partial\Delta G^0=(2.8\pm0.3)\cdot10^{-2}$ M^{-1} and $\partial(-m_u)/\partial\Delta G^0=-(1.7\pm0.9)\cdot10^{-2}$ M^{-1}. The tendamistat variants L14A and N25A (filled symbols) significantly differ from the other proteins. The data are taken from the global fits of the kinetic and equilibrium data of each protein.

The m_f –value of N25A is significantly increased indicating a ground state effect for the late transition state. However, the cross-interaction parameter p_{DS} for the late transition state is accompanied by too large uncertainties due to the less differences in stability of the two proteins L14A and N25A ($\Delta\Delta G^0_{(N25A-L14A)}$ = (2.1 ±0.2) kJ/mol).

The results are in good accordance with our previous results obtained from the temperature-denaturation perturbation of wild type, L14V, L14A and N25A revealing Hammond behavior for the early transition state, whereas the late transition state shows only little Hammond behavior accompanied with large ground state effects (chapter 3.1).

4.2.2.2 Tendamistat Variants with Complex Unfolding Kinetics

Unfolding of tendamistat wild type at pH 2.0 at high denaturant concentration consists of two unfolding reactions.[174] The major kinetic phase has a relative amplitude of about 98 %, which was attributed to the actual unfolding process.[174] The remaining 2 % of the amplitude is caused by the unfolding reaction of a native like intermediate (N*) (chapter 1.4).[174] Unfolding of N* is about tenfold faster than the unfolding reaction of the native molecule.[174]

Two unfolding reactions were observed for nearly all tendamistat variants (chapter 4.2.2.1). However, a sum of three exponentials is required to fit the unfolding reaction at various conditions for the tendamistat variants V36A, V36G, E38Q and D39A. All three mutated residues are located in the C-terminal β-hairpin (Figure 4-25). To elucidate the origin of the complex kinetics we performed interrupted refolding[121,122] and double-jump experiments[78] (chapter 1.3.3).

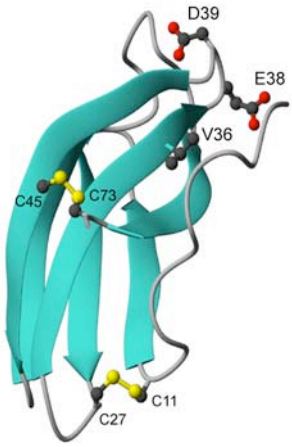

Figure 4-25: Schematic drawing of the structure of tendamistat. The disulfide bonds between Cys11-Cys27 and Cys45-Cys73 and Val36, Glu38 and Asp39 are shown as ball-and-stick models. The figure was generated using MOLMOL[194].

Folding and stability of the tendamistat variant V36A

The GdmCl-induced unfolding transition states of V36A were measured at pH 7 and pH 2 (Figure 4-26). A shift of the transition midpoint from 3.8 M to 1.1 M GdmCl occurs upon decreasing pH. The equilibrium unfolding transitions were cooperative without any apparent intermediate states and the data were fitted assuming a two-state mechanism. The results of the fits are given in Table 9.

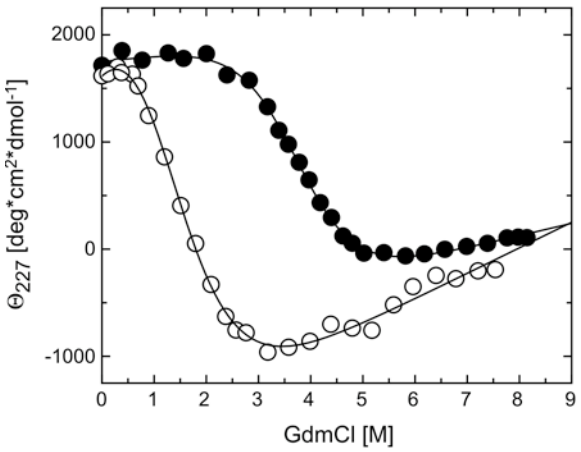

Figure 4-26: GdmCl-induced unfolding transition of the tendamistat variant V36A at pH 7 (●) and pH 2 (○) at 25°C monitored by ellipticity at 227 nm. Concentration was 10 µM in 100 mM cacodylic acid. The line represents the analysis assuming the two-state model. The results are given in Table 9.

The replacement of valine with alanine at position 36 decreases protein stability significantly for about 16 to 18 kJ/mol independent of pH. A decrease of m_{eq} for about 1 kJ/(mol·M) is observed at both pH values compared to wild type (Table 9). Changes in the m-values indicate a change in the compactness of the unfolded structure due to the correlation of m_{eq} and the changes in accessible surface area upon unfolding.[23]

Table 9: Comparison of the Gibbs free energy and the m-value of the tendamistat variant V36A and tendamistat wild type at pH 7 and pH 2 at 25°C. The data are results from the GdmCl-induced unfolding transition states. Data for wild type were taken from Schönbrunner et al.[173] *(pH 7) and from Pappenberger et al.*[174] *(pH 2).*

		ΔG^0 [kJ/mol]	m [kJ/(mol·M)]
pH 7	**Tendamistat**[173]	-(35.9 ±0.1)	5.48 ±0.01
	V36A	-(16.4 ±2.0)	4.37 ±0.52
pH 2	**Tendamistat**[174]	-(21.4 ±0.8)	5.21 ±0.19
	V36A	-(4.8 ±1.2)	4.26 ±0.34

The folding kinetics of V36A were measured following the change of the fluorescence signal after stopped-flow mixing and manual-mixing, respectively (appendix 9.5). The refolding kinetics are fitted well with a sum of three exponentials. The two slow rate constants with about 6 % and 8 % (Figure 4-27A and C) seems to be due to non-prolyl and prolyl-isomerization reactions as observed for the tendamistat wild type.[84,173,174] In contrast to the wild type, a sum of three exponentials is necessary to fit the unfolding

kinetics. The fastest unfolding rate constants has an amount of approximatly 8 % of the fluorescence amplitudes, whereas the two slower rates correspond to approximatly 43 % and 49 % of the fluorescence amplitudes (Figure 4-27A, B and C).

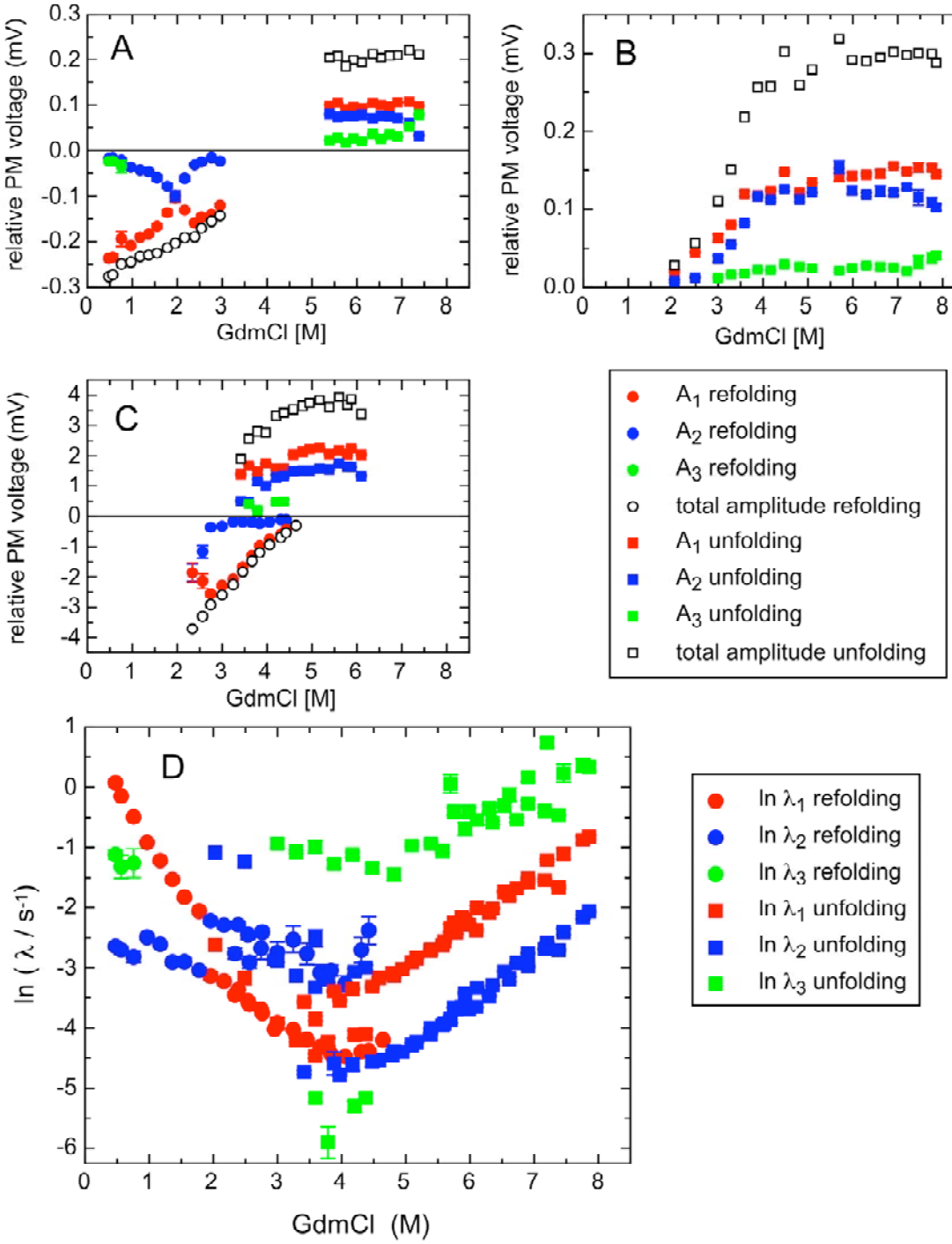

Figure 4-27: GdmCl dependence the apparent rate constants (D) and of the amplitudes A_i (A, B, C) of refolding (circles) and unfolding (squares) of the tendamistat variant V36A at 25°C and pH 7. (A, B) The kinetics were measured by stopped-flow mixing monitoring the change in fluorescence after initiation by 11-fold (A) and 26-fold (B) dilution, respectively. (C) The kinetics were measured by manual-mixing monitoring the change in fluorescence.

Figure 4-27D shows the GdmCl dependence of refolding and unfolding rate constants of V36A. Analysis of the refolding data reveals a deceleration of the apparent rate constants with the major amplitudes, λ_1, to a value of about 1.9 s^{-1} in the absence of denaturant compared to wild type (72 ±2 s^{-1}) (Figure 4-27D and Table 5). The second fastest phase is about tenfold slower ($\lambda_3 \approx 0.3$ s^{-1}) compared to wild type and the other tendamistat variants with an apparent two-state behavior (chapter 4.2.2.1). The apparent rate constant of the slow phase, which was assumed to belong to the prolyl-isomerization reaction, is identical to the rate constant observed in tendamistat wild type ($\lambda_2 \approx 0.07$ s^{-1}) (chapter 4.2.2.1). All three unfolding rate constants show a very similar GdmCl dependence. However, we cannot distinguish, which of the phases belongs to the unfolding of native like intermediate (N*)[174] nor can we tell anything about the origin of the third unfolding phase. It is also not obvious which of the unfolding rate constants belongs to unfolding of native protein.

To further investigate the folding mechanism of the tendamistat variant V36A we performed kinetic studies at pH 2 and 25°C, conditions that destabilize the protein with a $\Delta\Delta G^0$ of (12 ±3) kJ/mol but do not change the m_{eq}-value (Table 9). Refolding and unfolding could be fitted with a sum of three exponentials (appendix 9.5). However, Figure 4-28 shows that the folding kinetics are complex. The apparent rate constants for refolding do not change significantly upon decreasing pH, in contrast to the unfolding rate constants, which accelerate. Coupling of the two major unfolding phases leads to scattered data (Figure 4-28). Fitting the data with fixed ratio of the amplitudes of unfolding does not improve the results significantly.

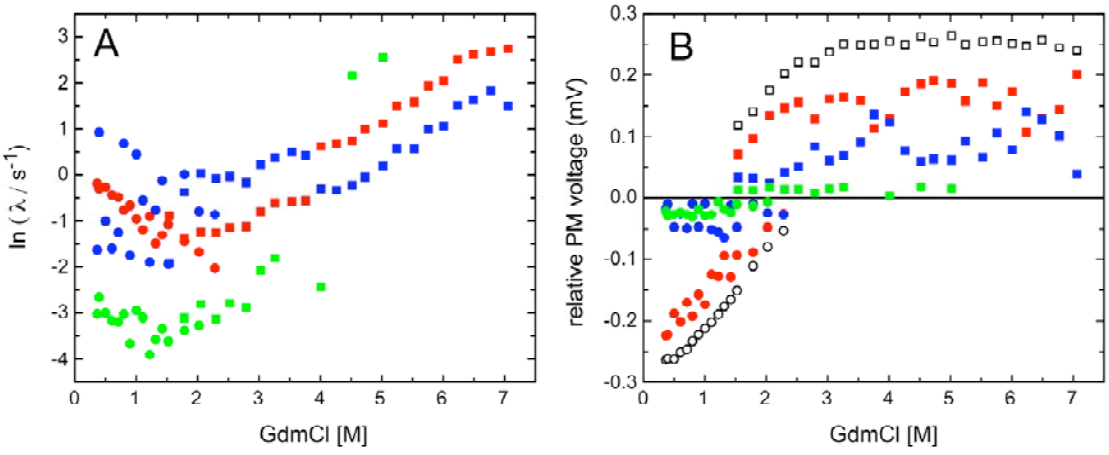

Figure 4-28: GdmCl dependence of the apparent rate constants (A) and the amplitudes (B) of refolding (circles) an unfolding (squares) of the tendamistat variant V36A at 25°C and pH 2.

Formation of native molecules during V36A folding

To understand the origin of the unfolding rate constants, we performed an interrupted refolding experiment[121,122] (chapter 1.3.3) in order to follow the time course of formation of the unfolding reactions during folding. Interrupted refolding experiments of tendamistat wild type at pH 2 revealed an additional slow folding reaction (λ = 0.008 s^{-1}) with an amplitude of 12 %, caused by the interconversion of a highly structured intermediate, N*, to native tendamistat.[174] To find out, which of the three unfolding phases are caused by unfolding of N*, we refolded the tendamistat variant V36A in 0.6 M GdmCl (pH 7 and 25°C) for a certain time (t_i) and then transferred to denaturing conditions (6.9 M GdmCl, pH 7) to initiate unfolding. Triple exponential unfolding kinetics are observed at all folding times with rate constants of : λ_1 = (0.224 ±0.001) s^{-1}, λ_2 = (5.36 ±0.02)·10^{-2} s^{-1} and λ_3 = (1.50 ±0.02) s^{-1}. The rate constants of the unfolding reactions do not depend on the age times (Figure 4-29B).

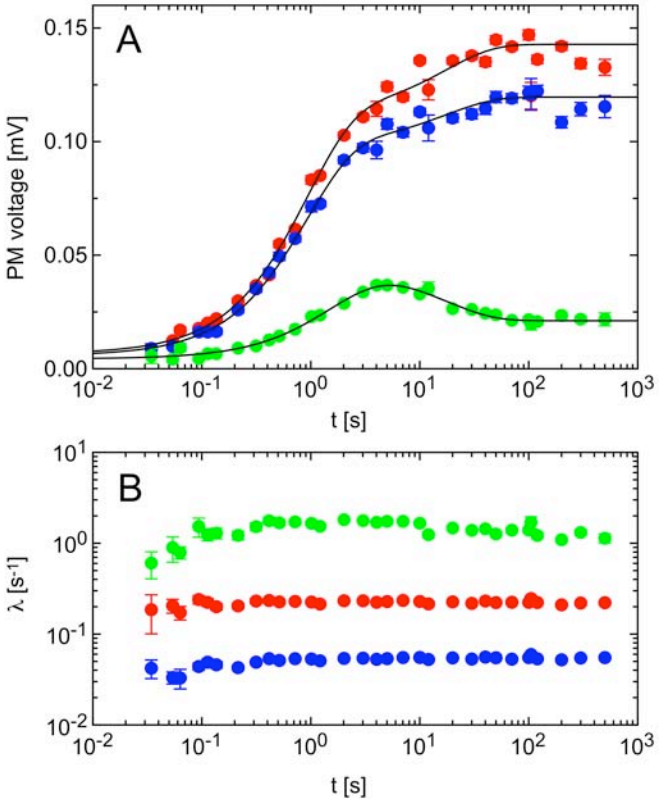

Figure 4-29: (A) Refolding of tendamistat variant V36A at 0.6 M GdmCl, pH 7 and 25°C monitored by an interrupted refolding experiment which allows us to follow the formation of the native state (● , ●) and of the native-like intermediate (●). The lines represent a global fit. The rate constants of the fits are given in Table 10. (B) Rate constants of the slow unfolding reactions (● , ●) and the fast unfolding reaction of the native-like intermediate (●) as a function of the refolding time.

Figure 4-29A shows the amplitudes of the three unfolding phases as the function of the refolding time (t_i). The fast unfolding reaction shows similar behavior as observed for the formation of the native-like intermediate N*.[174] The two slower unfolding molecules rise in parallel. All three refolding phases could be fitted with the sum of two exponentials. Comparison of the apparent rate constants reveals that the fast increase of the two slow-unfolding molecules are identical within errors, whereas the slow increase of the two slow-unfolding molecules mirrors the decay of the fast-unfolding molecules, which is the slow interconversion of N* to the native state during folding of tendamistat (Table 10). Therefore, we fitted the data globally with a value of (0.06 ±0.01) s^{-1} for the interconversion and a rate constant for the fast increase of the two slow-unfolding molecules of (1.10 ±0.05) s^{-1} (Table 10). The relative amplitudes of the end values are in good agreement with the results of the direct unfolding kinetics (Figure 4-27). The same refolding rate constants for the two slow-unfolding molecules, which are virtually identical to the recovery of the fluorescence signal in direct refolding (Figure 4-27), reveal that both reflect the formation of native protein.

The refolding experiments clearly revealed that unfolding of N* causes the fast unfolding rate constant. However, the amplitudes of the decay of N* are significantly smaller than the amplitudes for the slow increase of the two slow-unfolding molecules.

Table 10: Apparent rate constants (λ_i) and amplitudes (A_i) of V36A folding at 0.6 M GdmCl, pH 7 and 25°C. Positive amplitudes were assigned to the formation of a species and negative amplitudes to its decay. The data are from the interrupted refolding assay (Figure 4-29).

		Formation of N	Formation of N	Formation of N*
single fit	**λ_1 (s^{-1})**	1.14 ±0.09	1.12 ±0.06	
	A_1 (%)	37.6 ±1.4	35.2 ±0.8	
	λ_2 (s^{-1})			0.60 ±0.06
	A_2 (%)			14.8 ±0.9
	λ_3 (s^{-1})	0.06 ±0.02	0.03 ±0.01	0.06 ±0.01
	A_3 (%)	12.6 ±1.4	8.1 ±0.8	-(8.4 ±0.9)
	ΣA_i (%)	50.2	43.3	6.4
global fit	**λ_1 (s^{-1})**	1.10 ±0.05	1.10 ±0.05	
	A_1 (%)	39.6 ±1.0	34.7 ±0.9	
	λ_2 (s^{-1})			0.60 ±0.10
	A_2 (%)			15.8 ±1.2
	λ_3 (s^{-1})	0.06 ±0.01	0.06 ±0.01	0.06 ±0.01
	A_3 (%)	11.5 ±1.0	7.9 ±0.9	-(8.8 ±1.2)
	ΣA_i (%)	51.1	42.6	7.0

Double Jump experiments

Native protein and the native-like intermediate have virtual identical fluorescence amplitudes in tendamistat wild type at pH 2, thus it could not detect with direct refolding kinetics.[174] Interrupted refolding experiments revealed, however, that the rate constant for the slow interconversion of the native-like intermediate to the native state during folding of the tendamistat variant V36A is virtually identical to the slow refolding rate constant observed by direct kinetic measurements (Table 10; Figure 4-27). This slow phase was originally assumed to be due to the prolyl-isomerization reaction. To investigate the origin of the slow refolding reaction and to detect possible populated intermediates during unfolding, we performed double-jump measurements[78] (chapter 1.3.3).

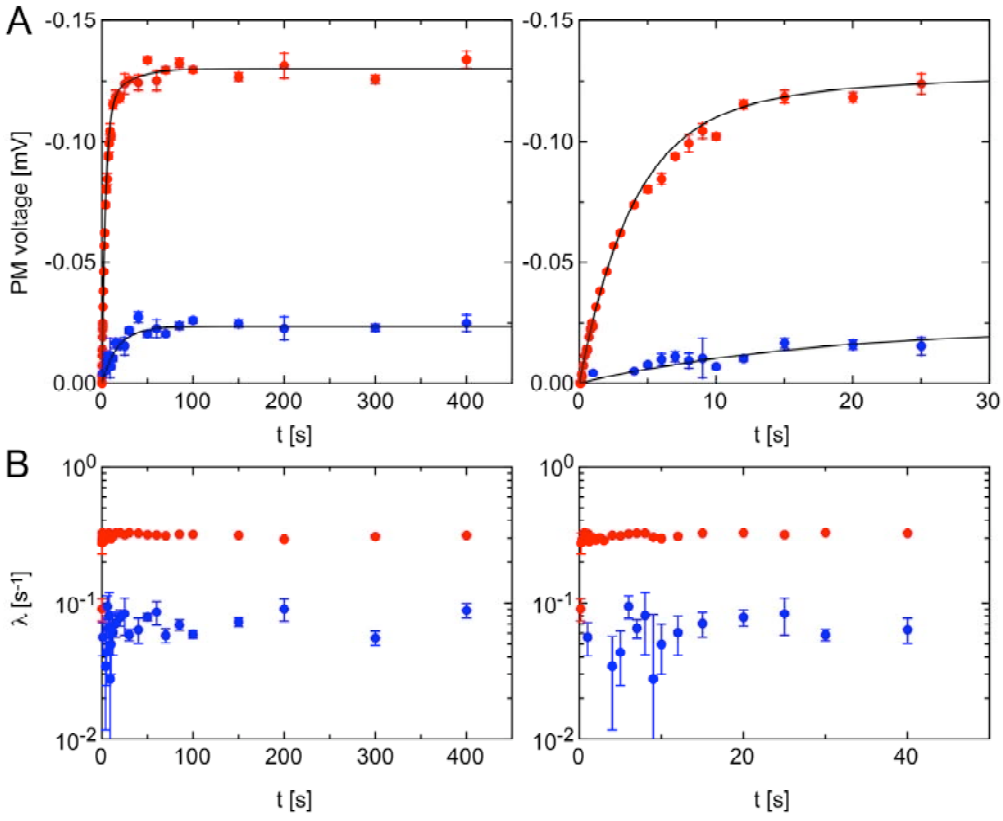

Figure 4-30: (A) Time course of formation of the fast refolding (●) and of the slow refolding molecules (●) of tendamistat variant V36A in 7.0 M GdmCl, pH 7 and 25 °C, obtained by double-jump experiments. The formation of the fast refolding phase occurs with rate constants of (0.26 ±0.01) s^{-1} and (0.04 ±0.01) s^{-1}. The slow refolding phase is formed with an apparent rate constant of (0.058 ±0.004) s^{-1}. (B) Rate constants of the fast refolding (●) and the slow refolding reaction (●) as a function of the unfolding time.

Double-jump experiments allow discrimination between unfolded states that are populated immediately after unfolding and states produced by slow equilibration processes in U. An equilibration step following the unfolding reaction would produce a lag phase in the appearance of the amplitude of the slow refolding reaction. Native protein is unfolded in 7.0 M GdmCl. After various times of unfolding (t_i) the protein is transferred to strongly native solvent conditions (1.2 M GdmCl), which allows refolding to occur. Till a delay time t_i of about 4 s^{-1} the refolding traces can well be fitted with single exponentials with a rate constant of $(31.1 \pm 0.1) \cdot 10^{-2}$ s^{-1}. Above 4 s^{-1}, a fit with two exponentials is necessary to describe the kinetics with a slower rate constant of $(6.5 \pm 0.2) \cdot 10^{-2}$ s^{-1} (Figure 4-30A). Figure 4-30B shows that the slow phase are formed more slowly than unfolding occurs, indicating these reactions to be due to slow folding molecules, which are produced by slow equilibration processes in the unfolded state. The rate constant of (0.058 ± 0.004) s^{-1} is compatible with prolyl isomerization reactions. By contrast, the fast refolding reaction appears soon after the molecules have been unfolded with a rate constant of (0.26 ± 0.1) s^{-1} and a slower rate constant of (0.04 ± 0.01) s^{-1}, revealing that the fastest refolding pathway represents the folding of unfolded molecules with all peptide bonds in the native *trans* state. The slow rate constant has the same value as observed for the formation of the slow refolding molecules. Comparison of the fast formation of the fast refolding reaction with the fluorescence signal in direct unfolding (Figure 4-27) reveals that the main unfolding phase with a relative amplitude of 49 % is caused by unfolding of the native molecule.
For a better characterization of the mechanism and to accelerate the unfolding reaction, we performed double-jump experiments at pH 2. The native tendamistat variant V36A was diluted to a final GdmCl concentration of 7 M at pH 2. After various delay time t_i, unfolding was interrupted and the protein was allowed to refold at 1.2 M GdmCl at pH 7. In contrast to the double-jump experiments at pH 7, two exponentials are necessary to fit the kinetic traces at all t_i with values of: $\lambda_1 = (32.2 \pm 0.2) \cdot 10^{-2}$ s^{-1} and $\lambda_2 = (7.0 \pm 0.2) \cdot 10^{-2}$ s^{-1} (Figure 4-31B). The formation of fast refolding molecules is significantly accelerated ((13.3 ± 0.1) s^{-1}) and shows a significant delay, which mirrors the formation of slow refolding molecules, both in amplitude and in the rate constant (Figure 4-31A). This confirms our previous observation that the slow refolding phase is caused by prolyl isomerization.

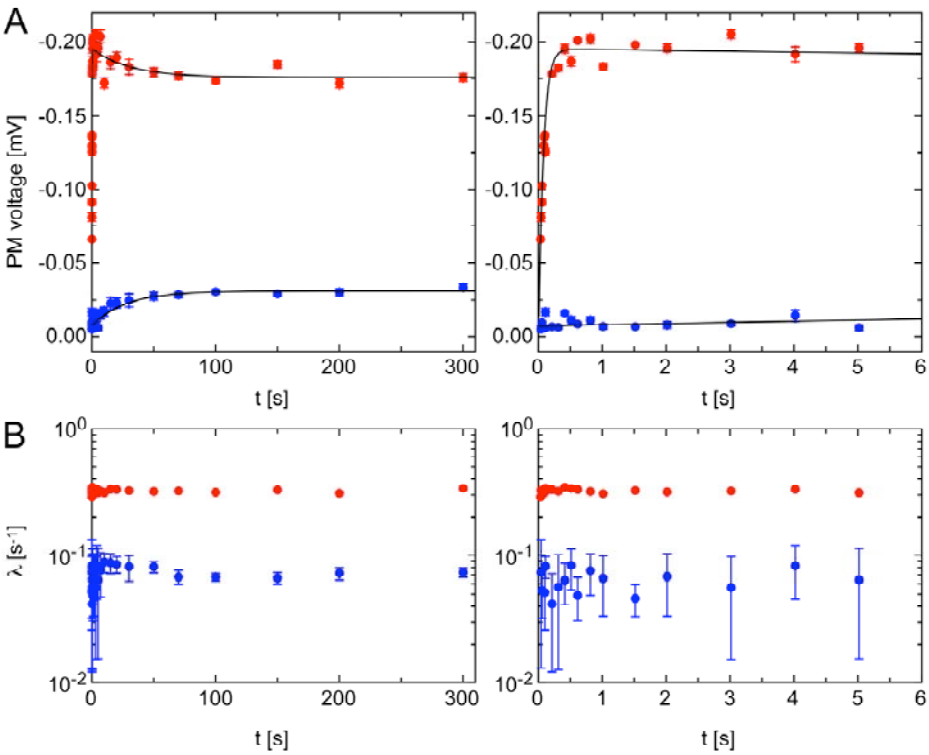

Figure 4-31: (A) Time course of formation of the fast refolding (●) and of the slow refolding molecules (●) of tendamistat variant V36A in 7.0 M GdmCl, pH 2 and 25 °C, obtained by double-jump experiments. The formation of the fast refolding phase occurs with a rate constant of (13.3 ±0.1) s^{-1} and its decay can be fit with a rate constant of (0.03 ±0.01) s^{-1}. The slow refolding phase is formed with an apparent rate constant of (0.037 ±0.008) s^{-1}. (B) Rate constants of the fast refolding (●) and the slow refolding reaction (●) as a function of the unfolding time.

Folding and stability of the tendamistat variant V36G

To investigate the equilibrium unfolding behavior of V36G, we measured GdmCl-induced unfolding transitions at 25°C and 45°C at pH 7 (Figure 4-32). The equilibrium transitions were cooperative with no apparent intermediate.

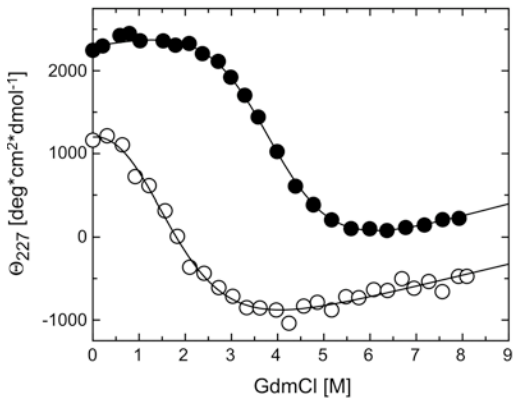

Figure 4-32: GdmCl-induced unfolding transition of the tendamistat variant V36G at 25°C (●) and 45°C (○) at pH 7 monitored by ellipticity at 227 nm. Concentration was 10 µM in 100 mM cacodylic acid. The line represents the analysis assuming the two-state model. The results are given in Table 11.

Table 11: Comparison of the Gibbs free energy and the m-value of the tendamistat variant V36G and tendamistat wild type at 25°C and 45°C at pH 7. The data are results from the GdmCl-induced unfolding transition states (Figure 4-32). Data for wild type were taken from Schönbrunner et al.[173].

	ΔG^0 [kJ/mol]	m [kJ/(mol·M)]
Tendamistat[173]	-(35.9 ±0.1)	5.48 ±0.01
V36G, 25°C	-(13.6 ±1.3)	3.57 ±0.34
V36G, 45°C	-(4.0 ±5.9)	3.62 ±1.15

Substitution of Val36 by glycine leads to a destabilization of 22.3 kJ/mol, which is 2.8 kJ/mol less stable than V36A. Increasing the temperature leads to a change in Gibbs free energy of about 9.6 kJ/mol but no changes in m_{eq} occur (Table 11).

The sum of three exponentials is necessary to fit the refolding and unfolding traces of V36G at 25°C measured by following the change of the fluorescence signal after stopped-flow and manual mixing (Figure 4-33). As we pointed out for V36A using interrupted refolding experiments, the unfolding of native like intermediate probably causes the fastest unfolding rate constant with relative amplitudes of 7 %. The two slower rates correspond to 68 % and 25 % of the fluorescence amplitudes (Figure 4-33).

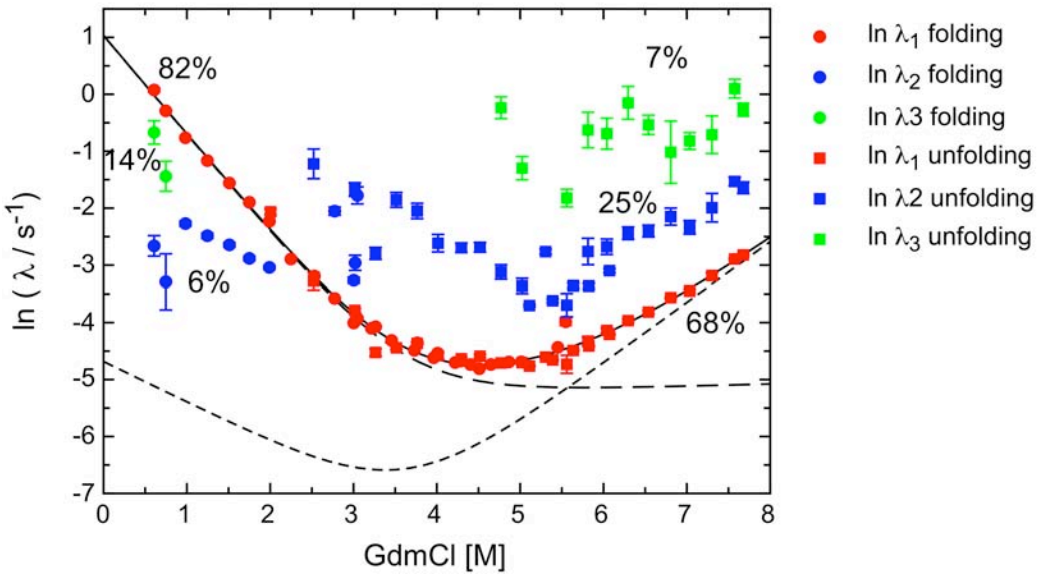

Figure 4-33: GdmCl-dependence of the apparent rate constants of refolding (circles) and unfolding (squares) of V36G at 25°C and pH 7. The mean amounts of the relative amplitudes of the apparent rate constants are indicated. The lines are the results of the fit using parallel two-state reaction mechanism of the rate constants with the major amplitudes λ_1.

Analysis of the rate constants with the major kinetic phase reveals an upward curvature near the midpoint of the unfolding transition. Assuming parallel pathways, the reaction with the most native-like transition state will be most sensitive to a reduced stability of the native-state and thus, a more unfolded-like transition state will become rate-limiting leading to an upward curvature in Chevron plots.[59]

For a better characterization of the upward curvature, we measured the folding kinetics at 45°C which destabilizes the protein and thus should affect parallel pathways (Table 11). Refolding and unfolding traces were well be fitted with the sum of two exponentials with relative amplitudes of 78 % and 22 % for the refolding and 63 % and 37 % for the unfolding traces (Figure 4-34). The slow unfolding phase has the major amplitudes and shows clearly an upward curvature between 5 and 6 M GdmCl. No upward curvature was observed, however, in the fast unfolding phase.

The rate constant of the major phase was fitted using a parallel two-state reaction mechanism and the results are given in Table 12. The results of the fits reveal a very native-like transition state (α_D = 0.98 and 0.91) as rate-limiting step at low denaturant concentrations. Around 5.5 M (25°C) and 5 M (45°C) GdmCl, respectively, a switch to a less native-like transition state occurs with α_D–values of 0.40 and 0.60 (Figure 4-33, Figure 4-34). However, the results are not reliable since we do not know the origin of the third unfolding phase.

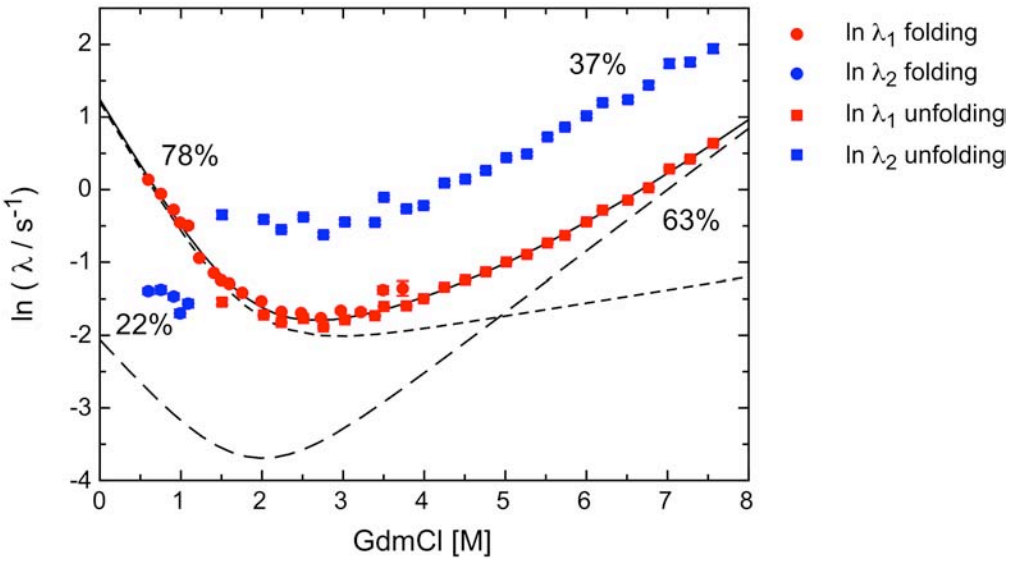

Figure 4-34: GdmCl-dependence of the apparent rate constants of refolding (circles) and unfolding (squares) of V36G at 45°C and pH 7. The mean amounts of the relative amplitudes of the apparent rate constants are indicated. The lines are the results of the fit using parallel two-state reaction mechanism of the rate constants with the major amplitudes λ_1.

Table 12: Kinetic and equilibrium parameters of tendamistat variants at pH 7 and 25°C. All data were resulted from global fit of equilibrium and kinetic data. The microscopic rate constants were extrapolated to 0 M GdmCl. Data for wild type were taken from Schönbrunner et al.[173]

		k_f (s^{-1})	k_u (s^{-1})	m_f (kJ/molM)	$-m_u$ (kJ/molM)	$\alpha_D = m_f/m_{eq}$
25°C	**TS1**	0.01 ±0.01	$(2 \pm 1)\cdot 10^{-5}$	1.77 ±0.23	-(2.64 ±0.31)	0.40 ±0.09
	TS2	2.8 ±0.5	$(5 \pm 4)\cdot 10^{-3}$	4.32 ±0.54	-(0.09 ±0.59)	0.98 ±0.10
45°C	**TS1**	0.1 ±0.1	$(3 \pm 2)\cdot 10^{-3}$	3.32 ±0.83	-(2.23 ±0.24)	0.60 ±0.12
	TS2	3.3 ±0.3	$(7 \pm 1)\cdot 10^{-2}$	5.08 ±0.32	-(0.47 ±0.27)	0.91 ±0.09

Folding and stability of the tendamistat variants E38Q and D39A

The GdmCl-induced unfolding transitions of the tendamistat variants E38Q and D39A will be discussed in more detail in chapter 4.2.2.3. Both transition states were cooperative and were fitted assuming a two-state mechanism. The results of the two-state fits are given in Table 13. Both tendamistat variants are destabilized compared to wild type with a $\Delta\Delta G^0$ of 15.7 kJ/mol (E38Q) and 21.9 kJ/mol (D39A).

Table 13: Comparison of the Gibbs free energy and the m-value of tendamistat and the tendamistat variants E38Q and D39A at pH 7 and 25°C. The data are results from GdmCl-induced unfolding transition states assuming the two-state model. Data for wild type were taken from Schönbrunner et al.[173]

	ΔG^0 [kJ/mol]	m [kJ/(mol·M)]
Tendamistat[173]	-(35.9 ±0.1)	5.48 ±0.01
E38Q	-(20.2 ±2.6)	3.52 ±0.58
D39A	-(14.0 ±2.2)	4.12 ±0.59

The folding kinetics of E38Q and D39A were measured following the change of fluorescence signal above 320 nm after excitation at 276 nm. The refolding and unfolding kinetic traces can well be fitted to a sum of three exponentials as already observed for V36A and V36G (appendix 9.5). Comparison of refolding of both proteins reveals a deceleration of the rate constants of the main refolding phase from about 27 s^{-1} for E38Q to 3 s^{-1} for D39A (Figure 4-35). Interestingly, the second rate constant for E38Q with a relative amplitude of 10 % ($\lambda_3 \approx 2\ s^{-1}$) is accelerated compared to D39A, V36A and V36G, and has nearly the same value as observed for wild type and the other variants with an apparent two state behaviour ($\lambda_3 \approx 4\ s^{-1}$; chapter 4.2.2.1).

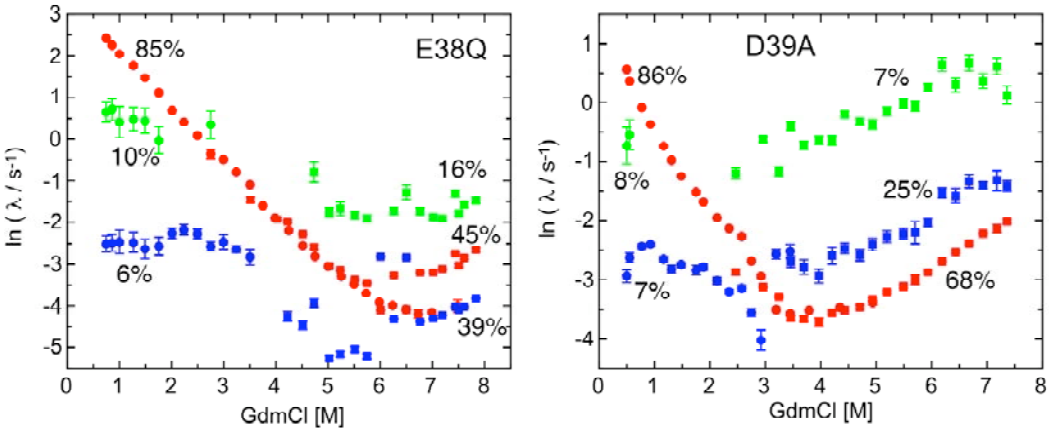

Figure 4-35: GdmCl dependence of the apparent rate constants of refolding (circle) and unfolding (square) of E38Q and D39A at 25°C and pH 7. The mean amounts of the relative amplitudes of the apparent rate constants are indicated.

Like observed for V36A and V36G, the three unfolding rate constants show similar denaturant dependences (Figure 4-35). The fastest unfolding rate constant is probably due to unfolding of native like intermediate as pointed out for V36A.

In Table 14 we compare the relative mean amplitudes and the stability of the four tendamistat variants V36A, V36G, E38Q and D39A. The fastest unfolding rate constant, which is due to unfolding of native like intermediate (N*)[174], has about twice the amount of relative amplitude for E38Q compared to the other three variants with about 7 % amplitude. The two most destabilized variants V36G and D39A have the same relative amplitude of 68 % for the slowest unfolding reaction. In contrast, the slowest unfolding reaction of the tendamistat variants V36A and E38Q have amplitudes of 43 and 39 %, whereas the major amplitudes correspond to the faster unfolding reaction. Interestingly, the ratio of the amplitudes for the two slow phases correlates with the protein stability.

Table 14: Relative mean amplitudes of the tendamistat variants with three unfolding phases.

	ΔG^0 (kJ/mol)	A_1 (%)	A_2 (%)	A_3 (%)
V36A	-16 ±2	49 ±3	43 ±3	8 ±1
V36G	-14 ±1	68 ±3	25 ±2	7 ±2
E38Q	-20 ±3	45 ±2	39 ±4	16 ±3
D39A	-14 ±2	68 ±6	25 ±6	7 ±1

Possible folding mechanism of tendamistat variant V36A

To elucidate the folding mechanism, we combined the results of direct folding kinetics at various GdmCl concentrations of the variant V36A at pH 7 with the results obtained from interrupted refolding and double-jump measurements. Figure 4-36 shows the results of all three measurements. The main question to solve the folding mechanism was to elucidate the origin of the three unfolding phases. With the interrupted refolding experiment we could clearly show that the fast unfolding phase with a relative amplitude of (8 ±1) % (Table 14) belongs to the unfolding reaction of the native-like intermediate N*[174] (Table 10 and Figure 4-29). The interrupted refolding experiment also revealed that the two slow-unfolding molecules refold into native molecule (Table 10 and Figure 4-29). Since no change of fluorescence signal was observed in the deadtime of the measurements for all four tendamistat variants with complex unfolding kinetics (appendix 9.5), we assume that the major refolding phase is caused by formation of native molecules from the unfolded polypeptide chain without transiently populated intermediate. Double-jump experiments confirm our previous assumption that the slow refolding phase belongs to the *cis-trans* prolyl-isomerization reaction (Figure 4-30). It also reveals that the major unfolding phase is probably due to the unfolding reaction of native molecules (Figure 4-30). No transiently populated intermediate was observed in double-jump experiments.

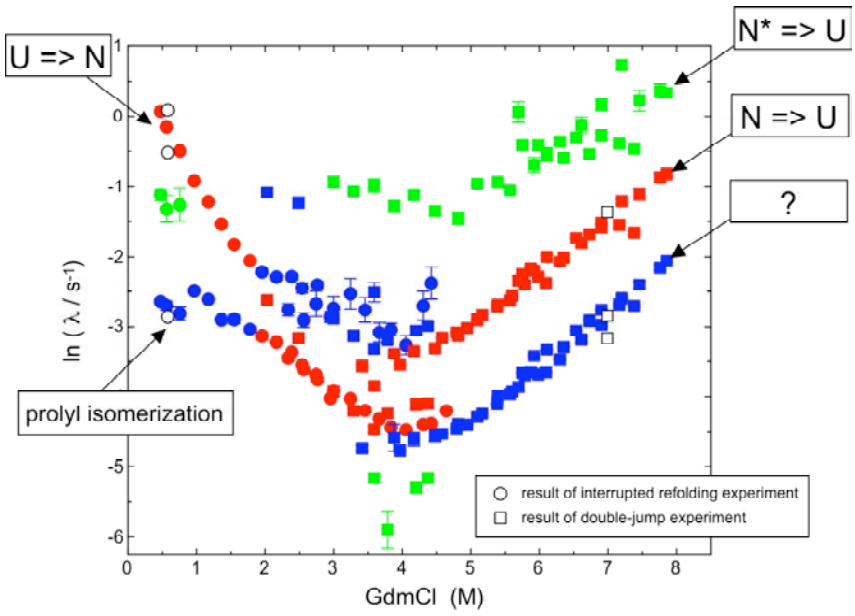

Figure 4-36: GdmCl dependence the apparent rate constants of refolding (circles) an unfolding (squares) of the tendamistat variant V36A at 25°C and pH 7. The results of the interrupted refolding experiment and double-jump experiment are indicated.

But what is the origin of the slow unfolding phase with relative amplitude of (43 ±3) %? A possible answer is either it is due to unfolding of native molecules to an intermediate or unfolding of an intermediate. Three possible pathways exist for folding with a single intermediate (chapter 1.3.3). Combination of our results of the tendamistat variant V36A and the observed upward curvature in unfolding of the variant V36G revealed a possible triangular mechanism:

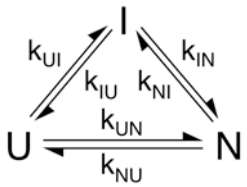

(4.13)

If $k_{UN} >> k_{UI}$ at low GdmCl concentration, then only the reaction U ⇒ N will be observed. For the unfolding reaction, two possible cases exist:

a) $k_{IU} >> k_{NU} > k_{NI}$: both reactions, N ⇒ U and N ⇒ I will be observed, followed by a fast interconversion of the intermediate to the unfolded polypeptide chain.

b) k_{NI} and $k_{IN} >> k_{NU} > k_{IU}$: the interconversion of native molecules and the intermediate is very fast compared to unfolding of N and I.

With both mechanisms we can explain the results of the kinetic data. However, up to now we cannot fit the data to one of the possible models. Thus, further investigations are necessary to solve the folding mechanism of all four proteins, which show complex unfolding kinetics.

4.2.2.3 Influence of Surface-Exposed Charges on the Stability of Tendamistat

Proteins are stabilized primarily by noncovalent interactions, such as hydrophobic, van der Waals, coulombic and hydrogen bonded interactions. There is a multitude of interactions, but all of them are weak. They must balance the loss of interactions with the aqueous solvent and must compensate for the enormous decrease in chain entropy upon folding. Thus, most proteins are only marginally stable. The dissection of the overall protein stability into individual components remains difficult, because interactions in proteins are often cooperative and thus any partitioning is ambiguous.[26,246] Rather than focusing on the contributions of certain types of interactions, it is more straightforward to concentrate on the contributions of individual residues or residue types to stability.[247]

The contributions of charged residues to protein stability are thought to be small, but there is a broad agreement between experimentalists and theoreticians that surface-exposed charged residues can be important for the stability of proteins.[246,248-252] In tendamistat, the surface-exposed C-terminal β-hairpin between the amino acids 37 and 40 is formed of primarily acidic amino acids like aspartic acid and glutamic acid (Figure 4-37). In contrast, the opposite turn between the amino acids 58 and 68 consists basic amino acids like arginine and histidine residues (Figure 4-14). To elucidate the influence of the acidic amino acids of the C-terminal β-hairpin on the total stability of tendamistat, we measured the stability of five loading variants: E38Q, D39N, D39A, D40N and E42Q.

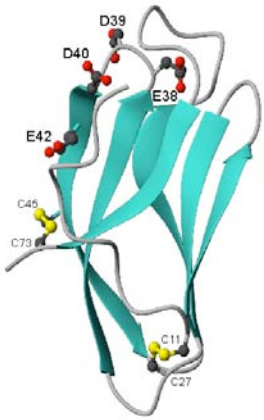

Figure 4-37: Schematic drawing of the structure of tendamistat. The disulfide bonds between Cys11-Cys27 and Cys45-Cys73 and the residues Glu38, Asp39, Asp40 and Glu42 are shown as ball-and-stick models. The figure was generated using MOLMOL[194].

Effect of acidic amino acid replacements on stability of tendamistat

The carboxylate group of Glu38, Asp39, Asp40 and Glu42 were substituted into an amide group to destroy the surface salt bridges. Additionally, Asp40 was substituted with an alanine. To obtain the stability of the tendamistat variants we measured the GdmCl-induced unfolding transitions at 25°C and pH 7.0 (Figure 4-38).

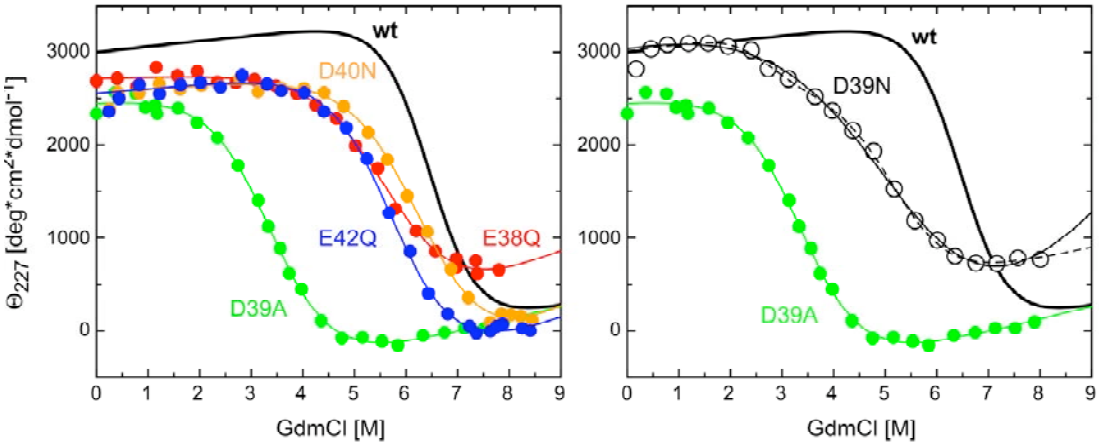

Figure 4-38: GdmCl-induced unfolding transition of the tendamistat variants E38Q, D39A, D39N, D40N and E42Q at pH 7 and 25°C monitored by ellipticity at 227 nm. Concentration was 10 µM in 100 mM cacodylic acid. The solid lines represent the analysis assuming the two-state model. The results are given in Table 15. The dotted line is the fit for the variant D39N assuming a three state model. The result is described in the text. Data for the fit of wild type was taken from Schönbrunner et al. [173].

The equilibrium unfolding transitions were cooperative without any apparent intermediate states and the data were fitted assuming a two-state mechanism except for the variant D39N (Figure 4-38). The results of the two-state fits are given in Table 15. The equilibrium unfolding transition of D39N could not be fitted well with a two-state mechanism (Figure 4-38). Thus, it was fitted assuming a three-state mechanism (Figure 4-38). The Gibbs free energy for the formation of an intermediate is ΔG^0 (U→I) = -(16.8 ±13.4) kJ/mol and with m (U→I) =(6.64 ±6.52) kJ/(mol·M). The interconversion of the intermediate to the native state is accompanied by a Gibbs free energy ΔG^0 (I→N) of -(23.2 ±12.8) kJ/mol and a m-value of (4.40 ±1.98) kJ/(mol·M). The results are accompanied by large errors due to the less well-defined denaturant dependent baseline of the intermediate state. Re-measuring the equilibrium unfolding transition with significant more data points would provide a better insight into a possible population of an intermediate.

Table 15: Comparison of the Gibbs free energy and the m-value of tendamistat and the tendamistat variants E38Q, D39A, D39N, D40N and E42Q at pH 7 and 25°C. The data are results from GdmCl-induced unfolding transition states assuming the two-state model. Data for wild type were taken from Schönbrunner et al.[173]

	ΔG° **[kJ/mol]**	**m** **[kJ/(mol·M)]**	**ΔΔG°** **[kJ/mol]**	**m_{wt} / $m_{variant}$**
Tendamistat[173]	-(35.9 ±0.1)	5.48 ±0.01	--	--
E38Q	-(20.2 ±2.6)	3.52 ±0.58	15.7 ±2.7	0.64
D39N	-(12.5 ±1.9)	2.26 ±0.48	23.4 ±2.0	0.41
D39A	-(14.0 ±2.2)	4.12 ±0.59	21.9 ±2.3	0.75
D40N	-(22.7 ±1.8)	3.55 ±0.37	13.2 ±1.9	0.65
E42Q	-(24.6 ±1.2)	4.27 ±0.24	11.3 ±1.3	0.78

The replacements of the acidic amino acids in the C-terminal β-turn significantly reduce the protein stability at all four positions (Table 15). The replacing of the carboxyl group with an amide group of the residues Glu38, Asp40 and Glu42 destabilizes the protein of about 11 - 16 kJ/mol. In contrast, the replacing and removing of the carboxyl group of the residue Asp39 destabilize the protein significantly compared to wild type.

For all variants a significantly decrease of the m-value are observed (Table 15). For the variants E38Q, D39A, D40N and E42Q the m-value decreases between 64 and 78 %. The significant low m-value for D39N could also be an indication that the two-state model is not valid to analyze the GdmCl-induced unfolding transition. An increase or decrease in the m-value reflects a change in the compactness of the folded and/or unfolded structure due to the proportionality of the m_{eq}-values to the change in solvent accessible surface area (ASA) upon unfolding of the protein.[23] The substitution of the carboxylate group decreases therefore the change in ASA. The reducing of the overall net charge of the native protein leads to a more compact structure.

Study of possible salt bridges of surface-exposed charges in tendamistat

To search for possible salt bridges, mean distances between the acidic amino acids Glu38, Asp39, Asp40, Glu42 and basic amino acids in the protein were determined using the program MOLMOL[194]. The atomic coordinates of tendamistat were obtained from the Brookhaven Protein Databank.[166,168] The three-dimensional structure of tendamistat was determined by NMR spectroscopy in aqueous solution[166] and by X-ray crystallography in single crystals[168]. There is a very good agreement between

coordinates determined by these two methods with only subtle differences in the degree of disorder for residues near the solvent-exposed surface of the protein.[169] Near the protein surface areas the solution structure appears more disordered than the crystal structure.

To obtain possible salt bridges, the distances between the oxygen atoms of the carboxyl group of the acidic amino acids and the nitrogen atoms of basic amino acids were calculated. The calculations were done for the structure obtained by X-ray[168] and the different solution structures obtained by NMR spectroscopy[166]. The nine solution structures differ slightly in the orientation of the side chains. The relevant distances resulting of this study are reported in Table 16. Distances between oppositely charged groups shorter than 4 Å are converted into stabilizing salt-bridges in Figure 4-39.

Table 16: Distances (Å, smaller than 4 Å) between the oxygen atoms of the carboxyl groups of the acidic amino acids Glu38, Asp39, Asp40 and Glu42 and the nitrogen atoms of the basic amino acids Arg 68, His64 and Lys34.

acidic	**basic amino acids**			
amino acid	**X-ray**	**Distance [Å]**	**NMR**	**Distance [Å]**
Glu38	--	--	Arg68	2.49 – 4.00 (6)[1]
Asp39	His64	2.87	His64	2.49 – 3.26 (7)[1]
Asp40	Arg68	2.97 – 3.06	--	--
Glu42	Lys34	2.83	Lys34	2.68 - 3.85 (3)[1]

[1] In brackets are the numbers of structures with a distance smaller than 4 Å.

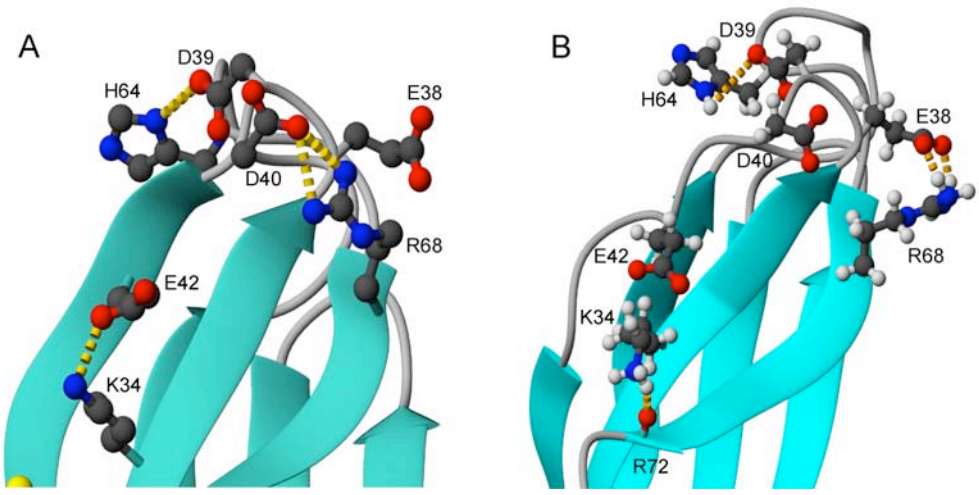

Figure 4-39: Schematic drawing of the structure of tendamistat based on the (A) X-ray[168] and (B) NMR[166] data, respectively. The residues Glu38, Asp39, Asp40, Glu42, Lys34, His64 and Arg68 and the backbone carbonyl oxygen of Arg72 are shown as ball-and-stick models. The possible salt bridges and H-bonds, respectively, are indicated as dotted lines. The figure was generated using MOLMOL[194].

From comparison of the results of the distances found in the solution and crystal structure can be concluded that a surface salt bridge is formed between the Asp39 and His64 (Table 16 and Figure 4-39). The longest distance between the carbonyl group of Asp39 and the nitrogen atom Nδ1 of the imidazole side chain of His64 are 4.77 Å.

In the X-ray structure, a salt bridge is formed between Arg68 and Asp40 (Figure 4-39A), whereas these interactions are not found in the solution structure measured by NMR spectroscopy (Table 16). The distance between Arg68 and Glu38 are significantly smaller in solution than between Arg68 and Glu38 (Table 16 and Figure 4-39B). The distances between Arg68 and Glu38 found in X-ray structure is 4.30 Å. The question arose of a possible salt bridge triad between Glu38-Arg68-Asp40 with the guanido group of Arg68 switching between the two carboxyl groups. However, uncertainties and artifacts of the measurements could explain the difference.

Small distances between Glu42 and Lys34 are found in the structure solved by X-ray diffraction and in three of the nine NMR structures (Table 16 and Figure 4-39A). In the other six solution structures a H-bond was found between one of the hydrogen bonds of the methylene group of Lys34 and the backbone carbonyl oxygen of Arg72 with a distance of 1.69 Å and an angle of 160.4° (Figure 4-39B).

Stabilization effect of surface-exposed charges in tendamistat

The contribution of electrostatic interactions to protein stability has been controversial since it was first proposed by Perutz & Raidt in 1975.[253] It has been argued that solvent-exposed ion pairs do not stabilize proteins because of the large desolvation penalty and entropic cost of fixing two charged side-chains.[252] However, there is growing evidence to support the role of electrostatic interactions in the thermostability of proteins.[247,249,251,252,254,255]

Analyses of thermophilic proteins revealed more charged residues at their surfaces than their mesophilic homologues.[256] This renewed the interest in ion pairs at the protein surface. Various mutational and theoretical analyses support the influence of surface-exposed charged residues to protein stability.[248,250,254,257-261]

A simplistic approach to determine the contributions of the surfaced-exposed charged residues to protein stability is to determine distances in protein structures shorter than a certain cut-off and translate them into stabilizing ion pairs. However, interactions between charges of opposite sign are, in general, not very effective since the enthalpic gain is balanced with a loss of entropy due to mobility restrictions in the side chains.[252]

In fact, the surface charges in thermophilic proteins are apparently arranged as ion networks rather than as isolated ion pairs. This finding is expected due to the long-range nature of Coulombic interactions and the high mobility of charged groups at the protein surface[252]. In this ion networks the ion charges are optimally placed to improve the overall electrostatic interactions.

In tendamistat, the analysis of distances of the surface-exposed acidic amino acids of the C-terminal β-hairpin revealed a possible salt bridge triad between Glu38, Arg68 and Asp39. Such an ion-network can have a stabilizing effect on the stability of tendamistat. Indeed, substitutions of the carboxyl group with an amide group of the two acidic amino acids have the same destabilizing effect on the protein. A similar decrease in protein stability was observed for E42Q. Here, the possible salt-bridge partner Lys34 is able to form a H-bond with the backbone carbonyl oxygen of Arg72 and can thus compensate the loss of the salt-bridge with Asp42. The strongest stabilizing effect has Asp39, which make strong interaction with His64 found in all structures.

To further elucidate the contribution of the single acidic amino acids to the stability of tendamistat, determination of the protein stability with variation of pH, salt concentrations and temperature would be useful.

Effect of replacement of the acidic amino acids Glu38 and Asp39 on the folding kinetics of tendamistat

The folding kinetics of the tendamistat variants E38Q and D39A were measured at 25°C and pH 7. The refolding kinetic traces can well be fitted to a sum of three exponentials as for wild type (appendix 9.5). As previously shown for wild type[84,173], the two slow components with an amount of approximate 8 % and 6 % of the fluorescence amplitudes are due to non-prolyl and prolyl isomerization, respectively (appendix 9.5). In contrast to wild type, a sum of three exponential functions is needed to describe the unfolding kinetic traces (appendix 9.5). This additional unfolding phase was also observed for the unfolding kinetics for the tendamistat variants V36A and V36G and will be discussed in detail in chapter 4.2.2.2. On the following, we will focus our analysis of the refolding data on the main refolding phase, which correspond to folding of the unfolding molecule with all native prolyl and non-prolyl peptide bond isomers (Figure 4-40).

Comparison of the kinetic data reveals a deceleration of the refolding rates for E38Q and D39A compared to wild type (Figure 4-40). The apparent rate constant, λ, at 1 M GdmCl decrease from 15.4 s^{-1} for wild type[173] upon replacement of the carboxyl group with an amide group at position 38 to (7.7 ±0.2) s^{-1}. Refolding of the variant D39A is significantly decelerated with λ = (0.69 ±0.02) s^{-1}. Removing of the carboxyl group seems to have a much stronger effect on the refolding rates than replacing with an amide group. However, as discussed above, analysis of the equilibrium transition of the variant D39N reveals also a strong destabilizing effect (Figure 4-38). The strong influence of the removing of the surface exposed carboxyl group on the refolding rate could be an indication of an early formation of the interaction between Asp39 and His64 (Figure 4-39) during folding of tendamistat. The replacement of the carboxyl group in Glu38 has less effect on the refolding rates of tendamistat. This may be due to a compensating effect of formation of the salt bridge by Asp40 in the possible salt bridge triad Glu38-Arg68-Asp40 (Figure 4-39 and Table 16). The decelerations of the refolding rate combined with a decrease in stability are an indication of an early formation of the C-terminal β-hairpin. However, the origin of the additional unfolding phase is still not solved and thus, the exact folding mechanism of these variants are still unknown.

A careful investigation of the folding mechanism of all five salt-deficient variants under various conditions such as variation of pH and salt concentrations would provide a more detailed insight into the influence of the surface-exposed charges on folding of tendamistat.

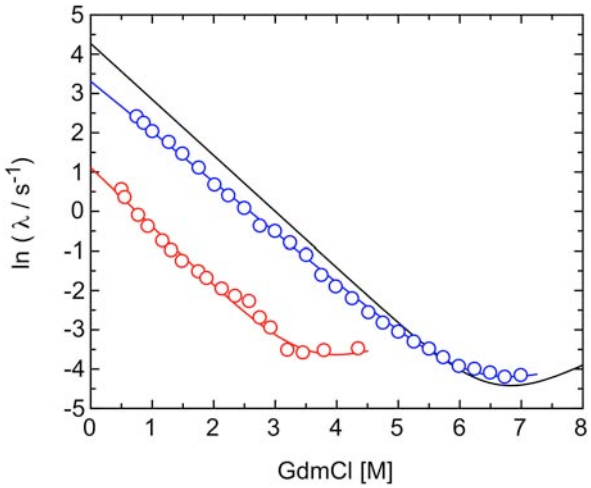

Figure 4-40: GdmCl-dependence of the refolding rates of the tendamistat variants E38Q (○) and D39A (○) at pH 7 and 25°C. Only the rate constant with the major amplitude is plotted. The solid line represent the fit of tendamistat wild type taken from Schönbrunner et al.[173].

4.2.3 Effect of Sodium Sulfate on the Folding Reaction of the Tendamistat Variants L14A and N25A

Stabilization of proteins upon addition of salts was first described in 1888, when Hofmeister studied the precipitation of proteins from whole egg white by various salts.[262] He found the regular series of anions and cations that bears his name. One of the salts, where the stabilization effect is described in detail, is sodium sulfate.[263,264] The stabilization of folded states in proteins with sodium sulfate is mainly due to two mechanism.[263] The first mechanism is reduction of the net positive charge on proteins by specific anion binding to shield the charge repulsion. However, the most important mechanism is the effect of sodium sulfate on water, which enhances hydrophobic interactions and stabilize the native structure of proteins.

The denaturant dependence of the folding rate constant of tendamistat shows a pronounced curvature in the presence of sodium sulfate at low denaturant concentrations without evidence of intermediates.[265] The curvature is unlikely to be an unspecific effect of the salt due to the observation of linear Chevron plots in the presence of sodium sulfate described in literature.[110,178,266]

To further investigate the effect of sodium sulfate on tendamistat folding, the stability and folding of the tendamistat variants L14A and N25A were studied in the presence of sodium sulfate at pH 7 and 25°C. L14A and N25A are the two most destabilized tendamistat variants with intact disulfide bridges (chapter 4.2.2.1). The folding kinetics at various temperatures of both proteins have been analyzed in detail and no deviation of the linear denaturant concentrations dependence of the rate constants could be observed (chapter 3.1). In addition, the effect of sodium sulfate on the folding rates was compared with tendamistat and the proline free variant.

Effect of sodium sulfate on folding and stability of N25A

The effect of sodium sulfate on stability and folding of N25A was measured at 4 different concentrations of sodium sulfate: 0.125, 0.25, 0.35 and 0.45 M. The addition of sodium sulfate leads to a shift of the GdmCl-induced unfolding transition midpoints from 2.0 M GdmCl in the absence of salt to 3.1 M GdmCl upon addition of 0.45 M sodium sulfate (Figure 4-41). The addition of 0.45 M sodium sulfate stabilizes the protein for a $\Delta\Delta G^0$ of 5.6 kJ/mol (Table 17), which is only halve of the stabilization effect as observed for L14A (Table 18). The m_{eq}-values decrease upon addition of

sodium sulfate for about 1 kJ/(mol·M) (Table 17). This is in contrast to the effect of sodium sulfate on L14A, where an increase of the change in ASA is observed (Figure 4-43, Table 18).

Analysis of the kinetic data of the main refolding and unfolding phases, which correspond to folding and unfolding with all native prolyl and non-prolyl bonds isomers,[84,173,174] reveals linear Chevron plots as expected for a two-state folding reaction (Figure 4-41). Addition of sodium sulfate leads to an increase of the folding rate constants and a deceleration of the unfolding reaction is observed (Figure 4-41). The equilibrium and kinetic data are fitted globally using a two-state model and the results are given in Table 17.

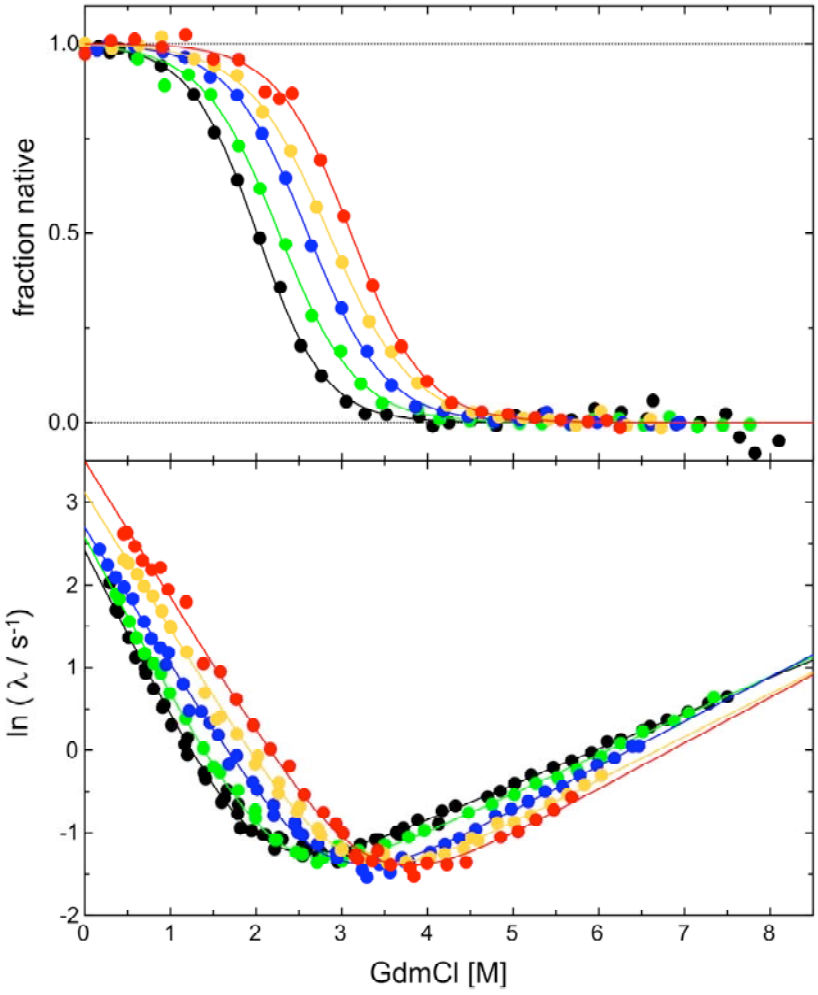

Figure 4-41: GdmCl-induced unfolding transition and GdmCl-dependence of the refolding and unfolding rates of the tendamistat variant N25A at pH 7 and 25°C in the absence (●) and in the presence of 0.125 (●), 0.25 (●), 0.35 (●) and of 0.45 M (●) sodium sulfate. The GdmCl-induced unfolding transition was monitored by ellipticity at 227 nm with a concentration of 10 µM in 100 mM cacodylic acid. The lines represents the global analysis of kinetic and equilibrium data assuming the two-state model.

Table 17: Kinetic and equilibrium parameters of the tendamistat variant N25A at different sodium sulfate concentrations. All data are results from the global fit of equilibrium and kinetic data.

Na_2SO_4 (M)	k_f (s^{-1})	k_u (s^{-1})	ΔG^0 (kJ/mol)	m_f (kJ/molM)	m_u (kJ/molM)	m_{eq} (kJ/molM)	$\alpha_D = m_f/m_{eq}$
0	11.1 ±0.4	(7.6 ±0.6)·10^{-2}	-12.35 ±0.10	5.08 ±0.08	1.07 ±0.14	6.15 ±0.07	0.83 ±0.02
0.125	13.1 ±0.6	(5.2 ±0.5)·10^{-2}	-13.55 ±0.11	4.78 ±0.07	1.17 ±0.14	5.95 ±0.07	0.80 ±0.02
0.25	14.8 ±0.4	(3.0 ±0.3)·10^{-2}	-15.19 ±0.16	4.13 ±0.05	1.34 ±0.10	5.47 ±0.05	0.76 ±0.02
0.35	22.7 ±0.9	(2.6 ±0.3)·10^{-2}	-16.40 ±0.11	4.13 ±0.05	1.29 ±0.09	5.43 ±0.04	0.76 ±0.01
0.45	33.0 ±1.5	(5.2 ±0.5)·10^{-2}	-18.05 ±0.45	4.10 ±0.07	1.37 ±0.16	5.47 ±0.09	0.75 ±0.02

Figure 4-42 shows the effect of increasing stability upon addition of sodium sulfate on α_D and on the *m*-values. With increasing sodium sulfate concentration the α_D-values decrease till it reach a value of about 0.76 and becomes salt-independent above 0.25 M sodium sulfate (Figure 4-42A and C, Table 17). Analysis of the *m*-values reveals that increasing the sodium sulfate concentration till 0.25 M m_{eq} and m_f decreases, whereas m_u increases with increasing protein stability (Figure 4-42B and C). Above 0.25 M sodium sulfate, m_{eq}, m_f and m_u do not change significantly (Figure 4-42B and C). Comparison with the results of the structure-denaturant perturbation (chapter 4.2.2.1) reveals that a change of the rate-limiting step occurs due to the stronger stabilization of the late transition state compared to the early transition barrier upon addition of sodium sulfate (Figure 4-42C and D). The change in α_D upon stabilization of the protein is in accordance with our previous assumption that N25A folds with the late-transition state as the rate-limiting step.

The effect of sodium sulfate on protein stability cannot be analyzed using rate-equilibrium free energy relationships due to the involvement of bimolecular interactions.[267]

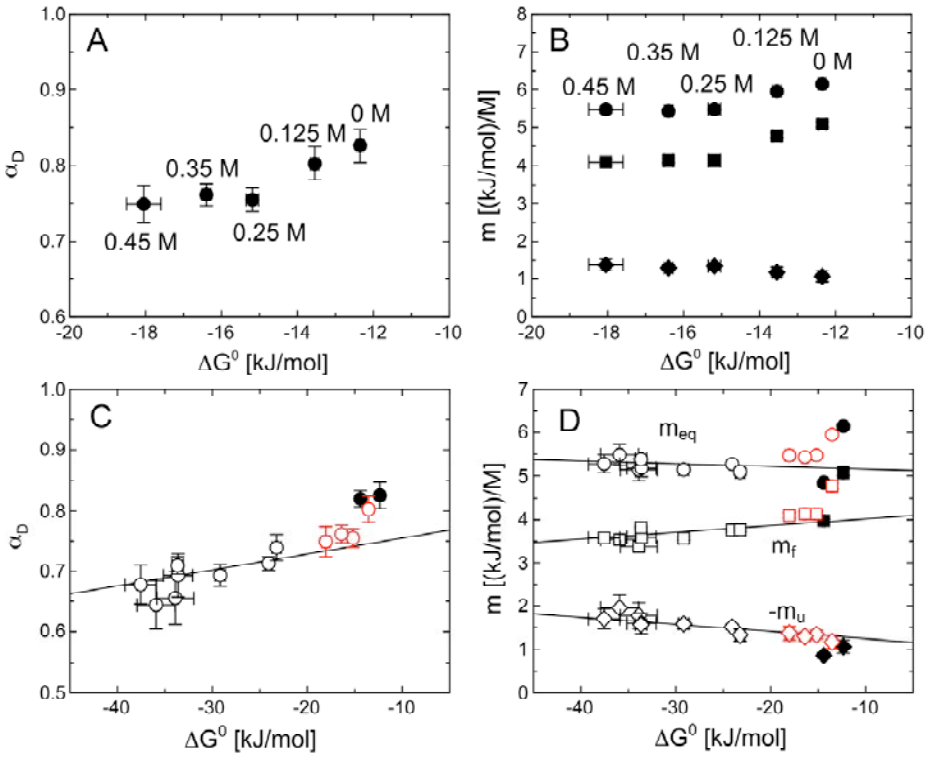

Figure 4-42: (A, B) Effect of ΔG° on α_D and on m_{eq} (●), m_f (■) and m_u (◆) for N25A in the absence and the presence of various sodium sulfate concentrations. The data are taken from global fits of the equilibrium and kinetic data. (C, D) Comparison of the effect of ΔG° on α_D and on m_{eq} (circles), m_f (squares) and m_u (diamonds) for the structure-denaturant perturbation on the early transition state (open symbols) and on the late transition state (filled symbols) and for the perturbation with sodium sulfate and denaturant (red symbols).

Effect of sodium sulfate on folding and stability of L14A

Figure 4-43 shows the GdmCl-induced unfolding transitions of L14A in the absence and presence of 0.5 M sodium sulfate. A shift of the transition midpoint from 2.8 M to 3.6 M GdmCl occurs upon addition of salt. The data were fitted assuming a two-state mechanism (Table 18).

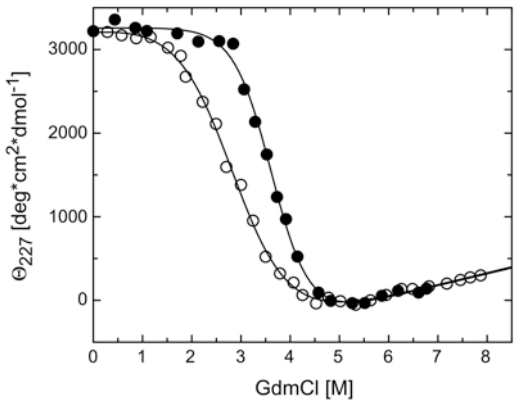

Figure 4-43: GdmCl-induced unfolding transition of the tendamistat variant L14A at pH 7 and 25°C in the absence (○) and in the presence (●) of 0.5 M sodium sulfate monitored by ellipticity at 227 nm. Concentration was 10 µM in 100 mM cacodylic acid. The line represents the analysis assuming the two-state model. The results are given in Table 18.

Table 18: Comparison of the Gibbs free energy and the m-value of the tendamistat variant L14A at pH 7 and 25°C in the presence and absence of sodium sulfate. The data are results from GdmCl-induced unfolding transition states.

Na_2SO_4 [M]	ΔG^0 [kJ/mol]	m_{eq} [kJ/(mol·M)]
0	-(14.4 ±1.0)	4.85 ±0.03
0.5	-(22.1 ±0.8)	6.00 ±0.48

The addition of 0.5 M sodium sulfate stabilize the protein with a $\Delta\Delta G^0$ = 7.7 kJ/mol and increase the m_{eq}-value for about 1 kJ/(molM) (Table 18). Due to the proportionality of the m_{eq}-values to the change in solvent accessible surface area (ASA) upon unfolding of the protein,[23] an increase or decrease in the m_{eq}-value reflect a change in the compactness of the folded and/or unfolded structure. The change in ΔASA caused by the addition of sodium sulfate is most likely due to changes of the unfolded state.

The refolding kinetics of L14A were measured following the change of the CD (Figure 4-44B) and fluorescence (Figure 4-44C, D) signal, respectively. The change in the fluorescence signal was measured by a 11-fold (Figure 4-44C) and 26-fold (Figure 4-44D) dilution, respectively, of unfolded protein into various GdmCl concentrations. The unfolding kinetics were measured only by monitoring the change of fluorescence signal by a 11-fold dilution of native protein. The unfolding kinetic traces can well be fitted to a sum of two exponential and the refolding ones to the sum of three exponentials, as in the absence of sodium sulfate (chapter 4.2.2.1, Appendix 9.4). On the following, we will focus our analysis of the kinetic data on the main refolding and unfolding phase, which corresponds to folding with all native prolyl and non-prolyl peptide bond isomers (Figure 4-44).

Upon addition of 0.5 M sodium sulfate to the folding conditions a significant curvature is observed at low denaturant concentration (Figure 4-44A). This leads to nearly identical folding rates as in the absence of sodium sulfate (Table 19). In a number of proteins the addition of sodium sulfate was found to increase the population of transient folding intermediates.[264,266,268-270] This is commonly correlated with a large fluorescence change in the deadtime of refolding. The initial values for both spectroscopic probes (Figure 4-44 B, C, D) do not show any burst phase at low denaturant concentrations and thus argue against a populated intermediate or collapsed state. These data support a three-state model with a high-energy intermediate for folding of L14A in the presence of sodium sulfate (Figure 4-44A).

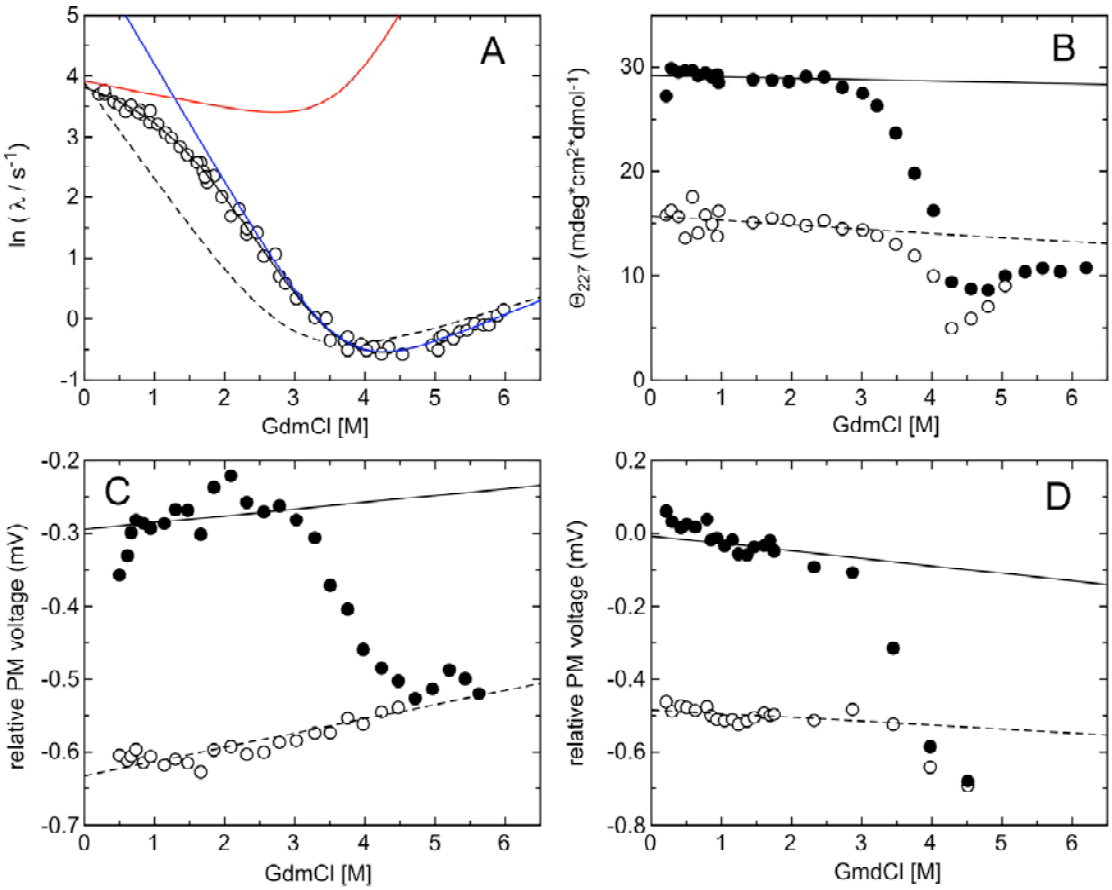

Figure 4-44: GdmCl dependence of folding of L14A at 25°C and pH 7 in the presence of 0.5 M sodium sulfate. (A) Apparent rate constant of refolding and unfolding. Only the rate constant with the major amplitude is plotted. The black line represents non-linear least-squares fits of the data according to the three-state model with a metastable intermediate. The result of the fit is given in Table 19. The red and blue lines represent the GdmCl-dependence of folding kinetics for folding limited by the early transition state (red) and late transition state (blue), respectively. The dashed line represent the fit of L14A in the absence of sodium sulfate. (B), (C), (D) Final (●) and initial values (○), respectively for the refolding kinetics. The kinetics was measured monitoring the change in ellipticity (D) and the change in fluorescence after initiation by 11-fold (B) and 26-fold (C) dilution, respectively, of unfolded protein into various denaturant concentrations.

Table 19: Kinetic parameters for the tendamistat variant L14A with and without sodium sulfate

	m_f [kJ/(mol·M)]	m_u [kJ/(mol·M)]	k_f [s^{-1}]	k_u [s^{-1}]	α_D
0.5 M Na_2SO_4					
early TS	0.55 ±0.26	-(5.45 ±0.12)	50 ±2	(7 ±2)·10^{-3}	0.09 ±0.05
late TS	4.83 ±0.43	-(1.17 ±0.05)	463 ±93	(63 ±7)·10^{-3}	0.80 ±0.14
0 M Na_2SO_4	3.98 ±0.04	-(0.87 ±0.07)	49 ±1	(146 ±7)·10^{-3}	0.82 ±0.01

The GdmCl-dependence of the observed rate constants and the GdmCl-induced unfolding transition were fitted globally and the results are given in Table 19. The results reveal that the solvent accessibility of the late transition state in the presence of 0.5 M sodium sulfate with $\alpha_D = 0.80$ is nearly identical to the α_D-value (= 0.82) of the transition state in the absence of sodium sulfate. The solvent accessibility of the early transition state ($\alpha_D = 0.09$) is significantly low indicating an unfolded-like transition state. The fit yields identical k_f –values in the presence and absence of sodium sulfate and thus the same activation free energy for folding, $\Delta G_f^{0\ddagger}$, with about 36 kJ/mol using a pre-exponential factor of 10^8 s^{-1} (Figure 4-35 and Table 19). The early transition state is 5.5 kJ/mol higher in free energy than the late transition state. At 1.3 M GdmCl concentration, the two barriers have identical free energies and the rate-limiting barrier changes from the early transition state to the late transition state.

The very low α_D-value arise the question after the origin of the curvature. Is it due to a change of the rate-limiting step or has it another origin? To answer this question we compared the effect of sodium sulfate on tendamistat folding.

Effect of sodium sulfate on the refolding reaction

Comparison of the effect of sodium sulfate on the refolding rates of tendamistat wild type[265], the proline free variant[265] and L14A reveals nearly identical k_f values in the range from 44 to 50 s^{-1} at zero denaturant (Figure 4-45). Thus, the activation free energy for folding, $\Delta G_f^{0\ddagger}$, is about 36 kJ/mol using a pre-exponential factor of 10^8 s^{-1}. All three proteins show a significant curvature nearly in the same range. In contrast, N25A shows a perfectly linear refolding branch with a k_f of 33 s^{-1} upon addition of 0.45 M sodium sulfate.

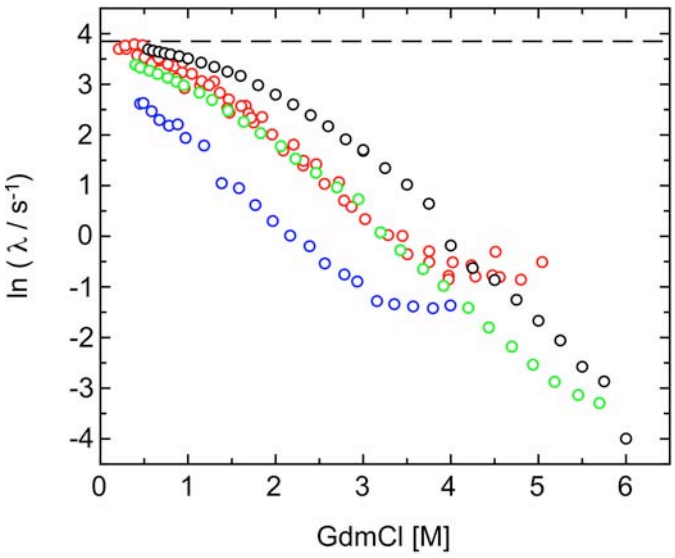

Figure 4-45: Comparison of the apparent rate constant of refolding at pH 7.0 and 25°C for tendamistat wild type (black), for a proline-free variant (green) and for L14A (red) in the presence of 0.5 M Na_2SO_4 and for N25A (blue) in the presence of 0.45 M Na_2SO_4. Only the rate constant with the major amplitude is plotted. The dashed line represent the maximum refolding rate of $\lambda = 50\ s^{-1}$. The data for tendamistat wild type and the proline-free variant was from ref.[265]

What is the origin of the non-linear GdmCl dependence of the folding rate constants in the presence of sodium sulfate? None of the proteins show a burst phase and the curvature is identical over a wide pH-range but temperature-dependent.[265] Due to the linear Chevron plots for N25A it is unlikely an unspecific effect of sodium sulfate.

The rate of folding of tendamistat seems to be limited upon addition of sodium sulfate with a maximal folding rate of about 20 ms. Analysis of the effect of point mutation on folding revealed that only the tendamistat variant L44A folds faster than wild type with a rate of about 10 ms (chapter 4.2.2.1). Folding of tendamistat seems to be limited by intrinsic dynamic. This could be due to the two disulfide bonds, which reduce conformational freedom.

Further investigations are necessary to understand the influence of sodium sulfate and to elucidate the origin of the folding limit in tendamistat.

Materials and Methods

Isolation and purification of tendamistat variants

Tendamistat variants were expressed in *Streptomyces lividans* and purified as described by Haas-Lauterbach *et al.*[242] The plasmids are gifts from Prof. Dr. Joachim W. Engels and Dr. Hüseyin Aygün. The mass was confirmed by electrospray ionization mass spectroscopy. The molecular masses for the mutated proteins are: Tendamistat wild type, 7961; S10M, 8005; L14A, 7919; L14V, 7947; R19L, 7918; S21A, 7945; S21G, 7931; N25A, 7918; V31A, 7933; T32A, 7931; V36A, 7933; V36G, 7919; E38Q, 7960; D39A, 7917; D39N, 7960; D40N, 7960; E42Q, 7960; L44A, 7919; I61M, 7979. Protein concentration was determined by UV absorption measurements using an absorption coefficient $A_{276}^{0.1\%}$ = 1.61 for tendamistat wild type and mutated proteins.[162]

Spectroscopic Techniques

Fluorescence spectra were recorded on a Aminco-Bowman fluorimeter with a thermostated cell holder and magnetic stirrer. The excitation wavelength was 276 nm. Protein concentrations were 5 μM in 10 mM KP_i at pH 7.

CD spectra were recorded in an Aviv 62A DS spectropolarimeter. Protein concentrations were 20 μM in 10 mM KP_i at pH 7. The ellipticity was measured in a thermostatted 1 mm cell.

Equilibrium unfolding transitions

The GdmCl-induced equilibrium transitions were monitored by the change in ellipticity at 227 nm in an Aviv 62A DS spectropolarimeter. Protein concentrations were 10 μM in 100 mM cacodylic acid. Samples were incubated for at least two hours before measurements. The ellipticity was measured in a thermostatted 1 cm cell.

The data were fit based on the two-state model and a linear dependence of the free energy of folding on the GdmCl concentration following the procedure described by Santoro & Bolen.[131] This yields the free energy in the absence of denaturant ($\Delta G_{H_2O}^0$) and the associated *m*-value.

Kinetic measurements

Fast refolding and unfolding kinetics were measured in an Applied Photophysics SX.18MV or π*-180 stopped-flow instrument. The change in fluorescence above 320 nm after excitation at 276 nm and the change in ellipticity at 227 nm, respectively,

were monitored. Unfolding or refolding was initiated by 11- and 26-fold dilution, respectively, of native or unfolded protein into various denaturant concentrations. Slow reactions were additionally measured by manual mixing and monitored by the change in fluorescence at 340 nm after excitation at 276 nm in an Aminco-Bowman Fluorimeter. Under conditions where the reactions could be measured by manual-mixing and by stopped-flow mixing, both methods gave identical rate constants. The final protein concentration for fluorescence and CD measurements were 3.8 and 10 μM, respectively.

Interrupted refolding experiments

The formation of native protein during refolding was monitored by stopped-flow interrupted refolding experiments at 25°C as described.[121,122] Unfolded protein at 3.6 M GdmCl in 10 mM glycine (pH 2) was diluted sixfold into final conditions of 0.6 M GdmCl, 100 mM cacodylic acid (pH 7) to initiate refolding. After various time (t_i), refolding was interrupted by transferring the solution into final conditions of 6.9 M GdmCl, 100 mM cacodylic acid (pH 7), and the resulting unfolding kinetic was monitored. Under these conditions tendamistat unfolds with three rate constants. The amplitude of these unfolding reactions were used as a measure for the amount of native protein that was present after the time t_i when refolding was interrupted.

Double jump measurements

The formation of the refolding phases of tendamistat at pH 7 and pH 2 were followed by double jump experiments.[78] Tendamistat in 1 M GdmCl, 100 mM cacodylic acid (pH 7), was first unfolded in 8.2 M GdmCl, 100 mM cacodylic acid (pH 7) to yield a final GdmCl concentration of 7.0 M. After various times of unfolding the solution was diluted sixfold into final refolding conditions of 1.2 M GdmCl, 100 mM cacodylic acid (pH 7), and the resulting refolding kinetics were monitored.

Analogously, double jump at pH 2 was measured. Therefore, tendamistat in 1 M GdmCl, 5 mM cacodylic acid (pH 7), was diluted sixfold into 8.2 M GdmCl, 10 mM glycine (pH 1.65) to a final GdmCl concentration of 7 M to a pH 2. After various times t_i, unfolding was interrupted by a second sixfold mixing step into refolding conditions of 100 mM cacodylic acid (pH 7) to a final concentration of 1.2 M GdmCl (pH 7).

Analysis of the kinetic data

The free energies of activation for folding ($\Delta G_f^{0\ddagger}$) and unfolding ($\Delta G_u^{0\ddagger}$) were calculated using transition state theory:[271]

$$k = k_0 \cdot e^{-\Delta G^{0\ddagger}/\mathrm{RT}} \tag{4.14}$$

where the pre-exponential factor, k_0 represents the maximum rate constant for protein folding in the absence of free energy barriers. This value was measured to be in the order of 10^7-10^8 s^{-1}.[49] A value of 10^8 s^{-1} was used. The pre-exponential factor was assumed to be temperature independent and does not change upon mutation.

The GdmCl dependence of the apparent rate constant (λ) for folding/unfolding was analyzed by using the two-state model with:

$$U \underset{k_u}{\overset{k_f}{\rightleftharpoons}} N \tag{4.15}$$

$$\lambda = k_f + k_u \tag{4.16}$$

$$\ln k_{f,u} = \ln k_{f,u}^{H_2O} - \frac{m_{f,u}}{\mathrm{RT}}[denaturant] \tag{4.17}$$

For the sequential three-state model with high-energy intermediate the apparent rate constant was analyzed according to following equation:[110]

$$U \underset{k_{IU}}{\overset{k_{UI}}{\rightleftharpoons}} I \underset{k_{NI}}{\overset{k_{IN}}{\rightleftharpoons}} N \tag{4.18}$$

$$\lambda_{1,2} = \frac{-B \pm \sqrt{B^2 - 4C}}{2} \tag{4.19}$$

with

$$B = -(k_{UI} + k_{IU} + k_{IN} + k_{NI}) \tag{4.20}$$
$$C = k_{UI} \cdot (k_{IN} + k_{NI}) + k_{IU} \cdot k_{NI}$$

The stability of the high-energy intermediate I cannot be determined, since it does not become populated, but the difference in free energy between both transition states ($\Delta G^0_{TS2/TS1}$) can be obtained. Therefore, the fitting of the data to the analytical solutions of the three-state model (equation (4.20)) allows the determination of k_{UI} and k_{NI} and their denaturant dependencies m_{UI} and m_{NI}, respectively. Only the ratios k_{IN}/k_{IU} and m_{IN}-m_{IU} are defined, which have to be used for data fitting.[110] Thus, k_f and k_u for the first transition state is given by:

$$k_f(TS1) = k_{UI} = k_0 e^{-\Delta G_f^{\ddagger}(TS1)/RT}$$
$$m_f(TS1) = m_{UI} \tag{4.21}$$

$$k_u(TS1) = \frac{k_{NI}}{k_{IN}} k_{IU} = k_{NI}\left(\frac{k_{IN}}{k_{IU}}\right)^{-1} = k_u(TS2)\left(\frac{k_{IN}}{k_{IU}}\right)^{-1}$$
$$m_u(TS1) = m_{IU} - m_{IN} + m_{NI} \tag{4.22}$$

In analogy, k_f and k_u for the second transition state can be expressed as:

$$k_f(TS2) = \frac{k_{UI}}{k_{IU}} k_{IN} = k_{UI} \frac{k_{IN}}{k_{IU}} = k_f(TS1) \frac{k_{IN}}{k_{IU}}$$
$$m_f(TS2) = m_{UI} + m_{IN} - m_{IU} \tag{4.23}$$

$$k_u(TS2) = k_{NI} = k_0 e^{-\Delta G_u^{\ddagger}(TS2)/RT}$$
$$m_u(TS2) = m_{NI} \tag{4.24}$$

Global analysis of kinetic and equilibrium data

For two-state folding the equilibrium constant (K) represents the ratio of the folding (k_f) and unfolding (k_u) rate constants ($K=k_f/k_u$). Comparison with equations (4.14), (4.17) and the relationship of the equilibrium constant (K) and the Gibbs free energy ($\Delta G^0 = -RT \ln K$) reveals at constant GdmCl concentration:

$$\Delta G_{eq}^0 = \Delta G_f^{0\ddagger} - \Delta G_u^{0\ddagger}$$
$$m_{eq} = m_f - m_u \tag{4.25}$$

These relationships were used for global fitting of the GdmCl dependence of equilibrium and kinetic data.

Determination of self- and cross-interaction parameters

A way to analyze the properties of the transition barriers is to measure the changes in activation free energy ($\Delta G^{0\ddagger}$) and in equilibrium free energy (ΔG^0) between the unfolded state and the native state upon addition of a perturbation ∂x.[123-125,272] To quantify the rate-equilibrium free energy relationships (REFERs) a proportionality constant can be defined:[124]

$$\alpha_x = \frac{\partial \Delta G^{0\ddagger} / \partial x}{\partial \Delta G^0 / \partial x}. \tag{4.26}$$

α_x is commonly used to obtain information on the structural properties of the transition state and it is a measure for the position of the transition state along the reaction

coordinate investigated by ∂x. The range of α_x is normally from 0 for an unfolded-like transition state to 1 for a native-like transition state.

To systematic analyze a shift in the position of the transition state along the reaction coordinate due to changes in equilibrium free energy upon addition of denaturant, the self-interaction parameter p_D was used.[148]

$$p_D = \frac{\partial \alpha_D}{\partial \Delta G_D^0} = \frac{\partial^2 \Delta G_f^{0\ddagger}}{\left(\partial \Delta G_D^0\right)^2} \tag{4.27}$$

A positive p_D-value indicates a movement of the transition state to the destabilized state according to Hammond or a change in the rate-limiting step, whereas anti-Hammond behaviour or parallel pathways could cause a negative value.[123]

To improve the sensitivity in the detection of transition state movements we analyzed the position of the transition state along the denaturant-induced reaction coordinate under different ΔG^0 caused by a second perturbation, such as structural changes: [148]

$$p_{DS} = \frac{\partial \alpha_D}{\partial \Delta G_S^0} = \frac{\partial^2 \Delta G_f^{0\ddagger}}{\left(\partial \Delta G_S^0\right)\left(\partial \Delta G_D^0\right)} = \frac{\partial \alpha_S}{\partial \Delta G_D^0} = \frac{\partial \phi_f}{\partial \Delta G_D^0} = p_{SD} \tag{4.28}$$

Hammond behaviour and ground state effects will yield positive p_{DS}-values. Negative p_{DS}-values indicate anti-Hammond behaviour or parallel pathways. To distinguish between these effects it is necessary to also determine the effect of ΔG_T^0 on the kinetic and equilibrium *m*-values.

5. Summary

The goal of this work was to improve our understanding of the properties of the free energy barriers in protein folding. We used the small all-β-sheet protein tendamistat as a model protein. Tendamistat contains two disulfide bridges and folds and unfolds in apparent two-state reactions. However, previous studies on disulfide variants demonstrated that tendamistat folds in at least two sequential steps with a high-energy intermediate. Elucidation of the properties of the free energy barriers by studying different tendamistat variants and various fragments provide a good insight into the underlying complexity of apparent two state folders. To obtain this information several approaches have been used in this work: we studied the combined influence of denaturant, temperature, structural variation and sodium sulfate on folding and stability; furthermore, we analysed the properties and stability of different fragments of tendamistat.

Multiple perturbation analysis was used to gain information on the shape of the free energy barriers in tendamistat folding. Analysis of denaturant and temperature as perturbations revealed transition state movement according to the Hammond postulate. Hammond behaviour is more pronounced in the early transition state compared to the late transition state where only small transition state movement was observed. The results suggest that the early transition state is rather broad compared to the late transition state. These results emphasized the importance of multiple perturbation analysis to test the shape of the free energy barriers in protein folding.

Determination of the activation parameters revealed less difference between both transition states. However, the denaturant dependence of the activation parameters of the transition states differs significantly. The results confirm our previous suggestion that the early transition state is broad and structurally less well defined, whereas the late transition state shows a rather narrow and structurally well-defined maximum.

We further studied the effect of denaturant and structural variation on folding and stability. The results confirmed Hammond behaviour of the early transition state. To know more about structural properties of the transition states we determined ϕ_f-values. The obtained results suggest a late formation of the N-terminal β-hairpin in tendamistat folding.

To test for parallel pathways in protein folding we measured the effect of denaturant and temperature on folding of the disulfide variant C11A/C27S. The denaturant dependence of the apparent folding rate constant revealed a change in the rate-limiting step at high denaturant concentrations. Multiple perturbation analysis of C11A/C27S revealed switches between parallel pathways at the early stage in folding. In contrast, the late transition state is rather insensitive to perturbations. Our results further demonstrated that multiple perturbation analysis offers a good possibility to detect parallel pathways in protein folding.

Folding studies on some variants revealed an additional unfolding phase. The denaturant dependence of the unfolding rate constant of one of these variants was found to have an upward curvature indicating parallel pathways. With the help of interrupted refolding and double-jump experiments, we concluded a triangular mechanism as the possible folding reaction of these tendamistat variants.

To know how the surface exposed charges contribute to tendamistat stability and folding we determined the effect of denaturant on folding stability of different loading variants. We found possible ion networks on the protein surface, which have significantly contributions to tendamistat stability.

The denaturant dependence of the folding rate constant of the tendamistat variant L14A was found to have a pronounced curvature upon addition of sodium sulfate. This effect was already observed for tendamistat wild type and for a proline free variant. Intrinsic dynamics as a rate-limiting step provides a possible explanation for the influence of sodium sulfate in tendamistat folding.

To determine the influence of the ten N-terminal amino acids on protein stability we analysed the structure formation and stability of a tendamistat fragment lacking these ten amino acids. The removal of these amino acids leads to a significant destabilisation and more compact state of the core.

Tendamistat was cleaved in the centre of the second β-sheet into two fragments. We could observe only small evidence for structure formation for both fragments. They did not show any tendency to associate. Cleavage in the centre of the second sheet seems to interrupt important structural properties, which are important to form native like structure.

To determine the tendency of the N-terminal β-hairpin to form secondary structure we analysed disulfide bond formation of a peptide consisting the sequence of this hairpin by using the concept of effective concentrations. Our results showed that this peptide behaves like a random coil. This argues for the importance of the disulfide bond at the base of the N-terminal β-hairpin to stabilise the secondary structure in tendamistat.

6. Acknowledgements

This work was completed from April 2001 to September 2005 in the laboratory of Prof. Dr. Thomas Kiefhaber in the Department of Biophysical Chemistry at the Biozentrum of the University of Basel, Switzerland.

First of all, thanks a lot to all people, who contributed to this work.

I would like to thank Thomas Kiefhaber for his excellent supervision. During my thesis I have learned a lot from his excellent scientific approach. He provided me with the necessary freedom and motivation to complete this work despite certain unplanned elements in my like.

Many thanks to the former and current members of the TK lab for many fruitful discussions, for giving moral and practical support and in particular the nice atmosphere in and outside the lab.

I want to thank Rita Müller for introducing me into the secrets of the expression and purification of tendamistat. Further I want to thank Hans, Leo and Gernot from the floor service group for the excellent technical support during my thesis. Thanks to Dr. Paul Jenö and Thierry Mini for mass spectrometry support.

I would also like to acknowledge the fruitful cooperation with Prof. Dr. Joachim Engels and Hüseyin Aygün who provided the tendamistat variants.

Many thanks to Prof. Dr. Rudolf Glockshuber for taking the time and effort to co-correct this work. I would also like to thank Rudi, Annett and Thomas for the enjoyable introduction to *Schafkopf*.

Special thanks to friends and family for all their support during the time.

Most of all I'm particularly deeply grateful to Axel and Lars, without whose support and patience none of this would have been possible. Without any further words, this work is dedicated to them.

7. References

1. Walter, S. & Buchner, J. Molecular chaperones - cellular machines for protein folding. *Angew. Chem. Int. Ed. Engl.* **41**, 1098-1113 (2003).
2. Schiene, C. & Fischer, G. Enzymes that catalyse the restructuring of proteins. *Curr Opin Struct Biol* **10**, 40-5 (2000).
3. Lang, K., Schmid, F.X. & Fischer, G. Catalysis of protein folding by prolyl isomerase. *Nature* **329**, 268-270 (1987).
4. Schiene-Fischer, C., Habazettl, J., Schmid, F.X. & Fischer, G. The hsp70 chaperone DnaK is a secondary amide peptide bond cis-trans isomerase. *Nat Struct Biol* **9**, 419-24 (2002).
5. Sevier, C.S. & Kaiser, C.A. Formation and transfer of disulphide bonds in living cells. *Nat Rev Mol Cell Biol* **3**, 836-47 (2002).
6. Collet, J.-F. & Bardwell, J.C. The catalysis of disulfide bond formation in prokaryotes. in *Protein Folding Handbook*, Vol. 3 (eds. Buchner, J. & Kiefhaber, T.) 358-376 (Wiley-VCH Verlag, Weinheim, 2005).
7. Anfinsen, C.B. Principles that govern the folding of protein chains. *Science* **181**, 223-230 (1973).
8. Tanford, C. Protein denaturation. Part B. The transition from native to denatured state. *Adv. Prot. Chem* **23**, 218-282 (1968).
9. Anfinsen, C.B., Haber, E., Sela, M. & White, F.H., Jr. The kinetics of formation of native ribonuclease during oxidation of the reduced polypeptide chain. *Proc Natl Acad Sci U S A* **47**, 1309-14 (1961).
10. Becktel, W.J. & Schellman, J.A. Protein stability curves. *Biopolymers* **26**, 1859-1877 (1987).
11. Jaenicke, R. Protein structure and function at low temperatures. *Philos Trans R Soc Lond [Biol]* **326**, 535-551; discussion 551-553 (1990).
12. Luque, I., Leavitt, S.A. & Freire, E. The linkage between protein folding and functional cooperativity: two sides of the same coin? *Annu. Rev. Biophys. Biomol. Struct.* **31**, 235-256 (2002).
13. Griko, Y.V., Privalov, P.L., Venyaminov, S.Y. & Kutyshenko, V.P. Thermodynamic study of the apomyoglobin structure. *J Mol Biol* **202**, 127-38 (1988).
14. Griko, Y.V., Privalov, P.L., Sturtevant, J.M. & Venyaminov, S. Cold denaturation of staphylococcal nuclease. *Proc Natl Acad Sci U S A* **85**, 3343-7 (1988).
15. Schönbrunner, N., Pappenberger, G., Scharf, M., Engels, J. & Kiefhaber, T. Effect of Pre-Formed Correct Tertiary Interactions on Rapid Two-State Tendamistat Folding: Evidence for Hairpins as Initiation Sites for β-Sheet Formation. *Biochemistry* **36**, 9057-9065 (1997).
16. Dunitz, J.D. Win some, lose some: enthalpy-entropy compensation in weak intermolecular interactions. *Chem Biol* **2**, 709-12 (1995).
17. Cooper, A., Johnson, C.M., Lakey, J.H. & Nollmann, M. Heat does not come in different colours: entropy-enthalpy compensation, free energy windows, quantum confinement, pressure perturbation calorimetry, solvation and the multiple causes of heat capacity effects in biomolecular interactions. *Biophys Chem* **93**, 215-30 (2001).

18. Makhatadze, G.I., Clore, G.M. & Gronenborn, A.M. Solvent isotope effect and protein stability. *Nat Struct Biol* **2**, 852-5 (1995).
19. Schellman, J.A. The thermodynamic stability of proteins. *Annu Rev Biophys Biophys Chem* **16**, 115-37 (1987).
20. Privalov, P.L. & Khechinashvili, N.N. A thermodynamic approach to the problem of stabilization of globular protein structure: a calorimetric study. *J Mol Biol* **86**, 665-84 (1974).
21. Spolar, R.S., Ha, J.H. & Record, M.T., Jr. Hydrophobic effect in protein folding and other noncovalent processes involving proteins. *Proc Natl Acad Sci U S A* **86**, 8382-5 (1989).
22. Baldwin, R.L. Temperature dependence of the hydrophobic interaction in protein folding. *Proc Natl Acad Sci U S A* **83**, 8069-72 (1986).
23. Myers, J.K., Pace, C.N. & Scholtz, J.M. Denaturant m values and heat capacity changes: relation to changes in accessible surface areas of protein unfolding. *Protein Sci* **4**, 2138-48 (1995).
24. Makhatadze, G.I. & Privalov, P.L. Heat capacity of proteins. I. Partial molar heat capacity of individual amino acid residues in aqueous solution: hydration effect. *J Mol Biol* **213**, 375-84 (1990).
25. Makhatadze, G.I. Heat capacities of amino acids, peptides and proteins. *Biophys Chem* **71**, 133-56 (1998).
26. Makhatadze, G.I. & Privalov, P.L. Energetics of protein structure. *Adv Protein Chem* **47**, 307-425 (1995).
27. Spolar, R.S., Livingstone, J.R. & Record, M.T., Jr. Use of liquid hydrocarbon and amide transfer data to estimate contributions to thermodynamic functions of protein folding from the removal of nonpolar and polar surface from water. *Biochemistry* **31**, 3947-55 (1992).
28. Robertson, A.D. & Murphy, K.P. Protein Structure and the Energetics of Protein Stability. *Chem Rev* **97**, 1251-1268 (1997).
29. Makhatadze, G.I. Thermal unfolding of proteins studied by calormetry. in *Protein Folding Handbook*, Vol. 1 (eds. Buchner, J. & Kiefhaber, T.) 70-98 (Wiley-VCH Verlag, Weinheim, 2005).
30. Loladze, V.V., Ermolenko, D.N. & Makhatadze, G.I. Heat capacity changes upon burial of polar and nonpolar groups in proteins. *Protein Sci* **10**, 1343-52 (2001).
31. Loladze, V.V., Ermolenko, D.N. & Makhatadze, G.I. Thermodynamic consequences of burial of polar and non-polar amino acid residues in the protein interior. *J Mol Biol* **320**, 343-57 (2002).
32. Yang, A.S., Sharp, K.A. & Honig, B. Analysis of the heat capacity dependence of protein folding. *J Mol Biol* **227**, 889-900 (1992).
33. Lazaridis, T., Archontis, G. & Karplus, M. Enthalpic contribution to protein stability: insights from atom-based calculations and statistical mechanics. *Adv Protein Chem* **47**, 231-306 (1995).
34. Makhatadze, G.I. & Privalov, P.L. Contribution of hydration to protein folding thermodynamics. I. The enthalpy of hydration. *J Mol Biol* **232**, 639-59 (1993).
35. Madan, B. & Sharp, K. Changes in water structure induced by a hydrophobic solute probed by simulation of the water hydrogen bond angle and radial distribution functions. *Biophys Chem* **78**, 33-41 (1999).
36. Creamer, T.P. & Rose, G.D. Side-chain entropy opposes alpha-helix formation but rationalizes experimentally determined helix-forming propensities. *Proc Natl Acad Sci U S A* **89**, 5937-41 (1992).

37. Doig, A.J. & Sternberg, M.J. Side-chain conformational entropy in protein folding. *Protein Sci* **4**, 2247-51 (1995).
38. Pickett, S.D. & Sternberg, M.J. Empirical scale of side-chain conformational entropy in protein folding. *J Mol Biol* **231**, 825-39 (1993).
39. Sternberg, M.J. & Chickos, J.S. Protein side-chain conformational entropy derived from fusion data--comparison with other empirical scales. *Protein Eng* **7**, 149-55 (1994).
40. Amzel, L.M. Calculation of entropy changes in biological processes: folding, binding, and oligomerization. *Methods Enzymol* **323**, 167-77 (2000).
41. Pace, C.N., Grimsley, G.R., Thomson, J.A. & Barnett, B.J. Conformational stability and activity of ribonuclease T1 with zero, one, and two intact disulfide bonds. *J Biol Chem* **263**, 11820-5 (1988).
42. Doig, A.J. & Williams, D.H. Is the hydrophobic effect stabilizing or destabilizing in proteins? The contribution of disulphide bonds to protein stability. *J Mol Biol* **217**, 389-98 (1991).
43. Betz, S.F. Disulfide bonds and the stability of globular proteins. *Protein Sci* **2**, 1551-8 (1993).
44. Clarke, J., Hounslow, A.M. & Fersht, A.R. Disulfide mutants of barnase. II: Changes in structure and local stability identified by hydrogen exchange. *J Mol Biol* **253**, 505-13 (1995).
45. Clarke, J., Henrick, K. & Fersht, A.R. Disulfide mutants of barnase. I: Changes in stability and structure assessed by biophysical methods and X-ray crystallography. *J Mol Biol* **253**, 493-504 (1995).
46. Balbach, J. et al. Structure and dynamic properties of the single disulfide-deficient a-amylase inhibitor C45A/C73A tendamistat: an NMR study. *Proteins: Struct. Funct. Genetics* **33**, 285-294 (1998).
47. Vogl, T. et al. Mechanism of protein stabilization by disulfide bridges: calorimetric unfolding studies on disulfide-deficient mutants of the α-amylase inhibitor tendamistat. *J. Mol. Biol.* **254**, 481-496 (1995).
48. Bieri, O. et al. The speed limit for protein folding measured by triplet-triplet energy transfer. *Proc. Natl. Acad. Sci. USA* **96**, 9597-9601 (1999).
49. Krieger, F., Fierz, B., Bieri, O., Drewello, M. & Kiefhaber, T. Dynamics of unfolded polypeptide chains as model for the earliest steps in protein folding. *J. Mol. Biol.* **332**, 265-274 (2003).
50. Bieri, O. & Kiefhaber, T. Elementary steps in protein folding. *Biol. Chem.* **380**, 923-929 (1999).
51. Kubelka, J., Hofrichter, J. & Eaton, W.A. The protein folding 'speed limit'. *Curr Opin Struct Biol* **14**, 76-88 (2004).
52. Levinthal, C. How to fold graciously. in *Mössbauer Spectroscopy in Biological Systems* 22-24 (Allerton House, Monticello, Ill., 1969).
53. Zwanzig, R., Szabo, A. & Bagchi, B. Levinthal's paradox. *Proc. Natl. Acad. Sci. USA* **89**, 20-22 (1992).
54. Neri, D., Billeter, M., Wider, G. & Wüthrich, K. NMR determination of residual structure in a urea-denatured protein, the 434-repressor. *Science* **257**, 1559-1563 (1992).
55. Klein-Seetharaman, J. et al. Long-range interactions within a nonnative protein. *Science* **295**, 1719-1722 (2002).
56. Dyson, H.J. & Wright, P.E. Unfolded proteins and protein folding studied by NMR. *Chem Rev* **104**, 3607-22 (2004).

57. Schwalbe, H. et al. Structural and Dynamical Properties of a Denatured Protein. Heteronuclear 3D NMR Experiments and Theoretical Simulations of Lysozyme in 8 M Urea. *Biochemistry* **36**, 8977-8991 (1997).
58. Kristjansdottir, S. et al. Formation of native and non-native interactions in ensembles of denatured ACBP molecules from paramagnetic relaxation enhancement studies. *J Mol Biol* **347**, 1053-62 (2005).
59. Sánchez, I.E. & Kiefhaber, T. Hammond behavior versus ground state effects in protein folding: evidence for narrow free energy barriers and residual structure in unfolded states. *J. Mol. Biol.* **327**, 867-884 (2003).
60. Tiffany, M.L. & Krimm, S. New chain conformations of poly(glutamic acid) and polylysine. *Biopolymers* **6**, 1379-82 (1968).
61. Shi, Z., Woody, R.W. & Kallenbach, N.R. Is polyproline II a major backbone conformation in unfolded proteins? *Adv Protein Chem* **62**, 163-240 (2002).
62. Shi, Z., Olson, C.A., Rose, G.D., Baldwin, R.L. & Kallenbach, N.R. Polyproline II structure in a sequence of seven alanine residues. *Proc Natl Acad Sci U S A* **99**, 9190-5 (2002).
63. Rucker, A.L. & Creamer, T.P. Polyproline II helical structure in protein unfolded states: lysine peptides revisited. *Protein Sci* **11**, 980-5 (2002).
64. Pappu, R.V. & Rose, G.D. A simple model for polyproline II structure in unfolded states of alanine-based peptides. *Protein Sci* **11**, 2437-55 (2002).
65. Ferreon, J.C. & Hilser, V.J. The effect of the polyproline II (PPII) conformation on the denatured state entropy. *Protein Sci* **12**, 447-57 (2003).
66. Chellgren, B.W. & Creamer, T.P. Short sequences of non-proline residues can adopt the polyproline II helical conformation. *Biochemistry* **43**, 5864-9 (2004).
67. Mezei, M., Fleming, P.J., Srinivasan, R. & Rose, G.D. Polyproline II helix is the preferred conformation for unfolded polyalanine in water. *Proteins* **55**, 502-7 (2004).
68. Kentsis, A., Mezei, M., Gindin, T. & Osman, R. Unfolded state of polyalanine is a segmented polyproline II helix. *Proteins* **55**, 493-501 (2004).
69. Whittington, S.J., Chellgren, B.W., Hermann, V.M. & Creamer, T.P. Urea Promotes Polyproline II Helix Formation: Implications for Protein Denatured States. *Biochemistry* **44**, 6269-75 (2005).
70. Huang, G.S. & Oas, T.G. Submillisecond folding of monomeric lambda repressor. *Proc Natl Acad Sci U S A* **92**, 6878-82 (1995).
71. Burton, R.E., Huang, G.S., Daugherty, M.A., Fullbright, P.W. & Oas, T.G. Microsecond protein folding through a compact transition state. *J Mol Biol* **263**, 311-22 (1996).
72. Mayor, U. et al. The complete folding pathway of a protein from nanoseconds to microseconds. *Nature* **421**, 863-7 (2003).
73. Perl, D. et al. Conservation of rapid two-state folding in mesophilic, thermophilic and hyperthermophilic cold shock proteins. *Nat Struct Biol* **5**, 229-35 (1998).
74. Ferguson, N., Johnson, C.M., Macias, M., Oschkinat, H. & Fersht, A. Ultrafast folding of WW domains without structured aromatic clusters in the denatured state. *Proc Natl Acad Sci U S A* **98**, 13002-7 (2001).
75. Robinson, C.R. & Sauer, R.T. Equilibrium stability and sub-millisecond refolding of a designed single-chain Arc repressor. *Biochemistry* **35**, 13878-84 (1996).

76. Morillas, M., Sánchez, I.E., Zobeley, E., Kiefhaber, T. & Glockshuber, R. Fast folding of the Semliki Forest Virus capsid protein explains cotranslational proteolytic activity. *To be submitted* (2003).
77. Garel, J.R. & Baldwin, R.L. Both the fast and slow folding reactions of ribonuclease A yield native enzyme. *Proc. Natl. Acad. Sci. U.S.A.* **70**, 3347-3351 (1973).
78. Brandts, J.F., Halvorson, H.R. & Brennan, M. Consideration of the possibility that the slow step in protein denaturation reactions is due to *cis-trans* isomerism of proline residues. *Biochemistry* **14**, 4953-4963 (1975).
79. Kiefhaber, T., Grunert, H.P., Hahn, U. & Schmid, F.X. Replacement of a cis proline simplifies the mechanism of ribonuclease T1 folding. *Biochemistry* **29**, 6475-6480 (1990).
80. Schmid, F.X. Prolyl isomerization in protein folding. in *Protein Folding Handbook*, Vol. 2 (eds. Buchner, J. & Kiefhaber, T.) 916-945 (Wiley-VCH Verlag, Weinheim, 2005).
81. Reimer, U. et al. Side-chain effects on peptidyl-prolyl cis/trans isomerisation. *J Mol Biol* **279**, 449-60 (1998).
82. Balbach, J. & Schmid, F.X. Proline isomerization and its catalysis in protein folding. in *Protein Folding: Frontiers in Molecular Biology* (ed. Pain, R.) (Oxford University Press, Oxford, 2000).
83. Odefey, C., Mayr, L.M. & Schmid, F.X. Non-prolyl cis-trans peptide bond isomerization as a rate-determining step in protein unfolding and refolding. *J Mol Biol* **245**, 69-78 (1995).
84. Pappenberger, G. et al. Nonprolyl cis peptide bonds in unfolded proteins cause complex folding kinetics. *Nat Struct Biol* **8**, 452-8 (2001).
85. Scherer, G., Kramer, M.L., Schutkowski, M., Reimer, U. & Fischer, G. Barriers to rotation of secondary amide peptide bonds. *J. Am. Chem. Soc.* **120**, 5568-5574 (1998).
86. Bachmann, A. & Kiefhaber, T. Kinetic mechanism in protein folding. in *Protein Folding Handbook*, Vol. 1 (eds. Buchner, J. & Kiefhaber, T.) 379-410 (Wiley-VCH Verlag, Weinheim, 2005).
87. Colon, W., Wakem, L.P., Sherman, F. & Roder, H. Identification of the predominant non-native histidine ligand in unfolded cytochrome c. *Biochemistry* **36**, 12535-41 (1997).
88. Yeh, S.-R., Takahashi, S., Fan, B. & Rousseau, D.L. Ligand exchange in unfolded cytochrome c. *Nat. Struct. Biol.* **4**, 51-56 (1998).
89. Yeh, S.-R. & Rousseau, D.L. Folding intermediates in cytochrome c. *Nat. Struct. Biol.* **5**, 222-228 (1998).
90. Ptitsyn, O. How molten is the molten globule? *Nat Struct Biol* **3**, 488-90 (1996).
91. Kauzmann, W. Some factors in the interpretation of protein denaturation. *Adv. Prot. Chem.* **14**, 1-63 (1959).
92. Baldwin, R.L. How does protein folding get started? *Trends Biochem Sci* **14**, 291-4 (1989).
93. Schellman, J.A. The stability of hydrogen-bonded peptide structures in aqueous solution. *C R Trav Lab Carlsberg [Chim]* **29**, 230-59 (1955).
94. Schwarz, G. On the kinetics of the helix-coil transition of polypeptides in solution. *J. Mol. Biol.* **11**, 64-77 (1965).
95. Karplus, M. & Weaver, D.L. Protein-folding dynamics. *Nature* **260**, 404-6 (1976).

96. Kim, P.S. & Baldwin, R.L. Specific intermediates in the folding reactions of small proteins and the mechanism of protein folding. *Annu. Rev. Biochem.* **51**, 459-489 (1982).
97. Kim, P.S. & Baldwin, R.L. Intermediates in the folding reactions of small proteins. *Annu. Rev. Biochem.* **59**, 631-660 (1990).
98. Karplus, M. & Weaver, D.L. Protein folding dynamics: the diffusion-collision model and experimental data. *Protein Sci* **3**, 650-68 (1994).
99. Hughson, F.M., Wright, P.E. & Baldwin, R.L. Structural characterization of a partly folded apomyoglobin intermediate. *Science* **249**, 1544-8 (1990).
100. Arai, M. & Kuwajima, K. Role of the molten globule state in protein folding. *Adv Protein Chem* **53**, 209-82 (2000).
101. Jennings, P.A. & Wright, P.E. Formation of a molten globule intermediate early in the kinetic folding pathway of apomyoglobin. *Science* **262**, 892-6 (1993).
102. Fierz, B. & Kiefhaber, T. Dynamics of unfolded polypeptide chains. in *Protein Folding Handbook*, Vol. 2 (eds. Buchner, J. & Kiefhaber, T.) 809-855 (Wiley-VCH Verlag, Weinheim, 2005).
103. Jackson, S.E. & Fersht, A.R. Folding of chymotrypsin inhibitor 2. 1. Evidence for a two-state transition. *Biochemistry* **30**, 10428-35 (1991).
104. Jackson, S.E. How do small single-domain proteins fold? *Fold Des* **3**, R81-91 (1998).
105. Fersht, A.R. Optimization of rates of protein folding: the nucleation-condensation mechanism and its implications. *Proc Natl Acad Sci U S A* **92**, 10869-73 (1995).
106. Inaba, K., Kobayashi, N. & Fersht, A.R. Conversion of two-state to multi-state folding kinetics on fusion of two protein foldons. *J Mol Biol* **302**, 219-33 (2000).
107. Wetlaufer, D.B. Nucleation, rapid folding, and globular intrachain regions in proteins. *Proc Natl Acad Sci U S A* **70**, 697-701 (1973).
108. Abkevich, V.I., Gutin, A.M. & Shakhnovich, E.I. Specific nucleus as the transition state for protein folding: evidence from the lattice model. *Biochemistry* **33**, 10026-36 (1994).
109. Silow, M. & Oliveberg, M. High-energy channeling in protein folding. *Biochemistry* **36**, 7633-7 (1997).
110. Bachmann, A. & Kiefhaber, T. Apparent two-state tendamistat folding is a sequential process along a defined route. *J. Mol. Biol.* **306**, 375-386 (2001).
111. Sánchez, I.E. & Kiefhaber, T. Evidence for sequential barriers and obligatory intermediates in apparent two-state protein folding. *J. Mol. Biol.* **325**, 367-376 (2003).
112. Jonsson, T., Waldburger, C.D. & Sauer, R.T. Nonlinear free energy relationship in arc repressor unfolding imply the existence of unstable, native-like folding intermediates. *Biochemistry* **35**, 4795-4802 (1996).
113. Walkenhorst, W.F., Green, S. & Roder, H. Kinetic evidence for folding and unfolding intermediates in staphylococcal nuclease. *Biochemistry* **36**, 5795-5805 (1997).
114. Wagner, C. & Kiefhaber, T. Intermediates can accelerate protein folding. *Proc. Natl. Acad. Sci. USA* **96**, 6716-6721 (1999).
115. Szabo, Z.G. Kinetic characterization of complex reaction systems. in *Comprehensive chemical kinetics*, Vol. 2 (eds. Bamford, C.H. & Tipper, C.F.H.) 1-80 (Elsevier Publishing Company, Amsterdam, 1969).

116. Ikai, A. & Tanford, C. Kinetics of unfolding and refolding of proteins. I. Mathematical Analysis. *J. Mol. Biol.* **73**, 145-163 (1973).
117. Fuchs, S., De Lorenzo, F. & Anfinsen, C.B. Studies on the mechanism of the enzymic catalysis of disulfide interchange in proteins. *J Biol Chem* **242**, 398-402 (1967).
118. Creighton, T.E. Disulfide bond formation in proteins. *Methods Enzymol* **107**, 305-29 (1984).
119. Elove, G.A., Bhuyan, A.K. & Roder, H. Kinetic mechanism of cytochrome c folding: involvement of the heme and its ligands. *Biochemistry* **33**, 6925-35 (1994).
120. Roder, H., Maki, K., Latypov, R.F., Cheng, H. & Ramachandra Shastry, M.C. Early events in protein folding explored by rapid mixing methods. in *Protein Folding Handbook*, Vol. 1 (eds. Buchner, J. & Kiefhaber, T.) 491-535 (Wiley-VCH Verlag, Weinheim, 2005).
121. Schmid, F.X. Mechanism of folding of ribonuclease A. Slow refolding is a sequential reaction via structural intermediates. *Biochemistry* **22**, 4690-4696 (1983).
122. Kiefhaber, T. Kinetic traps in lysozyme folding. *Proc. Natl. Acad. Sci. USA* **92**, 9029-9033 (1995).
123. Sánchez, I.E. & Kiefhaber, T. Non-linear rate-equilibrium free energy relationships and Hammond behavior in protein folding. *Biophys. Chem.* **100**, 397-407 (2003).
124. Leffler, J.E. Parameters for the description of transition states. *Science* **117**, 340-341 (1953).
125. Jencks, W.P. *Catalysis in Chemistry and Enzymology*, (McGraw-Hill Book Company, New York, 1969).
126. Grosman, C., Zhou, M. & Auerbach, A. Mapping the conformational wave of acetylcholine receptor channel gating. *Nature* **403**, 773-6 (2000).
127. Spiro, K. Uber die Beeinflussung der Eiweisscoagulation durch stickstoffhaltige Substanzen. *Z Physiol Chem* **30**, 182-199 (1900).
128. Ramsden, W. Some new properties of urea. *J Physiol* **28**, 23-27 (1902).
129. Greenstein, J.P. Sulfhydryl groups in proteins. *J Biol Chem* **125**, 501-513 (1938).
130. Pace, C.N., Grimsley, G.R. & Scholtz, J.M. Denaturation of proteins by urea and guanidinium hydrochloride. in *Protein Folding Handbook*, Vol. 1 (eds. Buchner, J. & Kiefhaber, T.) 45-69 (Wiley-VCH Verlag, Weinheim, 2005).
131. Santoro, M.M. & Bolen, D.W. Unfolding free energy changes determined by the linear extrapolation method. 1. Unfolding of phenylmethanesulfonyl alpha-chymotrypsin using different denaturants. *Biochemistry* **27**, 8063-8068 (1988).
132. Greene, R.F.J. & Pace, C.N. Urea and guanidine-hydrochloride denaturation of ribonuclease, lysozyme, alpha-chyomtrypsinn and beta-lactoglobulin. *J. Biol. Chem.* **249**, 5388-5393 (1974).
133. Tanford, C. Protein Denaturation. Part C. Theoretical models for the mechanism of denaturation. *Adv. Prot. Chem.* **24**, 1-95 (1970).
134. Ikai, A., Fish, W.W. & Tanford, C. Kinetics of unfolding and refolding of proteins. II. Results for cytochrome c. *J. Mol. Biol.* **73**, 165-184 (1973).
135. Matthews, C.R. Effect of point mutations on the folding of globular proteins. *Meth. Enzymol.* **154**, 498-511 (1987).

136. Bieri, O. & Kiefhaber, T. Kinetic models in protein folding. in *Protein Folding: Frontiers in Molecular Biology* (ed. Pain, R.) 34-64 (Oxford University Press, Oxford, 2000).
137. Fersht, A.R., Matouschek, A. & Serrano, L. The folding of an enzyme. I. Theory of protein engineering analysis of stability and pathway of protein folding. *J. Mol. Biol.* **224**, 771-782 (1992).
138. Guydosh, N.R. & Fersht, A.R. A guide to measuring and interpreting ϕ-values. in *Protein Folding Handbook*, Vol. 1 (eds. Buchner, J. & Kiefhaber, T.) 445-453 (Wiley-VCH Verlag, Weinheim, 2005).
139. Goldenberg, D.P., Frieden, R.W., Haack, J.A. & Morrison, T.B. Mutational analysis of a protein-folding pathway. *Nature* **338**, 127-32 (1989).
140. Sánchez, I.E. & Kiefhaber, T. Origin of unusual phi-values in protein folding: Evidence against specific nucleation sites. *J. Mol. Biol.* **334**, 1077-1085 (2003).
141. Itzhaki, L.S., Otzen, D.E. & Fersht, A.R. The structure of the transition state for folding of chymotrypsin inhibitor 2 analysed by protein engineering methods: evidence for a nucleation-condensation mechanism for protein folding. *J Mol Biol* **254**, 260-88 (1995).
142. Silow, M. & Oliveberg, M. Transient intermediates in protein folding are easilty mistaken for folding intermediates. *Proc. Natl. Acad. Sci. USA* **94**, 6084-6086 (1997).
143. Kiefhaber, T., Bachmann, A., Wildegger, G. & Wagner, C. Direct measurements of nucleation and growth rates in lysozyme folding. *Biochemistry* **36**, 5108-5112 (1997).
144. Wright, C.F., Lindorff-Larsen, K., Randles, L.G. & Clarke, J. Parallel protein-unfolding pathways revealed and mapped. *Nat Struct Biol* **10**, 658-62 (2003).
145. Wildegger, G. & Kiefhaber, T. Three-state model for lysozyme folding: triangular folding mechanism with an energetically trapped intermediate. *J. Mol. Biol.* **270**, 294-304 (1997).
146. Ikai, A. & Tanford, C. Kinetic evidence for incorrectly folded intermediate states in the refolding of denatured proteins. *Nature* **230**, 100-102 (1971).
147. Hammond, G.S. A correlation of reaction rates. *J. Am. Chem. Soc.* **77**, 334-338 (1955).
148. Jencks, D.A. & Jencks, W.P. On the characterization of transition states by structure-reactivity coefficients. *J. Am. Chem. Soc.* **99**, 7948-7960 (1977).
149. Jencks, W.P. A primer for the Bema Hapothle. An empirical approach to the characterization of changing transition-state structures. *Chem. Rev.* **85**, 511-527 (1985).
150. Farcasiu, D. The use and misuse of the Hammond postulate. *J. Chem. Ed.* **52**, 76-79 (1975).
151. Fersht, A.R., Itzhaki, L.S., elMasry, N.F., Matthews, J.M. & Otzen, D.E. Single versus parallel pathways of protein folding and fractional formation of structure in the transition state. *Proc. Natl. Acad. Sci. USA* **91**, 10426-10429 (1994).
152. Matthews, J.M. & Fersht, A.R. Exploring the energy surface of protein folding by structure-reactivity relationship and engineered proteins: Observation of Hammond behavior for the gross structure of the transitions state and anti-hammond behavior for structural elements for unfolding/folding of barnase. *Biochemistry* **34**, 6805-6814 (1995).
153. Nauli, S., Kuhlman, B. & Baker, D. Computer-based redesign of a protein folding pathway. *Nat. Struc. Biol.* **8**, 602-605 (2001).

154. Guo, Z. & Thirumalai, D. Kinetics of protein folding: nucleation mechanism, time scales, and pathways. *Biopolymers* **36**, 83-102 (1995).
155. Wolynes, P.G., Onuchic, J.N. & Thirumalai, D. Navigating the folding routes. *Science* **267**, 1619-1620 (1995).
156. Bieri, O., Wildegger, G., Bachmann, A., Wagner, C. & Kiefhaber, T. A salt-induced intermediate is on a new parallel pathway of lysozyme folding. *Biochemistry* **38**, 12460-12470 (1999).
157. Bieri, O. & Kiefhaber, T. Origin of apparent fast and non-exponential kinetics of lysozyme folding measured in pulse labeling experiments. *J. Mol. Biol.* **310**, 919-935 (2001).
158. Noyelle, K., Joniau, M. & Van Dael, H. The fast folding pathway in human lysozyme and its blockage by appropriate mutagenesis: a sequential stopped-flow fluorescence study. *J. Mol. Biol.* **308**, 807-819 (2001).
159. Krantz, B.A. & Sosnick, T.R. Engineered metal binding sites map the heterogeneous folding landscape of a coiled coil. *Nat. Struct. Biol.* **8**, 1042-1047 (2001).
160. Pappenberger, G., Saudan, C., Becker, M., Merbach, A.E. & Kiefhaber, T. Denaturant-induced movement of the transition state of protein folding revealed by high-pressure stopped-flow measurements. *Proc Natl Acad Sci U S A* **97**, 17-22 (2000).
161. Svensson, B., Fukuda, K., Nielsen, P.K. & Bonsager, B.C. Proteinaceous alpha-amylase inhibitors. *Biochim Biophys Acta* **1696**, 145-56 (2004).
162. Vértesy, L., Oeding, V., Bender, R., Zepf, K. & Nesemann, G. Isolation and structure elucidation of an α-amylase inhibitor from *Streptomyces tendae* 4158. *Eur. J. Biochem.* **141**, 505-512 (1984).
163. Renner, M., Hinz, H.-J., Scharf, M. & Engels, J.W. Thermodynamics of unfolding of the α-amylase inhibitor tendamistat: correlations between accessible surface area and heat capacity. *J. Mol. Biol.* **223**, 769-779 (1992).
164. Kraulis, P. MolScript: a program to produce both detailed and schematic plots of protein structures. *J. Appl. Cryst.* **24**, 946-950 (1991).
165. Merrit, E. & Bacon, D. Raster3D: photorealistic molecular graphics. *Methods Enzymol.* **277**, 505-524 (1997).
166. Kline, A.D., Braun, W. & Wüthrich, K. Determination of the complete three-dimensional structure of the α-amylase inhibitor tendamistat in aqueous solution by nuclear magnetic resonance and distance geometry. *J. Mol. Biol.* **204**, 675-724 (1988).
167. Kline, A.D. & Wüthrich, K. Secondary structure of the α-amylase polypeptide inhibitor tendamistat from streptomyces tendae determined in solution by 1H nuclear magnetic resonance. *J. Mol. Biol.* **183**, 503-507 (1985).
168. Pflugrath, J., Wiegand, I., Huber, R. & Vértesy, L. Crystal structure determination, refinement and the molecular model of the α-amylase inhibitor Hoe-467A. *J. Mol. Biol.* **189**, 383-386 (1986).
169. Billeter, M., Kline, A.D., Braun, W., Huber, R. & Wuthrich, K. Comparison of the high-resolution structures of the alpha-amylase inhibitor tendamistat determined by nuclear magnetic resonance in solution and by X-ray diffraction in single crystals. *J Mol Biol* **206**, 677-87 (1989).
170. Wiegand, G., Epp, O. & Huber, R. The crystal strucutre of porcine pancreatic α-amylase in complex with the microbial inhibitor tendamistat. *J. Mol Biol.* **247**, 99-110 (1995).

171. Richardson, J.S. The anatomy and taxonomy of protein structure. *Advan Prot Chem* **34**, 167-339 (1981).
172. Arai, M., OOuchi, N. & Murao, S. Inhibitory properties of an α-amylase inhibitor, Paim, from *Streptomyces corchorushii*. *Agric. Biol. Chem.* **49**, 987-991 (1985).
173. Schönbrunner, N., Koller, K.-P. & Kiefhaber, T. Folding of the disulfide-bonded β-sheet protein tendamistat: Rapid two-state folding without hydrophobic collapse. *J. Mol. Biol.* **268**, 526-538 (1997).
174. Pappenberger, G. et al. Kinetic mechanism and catalysis of a native-state prolyl isomerization reaction. *J Mol Biol* **326**, 235-46 (2003).
175. Bonvin, A.M. & van Gunsteren, W.F. beta-hairpin stability and folding: molecular dynamics studies of the first beta-hairpin of tendamistat. *J Mol Biol* **296**, 255-68 (2000).
176. Kiefhaber, T., Sánchez, I.E. & Bachmann, A. Characterization of protein folding barriers with rate equilibrium free energy relationships. in *Protein Folding Handbook*, Vol. 1 (eds. Buchner, J. & Kiefhaber, T.) 411-444 (Wiley-VCH Verlag, Weinheim, 2005).
177. Schindler, T. & Schmid, F.X. Thermodynamic properties of an extremely rapid protein folding reaction. *Biochemistry* **35**, 16833-42 (1996).
178. Kuhlman, B., Luisi, D.L., Evans, P.A. & Raleigh, D.P. Global analysis of the effects of temperature and denaturant on the folding and unfolding kinetics of the N-terminal domain of the protein L9. *J Mol Biol* **284**, 1661-70 (1998).
179. Vidugiris, G.J., Markley, J.L. & Royer, C.A. Evidence for a molten globule-like transition state in protein folding from determination of activation volumes. *Biochemistry* **34**, 4909-12 (1995).
180. Schellman, J.A. Solvent denaturation. *Biopolymers* **17**, 1305-1322 (1978).
181. Fersht, A.R., Itzhaki, L.S., Elmasry, N., Matthews, J.M. & Otzen, D.E. Single versus parallel pathways of protein folding and fractional formation of structure in the transition state. *Proc Natl Acad Sci USA* **91**, 10426-10429 (1994).
182. Goldberg, J.M. & Baldwin, R.L. A specific transition state for S-peptide combining with folded S-protein and then refolding. *Proc Natl Acad Sci U S A* **96**, 2019-24 (1999).
183. Sancho, J. & Fersht, A.R. Dissection of an enzyme by protein engineering. The N and C-terminal fragments of barnase form a native-like complex with restored enzymic activity. *J Mol Biol* **224**, 741-7 (1992).
184. Kippen, A.D. & Fersht, A.R. Analysis of the mechanism of assembly of cleaved barnase from two peptide fragments and its relevance to the folding pathway of uncleaved barnase. *Biochemistry* **34**, 1464-8 (1995).
185. de Prat Gay, G. & Fersht, A.R. Generation of a family of protein fragments for structure-folding studies. 1. Folding complementation of two fragments of chymotrypsin inhibitor-2 formed by cleavage at its unique methionine residue. *Biochemistry* **33**, 7957-63 (1994).
186. de Prat Gay, G., Ruiz-Sanz, J. & Fersht, A.R. Generation of a family of protein fragments for structure-folding studies. 2. Kinetics of association of the two chymotrypsin inhibitor-2 fragments. *Biochemistry* **33**, 7964-70 (1994).
187. Kobayashi, N., Honda, S., Yoshii, H., Uedaira, H. & Munekata, E. Complement assembly of two fragments of the streptococcal protein G B1 domain in aqueous solution. *FEBS Lett* **366**, 99-103 (1995).
188. Tasayco, M.L. & Chao, K. NMR study of the reconstitution of the beta-sheet of thioredoxin by fragment complementation. *Proteins* **22**, 41-4 (1995).

189. Georgescu, R.E., Garcia-Mira, M.M., Tasayco, M.L. & Sanchez-Ruiz, J.M. Heat capacity analysis of oxidized Escherichia coli thioredoxin fragments (1--73, 74--108) and their noncovalent complex. Evidence for the burial of apolar surface in protein unfolded states. *Eur J Biochem* **268**, 1477-85 (2001).
190. Jourdan, M. & Searle, M.S. Cooperative assembly of a nativelike ubiquitin structure through peptide fragment complexation: energetics of peptide association and folding. *Biochemistry* **39**, 12355-64 (2000).
191. De Sanctis, G. et al. Effect of axial coordination on the kinetics of assembly and folding of the two halves of horse heart cytochrome C. *J Biol Chem* **279**, 52860-8 (2004).
192. Blanco, F.J. & Serrano, L. Folding of protein G B1 domain studied by the conformational characterization of fragments comprising its secondary structure elements. *Eur J Biochem* **230**, 634-49 (1995).
193. Honda, S., Kobayashi, N., Munekata, E. & Uedaira, H. Fragment reconstitution of a small protein: folding energetics of the reconstituted immunoglobulin binding domain B1 of streptococcal protein G. *Biochemistry* **38**, 1203-13 (1999).
194. Koradi, R., Billeter, M. & Wuthrich, K. MOLMOL: a program for display and analysis of macromolecular structures. *J Mol Graph* **14**, 51-5, 29-32 (1996).
195. Searle, M.S. Design and stability of peptide beta-sheets. in *Protein Folding Handbook*, Vol. 1 (eds. Buchner, J. & Kiefhaber, T.) 314-342 (Wiley-VCH Verlag, Weinheim, 2005).
196. Doig, A.J., Errington, N. & Iqbalsyah, T.M. Stability and design of alpha-helices. in *Protein Folding Handbook*, Vol. 1 (eds. Buchner, J. & Kiefhaber, T.) 247-313 (Wiley-VCH Verlag, Weinheim, 2005).
197. Blanco, F.J. et al. NMR evidence of a short linear peptide that folds into a β-hairpin in aqueous solution. *J Am Chem Soc* **115**, 5887-5888 (1993).
198. Blanco, F.J., Rivas, G. & Serrano, L. A short linear peptide that folds into a native stable beta-hairpin in aqueous solution. *Nat Struct Biol* **1**, 584-90 (1994).
199. Blanco, F.J. et al. NMR solution structure of the isolated N-terminal fragment of protein-G B1 domain. Evidence of trifluoroethanol induced native-like beta-hairpin formation. *Biochemistry* **33**, 6004-14 (1994).
200. Cox, J.P., Evans, P.A., Packman, L.C., Williams, D.H. & Woolfson, D.N. Dissecting the structure of a partially folded protein. Circular dichroism and nuclear magnetic resonance studies of peptides from ubiquitin. *J Mol Biol* **234**, 483-92 (1993).
201. Searle, M.S., Zerella, R., Williams, D.H. & Packman, L.C. Native-like beta-hairpin structure in an isolated fragment from ferredoxin: NMR and CD studies of solvent effects on the N-terminal 20 residues. *Protein Eng* **9**, 559-65 (1996).
202. Honda, S., Kobayashi, N. & Munekata, E. Thermodynamics of a beta-hairpin structure: evidence for cooperative formation of folding nucleus. *J Mol Biol* **295**, 269-78 (2000).
203. Munoz, V., Thompson, P.A., Hofrichter, J. & Eaton, W.A. Folding dynamics and mechanism of beta-hairpin formation. *Nature* **390**, 196-9 (1997).
204. Blanco, F.J. et al. Tendamistat (12-26) fragment. NMR characterization of isolated beta-turn folding intermediates. *Eur J Biochem* **200**, 345-51 (1991).
205. Sefler, A.M., Kozlowski, M.C., Guo, T. & Bartlett, P.A. Design, Synthesis, and Evaluation of a Depsipeptide Mimic of Tendamistat. *J Org Chem* **62**, 93-102 (1997).

206. Lin, T.Y. & Kim, P.S. Urea dependence of thiol-disulfide equilibria in thioredoxin: confirmation of the linkage relationship and a sensitive assay for structure. *Biochemistry* **28**, 5282-7 (1989).
207. Creighton, T.E. An empirical approach to protein conformation stability and flexibility. *Biopolymers* **22**, 49-58 (1983).
208. Lin, T.Y. & Kim, P.S. Evaluating the effects of a single amino acid substitution on both the native and denatured states of a protein. *Proc Natl Acad Sci U S A* **88**, 10573-7 (1991).
209. Page, M.I. & Jencks, W.P. Entropic contributions to rate accelerations in enzymic and intramolecular reactions and the chelate effect. *Proc Natl Acad Sci U S A* **68**, 1678-83 (1971).
210. Creighton, T.E. Kinetics of refolding of reduced ribonuclease. *J Mol Biol* **113**, 329-41 (1977).
211. Munoz, V., Henry, E.R., Hofrichter, J. & Eaton, W.A. A statistical mechanical model for beta-hairpin kinetics. *Proc Natl Acad Sci U S A* **95**, 5872-9 (1998).
212. Huyghues-Despointes, B. & Nelson, J.W. Stabilities of disulfide bond intermediates in the folding of apamin. *Biochemistry* **31**, 1476-1483 (1992).
213. Russell, S.J. & Cochran, A.G. Designing stable β-hairpins: energetic contributions from cross-strand residues. *J Am Chem Soc* **122**, 12600-12601 (2000).
214. Cochran, A.G. et al. A minimal peptide scaffold for beta-turn display: optimizing a strand position in disulfide-cyclized beta-hairpins. *J Am Chem Soc* **123**, 625-32 (2001).
215. Blandl, T., Cochran, A.G. & Skelton, N.J. Turn stability in beta-hairpin peptides: Investigation of peptides containing 3:5 type I G1 bulge turns. *Protein Sci* **12**, 237-47 (2003).
216. Russell, S.J., Blandl, T., Skelton, N.J. & Cochran, A.G. Stability of cyclic beta-hairpins: asymmetric contributions from side chains of a hydrogen-bonded cross-strand residue pair. *J Am Chem Soc* **125**, 388-95 (2003).
217. Price-Carter, M., Bulaj, G. & Goldenberg, D.P. Initial disulfide formation steps in the folding of an omega-conotoxin. *Biochemistry* **41**, 3507-19 (2002).
218. Creighton, T.E. Disulphide bonds and protein stability. *Bioessays* **8**, 57-63 (1988).
219. Hawkins, H.C., de Nardi, M. & Freedman, R.B. Redox properties and cross-linking of the dithiol/disulphide active sites of mammalian protein disulphide-isomerase. *Biochem J* **275 (Pt 2)**, 341-8 (1991).
220. Lyles, M.M. & Gilbert, H.F. Catalysis of the oxidative folding of ribonuclease A by protein disulfide isomerase: dependence of the rate on the composition of the redox buffer. *Biochemistry* **30**, 613-9 (1991).
221. Zapun, A., Bardwell, J.C. & Creighton, T.E. The reactive and destabilizing disulfide bond of DsbA, a protein required for protein disulfide bond formation in vivo. *Biochemistry* **32**, 5083-92 (1993).
222. Regan, L., Rockwell, A., Wasserman, Z. & DeGrado, W. Disulfide crosslinks to probe the structure and flexibility of a designed four-helix bundle protein. *Protein Sci* **3**, 2419-27 (1994).
223. Peng, Z.Y., Wu, L.C. & Kim, P.S. Local structural preferences in the alpha-lactalbumin molten globule. *Biochemistry* **34**, 3248-52 (1995).
224. Tachibana, H. Propensities for the formation of individual disulfide bonds in hen lysozyme and in the size and stability of disulfide-associated submolecular structures. *FEBS Lett* **480**, 175-8 (2000).

225. Clarke, J., Hounslow, A.M., Bond, C.J., Fersht, A.R. & Daggett, V. The effects of disulfide bonds on the denatured state of barnase. *Protein Sci* **9**, 2394-404 (2000).
226. Robinson, C.R. & Sauer, R.T. Striking stabilization of Arc repressor by an engineered disulfide bond. *Biochemistry* **39**, 12494-502 (2000).
227. Jacobsen, H. & Stockmayer, W.H. Intramolecular reaction in polycondensations. I. The theory of linear systems. *J. Phys. Chem.* **18**, 1600-1606 (1950).
228. Cochran, A.G., Skelton, N.J. & Starovasnik, M.A. Tryptophan zippers: stable, monomeric beta -hairpins. *Proc Natl Acad Sci U S A* **98**, 5578-83 (2001).
229. Du, D., Zhu, Y., Huang, C.Y. & Gai, F. Understanding the key factors that control the rate of beta-hairpin folding. *Proc Natl Acad Sci U S A* **101**, 15915-20 (2004).
230. Honda, S., Yamasaki, K., Sawada, Y. & Morii, H. 10 residue folded peptide designed by segment statistics. *Structure (Camb)* **12**, 1507-18 (2004).
231. Ciani, B., Jourdan, M. & Searle, M.S. Stabilization of beta-hairpin peptides by salt bridges: role of preorganization in the energetic contribution of weak interactions. *J Am Chem Soc* **125**, 9038-47 (2003).
232. Maynard, A.J., Sharman, G.J. & Searle, M.S. Origin of β-hairpin stability in solution: structural and thermodynamic analysis of the folding of a model peptide supports hydrophobic stabilization in water. *J Am Chem Soc* **120**, 1996-2007 (1998).
233. Searle, M.S., Griffiths-Jones, S.R. & Skinner-Smith, H. Energetics of weak interactions in a b-hairpin peptide: electrostatic and hydrophobic contributions to stability from lysine salt bridges. *J Am Chem Soc* **121**, 11615-11620 (1999).
234. Griffiths-Jones, S.R., Maynard, A.J. & Searle, M.S. Dissecting the stability of a beta-hairpin peptide that folds in water: NMR and molecular dynamics analysis of the beta-turn and beta-strand contributions to folding. *J Mol Biol* **292**, 1051-69 (1999).
235. Santiveri, C.M., Santoro, J., Rico, M. & Jimenez, M.A. Thermodynamic analysis of beta-hairpin-forming peptides from the thermal dependence of (1)H NMR chemical shifts. *J Am Chem Soc* **124**, 14903-9 (2002).
236. Xu, Y., Oyola, R. & Gai, F. Infrared study of the stability and folding kinetics of a 15-residue beta-hairpin. *J Am Chem Soc* **125**, 15388-94 (2003).
237. Dyer, R.B. et al. The mechanism of beta-hairpin formation. *Biochemistry* **43**, 11560-6 (2004).
238. de Alba, E., Jimenez, M.A. & Rico, M. Turn residue sequence determines beta-hairpin conformation in designed peptides. *J Am Chem Soc* **119**, 175-183 (1997).
239. Synd, F.A., Espinosa, J.F. & Gellman, S.H. NMR-based quantification of beta-sheet populations in aqueous solution through use of reference peptides for the folded and unfolded states. *J Am Chem Soc* **121**, 11577-11578 (1999).
240. Gill, S.C. & von Hippel, P.H. Calculation of protein extinction coefficients from amino acid sequence data. *Anal. Biochem.* **182**, 319-326 (1989).
241. Wildegger, G. *Role of intermediates in lysozyme folding*, 158 (University of Basel, Basel, 1997).
242. Haas-Lauterbach, S. et al. High yield fermentation and purification of Tendamistat disulphide analogues secreted by Streptomyces lividans. *Appl Microbiol Biotechnol* **38**, 719-27 (1993).

243. Spudich, G.M., Miller, E.J. & Marqusee, S. Destabilization of the Escherichia coli RNase H kinetic intermediate: switching between a two-state and three-state folding mechanism. *J Mol Biol* **335**, 609-18 (2004).
244. O'Connell, J.F. et al. The nuclear-magnetic-resonance solution structure of the mutant alpha-amylase inhibitor [R19L] Tendamistat and comparison with wild-type Tendamistat. *Eur J Biochem* **220**, 763-70 (1994).
245. Raleigh, D.P. & Plaxco, K.W. The protein folding transition state: what are Phi-values really telling us? *Protein Pept Lett* **12**, 117-22 (2005).
246. Honig, B. & Yang, A.S. Free energy balance in protein folding. *Adv Protein Chem* **46**, 27-58 (1995).
247. Perl, D. & Schmid, F.X. Electrostatic stabilization of a thermophilic cold shock protein. *J Mol Biol* **313**, 343-57 (2001).
248. Xiao, L. & Honig, B. Electrostatic contributions to the stability of hyperthermophilic proteins. *J Mol Biol* **289**, 1435-44 (1999).
249. Perl, D., Mueller, U., Heinemann, U. & Schmid, F.X. Two exposed amino acid residues confer thermostability on a cold shock protein. *Nat Struct Biol* **7**, 380-3 (2000).
250. Wunderlich, M., Martin, A. & Schmid, F.X. Stabilization of the cold shock protein CspB from Bacillus subtilis by evolutionary optimization of Coulombic interactions. *J Mol Biol* **347**, 1063-76 (2005).
251. Loladze, V.V., Ibarra-Molero, B., Sanchez-Ruiz, J.M. & Makhatadze, G.I. Engineering a thermostable protein via optimization of charge-charge interactions on the protein surface. *Biochemistry* **38**, 16419-23 (1999).
252. Perl, D. & Schmid, F.X. Some like it hot: The molecular determinants of protein thermostability. *Chembiochem* **3**, 39-44 (2002).
253. Perutz, M.F. & Raidt, H. Stereochemical basis of heat stability in bacterial ferredoxins and in haemoglobin A2. *Nature* **255**, 256-9 (1975).
254. Makhatadze, G.I., Loladze, V.V., Ermolenko, D.N., Chen, X. & Thomas, S.T. Contribution of surface salt bridges to protein stability: guidelines for protein engineering. *J Mol Biol* **327**, 1135-48 (2003).
255. Makhatadze, G.I., Loladze, V.V., Gribenko, A.V. & Lopez, M.M. Mechanism of thermostabilization in a designed cold shock protein with optimized surface electrostatic interactions. *J Mol Biol* **336**, 929-42 (2004).
256. Jaenicke, R. & Bohm, G. The stability of proteins in extreme environments. *Curr Opin Struct Biol* **8**, 738-48 (1998).
257. Sanchez-Ruiz, J.M. & Makhatadze, G.I. To charge or not to charge? *Trends Biotechnol* **19**, 132-5 (2001).
258. Spassov, V.Z., Karshikoff, A.D. & Ladenstein, R. Optimization of the electrostatic interactions in proteins of different functional and folding type. *Protein Sci* **3**, 1556-69 (1994).
259. Spector, S. et al. Rational modification of protein stability by the mutation of charged surface residues. *Biochemistry* **39**, 872-9 (2000).
260. Shaw, K.L., Grimsley, G.R., Yakovlev, G.I., Makarov, A.A. & Pace, C.N. The effect of net charge on the solubility, activity, and stability of ribonuclease Sa. *Protein Sci* **10**, 1206-15 (2001).
261. Serrano, L., Horovitz, A., Avron, B., Bycroft, M. & Fersht, A.R. Estimating the contribution of engineered surface electrostatic interactions to protein stability by using double-mutant cycles. *Biochemistry* **29**, 9343-52 (1990).
262. Hofmeister, F. Zur Lehre von der Wirkung der Salze. Zweite Mittheilung. *Arch. Exptl. Pathol. Pharmakol.* **24**, 247-260 (1888).

263. Ramos, C.H. & Baldwin, R.L. Sulfate anion stabilization of native ribonuclease A both by anion binding and by the Hofmeister effect. *Protein Sci* **11**, 1771-8 (2002).
264. Hamada, D. & Goto, Y. Alcohol- and Salt-induced Partially Folded Intermediates. in *Protein Folding Handbook*, Vol. 2 (eds. Buchner, J. & Kiefhaber, T.) 884-915 (Wiley-VCH Verlag, Weinheim, 2005).
265. Pappenberger, G. *Characterization of the rate-limiting steps in tendamistat folding*, (University of Basel, Basel, 2000).
266. Ferguson, N.F., Capaldi, A.P., James, R., Kleanthous, C. & Radford, S.E. Rapid folding with and without populated intermediates in the homologous four-helix proteins Im7 and Im9. *J. Mol. Biol.* **286**, 1597-1608 (1999).
267. Bodenreider, C. & Kiefhaber, T. Interpretation of protein folding psi values. *J Mol Biol* **351**, 393-401 (2005).
268. Otzen, D.E. & Oliveberg, M. Salt-induced detour through compact regions of the protein folding landscape. *Proc. Natl. Acad. Sci. USA* **96**, 11746-11751 (1999).
269. Park, S.H., O'Neil, K.T. & Roder, H. An early intermediate in the folding reaction of the B1 domain of protein G contains a native-like core. *Biochemistry* **36**, 14277-83 (1997).
270. Khorasanizadeh, S., Peters, I.D. & Roder, H. Evidence for a three-state model for protein folding from kinetic analysis of ubiquitin variants with altered core residues. *Nat. Struct. Biol.* **3**, 193-205 (1996).
271. Eyring, H. The activated complex in chemical reactions. *J. Chem. Phys.* **3**, 107-115 (1935).
272. Grosman, C., Zhou, M. & Auerbach, A. Mapping the conformational wave of acetylcholine receptor channel gating. *Nature* **403**, 773-776 (2000).

8. Manuscripts Ready for Submission

8.1 Shape of Free Energy Barrier for Tendamistat Folding Measured by Multiple Perturbation Analysis

Shape of the Free Energy Barrier for Tendamistat Folding Measured by Multiple Perturbation Analysis

Manuela Schätzle and Thomas Kiefhaber*

Biozentrum der Universität Basel
Department of Biophysical Chemistry
Klingelbergstr. 70
CH-4056 Basel
Switzerland

Running title: Shape of protein folding barriers

*Correspondence should be addressed to T.K.: phone: ++41612672194; fax: ++41612672189; e-mail: t.kiefhaber@unibas.ch

Abstract

The characterization of the free energy barriers has been a major goal in studies on the mechanism of protein folding. Here we present experiments that allow to obtain information on the shape of the free energy barriers. By applying multiple perturbations, e.g. temperature and denaturant, transition state movements are more easily detected than by applying a single perturbation. We used the small α-amylase inhibitor tendamistat as a model protein. Tendamistat is an apparent two-state folder, but it was shown that its folding mechanism involves two consecutive transition states and a high energy intermediate. Measuring the effect of temperature and denaturant on the position of the transition state in tendamistat wild-type and several mutants showed, that the early transition state shows pronounced Hammond behavior. The position of the late transition state, in contrast, is almost insensitive to the applied perturbations. These results suggest that the barriers in protein folding become narrower as the native state is approached.

Introduction

Characterization of the transition barriers separating the ensemble of unfolded chains from the native state is an important step towards the understanding of the mechanism of protein folding. A common approach is the analysis of the rate-equilibrium free energy relationships (REFERs), which test the effect of a perturbation ∂x on the kinetics and the equilibrium of a reaction.(1-8) For many reactions changes in activation free energy ($\Delta G^{0\ddagger}$) induced by changes in solvent conditions or in structure are linearly related to the corresponding changes in equilibrium free energy (ΔG^{0}) between reactants and products (1, 6, 7). To quantify the energetic sensitivity of the transition states in respect to a perturbation, ∂x, a proportionality constant can be defined (1):

$$\alpha_x = \frac{\partial \Delta G^{0\ddagger} / \partial x}{\partial \Delta G^{0} / \partial x} \qquad [1]$$

α_x is commonly used to obtain information on the structural properties of the transition state and it is a measure for the position of the transition state along the reaction coordinate probed by ∂x. The range of α_x is typically between 0 for an unfolded-like transition state to 1 for a native-like transition state. Equation [1] shows that α_x can be experimentally determined by applying a perturbation ∂x and plotting the resulting values of $\Delta G_f^{0\ddagger}$ *vs* ΔG^0 or $\ln(k_f)$ *vs* $\ln(K_{eq})$ (Leffler plots). Information on different structural and thermodynamic properties of transition barriers are obtained by applying different perturbations ∂x (7, 8). The most common perturbation in protein folding is the addition of denaturants like urea and GdmCl (9). The α_D-value

$$\alpha_D = \frac{\partial \Delta G^{0\ddagger} / \partial[\text{Denaturant}]}{\partial \Delta G^{0} / \partial[\text{Denaturant}]} \qquad [2]$$

locates the transition state along the reaction coordinate in terms of accessible surface area (ASA) buried in the transition state relative to the ground states U (unfolded state) and N (native state) (10). Other solvent-induced perturbations that have been applied include effects of pressure (11, 12) and temperature (13-19). For structural characterization of protein folding transition states the effect of mutations on folding and stability is widely used (α_S- or φ-value) (20, 21).

Leffler plots obtained from various perturbations are linear over a wide range of experimental conditions for folding reactions of many proteins (7). This shows that transition state structures are frequently insensitive to perturbations and indicates that barriers for folding are narrow and robust maxima in the free energy landscape (6, 7, 22-24). However, deviations from linearity in REFERs have also been observed in protein folding and can have different origins: (i) a change from two-state folding to folding through a populated intermediate (25-27); (ii) a change in the rate-limiting step in an apparent two-state reaction (18, 28-31), (iii) a shift between parallel pathways (7, 32), (iv) Hammond behavior, i.e. a gradual movement of the transition state along the reaction coordinate caused by a broad barrier region (6, 7, 22-24) and (v) structural changes in the ground states (7). Elucidation of the origins of these non-linearities therefore yields information on the shape of the transition barriers and on the mechanism of protein folding (6-8).

Analysis of non-linear Leffler plots reported for a large number of apparent two-state folders showed that folding of these proteins is best explained by a sequential folding model with

consecutive transition states and at least one metastable high energy intermediate (31). Gradual transition state movements were reported for several proteins when the effect of mutations was investigated. However, in most proteins these effects could be attributed to changes in the structure of the unfolded state (7). This leads to a movement of the position of the transition state relative to the unfolded state, although the transition state structure remains unchanged (6-8, 33). A detailed analysis of data from mutagenesis showed that transition state structures are remarkably stable towards amino acids replacements in virtually all investigated proteins. This suggested that transition states represent structurally well-defined maxima on the folding free energy landscape (7) and showed that Hammond behavior is rare.

One of the clearest examples for Hammond behavior was reported for the α-amylase inhibitor tendamistat. Tendamistat shows perfectly linear Leffler plots induced by GdmCl (12, 34). Measuring the effect of pressure on folding and stability as a function of denaturant concentration showed, however, that the volume of the transition state increases with increasing denaturant concentrations and that the compactness (ΔASA) of the transition state increases with increasing pressure (8, 12). The observed transition state movements are not accompanied by ground state effects. These results suggested that Hammond behavior in protein folding may be revealed by applying several perturbations. To test, whether Hammond behavior can also be observed by other perturbations and to test the broadness of the different barriers encountered during tendamistat folding we used multiple perturbation analysis by measuring the effect of temperature and denaturant on tendamistat folding and stability

Material and Methods

Materials. Tendamistat wild-type protein was a gift from Klaus Koller (Hoechst, Frankfurt, Germany). The variants L14V and N25A were constructed, expressed in *Streptomyces lividans* and purified as described by Haas-Lauterbach *et al*. (35). Ultrapure GdmCl was obtained by Nigu Chemie (Waldkaiburg, Germany). All other chemicals were analysis grade and purchased from Merck (Darmstadt, Germany). All experiments were carried out in 100 mM glycine, pH 2.0 or in 100 mM cacodylic acid, pH 7.0.

Equilibrium unfolding transitions. The GdmCl-induced equilibrium transitions were monitored by the change in ellipticity at 227 nm in an Aviv 62A DS spectropolarimeter. Protein concentrations were 10 μM. The data were fitted to a two-state model following the procedure described by Santoro & Bolen (36).

Kinetic measurements. Refolding and unfolding kinetics were measured in an Applied Photophysics SX.18MV stopped-flow instrument. The change in fluorescence above 320 nm after excitation at 276 nm was monitored. The final protein concentration was 3.8 μM.

Analysis of the effect of temperature and denaturant on protein folding and stability. The free energies of activation for folding ($\Delta G_f^{0\ddagger}$) and unfolding ($\Delta G_u^{0\ddagger}$) were calculated using extra-thermodynamic relationships

$$k_f = k_f^0 \cdot e^{-\Delta G_f^{0\ddagger}/\mathrm{RT}} \quad \text{and} \quad k_u = k_u^0 \cdot e^{-\Delta G_u^{0\ddagger}/\mathrm{RT}} \qquad [3]$$

where the pre-exponential factor, k_0 represents the maximum rate constant for protein folding in the absence of free energy barriers. This value was estimated to be in the order of 10^7–10^8 s^{-1} (37, 38). A value of 10^8 s^{-1} was used in the fits. If the pre-exponential factor is independent

of the change in solvent conditions, the cross-interaction parameters are independent of the absolute value of k_0. However, the absolute values of $\Delta S_f^{0\ddagger}$ and $\Delta S_u^{0\ddagger}$ depend on k_0 and should thus be treated with caution.

The microscopic rate constants for folding (k_f) and unfolding (k_u) were determined from the apparent rate constant (λ) and the equilibrium constant (K_{eq}) according to the two-state model

$$\lambda = k_f + k_u \text{ and } K_{eq} = \frac{k_f}{k_u} \quad [4]$$

The effect of GdmCl on k_f and k_u was analyzed according to equ. [5] (8, 9)

$$\ln k_{f,u} = \ln k_{f,u}(H_2O) - \frac{m_{f,u}}{RT}[denaturant] \quad [5]$$

Leffler plots were calculated by determining k_f-values directly from the refolding limb of the chevron plot. k_f in the transition region and under unfolding conditions were calculated from the measured apparent rate constant (λ) using equ. [4]

The entropy changes for folding and unfolding were determined from the effect of temperature on the folding and unfolding rate constants at different denaturant concentrations using equ. [3] and [6]

$$\Delta G^{0\ddagger} = \Delta H^{0\ddagger}(T_0) - T \cdot \Delta S^{0\ddagger}(T_0) + \Delta C_p^{\ddagger}\left(T - T_0 - T \cdot \ln\frac{T}{T_0}\right) \quad [6]$$

with a reference temperature (T_0) of 298.15 K.

Global fitting of the effect of temperature and denaturant. To globally fit the Chevron plots measured at different temperatures we assumed that the activation parameters $\Delta H^{0\ddagger}$, $\Delta S^{0\ddagger}$ and $\Delta C_p^{0\ddagger}$ depend linearly on the denaturant concentration as observed for the respective equilibrium thermodynamic parameters (39). This allows a global fit of the data according to equation [7]

$$\Delta G^{0\ddagger}\left(T,[GdmCl]\right) = \left(\Delta H^{0\ddagger}(T_0,H_2O) + h(T_0)[GdmCl]\right) - T\left(\Delta S^{0\ddagger}(T_0,H_2O) + s(T_0)[GdmCl]\right) + \left(\Delta C_p^{0\ddagger}(H_2O) + c[GdmCl]\right)\left[T - T_0 - T\ln\left(T/T_0\right)\right] \quad [7]$$

with $h(T_0) = \partial\Delta H^{0\ddagger}/\partial[GdmCl]$, $s(T_0) = \partial\Delta S^{0\ddagger}/\partial[GdmCl]$ and $c = \partial\Delta C_p^{0\ddagger}/\partial[GdmCl]$. $\Delta H^{0\ddagger}(T_0,H_2O)$, $\Delta S^{0\ddagger}(T_0,H_2O)$ and $\Delta C_p^{0\ddagger}(H_2O)$ are the entropy, enthalpy and the heat capacity of activation in the absence of denaturant at the reference temperature T_0 = 298.15 K. With $m_{f,u}(T) = \partial\Delta G_{f,u}^{0\ddagger}\left(T,[GdmCl]\right)/\partial[GdmCl]$ and equation 7 we obtain the temperature dependence of the kinetic m-values:

$$m_{f,u}(T) = h_{f,u}(T_0) - T\cdot s_{f,u}(T_0) + c_{f,u}\cdot\left[T - T_0 - T\ln\left(T/T_0\right)\right] \quad [8]$$

Analysis of published data. The temperature dependence of the kinetic and equilibrium m-values reported for FKBP12 (40) and for a destabilized variant of T4 lysozyme (41, 42) were used to calculate cross-interactions parameters. For barnase (43) and CI2 (43) no ΔG^0 values were reported and the transition state movement could thus not be quantified. For *Bs*-CspB and *Bc*-Csp the denaturant dependence of ΔS^0 and $\Delta S_{f,u}^{0\ddagger}$ was reported (14, 44) and used for calculation of the p_{DT} value.

Data fitting. The program ProFit (Quantum Soft, Zürich, Switzerland) was used for all data fitting.

Result and Discussion

Transition state movement in tendamistat folding. A systematic way to analyze transition state movements was introduced by Jencks and co-workers by applying self-interaction and cross-interaction parameters (24, 45). A self-interaction parameter p_x measures the shift in the position of the transition state along the reaction coordinate in response to changes in ΔG^0 caused by a perturbation ∂x.

$$p_x = \frac{\partial \alpha_x}{\partial \Delta G_x^0} = \frac{\partial^2 \Delta G_f^{0\ddagger}}{\left(\partial \Delta G_x^0\right)^2} \qquad [9]$$

Such a shift causes a curvature in the corresponding Leffler plot. The sensitivity in the detection of transition state movements can be improved by measuring the position of the transition state along a reaction coordinate α_x when a second perturbation ∂y is applied.

$$p_{xy} = \frac{\partial \alpha_x}{\partial \Delta G_y^0} = \frac{\partial \alpha_y}{\partial \Delta G_x^0} = \frac{\partial^2 \Delta G_f^{0\ddagger}}{\left(\partial \Delta G_x^0\right)\left(\partial \Delta G_y^0\right)} \qquad [10]$$

By definition, Hammond behavior yields positive cross-interaction parameters p_{xy}, whereas negative values indicate anti-Hammond behavior or parallel pathways.

Wild-type tendamistat showed pronounced transition state movement when the effect of denaturant and pressure on folding and stability was probed at pH 2 (12). Chevron plots

measured at different pressures showed a positive denaturant-pressure cross-interaction parameter

$$p_{Dp} = \frac{\partial \alpha_D}{\partial \Delta G_p^0} = \frac{\partial \alpha_p}{\partial \Delta G_D^0} = 0.025 \pm 0.006 \text{ mol/kJ} \qquad [11]$$

without detectable ground state effects indicating real Hammond behavior (6, 8, 12). The low pH was chosen to decrease the effect of electrostriction. In addition wild-type tendamistat unfolds only at very high GdmCl concentrations at neutral pH. Thus, measurements at pH 2 give more reliable baselines for the equilibrium transition and facilitate determination of folding and unfolding rate constants in the linear parts of the chevron plots. To test whether transition state movement can also be induced by a change in temperature we measured Chevron plots at pH 2.0 and temperatures between 5° C and 46° C. Chevron plots with linear folding and unfolding limbs are observed at all temperatures (Fig. 1). Assuming a two-state model, the rate constants and kinetic m-values for the folding (m_f) and unfolding reaction (m_u) obtained from the Chevron plots agree well with equilibrium values (data not shown) supporting the previously described two-state behavior of tendamistat (12, 34). Figure 1B shows that a perfectly linear Leffler plot is obtained from the Chevron plot at 25 ºC, indicating that the change in ASA between unfolded state and the transition state is insensitive to denaturant concentration. Linear Leffler plots are also observed at all other investigated temperatures.

To test whether the structure of the transition state of tendamistat folding is sensitive to a change in temperature we determined the denaturant temperature cross-interaction parameter from the data shown in Figure 1 according to

$$p_{DT} = \frac{\partial^2 \Delta G^{0\ddagger}}{\partial \Delta G_D^0 \partial \Delta G_T^0} = \frac{\partial \alpha_D}{\partial \Delta G_T^0} = \frac{\partial \alpha_T}{\partial \Delta G_D^0} \qquad [12]$$

Equation 12 shows that p_{DT} can be determined in two different ways. The effect of temperature on α_D, i.e. on the relative change in ASA between unfolded state and transition state, can be measured. Alternatively, the effect of GdmCl-concentration on α_T, i.e. on the relative entropy change between unfolded state and transition state, can be determined. For real Hammond behavior the p_{DT} values obtained either way should be identical. Figure 1C shows the effect of a change in ΔG^0 induced by a change in temperature ($\Delta\Delta G_T^0$) on α_D. α_D increases significantly as tendamistat is destabilized by a change in temperature. A linear fit of the data gives a p_{DT}-value of $(8.1\pm0.8)\cdot10^{-3}$ mol/kJ. The change in α_D is caused by real Hammond behavior since it is not accompanied by ground state effects as indicated by the temperature-independence of the equilibrium m-value ($m_{eq} = \partial\Delta G^0 / \partial[GdmCl]$) (Fig. 1D). Hammond behavior is confirmed by analyzing the changes in ΔS^0 and $\Delta S^{0\ddagger}$ with denaturant concentration. Figure 1E shows that α_T increases as tendamistat is destabilized by increasing denaturant concentration while GdmCl has no effect on ΔS^0 (Fig. 1F) The change in α_T with denaturant concentrations gives a p_{DT} value of $(8.7\pm0.8)\cdot10^{-3}$ mol/kJ, which is essentially identical to the value observed for the change in α_D with temperature. The data shown in Figure 1 can be fitted globally to eq. [7], which results in $p_{DT}=(8.2\pm3.4)\cdot10^{-3}$ mol/kJ (see table 1).

These results show that the ASA of the transition state for tendamistat folding is sensitive to changes in temperature and that the entropy of the transition state is sensitive to denaturant concentration. This is a surprising finding since linear Chevron plots were observed for wild-

type tendamistat folding under all conditions. However, the results are in agreement with our previous observation of Hammond behavior induced in response to perturbation by pressure and denaturant. A detailed discussion of other thermodynamic properties of the transition state for folding of wild-type tendamistat and of the other variants investigated in this work will be given elsewhere (M.S. & T.K., manuscript in preparation).

Effect of pH on Hammond behavior. To test whether Hammond behavior is also observed at neutral pH we determined the p_{DT} value of the tendamistat L14V variant, which is destabilized by 11.9±0.2 kJ/mol compared to wild-type tendamistat at 25 ºC and pH 7. This allows reliable determination of kinetic and equilibrium parameters at pH 7. The L14V variant shows linear refolding and unfolding limbs of the chevron plot at all temperatures (Fig. 2A) resulting in linear Leffler plots over the complete accessible range of GdmCl concentrations (Fig. 2B) indicating a denaturant self-interaction parameter close to 0. The transition state of the L14V variant is structurally identical to the wt transition state with an α_D-value of 0.67 at 25 ºC. Figure 1C shows the effect of ΔG_T^0 on the α_D-value. As for the wild-type protein at pH 2 the L14V variant shows an increase in α_D-value with increasing ΔG_T^0, indicating temperature-induced transition state movement. The effect of ΔG_T^0 on the kinetic and equilibrium m-values (Fig. 1D) indicates the absence of ground state effects. The p_{DT}-value is $(8.5\pm0.7)\cdot10^{-3}$ mol/kJ, which is almost identical to the value observed for the wild-type protein at pH 2 (table 1). Essentially the same p_{DT}-value is obtained when the effect of GdmCl concentration on α_T is determined ($p_{TD}=(8.6\pm0.5)\cdot10^{-3}$ mol/kJ; Fig. 1E and table 1)). As for wild-type protein ΔS^0 is independent of denaturant concentrations, indicating the absence of ground state effects. The Chevron plots for the L14V variant measured at different temperatures can be fitted with a global p_{DT} value of $(8.5\pm2.1)\cdot10^{-3}$ mol/kJ.

Hammond behavior in the late transition state of tendamistat folding. In previous studies we have shown that tendamistat folding involves two sequential transition states (18). In wild-type tendamistat and in the L14V variant the early transition state is rate-limiting for folding and unfolding under all conditions. Some variants like tendamistat C45A/C73A show a GdmCl-dependent switch between the two transition states (18) whereas in other mutants the late transition state is rate-limiting under all conditions. An example of a tendamistat variant with a late transition state is tendamistat N25A, which is destabilized by 23.6 kJ/mol compared to the wild-type protein. The N25A variant shows two-state folding and unfolding kinetics under all conditions and a linear GdmCl-induced Leffler plot (Fig. 3A, B). However, the α_D-value of 0.83 at 25 ºC is significantly higher than for wild-type tendamistat (α_D=0.67) indicating that the mutations leads to a switch from the early to the late transition state. To test for Hammond behavior in the late transition state we measured Chevron plots at different temperatures and determined the p_{DT}-value. Figure 3C shows that α_D increases significantly as the protein is destabilized by temperature. Accordingly, α_T increases with decreasing protein stability upon addition of denaturant, indicating transition state movement (Fig. 3E). However, the change in α_T with ΔG_D^0 is non-linear in the N25A variant and a decreasing p_{DT}-value with decreasing protein stability is observed. In contrast to the wild-type protein and to the L14V variant the transition state movement in the N25A variant is accompanied by major ground state effects as indicated by the increase in m_{eq} and ΔS^0 upon decreasing protein stability (Fig. 3D, F). The increased m_{eq} value upon protein destabilization with increasing temperature is in accordance with residual structure in the unfolded state, which is destabilized as the intramolecular interactions are weakened. This leads to a more solvent-exposed unfolded state. As previously observed for the effect of mutations on the m-values in many proteins (7), the changes in m_{eq} and ΔS^0 correlate with the changes in the respective properties of the folding reactions, m_f and $\Delta S_f^{0\ddagger}$ (Fig. 4A,C). In contrast, the changes in m_u

and $\Delta S_u^{0\ddagger}$ are weakly anti-correlated with the changes in m_{eq} and ΔS^0. This indicates Hammond behavior in addition to ground state effects in this variant. We therefore corrected the properties of the refolding reaction for the ground state effects to quantify the extent of Hammond behavior (Fig. 4B,D). Cross interaction plots of the corrected α_D and α_T values against ΔG_T^0 and ΔG_D^0, respectively, are linear with a p_{DT} value around $2.5 \cdot 10^{-3}$ mol/kJ (Fig. 4BD; table 1). This is about 4-times smaller than the value of wild-type tendamistat and the L14V variant indicating significantly less movement of the late transition state region compared to the early transition state. This result is supported by the comparison of the absolute effect of the change in protein stability on m_u and $\Delta S_u^{0\ddagger}$ (table 1). Both parameters change less in the late transition state compared to the early transition state indicating that the movement of the late transition state towards the native state is less pronounced than the movement of the early transition state. The same result is observed for late transition states in other tendamistat variants (data not shown). These results suggest that the early transition state of tendamistat folding represents a broader region of the free energy landscape compared to the late transition state (Fig. 5).

Temperature-induced Hammond behavior in protein folding. The presented results show that both the early and the late transition state in tendamistat folding exhibit temperature-induced Hammond behavior, which can be probed by the denaturant-temperature, cross interaction parameter. To investigate whether temperature-induced Hammond behavior is common in protein folding, we calculated p_{DT}-values for published data on different proteins. Only few studies have been performed on the temperature dependence of the kinetic *m*-values or on the denaturant dependence of the activation entropies in protein folding. Often, constant *m*-values are assumed at different temperatures and the published results do not allow determination of p_{DT} (16, 46). Table 2 shows p_{DT} values for 6 different monomeric proteins

calculated from published data. For all proteins non-zero p_{DT} values are observed indicating transition state movements. One of the proteins, T4 lysozyme, has a negative cross-interaction parameter, arguing for parallel folding pathways (6, 7). A more detailed analysis of these data reveals additional strong ground state effects on the native state as indicated by the decreased m_{eq}-value upon destabilization by temperature. The other 5 proteins show positive cross-interaction parameters. For CI2 the apparent transition state movement is exclusively due to Hammond, whereas for barnase, CspB and Csp the transition state movements are caused by Hammond behavior in addition to ground state effects in the unfolded state. For CspB a non-linearity was observed for the temperature-dependence of the α_D-value indicating a change in the rate-limiting step. This is in accordance with our previous analysis on the denaturant-dependence of CspB folding, which indicated the presence of sequential transition states (31). For FKBP the apparent transition state movement seems to be caused by ground state effects in the native state but the errors of the analysis are large. In addition, it is not clear whether FKBP12 shows two-state equilibrium unfolding (31). These results show that temperature-induced Hammond behavior in protein folding is common. However, for all proteins the observed p_{DT} values are small.

Shape of the free energy barriers for protein folding. The results from the effect of temperature and denaturant on tendamistat folding show that Hammond behavior is only observed when multiple perturbations are applied. Applying single perturbations results in linear Leffler plots indicating that the transition state movement is weak. Similar results are obtained when p_{DT}-values are determined from published data on other proteins. Nearly all proteins show linear Leffler plots but exhibit Hammond behavior when the effect of temperature and denaturant is analyzed. Analysis of tendamistat variants that have different rate-limiting transition states show that the early transition state exhibits significantly stronger

Hammond behavior than the late transition state suggesting that the barriers become increasingly narrow and transition state structures become more defined as the folding polypeptide chain approaches the native state (Fig. 5). The observation of Hammond behavior is in accordance with previous results from the effect of pressure and denaturant on tendamistat folding. Combining the results from both studies suggests that the transition state moves along the entropy and volume reaction coordinates upon destabilization by denaturant and that the ASA of the transition state changes with destabilization by pressure or temperature. This is in contrast to our previous findings on the effect of mutations on the ASA of the transition state in a large number of proteins. This analysis showed that Hammond behavior is extremely rare and if observed only small (7). This suggested that protein folding transition states are structurally well-defined and native-like in topology. By applying multiple perturbations we could show that the broadness of the free energy barriers for protein folding is different for different reaction coordinates. Another interesting feature of the analysis of the effect of temperature and denaturant on folding of several proteins is the commonly observed absence of major ground state effects. This is again in contrast to results from mutational studies, which revealed major ground state effects on the unfolded state in most proteins (7). These results show that the ensemble of unfolded states is rather robust against changes in denaturant concentration and temperature, whereas its structure is often significantly changed by single mutations.

The temperature-induced transition state movement observed for tendamistat and other proteins presented in this work has important consequences for the comparison of folding simulations with experimental data. Since the ASA of the transition state is temperature dependent, the commonly performed high temperature simulations should give more compact transition state structures compared to the experimental data, which are usually obtained at

ambient temperatures. This supports the need for identical conditions in experiment and simulation.

Acknowledgements

This work was supported by a grant from the Swiss National Science Foundation.

Table 1. Effect of changes in protein stability induced by temperature ($\partial\Delta G_T^0$) on α_D and on m_{eq}, m_f and m_u and effect of changes in protein stability induced by denaturant ($\partial\Delta G_D^0$) on α_T and on ΔS_{eq}^0, $\Delta S_f^{0\ddagger}$ and $\Delta S_u^{0\ddagger}$.

	p_{DT}								
variant	$\partial\alpha_D/\partial\Delta G_T^0$	$\partial\alpha_T/\partial\Delta G_D^0$	global fit	$\partial m_{eq}/\partial\Delta G_T^0$	$\partial m_f/\partial\Delta G_T^0$	$-\partial m_u/\partial\Delta G_T^0$	$-\partial\Delta S_{eq}^0/\partial\Delta G_D^0$	$-\partial\Delta S_f^{0\ddagger}/\partial\Delta G_D^0$	$\partial\Delta S_u^{0\ddagger}/\partial\Delta G_D^0$
	(mol/kJ)·10^3	(mol/kJ)·10^3	(mol/kJ)·10^3	M^{-1} x10^2	$M^{-1}\cdot10^2$	$M^{-1}\cdot10^2$	$K^{-1}\cdot10^3$	$K^{-1}\cdot10^3$	$K^{-1}\cdot10^3$
wt	8.1 ±0.8	8.7 ±0.8	8.2 ±3.4	-0.2 ±1.0	3.7 ±0.8	-3.9 ±0.5	-0.2 ±0.3	2.2 ±0.2	-2.4 ±0.1
L14V	8.5 ±0.7	8.6 ±0.5	8.5 ±2.1	-0.2 ±0.8	4.2 ±0.9	-4.4 ±0.2	0.1 ±0.2	2.3 ±0.1	-2.2 ±0.1
N25A	4.6 ±0.5			9 ±1	10 ±1	-1.5 ±0.2	3.0 ±0.1	3.6 ±0.1	-0.8 ±0.1
N25A(c)	2.4 ±0.4	2.7 ±0.5		0	2.2 ±2.0	-1.5 ±0.2	0	0.6 ±0.1	-0.8 ±0.1

Table 2. p_{DT} values for proteins for which kinetic data on the effect of denaturant and temperature are available.

Protein	$p_{DT} = \partial\alpha_D / \partial\Delta G_T^0$ (mol/kJ) x10^3)	$\partial m_{eq} / \partial\Delta G_T^0$ (M^{-1} x10^2)	$\partial m_f / \partial\Delta G_T^0$ (M^{-1} x10^2)	$-\partial m_u / \partial\Delta G_T^0$ (M^{-1} x10^2)
Barnase[a] (43)	>0	>0	>0	<0
CI2[a] (43)	>0	~0	>0	<0
CspB[b,c] (14, 44)	8.6 ±0.1	7 ±5	9.1 ±3.3	-2.1 ±1.1
Csp[c] (44)	10.8 ±0.1	2.6 ±1.5	8.5 ±1.2	-5.3 ±0.6
FKBP12 (40)	7 ±26	-7 ±15	0.2 ±8.5	-9 ±7
T4 lysozyme (41, 42)	-17 ±2	-21 ±5	-42 ±8	23 ±5
tendamistat wt[e]	8.1 ±0.8	-0.2 ±1.0	3.7 ±0.8	-3.9 ±0.5
tendamistat L14V[e]	8.5 ±0.7	-0.2 ±0.8	4.2 ±0.9	-4.4 ±0.2
tendamistat N25A[e]	2.5 ±0.4	9 ±1	10 ±1	-1.5 ±0.2

[a] For these proteins no free energy data were available. Thus, we could only analyze the m-values against the temperature.
[b] The results of these proteins were calculated from the results of the global fits.
[c] Analysis of CspB reveals non-linearities for the changes of the a_D-values with decreasing the protein stability. Both p_{DT}-values are the different maxima.
[e] Data from this work.

References

1. Leffler, J. E. (1953) *Science* **117,** 340-341.

2. Leffler, J. E. & Grunwald, E. (1963) *Rates and equilibria of organic reactions* (Dover, New York).

3. Jencks, W. P. (1969) *Catalysis in Chemistry and Enzymology* (McGraw-Hill Book Company, New York).

4. Grosman, C., Zhou, M. & Auerbach, A. (2000) *Nature* **403,** 773-776.

5. Horovitz, A., Amir, A., Danziger, O. & Kafri, G. (2002) *Proc. Natl. Acad. Sci. U S A* **99,** 14095-14097.

6. Sánchez, I. E. & Kiefhaber, T. (2003) *Biophys. Chem.* **100,** 397-407.

7. Sánchez, I. E. & Kiefhaber, T. (2003) *J. Mol. Biol.* **327,** 867-884.

8. Kiefhaber, T., Sánchez, I. E. & Bachmann, A. (2005) in *Protein Folding Handbook*, eds. Buchner, J. & Kiefhaber, T. (Wiley/VCH, Weinheim), Vol. 1, pp. 411-453.

9. Tanford, C. (1970) *Adv. Prot. Chem.* **24,** 1-95.

10. Myers, J. K., Pace, C. N. & Scholtz, J. M. (1995) *Protein Sci.* **4,** 2138-2148.

11. Vidugiris, G. J. A., Markley, J. L. & Royer, C. A. (1995) *Biochemistry* **34,** 4909-4912.

12. Pappenberger, G., Saudan, C., Becker, M., Merbach, A. E. & Kiefhaber, T. (2000) *Proc. Natl. Acad. Sci. USA* **97,** 17-22.

13. Pohl, F. M. (1976) *FEBS Lett.* **65,** 293-296.

14. Schindler, T. & Schmid, F. X. (1996) *Biochemistry* **51,** 16833-16842.

15. Schönbrunner, N., Pappenberger, G., Scharf, M., Engels, J. & Kiefhaber, T. (1997) *Biochemistry* **36,** 9057-9065.

16. Scalley, M. L. & Baker, D. (1997) *Proc. Natl. Acad. Sci. USA* **94,** 10636-10640.

17. Kuhlman, B., Luisi, D. L., Evans, P. A. & Raleigh, D. P. (1998) *J. Mol. Biol.* **284,** 1661-1670.

18. Bachmann, A. & Kiefhaber, T. (2001) *J. Mol. Biol.* **306,** 375-386.

19. Jäger, M., Nguyen, H., Crane, J. C., Kelly, J. W. & Gruebele, M. (2001) *J. Mol. Biol.* **311,** 373-393.

20. Matthews, C. R. (1987) *Meth. Enzymol.* **154,** 498-511.

21. Fersht, A. R., Matouschek, A. & Serrano, L. (1992) *J. Mol. Biol.* **224,** 771-782.

22. Hammond, G. S. (1955) *J. Am. Chem. Soc.* **77,** 334-338.

23. Thornton, E. R. (1967) *J. Am. Chem. Soc.* **89,** 2915-2927.

24. Jencks, W. P. (1985) *Chem. Rev.* **85,** 511-527.

25. Ikai, A. & Tanford, C. (1973) *J. Mol. Biol.* **73,** 145-163.

26. Tanford, C., Aune, K. C. & Ikai, A. (1973) *J. Mol. Biol.* **73,** 185-197.

27. Bachmann, A. & Kiefhaber, T. (2005) in *Protein Folding Handbook*, eds. Buchner, J. & Kiefhaber, T. (Wiley/VCH, Weinheim), Vol. 1, pp. 379-410.

28. Jonsson, T., Waldburger, C. D. & Sauer, R. T. (1996) *Biochemistry* **35,** 4795-4802.

29. Kiefhaber, T., Bachmann, A., Wildegger, G. & Wagner, C. (1997) *Biochemistry* **36,** 5108-5112.

30. Walkenhorst, W. F., Green, S. & Roder, H. (1997) *Biochemistry* **36,** 5795-5805.

31. Sánchez, I. E. & Kiefhaber, T. (2003) *J. Mol. Biol.* **325,** 367-76.

32. Wright, C. F., Lindorff-Larsen, K., Randles, L. G. & Clarke, J. (2003) *Nat. Struct. Biol.* **10,** 658-662.

33. Farcasiu, D. (1975) *J. Chem. Ed.* **52,** 76-79.

34. Schönbrunner, N., Koller, K.-P. & Kiefhaber, T. (1997) *J. Mol. Biol.* **268,** 526-538.

35. Haas-Lauterbach, S., Scharf, M., Sprunkel, B., Neeb, M., Koller, K.-P. & Engels, J. (1993) *Appl. Microbiol. Biotech.* **38,** 719-727.

36. Santoro, M. M. & Bolen, D. W. (1988) *Biochemistry* **27,** 8063-8068.

37. Krieger, F., Fierz, B., Bieri, O., Drewello, M. & Kiefhaber, T. (2003) *J. Mol. Biol.* **332,** 265-274.

38. Fierz, B. & Kiefhaber, T. (2004) in *Protein Folding Handbook*, eds. Buchner, J. & Kiefhaber, T. (WILEY-VCH Verlag GmbH & Co KGaA, Weinheim), pp. 805-851.

39. Schellman, J. A. (1978) *Biopolymers* **17,** 1305-1322.

40. Main, E. R. G., Fulton, K. F. & Jackson, S. E. (1999) *J. Mol. Biol.* **291,** 429-444.

41. Chen, B. L., Baase, W. A. & Schellman, J. A. (1989) *Biochemistry* **28,** 691-699.

42. Chen, B. L. & Schellman, J. A. (1989) *Biochemistry* **28,** 685-691.

43. Matouschek, A., Otzen, D. E., Itzhaki, L., Jackson, S. E. & Fersht, A. R. (1995) *Biochemistry* **34,** 13656-13662.

44. Perl, D., Jacob, M., Bánó, M., Stupâk, M., Antalík, M. & Schmid, F. X. (2002) *Biophys. Chem.* **2-3,** 173-190.

45. Jencks, D. A. & Jencks, W. P. (1977) *J. Am. Chem. Soc.* **99,** 7948-7960.

46. Kuhlman, B. & Raleigh, D. P. (1998) *Prot. Sci.* **7,** 2405-2412.

Figure Legends

Figure 1. Effect of denaturant and temperature on folding of tendamistat wild type at pH 2. (A) GdmCl-dependence of the apparent rate constants for folding. The lines represent the result of the fit of the kinetic data. (B) Leffler plot of the effect of GdmCl concentration on the equilibrium (K_{eq}) and folding rate constant (k_f) calculated from the kinetic data at 25°C. The slope corresponds to the α_D-value and a linear fit gives a value of 0.67. (C-F) Analysis of the temperature-denaturant cross-interaction parameter p_{DT}. Effect of ΔG_T^0 on m_{eq}, m_f and $-m_u$ (D) and on α_D (C), respectively, and effect of ΔG_D^0 on $-\Delta S_{eq}^0$, $-\Delta S_f^{0\ddagger}$ and $\Delta S_u^{0\ddagger}$ (F) and on α_T (E), respectively. The data are taken from individual fits. The results of the linear fits are given in table 1.

Figure 2. Effect of denaturant and temperature on folding of the tendamistat variant L14V at pH 7. (A) GdmCl-dependence of the apparent rate constants for folding. The lines represent the result of the fit of the kinetic data. (B) Leffler plot of the effect of GdmCl concentration on the equilibrium (K_{eq}) and folding rate constant (k_f) calculated from the kinetic data at 25°C. The slope corresponds to the α_D-value and a linear fit gives a value of 0.71. (C-F) Analysis of the temperature-denaturant cross-interaction parameter p_{DT}. Effect of ΔG_T^0 on m_{eq}, m_f and $-m_u$ (D) and on α_D (C), respectively, and effect of ΔG_D^0 on $-\Delta S_{eq}^0$, $-\Delta S_f^{0\ddagger}$ and $\Delta S_u^{0\ddagger}$ (F) and on α_T (E), respectively. The data are taken from individual fits. The results of the linear fits are given in table 1.

Figure 3. Effect of denaturant and temperature on folding of the tendamistat variant N25A at pH 7. (A) GdmCl-dependence of the apparent rate constants for folding. The lines represent the result of the fit of the kinetic data. (B) Leffler plot of the effect of GdmCl concentration on the equilibrium (K_{eq}) and folding rate constant (k_f) calculated from the kinetic data at 25°C. The slope corresponds to the α_D-value and a linear fit gives a value of 0.83. (C-F) Analysis of the temperature-denaturant cross-interaction parameter p_{DT}. Effect of ΔG_T^0 on m_{eq}, m_f and $-m_u$ (D) and on α_D (C), respectively, and effect of ΔG_D^0 on $-\Delta S_{eq}^0$, $-\Delta S_f^{0\ddagger}$ and $\Delta S_u^{0\ddagger}$ (F) and on α_T (E), respectively. The data are taken from individual fits. The results of the linear fits are given in table 1.

Figure 4. Correlation of the changes in m_{eq} with changes in m_f and m_u (A) and correlation of the changes in ΔS_{eq}^0 with changes in $\Delta S_f^{0\ddagger}$ and $\Delta S_u^{0\ddagger}$ (C) for tendamistat variant N25A. Correction of the properties of the refolding reaction for the ground state effects leads to the cross interaction plots of the corrected α_D (B) and α_T values (D) against ΔG_T^0 and ΔG_D^0, respectively.

Figure 5. Schematic drawing of the free energy barrier for folding of tendamistat. The response of variation in temperature on the early transition states (TS1) is more sensitive than on the late one (TS2) due to the different broadness of the barriers.

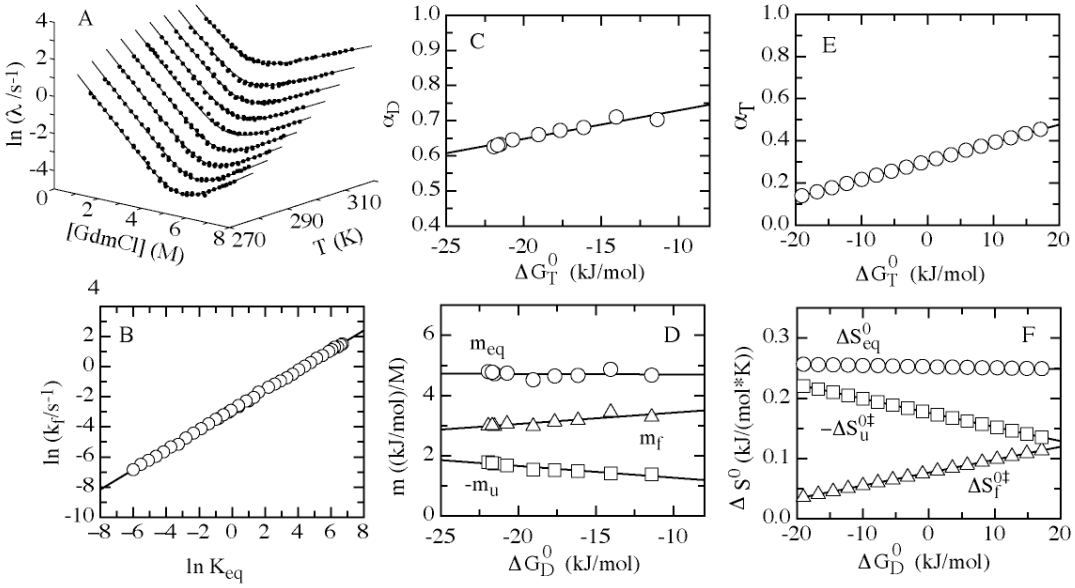
A
ln (λ /s-1)
[GdmCl] (M)
T (K)
B
ln (kf/s-1)
ln Keq
C
αD
ΔG0T (kJ/mol)
D
meq
mf
-mu
m ((kJ/mol)/M)
ΔG0D (kJ/mol)
E
αT
ΔG0T (kJ/mol)
F
ΔS0eq
-ΔS0‡u
ΔS0‡f
Δ S0 (kJ/(mol*K))
ΔG0D (kJ/mol)

Figure 1

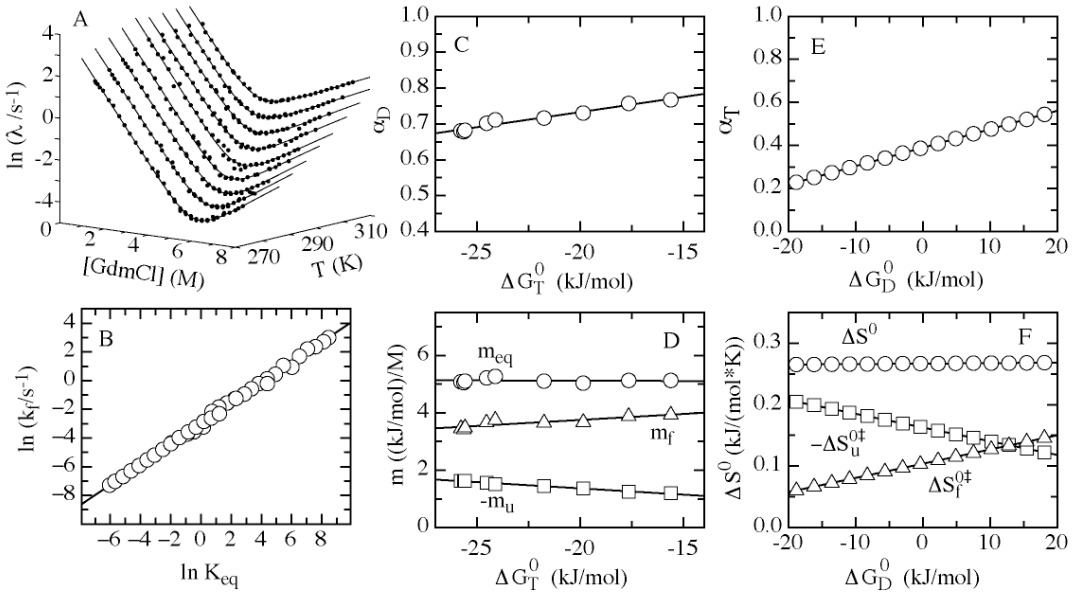
A
ln (λ /s-1)
[GdmCl] (M)
T (K)
B
ln (kf/s-1)
ln Keq
C
αD
ΔG0T (kJ/mol)
D
meq
mf
-mu
m ((kJ/mol)/M)
ΔG0T (kJ/mol)
E
αT
ΔG0D (kJ/mol)
F
ΔS0
-ΔS0‡u
ΔS0‡f
ΔS0 (kJ/(mol*K))
ΔG0D (kJ/mol)

Figure 2

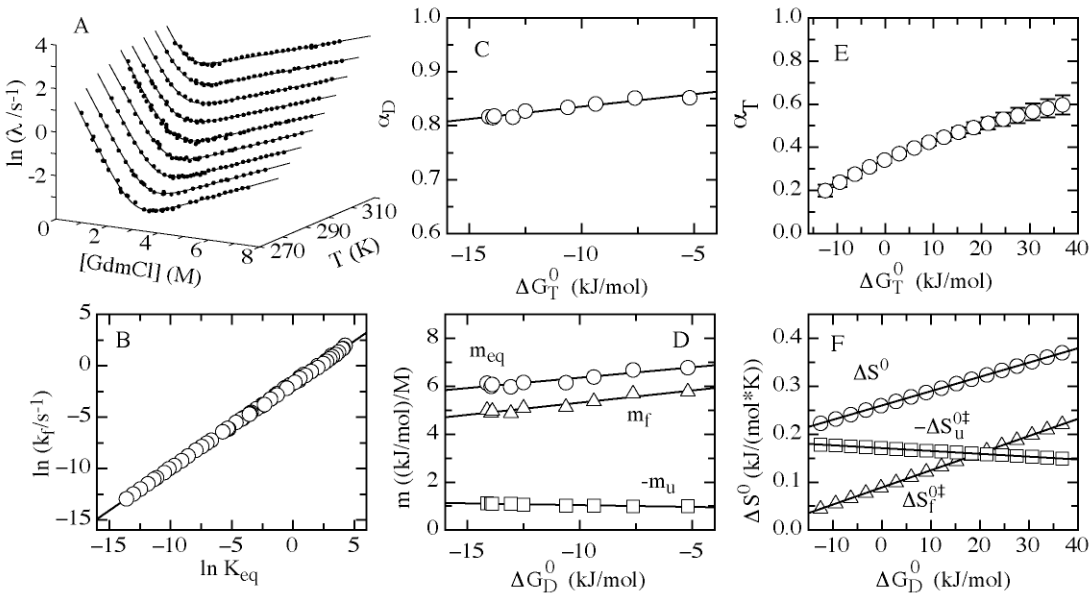
A
ln (λ /s-1)
[GdmCl] (M)
T (K)
B
ln (kf/s-1)
ln Keq
C
αD
ΔG0T (kJ/mol)
D
meq
mf
-mu
m ((kJ/mol)/M)
ΔG0D (kJ/mol)
E
αT
ΔG0T (kJ/mol)
F
ΔS0
−ΔS0‡u
ΔS0‡f
ΔS0 (kJ/(mol*K))
ΔG0D (kJ/mol)

Figure 3

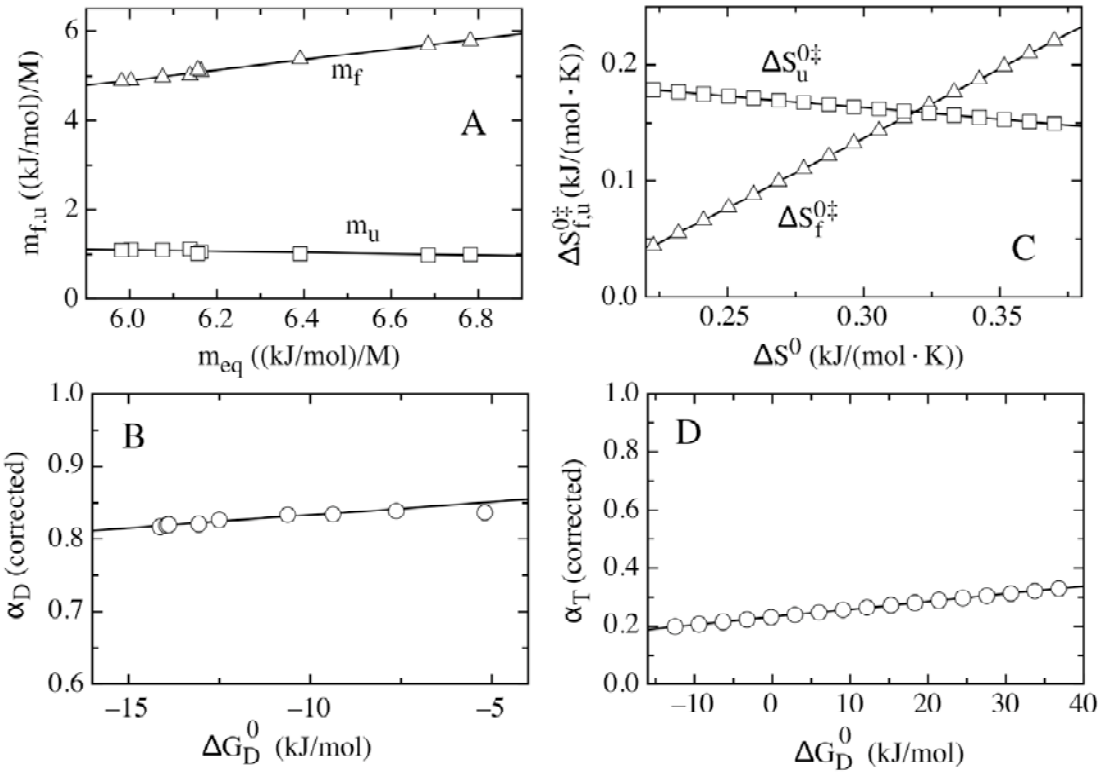
A
m_f
m_u
$m_{f,u}$ ((kJ/mol)/M)
m_{eq} ((kJ/mol)/M)
B
α_D (corrected)
ΔG_D^0 (kJ/mol)
C
$\Delta S_u^{0\ddagger}$
$\Delta S_f^{0\ddagger}$
$\Delta S_{f,u}^{0\ddagger}$ (kJ/(mol · K))
ΔS^0 (kJ/(mol · K))
D
α_T (corrected)
ΔG_D^0 (kJ/mol)

Figure 4

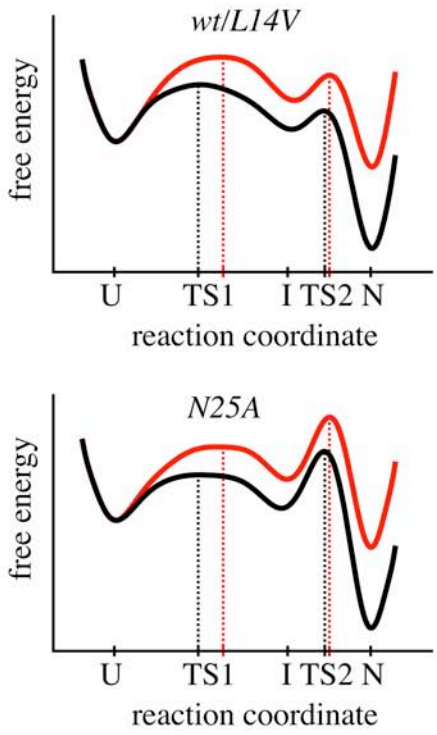
wt/L14V
free energy
U
TS1
I
TS2
N
reaction coordinate
N25A
free energy
U
TS1
I
TS2
N
reaction coordinate

Figure 5

8.2 Thermodynamic Properties of the Transition States in Tendamistat Folding

Thermodynamic Properties of the Free Energy Barriers in Tendamistat Folding

Manuela Schätzle and Thomas Kiefhaber

Biozentrum der Universität Basel
Department of Biophysical Chemistry
Klingelbergstr. 70
CH-4056
Switzerland

Running title: Free Energy Barriers in Tendamistat Folding

*Correspondence should be addressed to T.K.: phone: ++41612672194; fax: ++41612672189; e-mail: t.kiefhaber@unibas.ch

Abstract

Folding of the all-β-sheet protein tendamistat involves two sequential transition states. In our recent work we analyzed the shape of the free energy barriers for tendamistat folding using multiple perturbation analysis. Here, we further analyzed the activation parameters of the free energy barriers and their denaturant-dependence to characterize the thermodynamic properties of both transition states in tendamistat folding. Determination of the activation parameters revealed linear denaturant-dependence of $\Delta H^{0\ddagger}$, $\Delta S^{0\ddagger}$ and $\Delta C_p^{0\ddagger}$ confirming the linear free energy model. The activation parameters of both transition states show only less difference but differ significantly in their denaturant dependences. The denaturant dependence of the entropy-values is correlated with the temperature dependence of the m-values and therefore can also be used to test for transition state movement. Analysis of the denaturant dependence of $\Delta H^{0\ddagger}$ reveals a less well-defined transition structure for the early transition state, in contrast to the late transitions state. The results confirm our previous observation, that the early transition state is rather broad compared to the late transition state, which is a narrow and structurally well-defined barrier. It further reveals the importance of multiple perturbation analysis to test the properties of the free energy barriers.

Abbreviations: GdmCl, guanidinium chloride; ASA, accessible surface area; REFER, rate-equilibrium free energy relationship

Introduction

The structural and thermodynamic characterization of the energy barriers between unfolded and native protein is one of the major goals of protein folding studies and has been targeted by several experimental approaches. A systematic way to analyze transition states is to determine the rate-equilibrium free energy relationships (REFERs).[1-6] It was observed in many reactions that the changes in activation free energy ($\Delta G^{0\ddagger}$) induced by changes in the solvent or in structure are linearly related to the corresponding changes in equilibrium free energy (ΔG^{0}) between reactants and products.[1,4] The proportionality constant[1]

$$\alpha_x = \frac{\partial \Delta G^{0\ddagger} / \partial x}{\partial \Delta G^{0} / \partial x} \tag{1}$$

quantify the energetic sensitivity of the transition states in respect to a perturbation, ∂x, and is a measure for the position of the transition state along the reaction coordinate. α_x is commonly used in protein folding to obtain information on the structural properties of the transition state. The range of α_x is normally from 0 for an unfolded-like transition state to 1 for a native-like transition state. An experimentally way to determine α_x is to plot $\Delta G_f^{0\ddagger}$ versus ΔG^0 or $\ln(k_f)$ versus $\ln(K)$ obtained by applying a perturbation ∂x (Leffler plot).

The most common perturbation applied in protein folding is the addition of denaturants, such as urea and GdmCl. With the proportionality constants of the denaturant dependences of the activation free energies ($m_{f,u} = \partial \Delta G^{0\ddagger} / \partial [\text{Denaturant}]$) and the equilibrium free energy ($m_{eq} = \partial \Delta G^{0} / \partial [\text{Denaturant}]$) we can define an α_D-value:

$$\alpha_D = \frac{\partial \Delta G^{0\ddagger} / \partial [Denaturant]}{\partial \Delta G^{0} / \partial [Denaturant]} = \frac{m_{f,u}}{m_{eq}} \tag{2}$$

It defines the relative change in solvent accessible surface area between the unfolded state and the transition state.[7] Other possible perturbations are structural changes upon site-directed mutagenesis[8-10] and variation of temperature[11-15] and pressure[16,17].

Deviations from linearity in the REFERs are frequently observed. They are shown to be caused by four major effects: (i) a change in the rate limiting step[5,14,18,19], (ii) a change from two-state folding to folding through a populated intermediate[20-22], (iii) a

change to a parallel pathway[6,23], (iv) a movement of the transition state along the reaction coordinate (Hammond behavior)[24] and (v) structural changes in the ground states[6]. Determination of the origins of nonlinear REFERs reveal important features on the shape of the transition barriers and on the mechanism in protein folding.[4,6,25]

Jencks and coworkers proposed a method to analyze transition state movements by applying self-interaction and cross-interaction parameters.[26] A self-interaction parameter p_x measures the shift in the position of the transition state along the reaction coordinate due to changes in equilibrium free energy upon perturbation.

$$p_x = \frac{\partial \alpha_x}{\partial \Delta G^0} = \frac{\partial^2 \Delta G_f^{0\ddagger}}{\left(\partial \Delta G^0\right)^2} \tag{3}$$

A positive p_D-value causes a curvature in the corresponding Leffler plot. To improve the sensitivity in the detection of transition state movements we analyzed the position of the transition state along the reaction coordinate α_x under different ΔG^0 caused by a second perturbation, ∂y: [26]

$$p_{xy} = \frac{\partial^2 \Delta G_f^{0\ddagger}}{\left(\partial \Delta G_x^0\right)\left(\partial \Delta G_y^0\right)} = \frac{\partial \alpha_x}{\partial \Delta G_y^0} = \frac{\partial \alpha_y}{\partial \Delta G_x^0} \tag{4}$$

By definition, Hammond behaviour and ground state effects will yield positive p_{DT}-values. Negative p_{DT}-values indicate anti-Hammond behaviour or parallel pathways.

For many proteins, Leffler plots are linear over a wide range of experimental conditions indicating that transition states are narrow and robust maxima in the free energy landscape.[4,6] Analysis of the effect of mutations and denaturant in protein folding showed that Hammond behavior is extremely rare and most apparent transition state movements are due to ground state effects.[6] Multiple perturbation analysis of tendamistat folding revealed that the broadness of the free energy barriers is different for different reaction coordinates.[15,17,27] Folding of the small all-β-sheet protein tendamistat (figure 1) occurs in two sequential steps.[14] Applying single perturbations results in linear Leffler plots under all conditions.[15,17,27] In contrast, combining denaturant perturbation with variation in temperature or pressure revealed Hammond behavior supporting the importance of multiple perturbation analysis to test the shape of free energy barriers in protein folding.[4,6,15,17] Hammond behavior was observed at different pH.[15] Significantly less Hammond behavior was found for the late transition state compared to the early transition state indicating that the early

transition state is a rather broad barrier whereas the late-transition state is narrow and structurally well-defined maximum.

To examine the thermodynamic properties of the free energy landscape in tendamistat folding we further analyzed the temperature dependence of the folding kinetics. We further analyzed the effect of transition state movement on the other thermodynamic parameters. We also verify the differences between the two transition states in tendamistat folding and their denaturant dependences.

Materials and Methods

Materials. Tendamistat wild type protein was a gift from Klaus Koller (Hoechst, Frankfurt, Germany). The tendamistat variants L14V, L14A and N25A were constructed, expressed in *Streptomyces lividans* and purified as described by Haas-Lauterbach *et al.*[28]. Ultrapure GdmCl was obtained by Nigu Chemie (Waldkaiburg, Germany). All other chemicals were analysis grade and purchased from Merck (Darmstadt, Germany). All experiments were carried out in 100 mM cacodylic acid, pH 7.0 and 100 mM glycine, pH 2.0, respectively.

Equilibrium unfolding transitions. The GdmCl-induced equilibrium transitions were monitored by the change in ellipticity at 227 nm in an Aviv 62A DS spectropolarimeter. Protein concentrations were 10 μM. The data were fitted to a two-state model following the procedure described by Santoro & Bolen.[29]

Kinetic measurements. Refolding and unfolding kinetics were measured in an Applied Photophysics SX.18MV stopped-flow instrument. The change in fluorescence above 320 nm after excitation at 276 nm was monitored. The final protein concentration was 3.8 μM.

Transition state analysis. The free energies of activation for folding ($\Delta G_f^{0\ddagger}$) and unfolding ($\Delta G_u^{0\ddagger}$) were calculated using transition state theory[30]:

$$k = k_0 \cdot e^{-\Delta G^{0\ddagger}/\mathrm{RT}} \tag{5}$$

where the pre-exponential factor, k_0 represents the maximum rate constant for protein folding in the absence of free energy barriers. This value was measured to be in the order of 10^7-10^8 s^{-1}.[31,32] A value of 10^8 s^{-1} was used in the fits. The pre-exponential factor was assumed to be temperature independent and does not change upon mutation.

The GdmCl dependence of the apparent rate constant (λ) for folding (k_f) and unfolding (k_u) was determined according to the two-state model

$$\lambda = k_f + k_u \tag{6}$$

Rate constants at different denaturant concentration was calculated according to equation (7):

$$\ln k_{f,u} = \ln k_{f,u}^{H_2O} - \frac{m_{f,u}}{\mathrm{RT}}[denaturant] \tag{7}$$

The temperature dependence of the rate constants at various denaturant concentrations was analyzed using

$$\Delta G^{0\ddagger} = \Delta H^{0\ddagger}(T_0) - T \cdot \Delta S^{0\ddagger}(T_0) + \Delta C_p^{\ddagger}\left(T - T_0 - T \cdot \ln\frac{T}{T_0}\right) \tag{8}$$

with a reference temperature of T_0 = 298.15 K. Equation (8) assumes that $\Delta C_p^{0\ddagger}$ is itself independent of temperature.[33] The value for the entropy of activation ($\Delta S^{0\ddagger}$) depends critically on the correct pre-exponential factor, whereas the values for the enthalpy of activation ($\Delta H^{0\ddagger}$) and heat capacity of activation ($\Delta C_p^{0\ddagger}$) are nearly independent of the pre-exponential factor used.[14]

Global analysis of the kinetic data. To fit the kinetic data globally we assumed that the activation parameters $\Delta H^{\ddagger}$, $\Delta S^{\ddagger}$ and $\Delta C_p^{\ddagger}$ depend linearly on the denaturant concentration as shown for the equilibrium thermodynamic parameters[34]. This allows a global fit of the data according to equation (9)

$$\Delta G^{0\ddagger}\left(T,[GdmCl]\right) = \left(\Delta H^{\ddagger}(T_0,H_2O) + h(T_0)[GdmCl]\right) - T\left(\Delta S^{\ddagger}(T_0,H_2O) + s(T_0)[GdmCl]\right) \quad (9)$$
$$+\left(\Delta C_p^{\ddagger}(H_2O) + c[GdmCl]\right)\left[T - T_0 - T\ln\left(T/T_0\right)\right]$$

with $h(T_0) = \partial\Delta H^{\ddagger}/\partial[GdmCl]$, $s(T_0) = \partial\Delta S^{\ddagger}/\partial[GdmCl]$ and $c = \partial\Delta C_p^{\ddagger}/\partial[GdmCl]$. $\Delta H^{\ddagger}(T_0,H_2O)$, $\Delta S^{\ddagger}(T_0,H_2O)$ and $\Delta C_p^{\ddagger}(H_2O)$ are the entropy, enthalpy and the heat capacity of activation in the absence of denaturant at the reference temperature T_0 = 298.15 K. With $m_{f,u}(T) = \partial\Delta G_{f,u}^{0\ddagger}\left(T,[GdmCl]\right)/\partial[GdmCl]$ and equation (9) we receive the temperature dependence of the kinetic m-values:

$$m_{f,u}(T) = h_{f,u}(T_0) - T\cdot s_{f,u}(T_0) + c_{f,u}\cdot\left[T - T_0 - T\ln\left(T/T_0\right)\right] \quad (10)$$

The data were converted using equation (11):

$$\frac{h_{f,u}}{m_{eq}} = \frac{\partial\Delta H_{f,u}^{0\ddagger}}{\partial\Delta G_D^0};\ \frac{s_{f,u}}{m_{eq}} = \frac{\partial\Delta S_{f,u}^{0\ddagger}}{\partial\Delta G_D^0};\ \frac{c_{f,u}}{m_{eq}} = \frac{\partial\Delta C_{p\,f,u}^{\ddagger}}{\partial\Delta G_D^0} \quad (11)$$

Data fitting. The program ProFit (Quantum Soft, Zürich, Switzerland) was used for all data fitting.

Results and Discussions

Shape of the free energy barriers of tendamistat folding. Tendamistat folds in an apparent two-state behavior with perfectly linear Leffler plots.[15,27] Analysis of the effect of temperature and denaturant on tendamistat folding and stability revealed transition state movement according to the Hammond postulat.[15] Due to the high stability of the protein at pH 7, the measurements were performed at pH 2 to give more reliable baselines. To test for transition state movement at neutral pH we determined the effect of temperature and denaturant on folding and stability of the tendamistat variant L14V, which is destabilized by (11.9 ±0.2) kJ/mol compared to wild type. The folding kinetics of L14V show similar behavior like wild type at pH 2 with linear Leffler plots but a clear Hammond behavior was observed when the effect

of temperature and denaturant was analyzed. In previous studies it was shown that tendamistat folding involves two sequential transition states.[14] Tendamistat wild type and the variant L14V have similar α_D-values indicating that both have the same rate-limiting transition state. In contrast, the tendamistat variant N25A has a significantly higher α_D-value 0.83 ±0.02 than for wild type tendamistat at 25°C 0.64 ±0.01 indicating that the mutation leads to a switch from the early to the late transition state. To probe for transition state movement in the late transition state we determined the effect of denaturant and temperature on the tendamistat variant N25A. Using multiple perturbation analysis reveals that a major ground state effect accompany the transition state movement. Perfectly linear Leffler plots are obtained for all three proteins applying single perturbations.

To further verify the transition state movement of the late transition state we determine the effect of temperature and denaturant on the tendamistat variant L14A which has an α_D-value of 0.82 ±0.01 similar like α_D for the variant N25A (figure 2). Both mutated residues are located in the N-terminal β-hairpin (figure 1). Substitution of leucine with alanine leads to a decrease in protein stability by (21.5 ±0.1) kJ/mol at 25°C, which is 9.6 kJ/mol less stability than the replacement of leucine by valine. At all temperatures linear Leffler plots are obtained (figure 2). As shown in our previous work, transition state movements are only observed when the effect of multiple perturbations is analyzed.[6,15] The temperature-denaturant cross-interaction parameter

$$p_{DT} = \frac{\partial^2 \Delta G_f^{0\ddagger}}{\left(\partial \Delta G_T^0\right)\left(\partial \Delta G_D^0\right)} = \frac{\partial \alpha_D}{\partial \Delta G_T^0} = \frac{\partial \alpha_T}{\partial \Delta G_D^0} \tag{12}$$

can be determined in two different ways: analysis the effect of temperature on α_D (equation (2)), i.e. on the relative change in ASA between unfolded state and transition state, and the effect of denaturant concentration on α_T ($= \Delta S_f^{0\ddagger} / \Delta S_{eq}^0$), i.e. on the relative entropy change between unfolded state and transition state.[4,15,25] Figure 3B shows the effect of changes in ΔG^0 caused by variation of temperature on α_D. α_D increases as the protein is destabilized with increasing temperature with a p_{DT}-value of $(5.7 \pm 0.6) \cdot 10^3$ mol/kJ indicating transition state movement (table 1). We cannot determine the p_{DT}-value using the denaturant dependence of α_T due to the nonlinear dependence (figure 3E). To distinguish between ground state effects and Hammond behavior, determination of the effect of temperature on the kinetic and equilibrium m-

values and the denaturant concentration on the entropy-values, respectively, are required (figure 3A and D). The increase of m_{eq} and $-\Delta S^0_{eq}$ with decreasing protein stability reveals that the transition state movement is accompanied by a large ground state effect. To quantify the extend of Hammond behavior we corrected for the properties of the ground state effect (figure 3C and F). Corrected α-values are 3.6 ±0.8 and 3.9 ±0.9, respectively (table 1).

The result is in accordance with our previous results obtained for the late transition state received from the measurements of the tendamistat variant N25A.[15] Table 1 compares the cross-interaction parameters received from wild type, L14V, L14A and N25A. The p_{DT}-values obtained for the late transition states are about 2.2 to 3.5-fold smaller indicating significantly less movement compared to the early transition state. The results confirm that the barriers become increasingly narrow and structurally more defined upon folding of the protein (figure 4).[15]

Denaturant dependence of the activation parameters of the early transition state. As we have shown in our previous work, the denaturant dependence of entropy correlates with the temperature dependence of the m-values.[15] The origin of the denaturant dependence of enthalpy and the change in heat capacity is not as straightforward as for the entropy. ΔH^0 and ΔC^0_p have contributions from the solvent interaction with the protein, thus the values should change with denaturant concentrations. Changes in enthalpy in protein folding reactions contain contributions from the polypeptide chain and from its interactions with solvent. Figure 5A and B shows the changes of ΔH^0_{eq}, $\Delta H^{0‡}_f$ and $\Delta H^{0‡}_u$ with changes of ΔG^0 with increasing denaturant concentrations for tendamistat wild type and the variant L14V, which have both the early transition state rate-limiting. For both proteins, the denaturant dependencies of enthalpy show the same behavior. ΔH^0_{eq} and $\Delta H^{0‡}_u$ significantly decrease with decreasing protein stability, whereas $\Delta H^{0‡}_f$ shows no denaturant dependence. This reveal, that the denaturant has the same effect on the polypeptide chain in the unfolded and the transition state indicating that the structure of the early transition state has similar water accessibility than the unfolded state. The results of the denaturant dependencies of the activation parameters are given in table 2.

The results allow the denaturant dependence of α_H ($=\Delta H_f^{0\ddagger}/\Delta H_{eq}^0$), i.e. the relative enthalpy change between unfolded state and transition state (figure 5C and D). Uncertainties of α_H increase with decreasing protein stability. α_H of wild type and L14V show linear denaturant dependency within errors with a cross-interaction parameter p_{HD} of $-(5.5 \pm 0.8)\cdot 10^3$ mol/kJ and $-(2.9 \pm 0.5)\cdot 10^3$ mol/kJ, respectively (table 1).

ΔC_p^0 is entirely defined by differences in interactions of the protein side chains with the solvent and correlate well with m_{eq}.[7] Therefore, ΔC_p^0 should also show similar behavior than m_{eq}. The denaturant dependences of ΔC_p^0-values are accompanied with large uncertainties due to the strong dependence of the values on the slope of the denaturant dependence of the rate constants (table 2). The changes of heat capacity with changes in denaturant concentrations are slightly different for both proteins with the early transition state rate-limiting (figure 5E and F). $\Delta C_{p(u)}^{0\ddagger}$ shows a strong denaturant-dependence for the variant L14V but only small changes are observed with decreasing protein stability for wild type. In contrast, wild type shows a strong denaturant-dependence of $\Delta C_{p(f)}^{0\ddagger}$, whereas $\partial \Delta C_{p(f)}^{0\ddagger}/\partial \Delta G_D^0$ only slightly increase for L14V. Like for the kinetic m-values, the activation parameters of the change in heat capacity show different denaturant dependences according to Hammond postulate but with different magnitude. Thus, $\Delta C_{p(eq)}^0$ also change significantly with increasing denaturant concentration. This effect can be explained due to the fact, that m-values have mainly backbone contribution, whereas ΔC_p^0 has nearly none. The differences of the denaturant dependencies of $\Delta C_{p(f,u)}^{0\ddagger}$ and $\Delta C_{p(eq)}^0$ may be due to differences in pH.

α_C ($=\Delta C_{p(f)}^{0\ddagger}/\Delta C_{p(eq)}^0$) allows the characterization of a transition state in terms of its relative solvent exposure.[7] However, α_C is accompanied with significant large uncertainties at nearly all denaturant concentrations (figure 5G and H). Therefore, the cross-interaction parameter p_{CD} have large errors and are not well defined (table 1). The magnitude for p_{CD} is nearly identical for tendamstat wild type and the variant L14V with a value of $(4.6 \pm 2.5)\cdot 10^3$ mol/kJ and $(4.8 \pm 2.0)\cdot 10^3$ mol/kJ, respectively (table 1).

The observation of the denaturant dependences of the activation parameters of the early transition state confirms our previous results of a broad and less well structured transition barrier.

Denaturant dependence of Enthalpy and heat capacity on the late transition state. The denaturant dependence of enthalpy for the late transition state is not as homogeny as observed for the early transition state. $\Delta H_f^{0\ddagger}$ and $\Delta H_u^{0\ddagger}$ decreases with increasing protein stability for the tendamistat variants N25A and L14A but with different intensity (figure 6A and B; table 2). Thus, $-\partial\Delta H_{eq}^0/\partial\Delta G_D^0$ is slightly negative for N25A but shows a positive value for L14A. However, the denaturant dependence of the enthalpy-values of the late transition state are significantly smaller than for the early one indicating that the late transition barrier is more structured and robust against perturbations.

α_H show linear denaturant dependency within errors for L14A and N25A (figure 6C and D). The cross-interaction parameters, p_{HD}, for the early transition state have different signs compared to the late transition state with a value of $(10.5 \pm 0.7)\cdot 10^3$ mol/kJ and $(2.9 \pm 0.5)\cdot 10^3$ mol/kJ for L14A and N25A, respectively (table 1). The differences in the p_{HD}-values are due to denaturant dependences of $\Delta H_f^{0\ddagger}$ for the late transition state.

In contrast to changes in enthalpy with decreasing protein stability, $\partial\Delta C_{p(eq)}^0/\partial\Delta G_D^0$ and $\partial\Delta C_{p(f,u)}^{0\ddagger}/\partial\Delta G_D^0$ show similar behavior for L14A and N25A (figure 6E and F). $\Delta C_{p(u)}^{0\ddagger}$ is denaturant-independent, whereas $\Delta C_{p(f)}^{0\ddagger}$ and $\Delta C_{p(eq)}^0$ strongly depend on denaturant concentrations (table 2). This indicates that the side chains are well packed in the late transition state and thus, increasing denaturant concentration has no effect on $\Delta C_{p(u)}^{0\ddagger}$. Changes in ΔC_p^0 upon addition of denaturant concentrations are only due to changes of the ground states.

The values of the cross-interaction parameter p_{CD} are not very reliable due to the large uncertainties of α_C. $\Delta C_{p(eq)}^0$ and $\Delta C_{p(f,u)}^{0\ddagger}$-values of the late transition state significantly changes with decreasing protein stability, which is in contrast to the relative small changes for the early transition state (table 2).

Global analysis of the kinetic data. In accordance with the linear free energy model,[34] the changes in the Gibbs free energy, enthalpy, entropy and heat capacity have a linear dependence with denaturant concentration. Compared to the equilibrium thermodynamic parameters, where the linear denaturant dependence is proven for many proteins,[35-41] less data are available for the activation parameters.[42,43] Matthews and Co-workers measured the urea-dependence of the unfolding activation parameters of the α subunit of Tryptophan Synthase[42] and of the activation parameters of the unimolecular rearrangement of the dimer Trp Repressor[43]. Even though the data are scattered the linear dependence of the activation parameters on the urea concentration is clearly visible. As shown in figures 3, 5 and 6 the activation parameters of tendamistat folding show clearly a linear GdmCl dependence. Therefore we fitted the kinetic data globally using equation (9). Table 2 compares the results from the single and global fit of the thermodynamic parameters and their denaturant dependence. Both methods gave similar results within errors for the entropy and enthalpy-values at the measured denaturant concentrations. $\Delta C^{0\ddagger}_{p(f,u)}$ and $\Delta C^{0}_{p(eq)}$-values and their denaturant dependencies show larger differences between both fitting methods. The denaturant dependence of the change in heat capacity for the tendamistat variant L14A differ significantly. However, the values are accompanied with large uncertainties. This is due to small uncertainties of the GdmCl dependence of the rate constants, which results in large variations of the heat capacity. Interestingly, the change in heat capacity received from the global fits has similar behavior between L14A and L14V (table 2).

Comparison of α_D- and α_C-values. The *m* and ΔC^{0}_{p}-values correlate well with each other because both depend on the amount of protein surface which becomes exposed to solvent upon unfolding.[7] Thus, the two thermodynamic criteria are most often used in protein folding to locate the transition state with respect to the unfolded and the native state. Table 3 compares both α -values from the single fits as well as the global fits in the absence of denaturant and at 25°C. The results from the global fits and the single fits agree well within errors, except for α_C of L14A where the global fit is significantly larger. However as described above, the values are accompanied with large uncertainties due to the sensitivity of $\Delta C^{0\ddagger}_{p(f,u)}$ on the denaturant dependence of the apparent rate constants. α_C is 30 - 40 % lower than α_D. Higher α_D compared to α_C

is commonly observed in protein folding.[4] ΔC_p^0 have mainly contributions of side chains and nearly none from the backbone, in contrast to the m-values which have mainly backbone contributions. Therefore, the α_D-values report on the interactions of the transition state with the solvent, and the α_C-values report on the hydrophobic and polar hydration of the protein side chains in the transition state. Tendamistat wild type and the variant L14V have an α_C-value of 0.46 and 0.42, respectively. This is significantly smaller than the values obtained for the variants L14A ($\alpha_C = 0.59$) and N25A (α_C=0.56) confirming the change of the rate-limiting step for the two variants (table 3).

Thermodynamic properties of the free energy barriers in tendamistat folding. Figure 7 shows the changes in enthalpy, entropy and heat capacity during folding for the results of the global fit. The absolute value for $\Delta S^{0\ddagger}$ critically depends on the correct pre-exponential factor in the Eyring equation whereas the values of $\Delta H^{0\ddagger}$ and $\Delta C_p^{\ddagger}$ are nearly independent. Comparison of the results of tendamistat wild type at pH 2 and the variant L14V at pH 7 reveals nearly identical changes for the activation parameters relative to the folded state (figure 7 and table 2). There are small changes for the activation parameters relative to the unfolded state for both proteins.

Formation of the early and late transition states are enthalpically unfavorable and show relative small changes in entropy. Interestingly, both transition states show similar values for the reaction from the unfolded state to both transition states, whereas the formation of the native protein is accompanied with larger changes going from the early transition state (figure 7). Since ΔC_p^0 and m-values correlate with each other, formation of the transition states should have significantly larger changes in heat capacity for the late transition barrier (figure 7). Formation of the early transition state is accompanied with a value of –1.8 and –1.9 kJ/(mol·K), respectively, whereas the late transition state is formed with a decrease of $\Delta C_p^{0\ddagger}$ of –2.2 and –2.3 kJ/(mol·K), respectively (table 2).

These findings are in contrast to the results of the activation parameters observed for the tendamistat disulfide variant C45A/C73A with the early transition state representing only an enthalpic barrier, whereas the second step is an entropic barrier.

However, no transition state movement was observed for this variant indicating different folding mechanism.

Both transition states have similar thermodynamic properties but the denaturant-dependences of the activation parameters are quite different between both. These findings confirm our previous observation of the importance of multiple perturbation analysis to test the properties of the free energy barriers.

Conclusions

Tendamistat folding involves two sequential transition states. Multiple perturbation analysis for tendamistat wild type and three different variants suggest, that the early transition state is rather broad compared to the late transition state, which is a narrow and structurally well-defined barrier. Determination of the activation parameters of both transition states show only less difference in their activation parameters and are both entropic and enthalpic barriers. However, they show different behavior in their denaturant dependencies. Linear denaturant dependences are observed for all thermodynamic parameters according to the linear free energy model. Analysis of these denaturant dependencies of the activation parameters confirms our previous observation of a rather broad and structurally less well defined transition state. The results of the denaturant dependences of the activation heat capacity of early transition state is pH dependent, whereas the enthalpy shows the same behavior at all pH upon addition of denaturant. Analysis of the denaturant dependencies of the changes in activation heat capacity of tendamistat variants with the late transition state rate-limiting reveals ground state effect and only small changes are observed for the activation enthalpy indicating a structurally well defined transition barrier.

Acknowledgements

This work was supported by a grant from the Swiss National Science Foundation.

Table 1. Cross-interaction parameters of the folding reaction of wild type, L14V, L14A and N25A.

Cross-interaction parameter	wt	L14V	L14A	N25A
$p_{DT} = \partial\alpha_D / \partial\Delta G_T^0$ ((mol/kJ) x10^3)	8.1 ±0.8 [a]	8.5 ±0.7 [a]	5.7 ±0.6	4.6 ±0.4 [a]
$p_{DT,corr} = \partial\alpha_{D,corr} / \partial\Delta G_T^0$ ((mol/kJ) x10^3)			3.6 ±0.8	2.4 ±0.4 [a]
$p_{DT} = \partial\alpha_T / \partial\Delta G_D^0$ ((mol/kJ) x10^3)	8.7 ±0.8 [a]	8.6 ±0.5 [a]		
$p_{DT,corr} = \partial\alpha_{T,corr} / \partial\Delta G_D^0$ ((mol/kJ) x10^3)			3.9 ±0.9	2.7 ±0.5 [a]
$p_{HD} = \partial\alpha_H / \partial\Delta G_D^0$ ((mol/kJ) x10^3)	-5.5 ±0.8	-2.9 ±0.5	10.5 ±0.7	2.9 ±0.5
$p_{CD} = \partial\alpha_C / \partial\Delta G_D^0$ ((mol/kJ) x10^3)	4.6 ±2.5	4.8 ±2.0	5.2 ±2.9	4.7 ±1.4

[a] Data were taken from our previous work.[15]
[b] α-values were corrected for the properties of the refolding reaction for the ground state effect.

Table 2. Thermodynamic parameters of the folding reaction of the tendamistat wild type at pH 2 and the variants L14A, L14V and N25A at pH 7 and the effect of changes in protein stability induced by adding denaturant on the thermodynamic parameters.

	TM wt		TM L14V		TM N25A		TM L14A	
	single fit	global fit[a]	single fit	global fit[a]	single fit	global fit[a]	single fit	global fit[a]
ΔS_{eq}^{0} (J/(mol·K·M))	-257 ±8	-261 ±11	-265 ±9	-267 ±12	-223 ±5	-226 ±7	-214 ±4	-236 ±11
$\Delta S_{f}^{0\ddagger}$ (J/(mol·K·M))	-36 ±1	-37 ±3	-48 ±6	-49 ±2	-44 ±5	-46 ±4	-46 ±4	-49 ±5
$\Delta S_{u}^{0\ddagger}$ (J/(mol·K·M))	221 ±8	224 ±8	217 ±5	217 ±9	179 ±2	180 ±3	168 ±4	186 ±6
$-\partial\Delta S_{eq}^{0}/\partial\Delta G_{D}^{0}$ ($K^{-1}\cdot10^{3}$)	-0.2 ±0.3	-0.5 ±0.7	0.1 ±0.2	-0.2 ±0.5	3.0 ±0.1	3.0 ±1.0	4.8 ±0.2	3.5 ±1.2
$-\partial\Delta S_{f}^{0\ddagger}/\partial\Delta G_{D}^{0}$ ($K^{-1}\cdot10^{3}$)	2.2 ±0.2	2.0 ±0.5	2.3 ±0.1	2.1 ±0.3	3.6 ±0.1	3.6 ±0.9	5.6 ±0.2	5.0 ±0.9
$\partial\Delta S_{u}^{0\ddagger}/\partial\Delta G_{D}^{0}$ ($K^{-1}\cdot10^{3}$)	-2.4 ±0.1	-2.5 ±0.4	-2.2 ±0.1	-2.3 ±0.3	-0.8 ±0.1	-0.6 ±0.1	-0.8 ±0.1	-1.4 ±0.2
ΔH_{eq}^{0} (kJ/(mol·M))	-96 ±2	-97 ±3	-103 ±3	-103 ±3	-79 ±2	-80 ±2	-78 ±1	-85 ±3
$\Delta H_{f}^{0\ddagger}$ (kJ/(mol·M))	30 ±1	29 ±1	22 ±2	22 ±1	27 ±2	26 ±1	22 ±1	21 ±2
$\Delta H_{u}^{0\ddagger}$ (kJ/(mol·M))	125 ±2	126 ±2	124 ±2	125 ±3	105 ±1	106 ±8	100 ±1	106 ±2
$-\partial\Delta H_{eq}^{0}/\partial\Delta G_{D}^{0}$	-1.1 ±0.1	-1.2 ±0.3	-1.0 ±0.1	-1.0 ±0.2	-0.10 ±0.03	-0.11 ±0.27	0.41 ±0.06	0.04 ±0.33
$\partial\Delta H_{f}^{0\ddagger}/\partial\Delta G_{D}^{0}$	0.04 ±0.04	0.08 ±0.11	0.04 ±0.04	0.07 ±0.07	-0.25 ±0.03	-0.25 ±0.25	-0.84 ±0.06	-0.65 ±0.27
$\partial\Delta H_{u}^{0\ddagger}/\partial\Delta G_{D}^{0}$	-1.1 ±0.1	-1.1 ±0.1	-0.95 ±0.02	-0.96 ±0.10	-0.35 ±0.01	-0.36 ±0.03	-0.43 ±0.02	-0.61 ±0.08
$\Delta C_{p(eq)}^{0\ddagger}$ (kJ/(mol·K))	-3.9 ±0.4	-4.1 ±0.4	-4.4 ±0.5	-3.9 ±0.5	-3.8 ±0.3	-3.8 ±0.3	-3.9 ±0.2	-2.9 ±0.4
$\Delta C_{p(f)}^{0\ddagger}$ (kJ/(mol·K))	-1.8 ±0.1	-1.9 ±0.1	-1.9 ±0.3	-1.8 ±0.1	-2.1 ±0.3	-2.2 ±0.2	-2.3 ±0.2	-2.3 ±0.2
$\Delta C_{p(u)}^{0\ddagger}$ (kJ/(mol·K))	2.1 ±0.4	2.2 ±0.3	2.6 ±0.3	2.2 ±0.4	1.7 ±0.1	1.7 ±0.1	1.6 ±0.2	0.6 ±0.3
$-\partial\Delta C_{p(eq)}^{0}/\partial\Delta G_{D}^{0}$ ($K^{-1}\cdot10^{3}$)	25 ±12	20 ±25	-25 ±9	-11 ±2	90 ±5	84 ±33	97 ±10	-30 ±38
$-\partial\Delta C_{p(f)}^{0\ddagger}/\partial\Delta G_{D}^{0}$ ($K^{-1}\cdot10^{3}$)	33 ±8	32 ±14	6 ±7	10 ±9	90 ±5	83 ±30	94 ±10	8 ±27
$\partial\Delta C_{p(u)}^{0\ddagger}/\partial\Delta G_{T}^{0}$ ($K^{-1}\cdot10^{3}$)	-7 ±4	-13 ±12	-32 ±3	-21 ±1	-0.8 ±1.3	0.4 ±4.0	3 ±3	38 ±11

[a] The data are results from global fits of kinetic data at various temperatures.

Table 3. Comparison of the α_C-values and α_C-values from the single fits of tendamistat wild type, the tendamistat variants L14V, N25A and L14A. The results from the global fits are in bracket.

Protein	α_D (298K)	α_C (0M GdmCl)	α_C/α_D
wt	0.66 ±0.05 [a]	0.46 ±0.05	0.70
	(0.65 ±0.46) [b]	(0.46 ±0.08)	(0.70)
L14V	0.71 ±0.02 [a]	0.42 ±0.08	0.59
	(0.71 ±0.35) [b]	(0.45 ±0.09)	(0.63)
N25A	0.83 ±0.04 [a]	0.56 ±0.11	0.67
	(0.83 ±0.95) [b]	(0.57 ±0.08)	(0.68)
L14A	0.82 ±0.02 [a]	0.59 ±0.09	0.72
	(0.82 ±1.06) [b]	(0.79 ±0.18)	(0.96)

[a] Data are from single fits.
[b] Data were calculated from the results of the global fits.

Reference

1. Leffler, J.E. Parameters for the description of transition states. *Science* **117**, 340-341 (1953).
2. Jencks, W.P. *Catalysis in Chemistry and Enzymology*, (McGraw-Hill Book Company, New York, 1969).
3. Grosman, C., Zhou, M. & Auerbach, A. *Nature* **403**, 773-776 (2000).
4. Sánchez, I.E. & Kiefhaber, T. Non-linear rate-equilibrium free energy relationships and Hammond behavior in protein folding. *Biophys. Chem.* **100**, 397-407 (2003).
5. Sánchez, I.E. & Kiefhaber, T. Evidence for sequential barriers and obligatory intermediates in apparent two-state protein folding. *J. Mol. Biol.* **325**, 367-376 (2003).
6. Sánchez, I.E. & Kiefhaber, T. Hammond behavior versus ground state effects in protein folding: evidence for narrow free energy barriers and residual structure in unfolded states. *J. Mol. Biol.* **327**, 867-884 (2003).
7. Myers, J.K., Pace, C.N. & Scholtz, J.M. Denaturant m values and heat capacity changes: relation to changes in accessible surface areas of protein unfolding. *Protein Sci* **4**, 2138-48 (1995).
8. Guydosh, N.R. & Fersht, A.R. A guide to measuring and interpreting ϕ-values. in *Protein Folding Handbook*, Vol. 1 (eds. Buchner, J. & Kiefhaber, T.) 445-453 (Wiley-VCH Verlag, Weinheim, 2005).
9. Fersht, A.R., Matouschek, A. & Serrano, L. The folding of an enzyme. I. Theory of protein engineering analysis of stability and pathway of protein folding. *J. Mol. Biol.* **224**, 771-782 (1992).
10. Matthews, C.R. Effect of point mutations on the folding of globular proteins. *Meth. Enzymol.* **154**, 498-511 (1987).
11. Schindler, T. & Schmid, F.X. Thermodynamic properties of an extremely rapid protein folding reaction. *Biochemistry* **35**, 16833-42 (1996).
12. Schönbrunner, N., Pappenberger, G., Scharf, M., Engels, J. & Kiefhaber, T. Effect of Pre-Formed Correct Tertiary Interactions on Rapid Two-State Tendamistat Folding: Evidence for Hairpins as Initiation Sites for β-Sheet Formation. *Biochemistry* **36**, 9057-9065 (1997).
13. Kuhlman, B., Luisi, D.L., Evans, P.A. & Raleigh, D.P. Global analysis of the effects of temperature and denaturant on the folding and unfolding kinetics of the N-terminal domain of the protein L9. *J Mol Biol* **284**, 1661-70 (1998).
14. Bachmann, A. & Kiefhaber, T. Apparent two-state tendamistat folding is a sequential process along a defined route. *J. Mol. Biol.* **306**, 375-386 (2001).
15. Schätzle, M. & Kiefhaber, T. Using temperature-denaturant cross interaction parameters to test the shape of free energy barriers for protein folding. submitted.
16. Vidugiris, G.J., Markley, J.L. & Royer, C.A. Evidence for a molten globule-like transition state in protein folding from determination of activation volumes. *Biochemistry* **34**, 4909-12 (1995).
17. Pappenberger, G., Saudan, C., Becker, M., Merbach, A.E. & Kiefhaber, T. Denaturant-induced movement of the transition state of protein folding revealed by high-pressure stopped-flow measurements. *Proc Natl Acad Sci U S A* **97**, 17-22 (2000).

18. Jonsson, T., Waldburger, C.D. & Sauer, R.T. Nonlinear free energy relationship in arc repressor unfolding imply the existence of unstable, native-like folding intermediates. *Biochemistry* **35**, 4795-4802 (1996).
19. Walkenhorst, W.F., Green, S. & Roder, H. Kinetic evidence for folding and unfolding intermediates in staphylococcal nuclease. *Biochemistry* **36**, 5795-5805 (1997).
20. Ikai, A. & Tanford, C. Kinetic evidence for incorrectly folded intermediate states in the refolding of denatured proteins. *Nature* **230**, 100-102 (1971).
21. Wildegger, G. & Kiefhaber, T. Three-state model for lysozyme folding: Triangular folding mechanism with an energetically trapped intermediate. *J Mol Biol* **270**, 294-304 (1997).
22. Kiefhaber, T., Bachmann, A., Wildegger, G. & Wagner, C. Direct measurement of nucleation and growth rates in lysozyme folding. *Biochemistry* **36**, 5108-12 (1997).
23. Wright, C.F., Lindorff-Larsen, K., Randles, L.G. & Clarke, J. Parallel protein-unfolding pathways revealed and mapped. *Nat Struct Biol* **10**, 658-62 (2003).
24. Hammond, G.S. A correlation of reaction rates. *J. Am. Chem. Soc.* **77**, 334-338 (1955).
25. Kiefhaber, T., Sánchez, I.E. & Bachmann, A. Characterization of protein folding barriers with rate equilibrium free energy relationships. in *Protein Folding Handbook*, Vol. 1 (eds. Buchner, J. & Kiefhaber, T.) 411-444 (Wiley-VCH Verlag, Weinheim, 2005).
26. Jencks, D.A. & Jencks, W.P. On the characterization of transition states by structure-reactivity coefficients. *J. Am. Chem. Soc.* **99**, 7948-7960 (1977).
27. Schönbrunner, N., Koller, K.-P. & Kiefhaber, T. Folding of the disulfide-bonded β-sheet protein tendamistat: Rapid two-state folding without hydrophobic collapse. *J. Mol. Biol.* **268**, 526-538 (1997).
28. Haas-Lauterbach, S. et al. High yield fermentation and purification of tendamistat disulfide analogues secreted by *Streptomyces lividans*. *Appl. Microbiol. Biotech.* **38**, 719-727 (1993).
29. Santoro, M.M. & Bolen, D.W. Unfolding free energy changes determined by the linear extrapolation method. 1. Unfolding of phenylmethanesulfonyl alpha-chymotrypsin using different denaturants. *Biochemistry* **27**, 8063-8068 (1988).
30. Eyring, H. The activated complex in chemical reactions. *J. Chem. Phys.* **3**, 107-115 (1935).
31. Krieger, F., Fierz, B., Bieri, O., Drewello, M. & Kiefhaber, T. Dynamics of unfolded polypeptide chains as model for the earliest steps in protein folding. *J. Mol. Biol.* **332**, 265-274 (2003).
32. Fierz, B. & Kiefhaber, T. Dynamics of unfolded polypeptide chains. in *Protein Folding Handbook*, Vol. 2 (eds. Buchner, J. & Kiefhaber, T.) 809-855 (Wiley-VCH Verlag, Weinheim, 2005).
33. Becktel, W.J. & Schellman, J.A. Protein stability curves. *Biopolymers* **26**, 1859-1877 (1987).
34. Schellman, J.A. Solvent denaturation. *Biopolymers* **17**, 1305-1322 (1978).
35. Makhatadze, G.I. & Privalov, P.L. Protein interactions with urea and guanidinium chloride. A calorimetric study. *J Mol Biol* **226**, 491-505 (1992).
36. Agashe, V.R. & Udgaonkar, J.B. Thermodynamics of denaturation of barstar: evidence for cold denaturation and evaluation of the interaction with guanidine hydrochloride. *Biochemistry* **34**, 3286-99 (1995).

37. Nicholson, E.M. & Scholtz, J.M. Conformational stability of the Escherichia coli HPr protein: test of the linear extrapolation method and a thermodynamic characterization of cold denaturation. *Biochemistry* **35**, 11369-78 (1996).
38. Chiti, F. et al. Conformational stability of muscle acylphosphatase: the role of temperature, denaturant concentration, and pH. *Biochemistry* **37**, 1447-55 (1998).
39. Reddy, G.B. et al. Linear free-energy model description of the conformational stability of uracil-DNA glycosylase inhibitor A thermodynamic characterization of interaction with denaturant and cold denaturation. *Eur J Biochem* **261**, 610-7 (1999).
40. Felitsky, D.J. & Record, M.T.J. Thermal and urea-induced unfolding of the marginally stable lac repressor DNA-binding domain: a model system for analysis of solute effects on protein processes. *Biochemistry* **42**, 2202-2217 (2003).
41. Neira, J.L. & Gomez, J. The conformational stability of the Streptomyces coelicolor histidine-phosphocarrier protein. Characterization of cold denaturation and urea-protein interactions. *Eur J Biochem* **271**, 2165-81 (2004).
42. Chen, X. & Matthews, C.R. Thermodynamic properties of the transition state for the rate-limiting step in the folding of the alpha subunit of tryptophan synthase. *Biochemistry* **33**, 6356-62 (1994).
43. Gloss, L.M. & Matthews, C.R. The barriers in the bimolecular and unimolecular folding reactions of the dimeric core domain of Escherichia coli Trp repressor are dominated by enthalpic contributions. *Biochemistry* **37**, 16000-10 (1998).
44. Koradi, R., Billeter, M. & Wuthrich, K. MOLMOL: a program for display and analysis of macromolecular structures. *J Mol Graph* **14**, 51-5, 29-32 (1996).

Figure Legends

Figure 1. Schematic drawing of the structure of tendamistat. The cysteine residues involved in the two disulfide bridges and the residues Leu14 and Asn25 are indicated as ball-and-stick model. The figure was generated using the program MOLMOL[44].

Figure 2. (A) GdmCl-dependence of the apparent rate constants for folding of the tendamistat variant L14A at various temperatures at pH 7.0. The lines represent the result of the global fit of the kinetic data. (B) Leffler plot of the effect of GdmCl concentration on the equilibrium (K_{eq}) and folding rate constant (k_f) calculated from the kinetic data at 25°C. The slope corresponds to the α_D-value.

Figure 3. Analysis of the temperature-denaturant cross-interaction parameter p_{DT} for the tendamistat variant L14A. Effect of ΔG_T^0 on m_{eq}, m_f and $-m_u$ (A) and on α_D (B), respectively, and effect of ΔG_D^0 on $-\Delta S_{eq}^0$, $-\Delta S_f^{0\ddagger}$ and $\Delta S_u^{0\ddagger}$ (D) and on α_T (E), respectively. (C, F) Both α-values were corrected for the properties of the refolding reaction for the ground state effects. The data are taken from individual fits. (A) The linear fits gives values of $\partial m_{eq} / \partial \Delta G_T^0 = (0.11 \pm 0.01)\mathrm{M}^{-1}$, $\partial m_f / \partial \Delta G_T^0 = (0.13 \pm 0.01)\mathrm{M}^{-1}$ and $\partial(-m_u) / \partial \Delta G_T^0 = -(0.017 \pm 0.004)\mathrm{M}^{-1}$. (B-F) The results of the linear fits are given in table 1 and 2.

Figure 4. Schematic drawing of the free energy barrier for folding of tendamistat wild type and tendamistat variants L14V, L14A and N25A. The response of variation in temperature on the early transition states (TS1) is more sensitive than on the late one (TS2) due to the different broadness of the barriers.

Figure 5. Denaturant dependences of enthalpy and changes in heat capacity of the early transition state. Effect of ΔG_D^0 on $-\Delta H_{eq}^0$, $\Delta H_f^{0\ddagger}$ and $\Delta H_u^{0\ddagger}$ (A, B), on $-\Delta C_{p(eq)}^0$, $-\Delta C_{p(f)}^{0\ddagger}$ and $\Delta C_{p(u)}^{0\ddagger}$ (E, F) and on α_H (C, D) and on α_C (G, H), respectively, on tendamistat wild type (A, C, E, G) and variant L14V (B, D, F, H). The data are taken from individual fits. The results of the linear fits are given in table 1 and 2.

Figure 6. Denaturant dependences of enthalpy and changes in heat capacity of the late transition state. Effect of ΔG_D^0 on $-\Delta H_{eq}^0$, $\Delta H_f^{0\ddagger}$ and $\Delta H_u^{0\ddagger}$ (A, B), on $-\Delta C_{p(eq)}^0$, $-\Delta C_{p(f)}^{0\ddagger}$ and $\Delta C_{p(u)}^{0\ddagger}$ (E, F) and on α_H (C, D) and on α_C (G, H), respectively, on tendamistat variants N25A (A, C, E, G) and L14A (B, D, F, H). The data are taken from individual fits. The results of the linear fits are given in table 1 and 2.

Figure 7. Changes in H, T·S and C_p during folding of tendamistat wild type (○), L14V (●), N25A (●) and L14A (●) at 25°C. For comparison the respective values of the native proteins were arbitrarily set to 0. Data were taken from the fit parameters given in table 2.

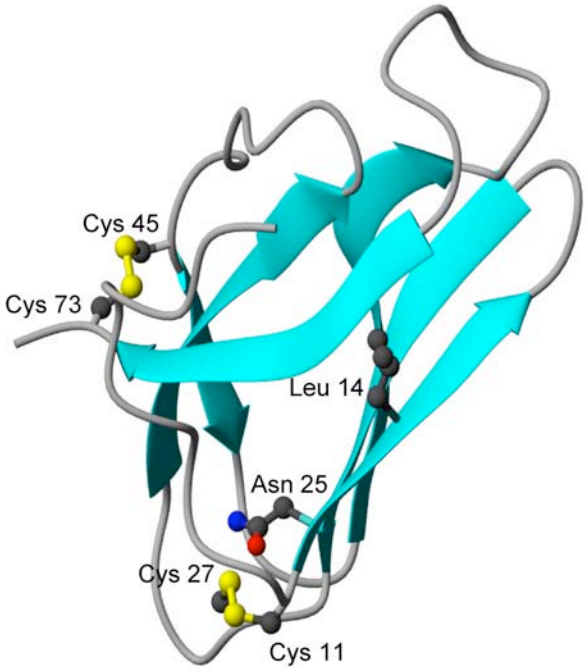

Figure 1

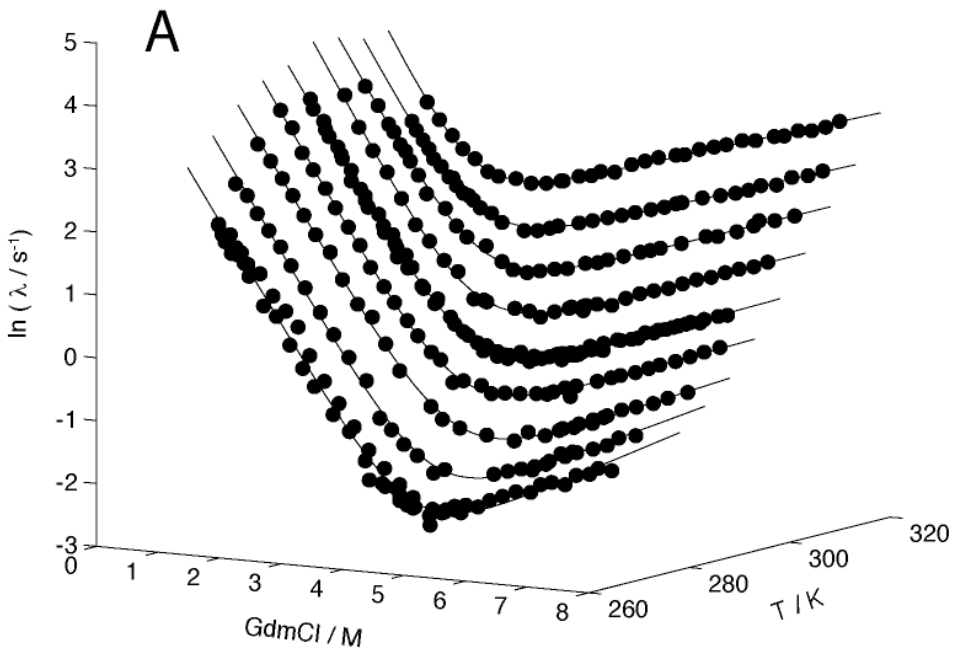
A
ln (λ / s-1)
5
4
3
2
1
0
-1
-2
-3
0
1
2
3
4
5
6
7
8
GdmCl / M
260
280
300
320
T / K

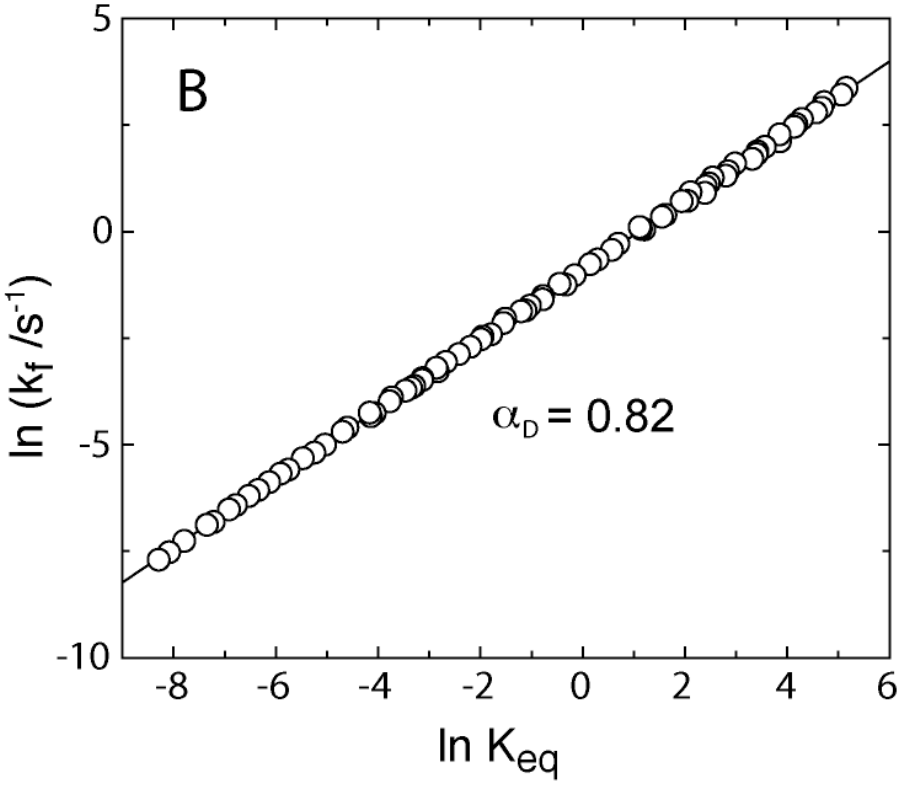
B
5
0
-5
-10
ln (kf /s-1)
αD = 0.82
-8
-6
-4
-2
0
2
4
6
ln Keq

Figure 2

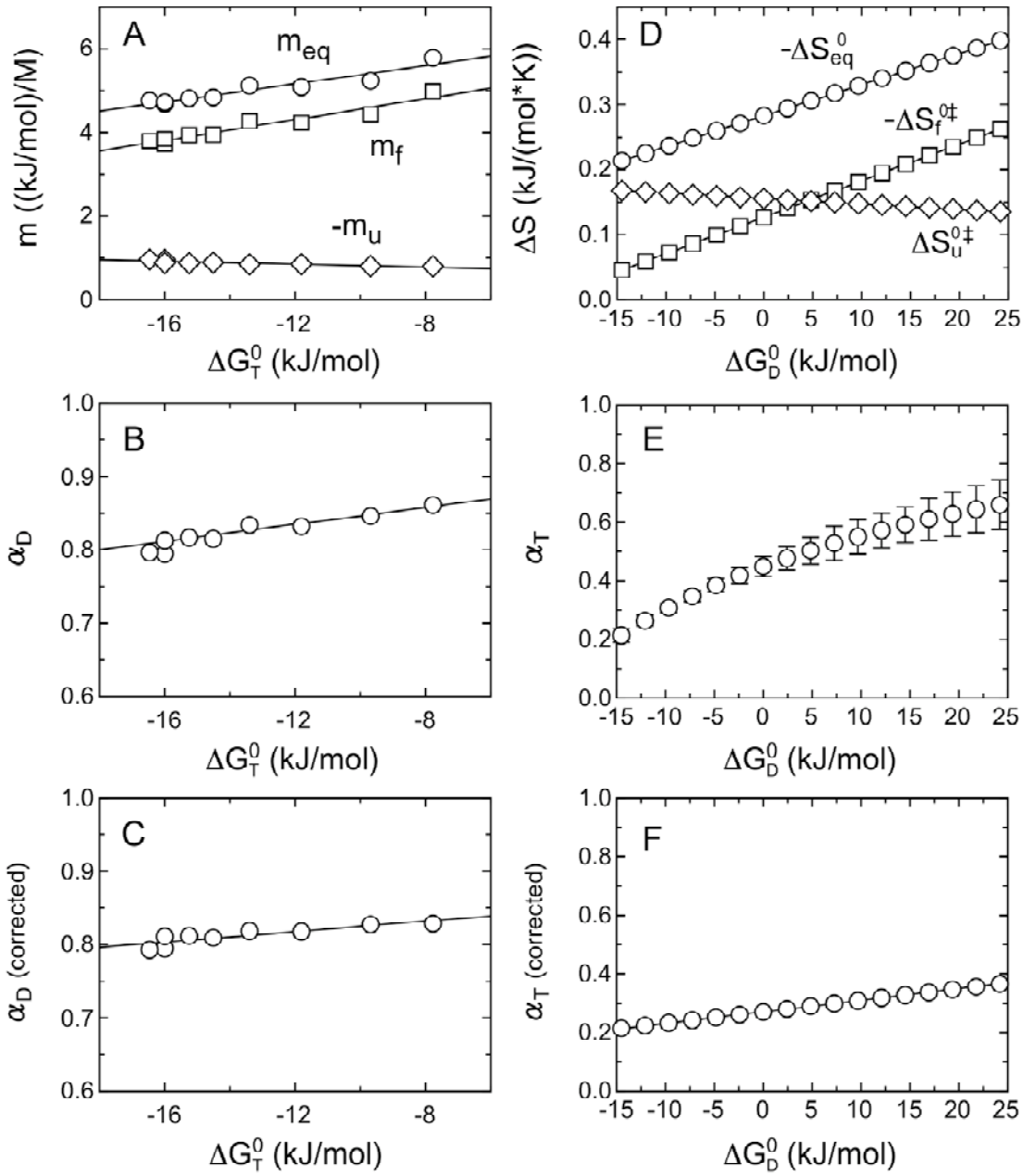
A
m_{eq}
m_f
$-m_u$
m ((kJ/mol)/M)
ΔG_T^0 (kJ/mol)
D
$-\Delta S_{eq}^0$
$-\Delta S_f^{0\ddagger}$
$\Delta S_u^{0\ddagger}$
ΔS (kJ/(mol*K))
ΔG_D^0 (kJ/mol)
B
α_D
ΔG_T^0 (kJ/mol)
E
α_T
ΔG_D^0 (kJ/mol)
C
α_D (corrected)
ΔG_T^0 (kJ/mol)
F
α_T (corrected)
ΔG_D^0 (kJ/mol)

Figure 3

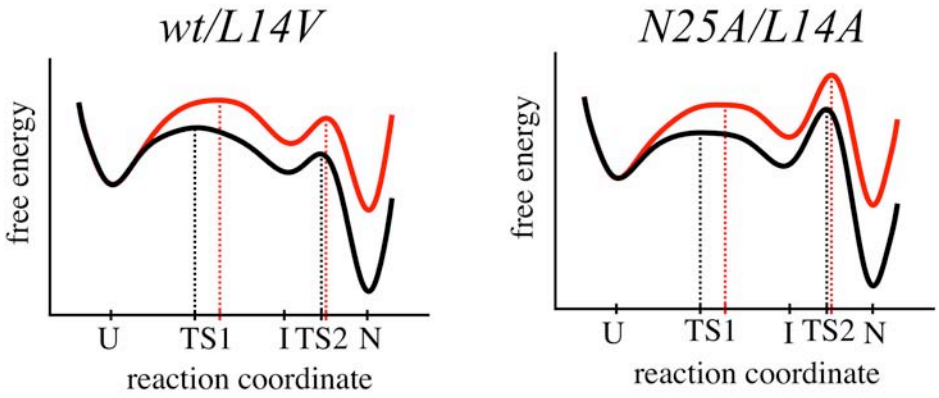
wt/L14V
free energy
U
TS1
I
TS2
N
reaction coordinate
N25A/L14A
free energy
U
TS1
I
TS2
N
reaction coordinate

Figure 4

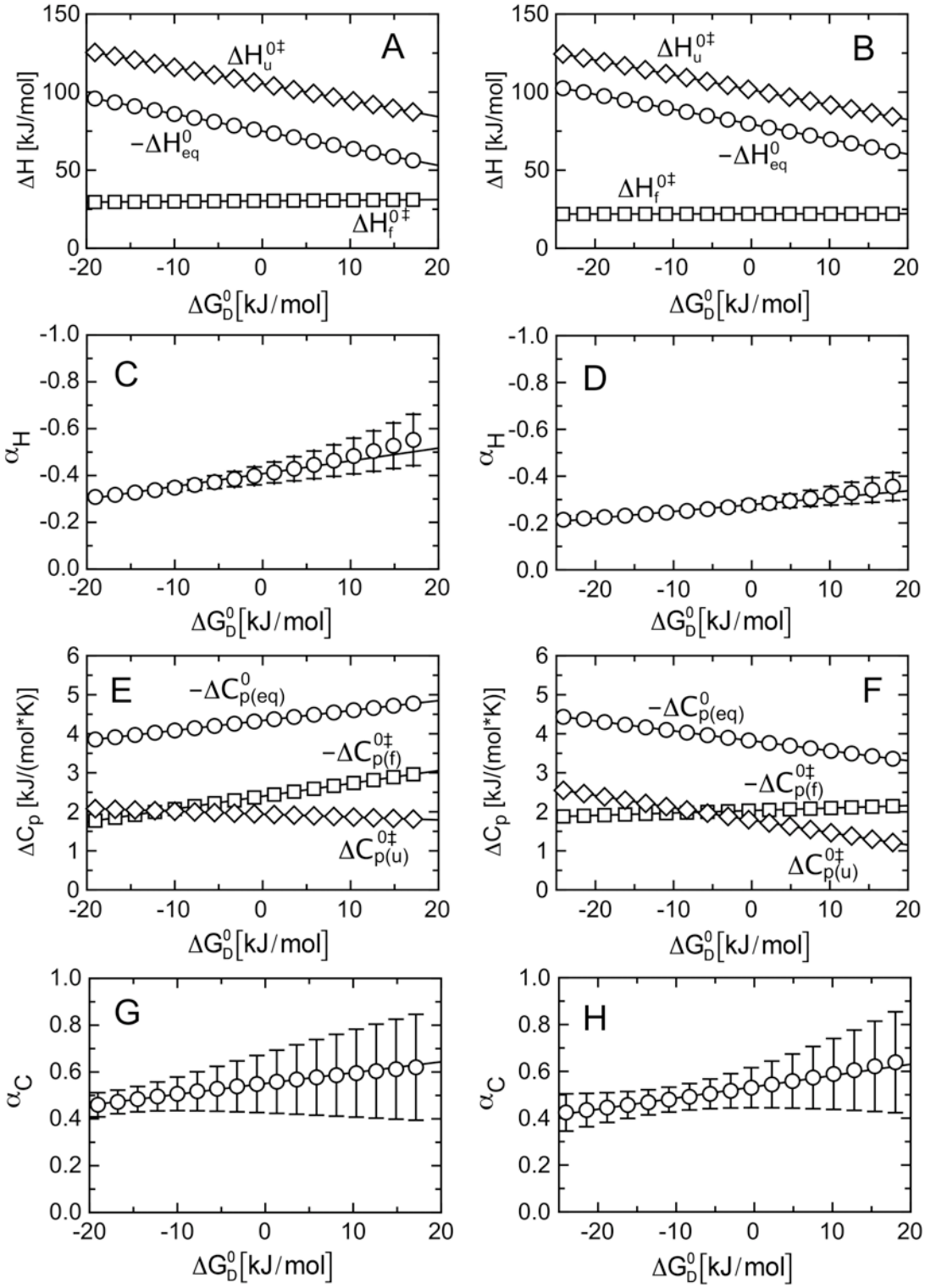
A
B
C
D
E
F
G
H
ΔH [kJ/mol]
$\Delta H_u^{0\ddagger}$
$-\Delta H_{eq}^0$
$\Delta H_f^{0\ddagger}$
α_H
ΔC_p [kJ/(mol*K)]
$-\Delta C_{p(eq)}^0$
$-\Delta C_{p(f)}^{0\ddagger}$
$\Delta C_{p(u)}^{0\ddagger}$
α_C
ΔG_D^0[kJ/mol]

Figure 5

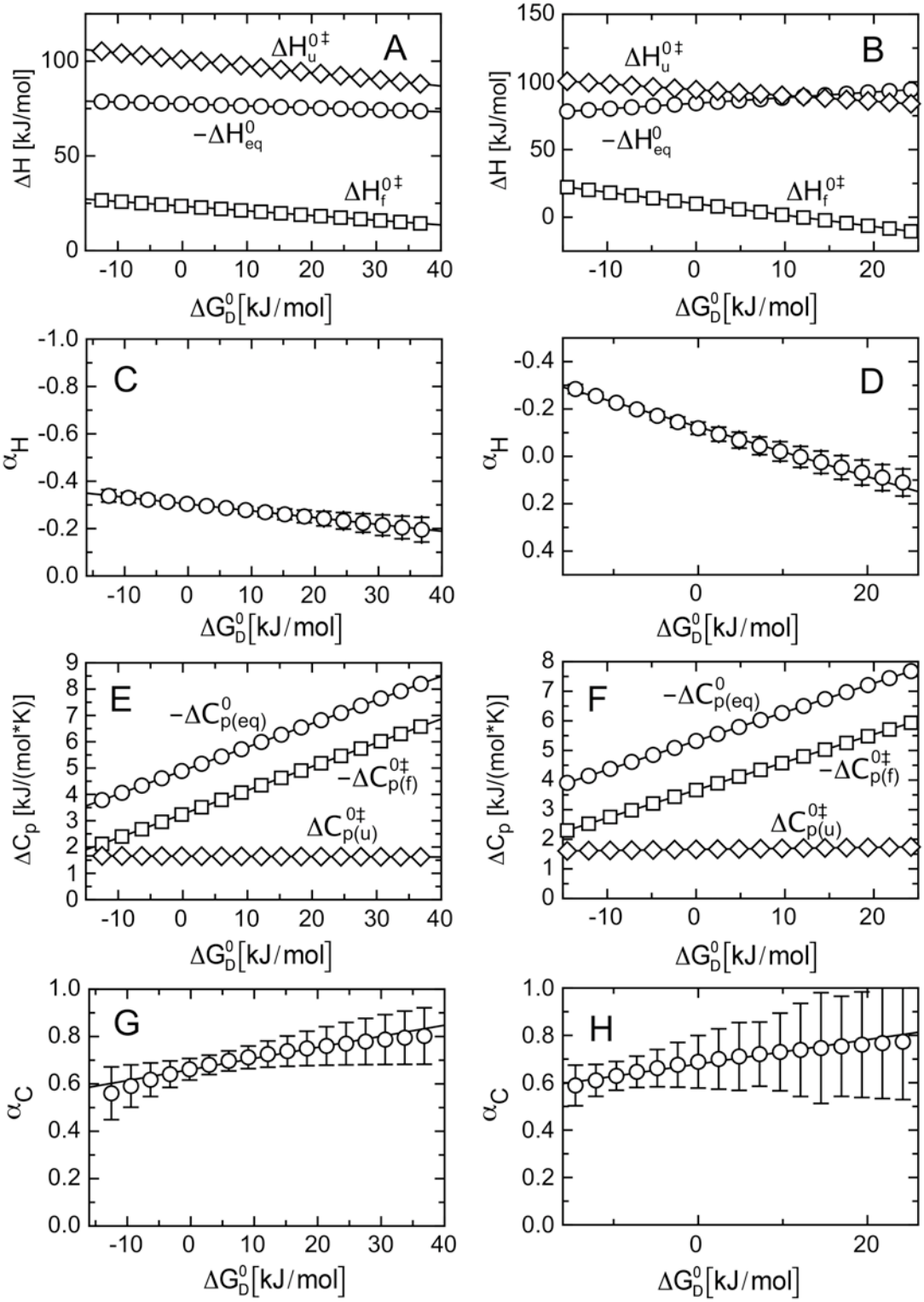
A
B
C
D
E
F
G
H
ΔH [kJ/mol]
$\Delta H_u^{0\ddagger}$
$-\Delta H_{eq}^{0}$
$\Delta H_f^{0\ddagger}$
ΔG_D^0[kJ/mol]
α_H
α_C
ΔCp [kJ/(mol*K)]
$-\Delta C_{p(eq)}^{0}$
$-\Delta C_{p(f)}^{0\ddagger}$
$\Delta C_{p(u)}^{0\ddagger}$

Figure 6

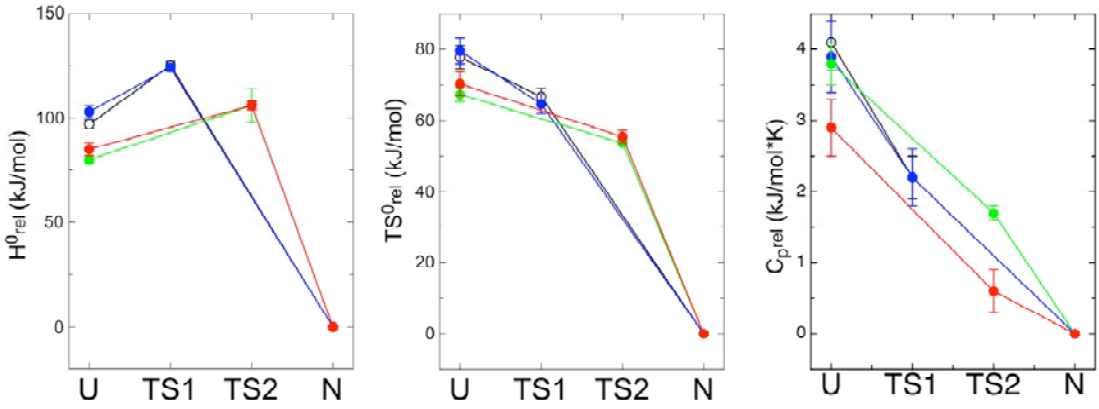
150
100
50
0
H^0_{rel} (kJ/mol)
U
TS1
TS2
N
80
60
40
20
0
TS^0_{rel} (kJ/mol)
U
TS1
TS2
N
4
3
2
1
0
$C_{p\,rel}$ (kJ/mol*K)
U
TS1
TS2
N

Figure 7

8.3 Evidence for Parallel Pathways at the Early Stage of Tendamistat Folding

Evidence for Parallel Pathways at the Early Stage of Tendamistat Folding

Manuela Schätzle and Thomas Kiefhaber

Biozentrum der Universität Basel
Department of Biophysical Chemistry
Klingelbergstr. 70
CH-4056
Switzerland

Running title: Parallel Pathways in Tendamistat Folding

*Correspondence should be addressed to T.K.: phone: ++41612672194; fax: ++41612672189; e-mail: t.kiefhaber@unibas.ch

Abstract

Although predicted, parallel pathways are not often observed in protein folding. In our recent work we revealed the importance of multiple perturbation analysis to improve the sensitivity to test the properties of the free energy barriers. To test for parallel pathways, we therefore measured the effect of denaturant and temperature on the folding kinetics of a tendamistat variant lacking one of the two disulfide bonds. Replacement of the disulfide bond leads to a change of the rate-limiting step at high denaturant concentrations. Determination of the temperature-denaturant cross-interaction parameters revealed switches between parallel pathways at the early stage in folding. In contrast, no transition state movement is observed for the late transition state. Analysis of the denaturant dependence of the activation parameters revealed that the late transition state is rather insensitive to the addition of perturbations. These are in accordance with our previous observations that the barriers become increasingly narrow and transition state structures become more defined as the folding polypeptide chain approaches the native state.

Our results confirm the importance to use multiple perturbation analysis to test the shape of the free energy barrier in protein folding and to reveal underlying complexities of apparent two-state protein folding.

Abbreviations: GdmCl, guanidinium chloride; ASA, accessible surface area; REFER, rate-equilibrium free energy relationship

Introduction

Elucidation of structural and thermodynamic properties of the transition barriers separating the ensemble of unfolded polypeptide chains from the native state are one of the major goal in protein folding. A way to analyze the properties of the transition barriers is to measure the changes in activation free energy ($\Delta G^{0\ddagger}$) and in equilibrium free energy (ΔG^{0}) between the unfolded state and the native state upon addition of a perturbation ∂x.[1-4] To quantify the rate-equilibrium free energy relationships (REFERs) a proportionality constant can be defined:[1]

$$\alpha_x = \frac{\partial \Delta G^{0\ddagger} / \partial x}{\partial \Delta G^{0} / \partial x}. \tag{1}$$

α_x is commonly used to obtain information on the structural properties of the transition state and it is a measure for the position of the transition state along the reaction coordinate investigated by ∂x. The range of α_x is normally from 0 for an unfolded-like transition state to 1 for a native-like transition state.

The most common perturbation applied in protein folding is a change in denaturant concentration. Linear denaturant dependencies of the activation free energies ($\Delta G^{0\ddagger}$) for refolding and unfolding lead to a V-shaped plot of $ln\lambda$ ($\lambda=k_f+k_u$) *versus* chemical denaturant concentration, commonly called chevron plots.[5] With the proportionality constants of the denaturant dependences of the activation free energies ($m_{f,u} = d\Delta G^{0\ddagger}_{f,u} / d[Denaturant]$) and the equilibrium free energy ($m_{eq} = d\Delta G^{0} / d[Denaturant]$) we can define an α_D-value:

$$\alpha_D = \frac{\partial \Delta G^{0\ddagger} / \partial [denaturant]}{\partial \Delta G^{0} / \partial [denaturant]} = \frac{m_{f,u}}{m_{eq}} \tag{2}$$

It was shown that the m-values are proportional to the changes in solvent accessible surface area.[6] Thus, α_D defines the relative change in solvent accessible surface area between the unfolded state and the transition state. Other possible perturbations are structural changes upon site-directed mutagenesis and variation of temperature and pressure.

It was observed in many reactions that the changes in activation free energy ($\Delta G^{0\ddagger}$) induced by changes in the solvent or in structure are linearly related to the corresponding changes in equilibrium free energy (ΔG^{0}) between reactants and

products (Leffler plot).[1,4,7] The slope of the Leffler plot gives α_x. Due to the uncertainty of the absolute value of $\Delta G^{0‡}$, a plot of the rate constant for folding (k_f) versus the equilibrium constant (K_{eq}) determined under the same conditions is a more practical way to analyze REFERs.[7] This will not influence the slope of the Leffler plot but it avoids some uncertainty on the absolute value of $\Delta G^{0‡}$.

Deviations from linearity in the REFERs upon mutation or changes in solvent conditions are frequently observed in protein folding. They were shown to be caused by four major effects: (i) a change in the rate limiting step[8-11], (ii) a change from two-state folding to folding through a populated intermediate[12-14], (iii) a change to a parallel pathway[15,16], (iv) a movement of the transition state along the reaction coordinate (Hammond behavior)[17] and (v) structural changes in the ground states[15]. Therefore, analysis of nonlinearities reveals important features on the shape of the transition barriers.

According to the Hammond postulate the position of a transition state is shifted towards the ground state that is destabilized by the perturbation relative to the unfolded state, leading to an increase in α_x and downward curvatures in the Leffler plots. In contrast, a decrease in α_x with decreasing protein stability is sometimes referred to as anti-Hammond behavior.[18,19] However, this phenomenon could be also explained due to a change of the transition state on parallel pathways.[15]

For a large number of apparent two-state folders non-linear Leffler plots were reported for the denaturant dependence of $\Delta G^{0‡}$ for refolding and unfolding. Detailed studies of these proteins showed that folding is best explained by a sequential folding model with consecutive transition states and at least one metastable high energy intermediate.[11] Most of the apparent transition state movements reported for several proteins when the effect of mutations was investigated revealed that these apparent Hammond behavior are due to ground state effects in the unfolded state.[15] Changes in the structure of the unfolded state leads to a movement of the position of the transition state relative to the unfolded state, although the transition state structure remains unchanged. This indicates that transition barriers in protein folding are rather narrow and remarkably stable towards amino acids replacements. Sensitivity to detect transition state movement can be improved by applying multiple perturbations.[20]

In contrast to the sequential transition states, parallel pathways are rare in protein folding.[11,15] However, theoretical studies suggested the presence of a manifold of

parallel routes to the native state.[21,22] For lysozyme folding at least three parallel pathways were described, some of which are detectable only under certain conditions.[23-26] Evidence for parallel pathways in the absence of intermediates is rare. A clear upward curvature in the chevron plot was reported for a titin domain, which is the clearest example for parallel pathways in two-state folding.[16] The existence of parallel pathways was also suggested for the formation of the first helix of barnase[18,27], and for protein G[28]. In parallel pathways a shift in the rate-limiting step to a more native-like transition state occurs upon destabilization of the protein. This leads to a decrease in α_x with decreasing protein stability, which is also sometimes referred to as anti-Hammond behavior.[15,18,19]

We used the small all-β-sheet protein tendamistat (figure 1A) as a model to test for parallel pathways in protein folding using multiple perturbation analysis. In previous studies it was shown that folding of tendamistat involves two sequential transition states.[10] Applying single perturbations on results in linear Leffler plots.[20,29,30] In contrast, combining the effect of denaturant and temperature or pressure on folding and stability revealed Hammond behavior supporting the importance of multiple perturbation analysis to test the shape of free energy barriers in protein folding.[20,30] Significantly less Hammond behavior was found for the late transition state leading to the conclusion that the transition barriers become increasingly narrow and structurally more defined as the folding polypeptide chain approaches the native state (figure 1B).

Tendamistat contains two disulfide bridges (Figure 1A). To test for parallel pathways in tendamistat folding, we measured the effect of denaturant and temperature on the folding kinetics of the tendamistat disulfide variant C11A/C27S.

Material and Methods

Materials. The tendamistat variant C11A/C27S was constructed, expressed in *Streptomyces lividans* and purified as described by Haas-Lauterbach *et al.*[31]. Ultrapure GdmCl was obtained by Nigu Chemie (Waldkaiburg, Germany). All other chemicals were analysis grade and purchased from Merck (Darmstadt, Germany). All experiments were carried out in 100 mM cacodylic acid, pH 7.0.

Kinetic measurements. Refolding and unfolding kinetics were measured in an Applied Photophysics SX.18MV stopped-flow instrument. The change in fluorescence above 320 nm after excitation at 276 nm was monitored. Unfolding or refolding was initiated by 11-fold dilution of native or unfolded protein into various denaturant concentrations. The final protein concentration was 3.8 μM.

Transition state analysis. The GdmCl dependence of the apparent rate constant (λ) for folding/unfolding was analyzed using the sequential three-state model with high-energy intermediate described by Bachmann & Kiefhaber:[10,32]

$$U \underset{k_{IU}}{\overset{k_{UI}}{\rightleftharpoons}} I \underset{k_{NI}}{\overset{k_{IN}}{\rightleftharpoons}} N \tag{3}$$

The high-energy intermediate is always less stable than U and N thus the analysis does not make any assumptions on the stability of the intermediate. Therefore, the fitting of the data to the analytical solutions of the three-state model allows the determination of k_{UI} and k_{NI} and their denaturant dependencies m_{UI} and m_{NI}, respectively. Only the ratios k_{IN}/k_{IU} and m_{IN}-m_{IU} are defined, which have to be used for data fitting. The determined values allows us to calculate k_f, k_u, m_f and m_u for the early and late transition state, respectively.

Rate constants at different denaturant concentrations were calculated according to equation (4):

$$\ln k_{f,u} = \ln k_{f,u}^{H_2O} - \frac{m_{f,u}}{\mathrm{RT}}[denaturant] \tag{4}$$

The free energies of activation for folding ($\Delta G_f^{0\ddagger}$) and unfolding ($\Delta G_u^{0\ddagger}$) were calculated using transition state theory[33]:

$$k = k_0 \cdot e^{-\Delta G^{0\ddagger}/\mathrm{RT}} \tag{5}$$

where the pre-exponential factor, k_0 represents the maximum rate constant for protein folding in the absence of free energy barriers. This value was measured to be in the order of 10^7-10^8 s^{-1}.[34,35] A value of 10^8 s^{-1} was used in the fits. The pre-exponential factor was assumed to be temperature independent. The temperature dependence of the rate constants at various denaturant concentrations was analyzed using equations (5) and (6)

$$\Delta G^{0\ddagger} = \Delta H^{0\ddagger}(T_0) - T \cdot \Delta S^{0\ddagger}(T_0) + \Delta C_p^{\ddagger}\left(T - T_0 - T \cdot \ln\frac{T}{T_0}\right) \tag{6}$$

with a reference temperature (T_0) of 298.15 K. Equation (6) assumes that $\Delta C_p^{0\ddagger}$ is itself independent of temperature.[36] The value for the entropy of activation ($\Delta S^{0\ddagger}$) depends critically on the correct pre-exponential factor, whereas the values for the enthalpy of activation ($\Delta H^{0\ddagger}$) and heat capacity of activation ($\Delta C_p^{0\ddagger}$) are nearly independent of the pre-exponential factor used.

For the Leffler plots the k_f-values were calculated from the measured apparent rate constant (λ).

To systematic analyze a shift in the position of the transition state along the reaction coordinate due to changes in equilibrium free energy upon addition of denaturant, the self-interaction parameter p_D was used.[4,37]

$$p_D = \frac{\partial \alpha_D}{\partial \Delta G_D^0} = \frac{\partial^2 \Delta G_f^{0\ddagger}}{\left(\partial \Delta G_D^0\right)^2} \tag{7}$$

A positive p_D-value indicates a movement of the transition state to the destabilized state according to Hammond or a change in the rate-limiting step, whereas anti-Hammond behavior or parallel pathways could cause negative values.

To improve the sensitivity in the detection of transition state movements we analyzed the position of the transition state along the reaction coordinate α_x under different ΔG^0 caused by the second perturbation, ∂y: [37]

$$p_{DT} = \frac{\partial^2 \Delta G_f^{0\ddagger}}{\left(\partial \Delta G_T^0\right)\left(\partial \Delta G_D^0\right)} = \frac{\partial \alpha_D}{\partial \Delta G_T^0} = \frac{\partial \alpha_T}{\partial \Delta G_D^0} \tag{8}$$

As equation (8) indicate and was shown in previous work[20], p_{DT} can be determined in two different ways: analysis the effect of temperature on α_D, i.e. on the relative change in ASA between unfolded state and transition state, and the effect of denaturant concentration on α_T, i.e. on the relative entropy change between unfolded state and transition state.

By definition, Hammond behavior and ground state effects will yield positive p_{DT}-values. Negative p_{DT}-values indicate anti-Hammond behavior or parallel pathways. To distinguish between these effects, determination of the effect of temperature on

the kinetic and equilibrium m-values and the denaturant concentration on the entropy-values, respectively, is necessary.

Global analysis of the kinetic data. To fit the kinetic data globally we assumed that the activation parameters $\Delta H^{\ddagger}$, $\Delta S^{\ddagger}$ and $\Delta C_p^{\ddagger}$ depend linearly on the denaturant concentration as shown for the equilibrium thermodynamic parameters[38]. This allows a global fit of the data according to equation (9)

$$\Delta G^{0\ddagger}\left(T,[GdmCl]\right) = \left(\Delta H^{\ddagger}(T_0,H_2O) + h(T_0)[GdmCl]\right) - T\left(\Delta S^{\ddagger}(T_0,H_2O) + s(T_0)[GdmCl]\right) + \left(\Delta C_p^{\ddagger}(H_2O) + c[GdmCl]\right)\left[T - T_0 - T\ln\left(T/T_0\right)\right] \quad (9)$$

with $h(T_0) = \partial\Delta H^{\ddagger}/\partial[GdmCl]$, $s(T_0) = \partial\Delta S^{\ddagger}/\partial[GdmCl]$ and $c = \partial\Delta C_p^{\ddagger}/\partial[GdmCl]$. $\Delta H^{\ddagger}(T_0,H_2O)$, $\Delta S^{\ddagger}(T_0,H_2O)$ and $\Delta C_p^{\ddagger}(H_2O)$ are the entropy, enthalpy and the heat capacity of activation in the absence of denaturant at the reference temperature T_0 = 298.15 K. With $m_{f,u}(T) = \partial\Delta G_{f,u}^{0\ddagger}(T,[GdmCl])/\partial[GdmCl]$ and equation (9) we receive the temperature dependence of the kinetic m-values:

$$m_{f,u}(T) = h_{f,u}(T_0) - T\cdot s_{f,u}(T_0) + c_{f,u}\cdot\left[T - T_0 - T\ln\left(T/T_0\right)\right] \quad (10)$$

The data were converted using equation (11):

$$\frac{h_{f,u}}{m_{eq}} = \frac{\partial\Delta H_{f,u}^{0\ddagger}}{\partial\Delta G_D^0};\ \frac{s_{f,u}}{m_{eq}} = \frac{\partial\Delta S_{f,u}^{0\ddagger}}{\partial\Delta G_D^0};\ \frac{c_{f,u}}{m_{eq}} = \frac{\partial\Delta C_{p\,f,u}^{\ddagger}}{\partial\Delta G_D^0} \quad (11)$$

Data fitting. The program ProFit (Quantum Soft, Zürich, Switzerland) was used for all data fitting.

Results and Discussions

Folding through an on-pathway high-energy intermediate. We studied the effect of temperature and GdmCl concentrations on folding and unfolding of the tendamistat variant C11A/C27S at pH 7. The microscopic rate constants for folding (k_f) and unfolding (k_u) were measured at a variety of different GdmCl concentrations between 1 and 8 M and at 7 different temperatures between 5°C and 35°C (figure 2A). At higher temperatures the unfolding limb clearly reveals a downward curvature near the transition region and reaches a constant value above 4 M GdmCl. The non-linearity can hardly be detected at lower temperatures due to the location of the curvature near the transition region. Thus, the downward curvature in the Chevron plot at 25°C in previous work escaped detection.[39] We re-measured the kinetic data with more data points in the unfolding limb and in the transition region revealing a small downward curvature (figure 2A and B). Analysis of the amplitudes reveals no evidence for intermediates at all investigated temperatures (data not shown).

Jencks and co-workers proposed a method to analyze transition state movements by applying self- and cross-interaction parameters (equations (7) and (8)).[37] A self-interaction parameter p_x measures the shift in the position of the transition state along the reaction coordinate due to changes in equilibrium free energy upon perturbation. Such a shift causes a curvature in the corresponding Leffler plot. By definition, Hammond behavior yields positive self-interaction parameters and a downward curvature in the Leffler plot. The Leffler plot obtained from the Chevron plot at 25°C clearly shows a downward curvature (Figure 2B). Nonlinear Leffler plots are also observed at all other investigated temperatures. At low temperatures, however, deviations from linearity are almost invisible as also seen from the nearly linear folding and unfolding limbs in the Chevron plots (figure 2A). Positive denaturant self-interaction parameters indicate Hammond behavior. However, a change in the rate limiting step causes also a downward curvature in Chevron plots.[4,8-11,32] Detailed studies of tendamistat showed sequential transition states in tendamistat folding.[11] Therefore, we fitted the data using the sequential three-state model with high-energy intermediate.[10,32]

Apparent transition state movement of the early transition state in tendamistat folding. As shown in our previous studies, transition state movements are only observed when the effects of multiple perturbations are analyzed.[15,20] The cross-interaction parameter p_{DT} (equation (8)) measures the position of the transition state along the denaturant-induced reaction coordinate α_D under different ΔG_T^0 which improves the detection of transition state movements.[37] Figure 3B shows the effect of changes in ΔG_T^0 caused by variation of temperature on α_D of the early transition state. α_D strongly decreases from 0.77 till 0.53 with increasing temperature. A linear fit of the data gives a negative p_{DT}-value of $-(39\pm4)\cdot10^{-3}$ mol/kJ for the early transition state (table 1). Negative cross-interaction parameters could be due to parallel pathways since the free energy of more native-like transition states would be more strongly increased when the native state is destabilized.[15] This would lead to an apparent movement to a more unfolded-like transition states often called anti-Hammond behavior. To distinguish between ground state effects and apparent transition state movements, the effect of changes in ΔG_T^0 on the equilibrium and kinetic *m*-values were analyzed (figure 3A). Large changes in m_u and m_f reveals transition state movements accompanied by a ground state effect as indicated by the increase in m_{eq} upon decreasing protein stability. Ground state effects in the unfolded state were also observed for the temperature-denaturant perturbation in tendamistat folding in our previous work.[20] This is in accordance with residual structure in the unfolded state. These intramolecular interactions are destabilized with increasing temperature leading to a more solvent-exposed unfolded state. Thus, the m_f and m_{eq}-values increases upon protein destabilization and contribute to the cross-interaction parameter p_{DT}. To quantify the extent of apparent transition state movement we therefore corrected the properties of the ground state effects. The corrected cross-interaction parameter p_{DT} is larger with a value of $-(48\pm4)\cdot10^{-3}$ mol/kJ (table 1; figure 3C).

An other way to determine p_{DT} is the determination of the effect of denaturant concentration on the relative entropy change between unfolded state and transition state $\alpha_T = \Delta S_f^{0\ddagger} / \Delta S_{eq}^0$ (equation (8)).[4,7,20] The parameters, received from the single fits of the Chevron plots at each temperature, allow the calculation of k_u and k_f at any given temperature and GdmCl concentration (figure 4) and thus, using equations (5) and (6), the determination of the GdmCl dependence of entropy, enthalpy and the

change in heat capacity (figures 3, 5 and 6; table 2). The magnitude of the activation entropies critically depend on the choice of the pre-exponential factor in the Eyring equation and therefore only relative values can be calculated from the kinetic data. The cross-interaction parameter p_{DT} is independent of the absolute value of the pre-exponential factor. The analysis of the disulfide variant C11A/C27S is accompanied by large errors due to the microscopic rate constant for folding (k_f) of the late transition state and the rate constant for unfolding (k_u) of the early transition state were less well defined (figure 4).

Analyzing the changes in ΔS^0 and $\Delta S^{0‡}$ with denaturant concentration confirm our observation found for the early transition state (figure 3D). In contrast to the temperature dependence of the α_D-values, the denaturant dependences of α_T shows no linear dependency accompanied by large uncertainties (figure 3E). The p_{DT}-value decreases with decreasing protein stability. Like for α_D, we corrected the properties of the refolding reaction for the ground state effects. Cross-interaction plot of the corrected α_T-values against ΔG_D^0 for the early transition state is linear with p_{DT}-value of $-(41\pm3)\cdot10^{-3}$ mol/kJ (figure 3F; table 1). The result is in good agreement with the p_{DT}-value obtained from the corrected α_D-value (figure 3C; table 1).

Origin of apparent anti-Hammond behavior. Theoretical studies on protein folding predict that multiple pathways between the folded and unfolded states exist for all proteins.[21,22] However, there has been little experimental evidence of multiple equivalent folding pathways to support these theories. One of the best-characterized case has involved intermediates acting as kinetic traps to folding.[13,40] At least three parallel pathways were described for lysozyme folding.[24] The existence of two parallel pathways in two-state folding was found for folding of the 27th immunoglobulin domain of the human giant muscle protein titin (TI I27).[16]

In the case of parallel pathways a perturbation should affect the transition states to different degrees. When the native state is destabilized the free energy of a more native-like transition states would be more affected. This leads to an apparent movement to a more unfolded-like transition states and negative cross-interaction parameters. Apparent transition state movements towards the unfolded state are sometimes explained as anti-Hammond behavior.[18,19] However, a more detailed analysis revealed that parallel pathways could also explain the effects.[15,16,41] No clear

example for anti-Hammond behavior for protein folding exist so far, in contrast, it was found that anti-Hammond behavior is not reasonable in protein folding.[4,7]

No parallel pathways could be observed for the tendamistat disulfide variant C11A/C27S analyzing Leffler plots at all measured temperatures (figure 2) confirming our previous observation that apparent transition state movement is only observed when multiple perturbations are applied.[20] Analysis of the denaturant dependence of folding of a tendamistat variant with intact disulfide bridges, however, clearly reveals an upward curvature indicating parallel pathways (unpublished results), which argues for parallel pathways rather than anti-Hammond behavior as origin of the apparent transition state movement.

Together with our previous results, we conclude that the early transition state is rather broad and less well-defined barrier with more pathways leading to the intermediate.

Late transition state is a rather narrow barrier in tendamistat folding. In contrast to the early transition state, the α_D-value of the late transition state is nearly temperature-independent with α_D-values between 0.90 and 0.91 and a small, positive p_{DT}-value of $(1.6\pm0.8)\cdot10^{-3}$ mol/kJ (table 1; figure 5B). Analysis of the changes of the kinetic *m*-values with increasing temperature reveals that the change in α_D is only caused by ground state effects in the unfolded state as indicated by the temperature-independence of m_u and of α_D corrected for the properties of the ground state effect with a p_{DT}-value of $-(0.1\pm0.7)\cdot10^{-3}$ mol/kJ (figure 5A, C; table 1). The results are confirmed by the denaturant independence of $\Delta S_u^{0\ddagger}$ (figure 5D). The change in α_T with ΔG_D^0 is non-linear in the late transition state as also observed for the early transition state (figures 5E and 3E). Figure 5F shows the corrected cross-interaction plot, which is linear with a p_{DT}-value of $(0.2\pm2.8)\cdot10^{-3}$ mol/kJ. Our observation is in accord with our previous results of the late transition state where only small Hammond behavior was observed.[20]

According to the linear free energy model,[38] changes in the activation parameters and the equilibrium thermodynamic parameters are linearly dependent on the GdmCl concentration and thus on the change of the Gibbs free energy ΔG_D^0. Table 2 compares the results from the global fit with the results from the individual fits of

the kinetic data. The result of the global fit for the denaturant dependence of ΔS^0 and $\Delta S^{0\ddagger}$ is in good agreement with the results of the single fits. The denaturant dependence of ΔS^0 and $\Delta S^{0\ddagger}$, however are accompanied with large uncertainties especially for the early transition state.

Denaturant dependences of the activation parameters. The origin of the GdmCl dependence of enthalpy and heat capacity is not as straightforward as the GdmCl dependence of entropy. Changes in enthalpy in protein folding reactions contain contributions from the polypeptide chain and from its interactions with solvent. Thus, the enthalpy-values should be dependend on the denaturant concentration. ΔH_{eq}^0 increases only slightly with increasing GdmCl concentrations (figure 6A and B). The activation enthalpies of the early transition state change significantly with decreasing protein stability, in contrast to the late transition state, where only small changes are observed (figure 6A and B; table 2). The results from the denaturant dependence of the enthalpy allow the definition of α_H ($\Delta H_f^{0\ddagger} / \Delta H_{eq}^0$), i.e. the relative enthalpy change between unfolded state and transition state. At high denaturant concentration α_H is accompanied by large uncertainties for both transition states (figure 6C and D). α_H shows linear dependency within errors with decreasing protein stability for the early and late transition state with cross-interaction parameters p_{HD} of $-(39\pm4)\cdot10^{-3}$ mol/kJ and p_{HD} of $-(4\pm3)\cdot10^{-3}$ mol/kJ. The results of the global fit are in good agreement with the results obtained from the single fits (table 2).

Comparison of the results of the global and single fits for the change in heat capacity received nearly similar results within errors for ΔC_p^0 and $\Delta C_p^{0\ddagger}$ (table 2). The denaturant dependences of the change in heat capacity, however, show quite differences between both fitting methods (table 2). The values of heat capacity strongly depend on the denaturant concentration of the rate constants. Small uncertainties in the GdmCl dependence of the rate constants result in large variations of the heat capacity. The errors significantly increase with decreasing protein concentration. The results of the denaturant dependence of the change in heat capacity for the global fit is accompanied with large uncertainties as also observed for the denaturant dependence of the entropy and enthalpy values. Despite from the differences of the results of both fitting methods, comparison of both reveals that

changes in heat capacity show a strong denaturant concentration dependence (figure 6E and F; table 2). In contrast to $\Delta C^{0\ddagger}_{p(u)}$ where only small changes with increasing denaturant concentration was observed, $\Delta C^{0}_{p(eq)}$ and $\Delta C^{0\ddagger}_{p(f)}$-values significantly increase with decreasing protein stability for both transition states.

ΔC^{0}_{p} is entirely defined by difference in interactions of the protein with the solvent thus α_C ($= \Delta C^{0\ddagger}_{p(f)} / \Delta C^{0}_{p(eq)}$) allows the characterization of a transition state in terms of its relative solvent exposure. The α_C-values are accompanied by very large errors (table 2) and are not defined at higher denaturant concentration due to the change of sign of $\Delta C^{0}_{p(eq)}$ (figure 6E-H). m_{eq} and ΔC^{0}_{p} -values correlate well with each other because both depend on the amount of protein surface which becomes exposed to solvent upon unfolding.[6] Thus, the two thermodynamic criteria are most often used in protein folding to locate the transition state with respect to the unfolded and the native state. α_D report on the interactions of the transition state with the solvent, and α_C report on the hydrophobic and polar hydration of the protein in the transition state. Table 3 compares α_C and α_D in absence of denaturant and at 25°C. The single and global fit results of α_D are in good agreement. However, the results for the global fits are accompanied with large uncertainties. Comparison of the results of the single and global fits of α_C differs significantly but is accompanied with large errors for either fitting method. For the late transition state, the α_D-value is higher than the α_C-value, which is commonly observed in protein folding.[4] In contrast, α_D is smaller than α_C for the early transition state which is very unusual.

In summary, the activation parameters of the early transition state significantly change with increasing denaturant concentration compared to the late transition state, where only small changes are observed (table 2). This is in accord with the assumption that the late transition state is rather narrow and well defined and does not significantly change with changes in solvent conditions. In contrast, it is difficult to interpret the data of the early transition states since folding occurs via parallel pathways.

Influence of the disulfide bridges on tendamistat folding. Replacement of the disulfide bond C11-C27 in tendamistat results in a large decrease in stability and to a deceleration of the refolding rates.[10,39] Similar like the removing of the other

disulfide bond C45-C73 in tendamistat, a change in the rate-limiting step occurs at high denaturant concentrations.[10] Our results of the late transition state of the disulfide variant C11A/C27S is in accordance with our previous finding that the late transition state is a rather narrow and structurally well-defined barrier.[20] Folding of the early stage in folding of C11A/C27S occurs over different parallel pathways. A destabilization of the protein leads to switches between parallel pathways. Parallel pathways without population of intermediates are not observed during folding of tendamistat wild type and other tendamistat variants so far. This indicates the importance of the disulfide bond connecting the N-terminal β-hairpin for the early folding of tendamistat. Formation of this hairpin is not favorable (M.S. and T.K., unpublished results) leading to the conclusion of the importance of the disulfide bond to stabilize the hairpin. Removing of this disulfide bond seems to lead to different possibilities to reach the intermediate state, whereas the late transition state is not affected confirming our observation of a well-structured late transition barrier. The use of multiple perturbation analysis reveals important features of the shape of the free energy barrier and the underlying complexities in tendamistat folding.

Acknowledgements

This work was supported by a grant from the Swiss National Science Foundation.

Table 1. Effect of changes in protein stability induced by temperature ($\partial\Delta G_T^0$) on α_D and on m_{eq}, m_f and m_u and effect of changes in protein stability induced by denaturant ($\partial\Delta G_D^0$) on α_T and on ΔS_{eq}^0, $\Delta S_f^{0\ddagger}$ and $\Delta S_u^{0\ddagger}$ of the folding reaction of the tendamistat disulfide variant C11A/C27S at pH 7.

	TS1	TS2	TS1 corrected [a]	TS2 corrected [a]
p_{DT}				
$\partial\alpha_D/\partial\Delta G_T^0$ ((mol/kJ)·10^3)	-39 ±4	1.6 ±0.8	-48 ±4	-0.1 ±0.7
$\partial\alpha_T/\partial\Delta G_D^0$ ((mol/kJ) ·10^3)			-41 ±3	0.2 ±2.8
$\partial m_{eq}/\partial\Delta G_T^0$ ($M^{-1}\cdot10^2$)	13 ±5		0	
$\partial m_f/\partial\Delta G_T^0$ ($M^{-1}\cdot10^2$)	-21 ±5	13 ±5	-33 ±12	-0.1 ±0.5
$-\partial m_u/\partial\Delta G_T^0$ ($M^{-1}\cdot10^2$)	34 ±3	0.1 ±0.5	34 ±3	0.1 ±0.5
$-\partial\Delta S_{eq}^0/\partial\Delta G_D^0$ ($K^{-1}\cdot10^3$)	2.3 ±0.5		0	
$-\partial\Delta S_f^{0\ddagger}/\partial\Delta G_D^0$ ($K^{-1}\cdot10^3$)	-7.7 ±0.8	2.4 ±0.5	-10.0 ±0.8	-0.04 ±0.50
$\partial\Delta S_u^{0\ddagger}/\partial\Delta G_D^0$ ($K^{-1}\cdot10^3$)	10.0 ±0.6	-0.04 ±0.05	10.0 ±0.6	-0.04 ±0.05

[a] Data were corrected of the properties of the refolding reaction for the ground state effect.

Table 2. Thermodynamic parameters of the folding reaction of the tendamistat disulfide variant C11A/C27S at pH 7 and the effect of changes in protein stability induced by adding denaturant on the thermodynamic parameters.

	TM C11A/C27S single fit		TM C11A/C27S global fit[a]	
	TS1	TS2	TS1	TS2
ΔS^0_{eq} (J/(mol·K·M))	-243 ±8		-257 ±21	
$\Delta S^{0‡}_{f}$ (J/(mol·K·M))	-213 ±21	-91 ±15	-201 ±7	-104 ±20
$\Delta S^{0‡}_{u}$ (J/(mol·K·M))	30 ±25	153 ±10	56 ±14	152 ±1
$-\partial\Delta S^0_{eq}/\partial\Delta G^0_D$ ($K^{-1}\cdot10^3$)	2.3 ±0.5		2.0 ±9.7	
$-\partial\Delta S^{0‡}_{f}/\partial\Delta G^0_D$ ($K^{-1}\cdot10^3$)	-7.7 ±0.8	2.4 ±0.5	-8.2 ±31.2	2.0 ±9.7
$\partial\Delta S^{0‡}_{u}/\partial\Delta G^0_D$ ($K^{-1}\cdot10^3$)	10.0 ±0.6	-0.04 ±0.05	10.3 ±38.6	-0.005 ±0.019
ΔH^0_{eq} (kJ/(mol·M))	-83 ±2		-88 ±6	
$\Delta H^{0‡}_{f}$ (kJ/(mol·M))	-23 ±6	11 ±4	-19 ±2	7 ±6
$\Delta H^{0‡}_{u}$ (kJ/(mol·M))	60 ±8	95 ±3	68 ±4	95 ±1
$-\partial\Delta H^0_{eq}/\partial\Delta G^0_D$	-0.3 ±0.1		-0.4 ±2.1	
$\partial\Delta H^{0‡}_{f}/\partial\Delta G^0_D$	2.9 ±0.2	0.2 ±0.1	3.1 ±11	0.3 ±1.8
$\partial\Delta H^{0‡}_{u}/\partial\Delta G^0_D$	2.6 ±0.2	-0.10 ±0.02	2.7 ±10.0	-0.1 ±0.4
$\Delta C^0_{p(eq)}$ (kJ/(mol·K))	-3.2 ±0.3		-2.7 ±0.6	
$\Delta C^{0‡}_{p(f)}$ (kJ/(mol·K))	-3.9 ±0.9	-1.3 ±0.6	-2.8 ±0.3	-0.4 ±0.5
$\Delta C^{0‡}_{p(u)}$ (kJ/(mol·K))	-0.7 ±1.1	2.0 ±0.4	-0.1 ±0.4	2.4 ±0.1
$-\partial\Delta C^0_{p(eq)}/\partial\Delta G^0_D$ ($K^{-1}\cdot10^3$)	-82 ±19		-69 ±293	
$-\partial\Delta C^{0‡}_{p(f)}/\partial\Delta G^0_D$ ($K^{-1}\cdot10^3$)	-168 ±29	-78 ±22	-77 ±314	-61 ±26
$\partial\Delta C^{0‡}_{p(u)}/\partial\Delta G^0_T$ ($K^{-1}\cdot10^3$)	86 ±18	-3.8 ±2.3	8 ±38	-7.8 ±31

[a] The data are results from global fits of kinetic data at various temperatures.

Table 3. Comparison of the α_D- and α_C-values from the single and global fits of the tendamistat variant C11A/C27S at 25°C and absence of denaturant.

	single fit		global fit	
	α_D	α_C	α_D	α_C
TS1	0.62 ±0.11	1.21 ±0.41	0.60 ±1.01	1.04 ±0.34
TS2	0.91 ±0.14	0.40 ±0.24	0.90 ±1.74	0.13 ±0.23

Reference

1. Leffler, J.E. Parameters for the description of transition states. *Science* **117**, 340-341 (1953).
2. Jencks, W.P. *Catalysis in Chemistry and Enzymology*, (McGraw-Hill Book Company, New York, 1969).
3. Grosman, C., Zhou, M. & Auerbach, A. Mapping the conformational wave of acetylcholine receptor channel gating. *Nature* **403**, 773-776 (2000).
4. Sánchez, I.E. & Kiefhaber, T. Non-linear rate-equilibrium free energy relationships and Hammond behavior in protein folding. *Biophys. Chem.* **100**, 397-407 (2003).
5. Tanford, C. Protein denaturation. Part B. The transition from native to denatured state. *Adv. Prot. Chem* **23**, 218-282 (1968).
6. Myers, J.K., Pace, C.N. & Scholtz, J.M. Denaturant m values and heat capacity changes: relation to changes in accessible surface areas of protein unfolding. *Protein Sci.* **4**, 2138-2148 (1995).
7. Kiefhaber, T., Sánchez, I.E. & Bachmann, A. Characterization of protein folding barriers with rate equilibrium free energy relationships. in *Protein Folding Handbook*, Vol. 1 (eds. Buchner, J. & Kiefhaber, T.) 411-444 (Wiley-VCH Verlag, Weinheim, 2005).
8. Jonsson, T., Waldburger, C.D. & Sauer, R.T. Nonlinear free energy relationship in arc repressor unfolding imply the existence of unstable, native-like folding intermediates. *Biochemistry* **35**, 4795-4802 (1996).
9. Wallenhorst, W.F., Green, S.M. & Roder, H. Kinetic evidence for folding and unfolding intermediates in staphylococcal nuclease. *Biochemistry* **36**, 5795-5805 (1997).
10. Bachmann, A. & Kiefhaber, T. Apparent two-state tendamistat folding is a sequential process along a defined route. *J Mol Biol* **306**, 375-386 (2001).
11. Sánchez, I.E. & Kiefhaber, T. Evidence for sequential barriers and obligatory intermediates in apparent two-state protein folding. *J. Mol. Biol.* **325**, 367-376 (2003).
12. Ikai, A. & Tanford, C. Kinetic evidence for incorrectly folded intermediate states in the refolding of denatured proteins. *Nature* **230**, 100-102 (1971).
13. Wildegger, G. & Kiefhaber, T. Three-state model for lysozyme folding: Triangular folding mechanism with an energetically trapped intermediate. *J Mol Biol* **270**, 294-304 (1997).
14. Kiefhaber, T., Bachmann, A., Wildegger, G. & Wagner, C. Direct measurement of nucleation and growth rates in lysozyme folding. *Biochemistry* **36**, 5108-12 (1997).
15. Sánchez, I.E. & Kiefhaber, T. Hammond behavior versus ground state effects in protein folding: evidence for narrow free energy barriers and residual structure in unfolded states. *J. Mol. Biol.* **327**, 867-884 (2003).
16. Wright, C.F., Lindorff-Larsen, K., Randles, L.G. & Clarke, J. Parallel protein-unfolding pathways revealed and mapped. *Nat Struct Biol* **10**, 658-62 (2003).
17. Hammond, G.S. A correlation of reaction rates. *J. Am. Chem. Soc.* **77**, 334-338 (1955).
18. Matthews, J.M. & Fersht, A.R. Exploring the energy surface of protein folding by structure-reactivity relationship and engineered proteins: Observation of Hammond behavior for the gross structure of the transitions

state and anti-hammond behavior for structural elements for unfolding/folding of barnase. *Biochemistry* **34**, 6805-6814 (1995).
19. Fersht, A.R., Itzhaki, L.S., Elmasry, N., Matthews, J.M. & Otzen, D.E. Single versus parallel pathways of protein folding and fractional formation of structure in the transition state. *Proc Natl Acad Sci USA* **91**, 10426-10429 (1994).
20. Schätzle, M. & Kiefhaber, T. Using temperature-denaturant cross interaction parameters to test the shape of free energy barriers for protein folding. submitted.
21. Guo, Z. & Thirumalai, D. Kinetics of protein folding: nucleation mechanism, time scales, and pathways. *Biopolymers* **36**, 83-102 (1995).
22. Wolynes, P.G., Onuchic, J.N. & Thirumalai, D. Navigating the folding routes. *Science* **267**, 1619-1620 (1995).
23. Wildegger, G. & Kiefhaber, T. Three-state model for lysozyme folding: triangular folding mechanism with an energetically trapped intermediate. *J. Mol. Biol.* **270**, 294-304 (1997).
24. Bieri, O., Wildegger, G., Bachmann, A., Wagner, C. & Kiefhaber, T. A salt-induced intermediate is on a new parallel pathway of lysozyme folding. *Biochemistry* **38**, 12460-12470 (1999).
25. Bieri, O. & Kiefhaber, T. Origin of apparent fast and non-exponential kinetics of lysozyme folding measured in pulse labeling experiments. *J. Mol. Biol.* **310**, 919-935 (2001).
26. Noyelle, K., Joniau, M. & Van Dael, H. The fast folding pathway in human lysozyme and its blockage by appropriate mutagenesis: a sequential stopped-flow fluorescence study. *J. Mol. Biol.* **308**, 807-819 (2001).
27. Fersht, A.R., Itzhaki, L.S., elMasry, N.F., Matthews, J.M. & Otzen, D.E. Single versus parallel pathways of protein folding and fractional formation of structure in the transition state. *Proc. Natl. Acad. Sci. USA* **91**, 10426-10429 (1994).
28. Nauli, S., Kuhlman, B. & Baker, D. Computer-based redesign of a protein folding pathway. *Nat. Struc. Biol.* **8**, 602-605 (2001).
29. Schönbrunner, N., Koller, K.-P. & Kiefhaber, T. Folding of the disulfide-bonded β-sheet protein tendamistat: Rapid two-state folding without hydrophobic collapse. *J. Mol. Biol.* **268**, 526-538 (1997).
30. Pappenberger, G., Saudan, C., Becker, M., Merbach, A.E. & Kiefhaber, T. Denaturant-induced movement of the transition state of protein folding revealed by high-pressure stopped-flow measurements. *Proc Natl Acad Sci U S A* **97**, 17-22 (2000).
31. Haas-Lauterbach, S. et al. High yield fermentation and purification of tendamistat disulfide analogues secreted by *Streptomyces lividans*. *Appl. Microbiol. Biotech.* **38**, 719-727 (1993).
32. Bachmann, A. & Kiefhaber, T. Kinetic mechanism in protein folding. in *Protein Folding Handbook*, Vol. 1 (eds. Buchner, J. & Kiefhaber, T.) 379-410 (Wiley-VCH Verlag, Weinheim, 2005).
33. Eyring, H. The activated complex in chemical reactions. *J. Chem. Phys.* **3**, 107-115 (1935).
34. Krieger, F., Fierz, B., Bieri, O., Drewello, M. & Kiefhaber, T. Dynamics of unfolded polypeptide chains as model for the earliest steps in protein folding. *J. Mol. Biol.* **332**, 265-274 (2003).

35. Fierz, B. & Kiefhaber, T. Dynamics of unfolded polypeptide chains. in *Protein Folding Handbook*, Vol. 2 (eds. Buchner, J. & Kiefhaber, T.) 809-855 (Wiley-VCH Verlag, Weinheim, 2005).
36. Becktel, W.J. & Schellman, J.A. Protein stability curves. *Biopolymers* **26**, 1859-1877 (1987).
37. Jencks, D.A. & Jencks, W.P. On the characterization of transition states by structure-reactivity coefficients. *J. Am. Chem. Soc.* **99**, 7948-7960 (1977).
38. Schellman, J.A. Solvent denaturation. *Biopolymers* **17**, 1305-1322 (1978).
39. Schönbrunner, N., Pappenberger, G., Scharf, M., Engels, J. & Kiefhaber, T. Effect of Pre-Formed Correct Tertiary Interactions on Rapid Two-State Tendamistat Folding: Evidence for Hairpins as Initiation Sites for β-Sheet Formation. *Biochemistry* **36**, 9057-9065 (1997).
40. Bieri, O., Wildegger, G., Bachmann, A., Wagner, C. & Kiefhaber, T. A salt-induced kinetic intermediate is on a new parallel pathway of lysozyme folding. *Biochemistry* **21**, 12460-70 (1999).
41. Fowler, S.B. & Clarke, J. Mapping the folding pathway of an immunoglobulin domain: structural detail from Phi value analysis and movement of the transition state. *Structure (Camb)* **9**, 355-66 (2001).
42. Kraulis, P. MolScript: a program to produce both detailed and schematic plots of protein structures. *J. Appl. Cryst.* **24**, 946-950 (1991).
43. Merrit, E. & Bacon, D. Raster3D: photorealistic molecular graphics. *Methods Enzymol.* **277**, 505-524 (1997).

Figure Legends

Figure 1. (A) Schematic drawing of the structure of tendamistat. The cysteine residues involved in the two disulfide bridges are indicated as ball-and-stick model. The figure was generated using the programs MOLSCRIPT[42] and Raster3D[43]. (B) Schematic drawing of the free energy barrier for folding of tendamistat wild type. The response of variation in temperature or pressure on the early transition states (TS1) is more sensitive than on the late one (TS2) due to the different broadness of the barriers.

Figure 2. (A) GdmCl-dependence of the apparent rate constants for folding of the tendamistat variant C11A/C27S at various temperatures at pH 7.0. The lines represent the result of the global fit of the kinetic data. (B) Leffler plot of the effect of GdmCl concentration on the equilibrium (K_{eq}) and folding rate constant (k_f) calculated from the kinetic data at 25°C. The lines represent hypothetical Leffler plots for the early transition state (TS1) and for the late transition state (TS2), respectively.

Figure 3. Analysis of the temperature-denaturant cross-interaction parameter p_{DT} for the early transition state in C11A/C27S folding. Effect of ΔG_T^0 on m_{eq}, m_f and $-m_u$ (A) and on α_D (B), respectively, and effect of ΔG_D^0 on $-\Delta S_{eq}^0$, $-\Delta S_f^{0\ddagger}$ and $\Delta S_u^{0\ddagger}$ (D) and on α_T (E), respectively. (C, F) Both α-values were corrected for the properties of the refolding reaction for the ground state effects. The data are taken from individual fits. The results of the linear fits are given in table 1.

Figure 4. Temperature dependence of the microscopic rate constants, k_f (A, C) and k_u (B, D) of the early (A, B) and late (C, D) transition state at various GdmCl concentrations. Microscopic rate constants at 0 M GdmCl were determined by fitting the kinetic data using the three-state model with metastable intermediate. The results were used to calculate the microscopic rate constants at various GdmCl concentrations according to equation (5). The data were fitted using equations (3) and (6). The resulting parameters are displayed in Figures 3, 5 and 6 and are given in table 2.

Figure 5. Analysis of the temperature-denaturant cross-interaction parameter p_{DT} for the late transition state in C11A/C27S folding. Effect of ΔG_T^0 on m_{eq}, m_f and $-m_u$ (A) and on α_D (B), respectively, and effect of ΔG_D^0 on $-\Delta S_{eq}^0$, $-\Delta S_f^{0\ddagger}$ and $\Delta S_u^{0\ddagger}$ (D) and on α_T (E), respectively. (C, F) Both α-values were corrected for the properties of the refolding reaction for the ground state effects. The data are taken from individual fits. The results of the linear fits are given in table 1.

Figure 6. Analysis of the denaturant-dependences of enthalpy and heat capacity, respectively, of the early (A, C, E, G) and late (B, D, F, H) transition state in C11A/C27S folding. Effect of ΔG_D^0 on enthalpy (A, B) and heat capacity (E, F) and on the corresponding α-values, α_H (C, D) and α_C (G, H), respectively. The data are taken from individual fits. The results of the linear fits for the denaturant-dependences of enthalpy and heat capacity are given in table 2. (C, D) The results of the cross-interaction parameters p_{HD} for the early and late transition states are $-(39 \pm 4)\cdot 10^{-3}$ mol/kJ and $-(4\pm 3)\cdot 10^{-3}$ mol/kJ, respectively.

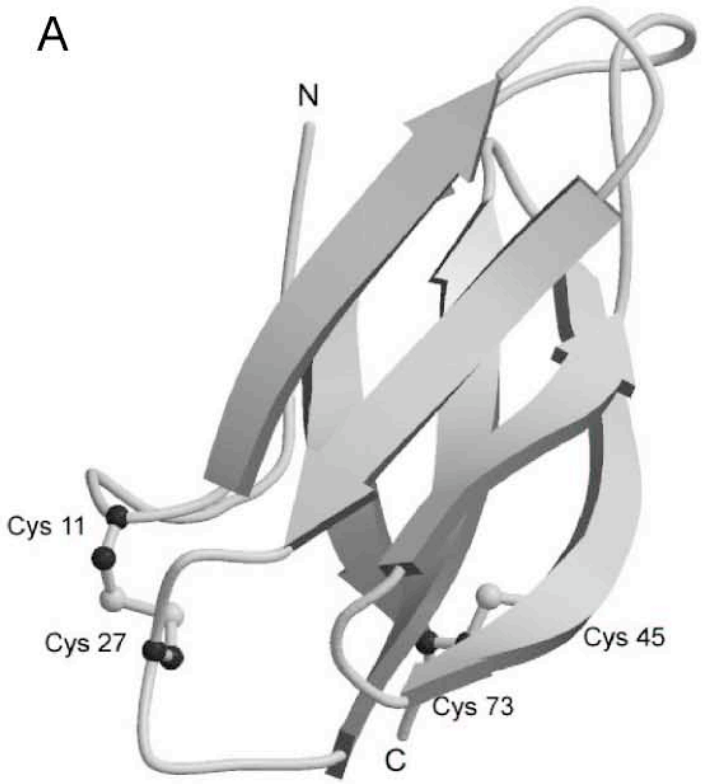
A
N
Cys 11
Cys 27
Cys 45
Cys 73
C

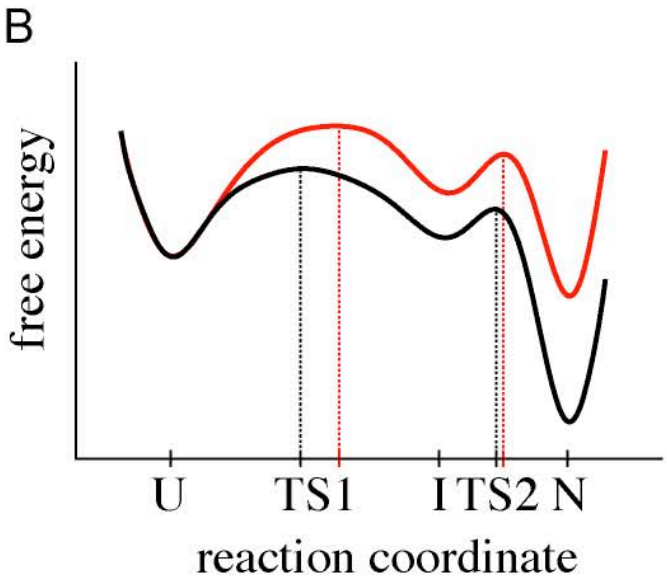
B
free energy
U
TS1
I
TS2
N
reaction coordinate

Figure 1

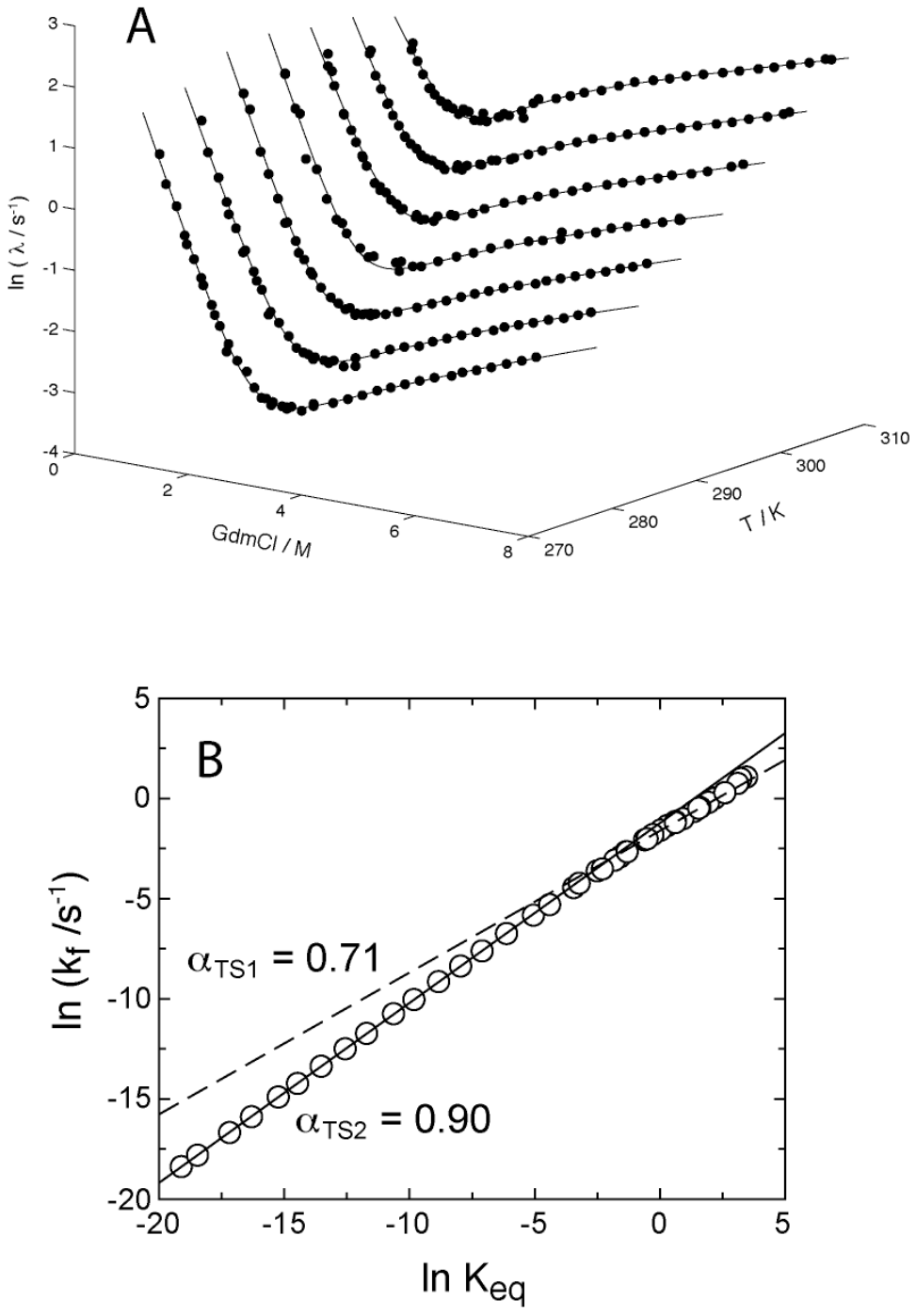
A
ln (λ / s-1)
3
2
1
0
-1
-2
-3
-4
0
2
4
6
8
GdmCl / M
270
280
290
300
310
T / K
B
ln (kf /s-1)
5
0
-5
-10
-15
-20
αTS1 = 0.71
αTS2 = 0.90
-20
-15
-10
-5
0
5
ln Keq

Figure 2

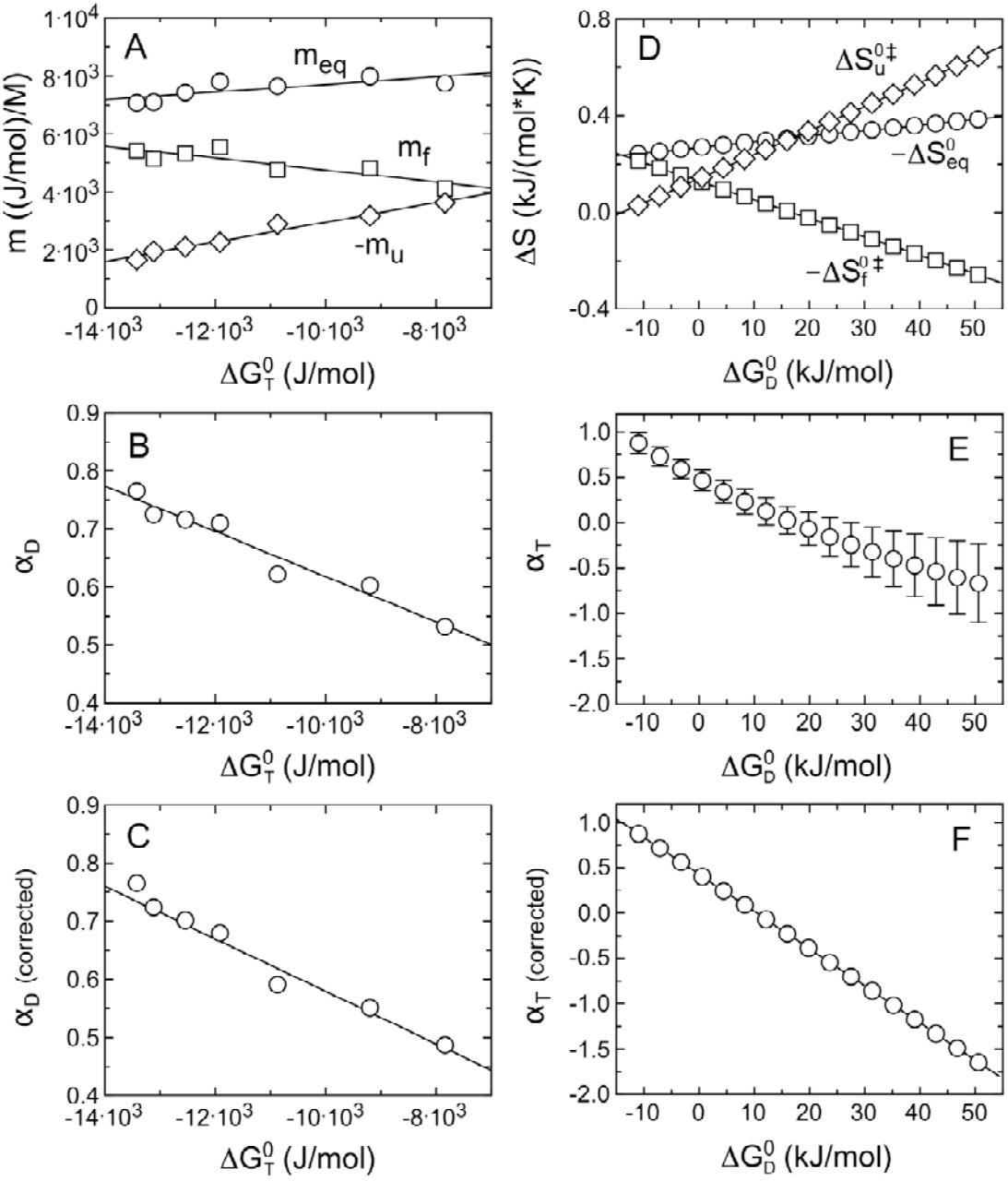
A
m_{eq}
m_f
$-m_u$
m ((J/mol)/M)
ΔG_T^0 (J/mol)
D
$\Delta S_u^{0\ddagger}$
$-\Delta S_{eq}^0$
$-\Delta S_f^{0\ddagger}$
ΔS (kJ/(mol*K))
ΔG_D^0 (kJ/mol)
B
α_D
ΔG_T^0 (J/mol)
E
α_T
ΔG_D^0 (kJ/mol)
C
α_D (corrected)
ΔG_T^0 (J/mol)
F
α_T (corrected)
ΔG_D^0 (kJ/mol)

Figure 3

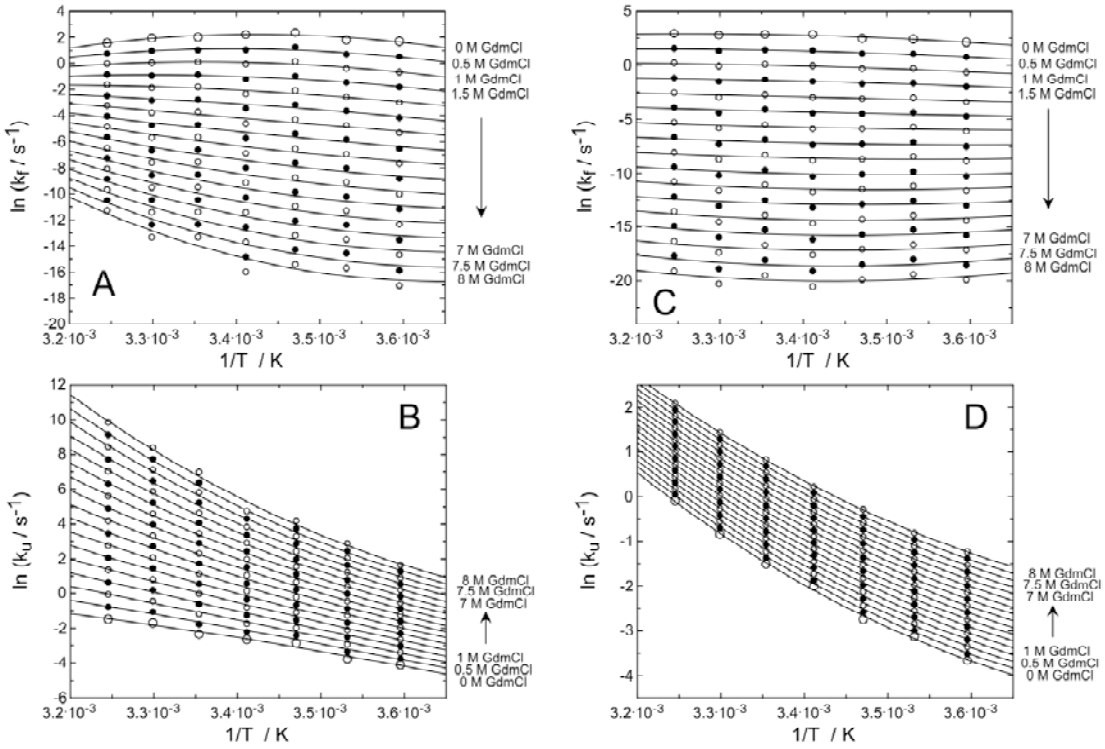
A
B
C
D
ln (k_f / s^-1)
ln (k_u / s^-1)
1/T / K
0 M GdmCl
0.5 M GdmCl
1 M GdmCl
1.5 M GdmCl
7 M GdmCl
7.5 M GdmCl
8 M GdmCl

Figure 4

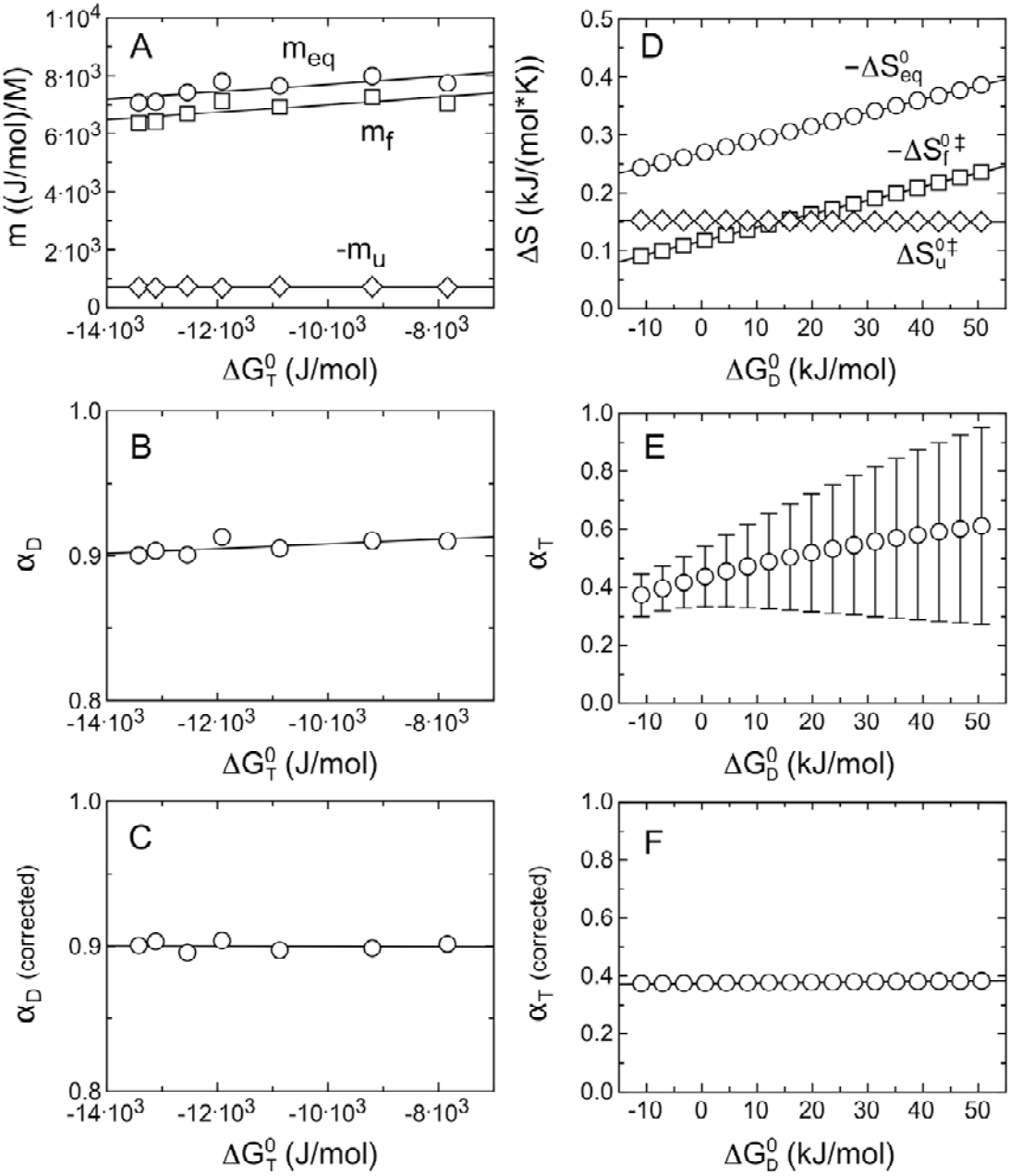
A
m_eq
m_f
-m_u
m ((J/mol)/M)
ΔG_T^0 (J/mol)
D
-ΔS_eq^0
-ΔS_f^0‡
ΔS_u^0‡
ΔS (kJ/(mol*K))
ΔG_D^0 (kJ/mol)
B
α_D
ΔG_T^0 (J/mol)
E
α_T
ΔG_D^0 (kJ/mol)
C
α_D (corrected)
ΔG_T^0 (J/mol)
F
α_T (corrected)
ΔG_D^0 (kJ/mol)

Figure 5

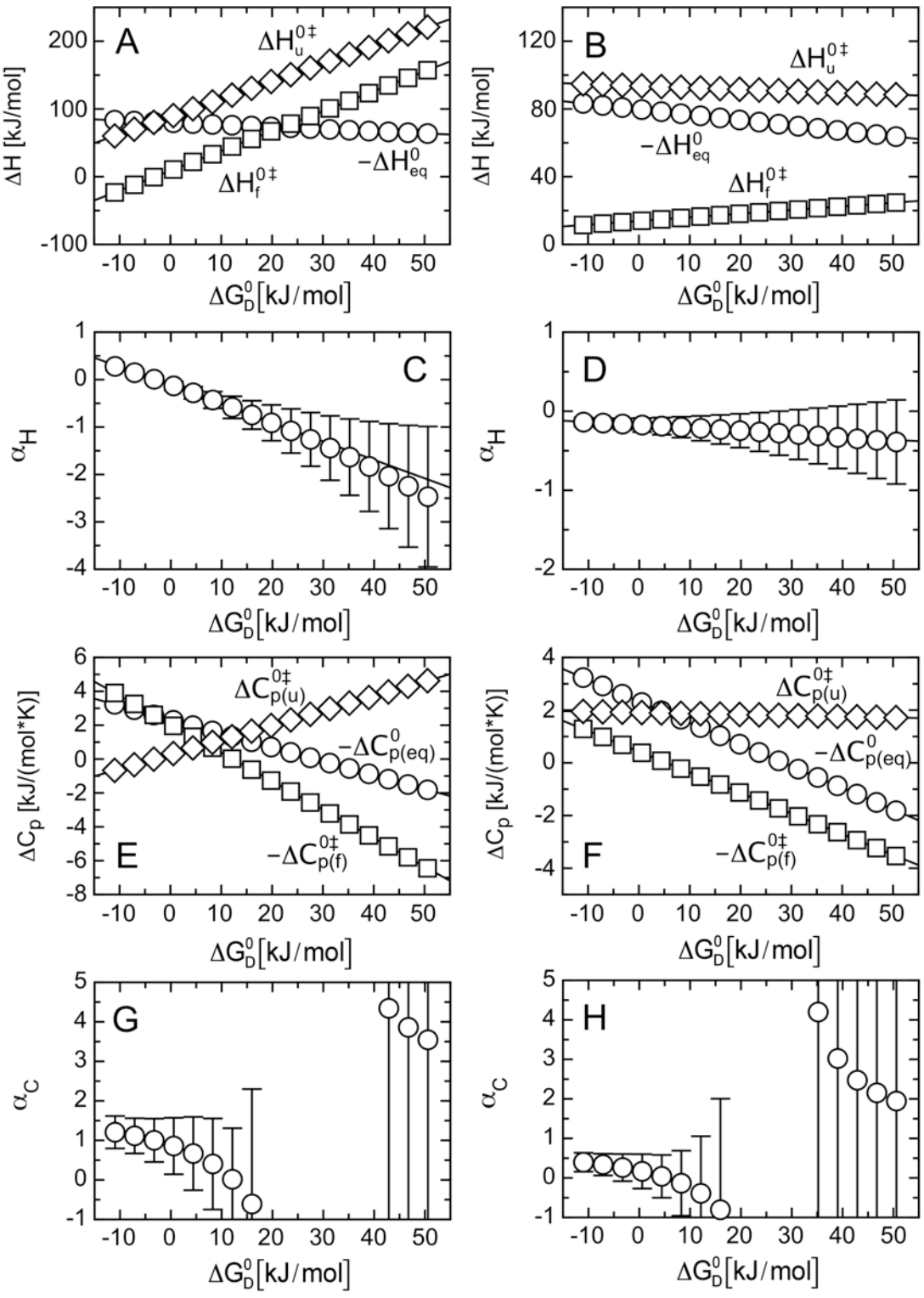
A
B
C
D
E
F
G
H
ΔH [kJ/mol]
ΔG⁰D [kJ/mol]
ΔH⁰‡u
−ΔH⁰eq
ΔH⁰‡f
αH
ΔCp [kJ/(mol*K)]
ΔC⁰‡p(u)
−ΔC⁰p(eq)
−ΔC⁰‡p(f)
αC

Figure 6

9. Appendix

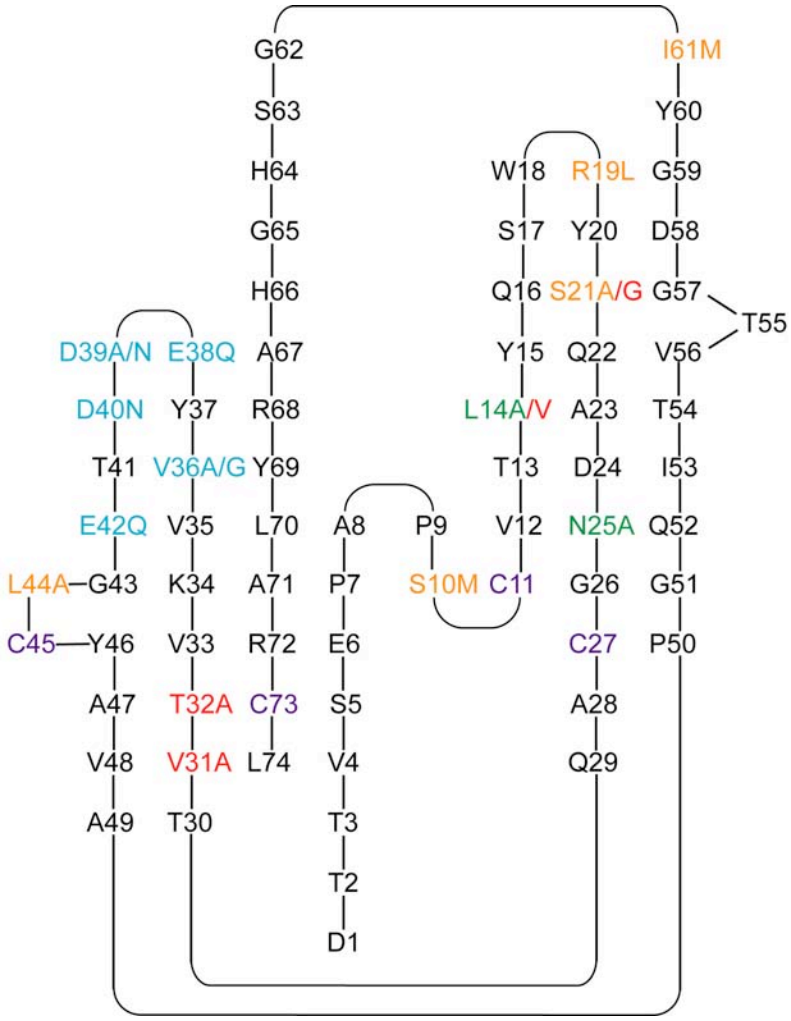

Figure 9-1: Schematic representation of the backbone structure of tendamistat. The four cysteine residues, which are connected via a disulfide bridge, are indicated in violet. The amino acid replacements, which folds and unfolds with the early transition state rate-limiting and a stability like wild type are colored in orange, whereas the less stable ones are colored in red. The two variants with the late transition state rate-limiting are colored in green. The variants, where a third unfolding phase was found, are colored in blue.

9.1 Temperature-dependence of Tendamistat wild type at pH 2

A detailed analysis of the data are described in "*Shape of Free Energy Barrier for Tendamistat Folding*", Schätzle, M. & Kiefhaber, T., 2005, to be submitted and "*Thermodynamic Properties of the Transition States in Tendamistat Folding*", Schätzle, M. & Kiefhaber, T., 2005, to be submitted. The results are summarized in chapter 3.1.

Equilibrium and kinetic data were measured for tendamistat wild type at pH 2 at various temperatures. Equilibrium data were obtained with 10 µM protein in 100 mM glycine, pH 2, by monitoring the ellipticity at 227 nm. The kinetics were measured monitoring the change in fluorescence after initiation by 11-fold dilution of native and unfolded protein, respectively, into various denaturant concentration to a final concentration of 4 µM protein in 100 mM glycine, pH 2.

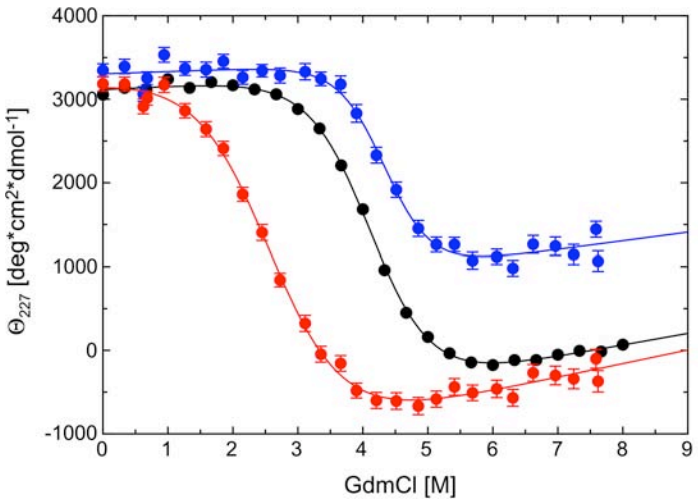

Figure 9-2: GdmCl-induced unfolding transition of tendamistat wild type at pH 2 at 5°C (●), 25°C (●) and 46°C (●). Data at 25°C were measured from Günter Papppenberger and were taken from ref.[174]. The lines represent the analysis assuming the two-state model.

Figure 9-3 – Figure 9-11: (following pages): GdmCl-dependence of the apparent rate constants λ_i (A), the amplitudes A_i (B) and the final and initial values for tendamistat wild type folding at pH 2 at different temperatures. The values for the refolding reaction are plotted as circles, for the unfolding reaction as squares.
Figure 9-7: Data at 25°C were measured from Günter Pappenberger and were taken from ref.[265].

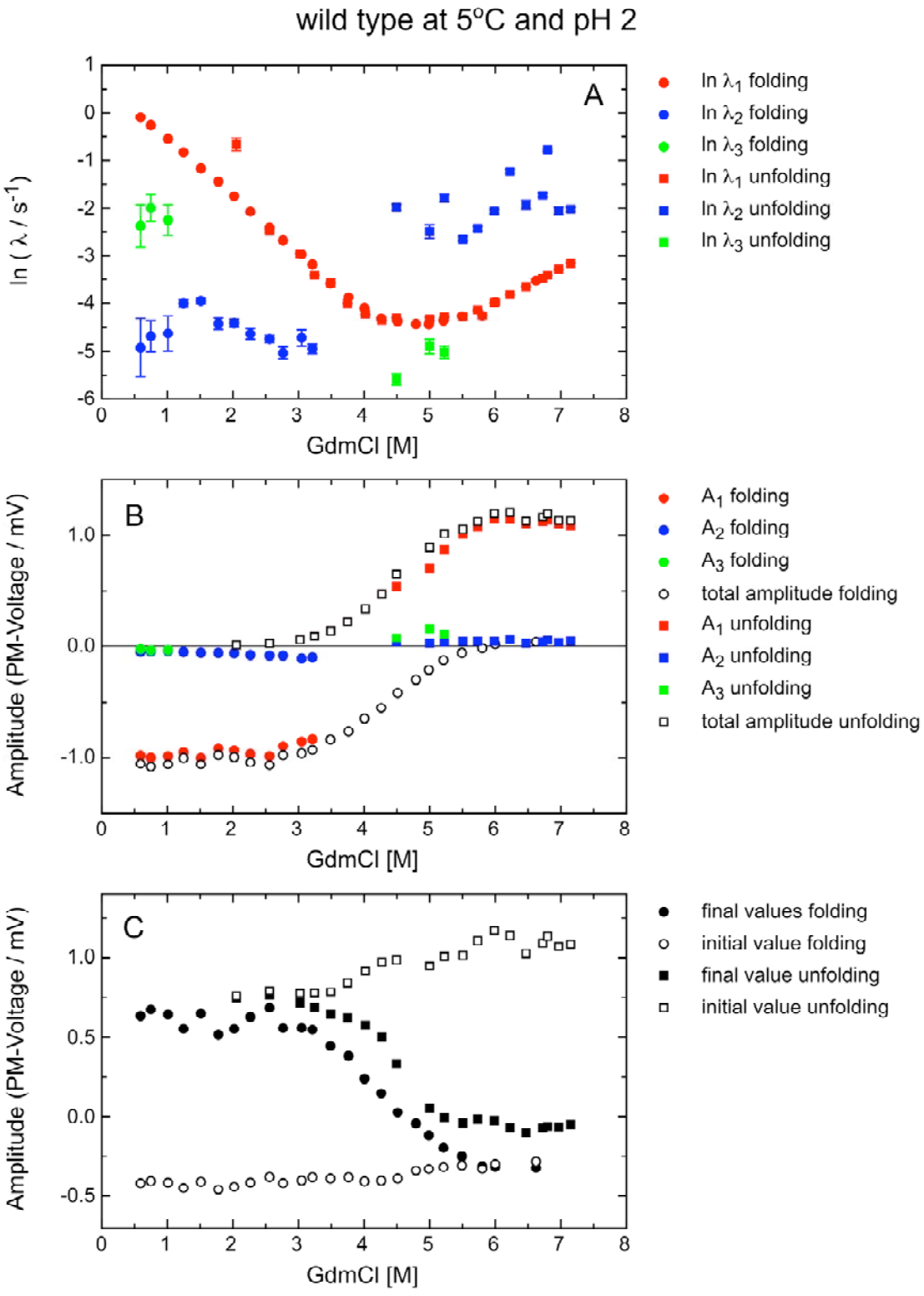
wild type at 5°C and pH 2
A
ln (λ / s-1)
GdmCl [M]
ln λ1 folding
ln λ2 folding
ln λ3 folding
ln λ1 unfolding
ln λ2 unfolding
ln λ3 unfolding
B
Amplitude (PM-Voltage / mV)
GdmCl [M]
A1 folding
A2 folding
A3 folding
total amplitude folding
A1 unfolding
A2 unfolding
A3 unfolding
total amplitude unfolding
C
Amplitude (PM-Voltage / mV)
GdmCl [M]
final values folding
initial value folding
final value unfolding
initial value unfolding

Figure 9-3

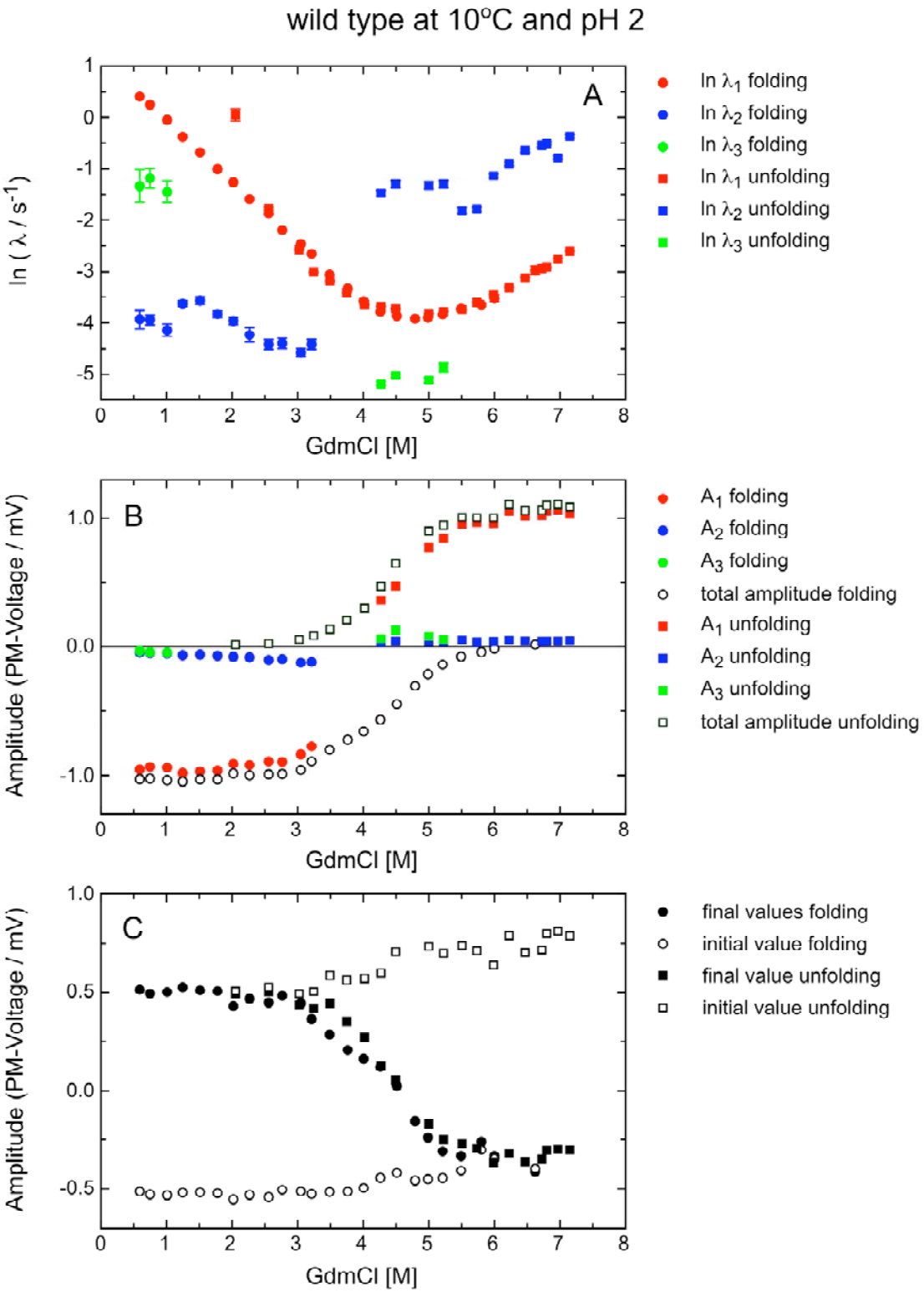
wild type at 10°C and pH 2
A
ln (λ / s-1)
GdmCl [M]
ln λ1 folding
ln λ2 folding
ln λ3 folding
ln λ1 unfolding
ln λ2 unfolding
ln λ3 unfolding
B
Amplitude (PM-Voltage / mV)
GdmCl [M]
A1 folding
A2 folding
A3 folding
total amplitude folding
A1 unfolding
A2 unfolding
A3 unfolding
total amplitude unfolding
C
Amplitude (PM-Voltage / mV)
GdmCl [M]
final values folding
initial value folding
final value unfolding
initial value unfolding

Figure 9-4

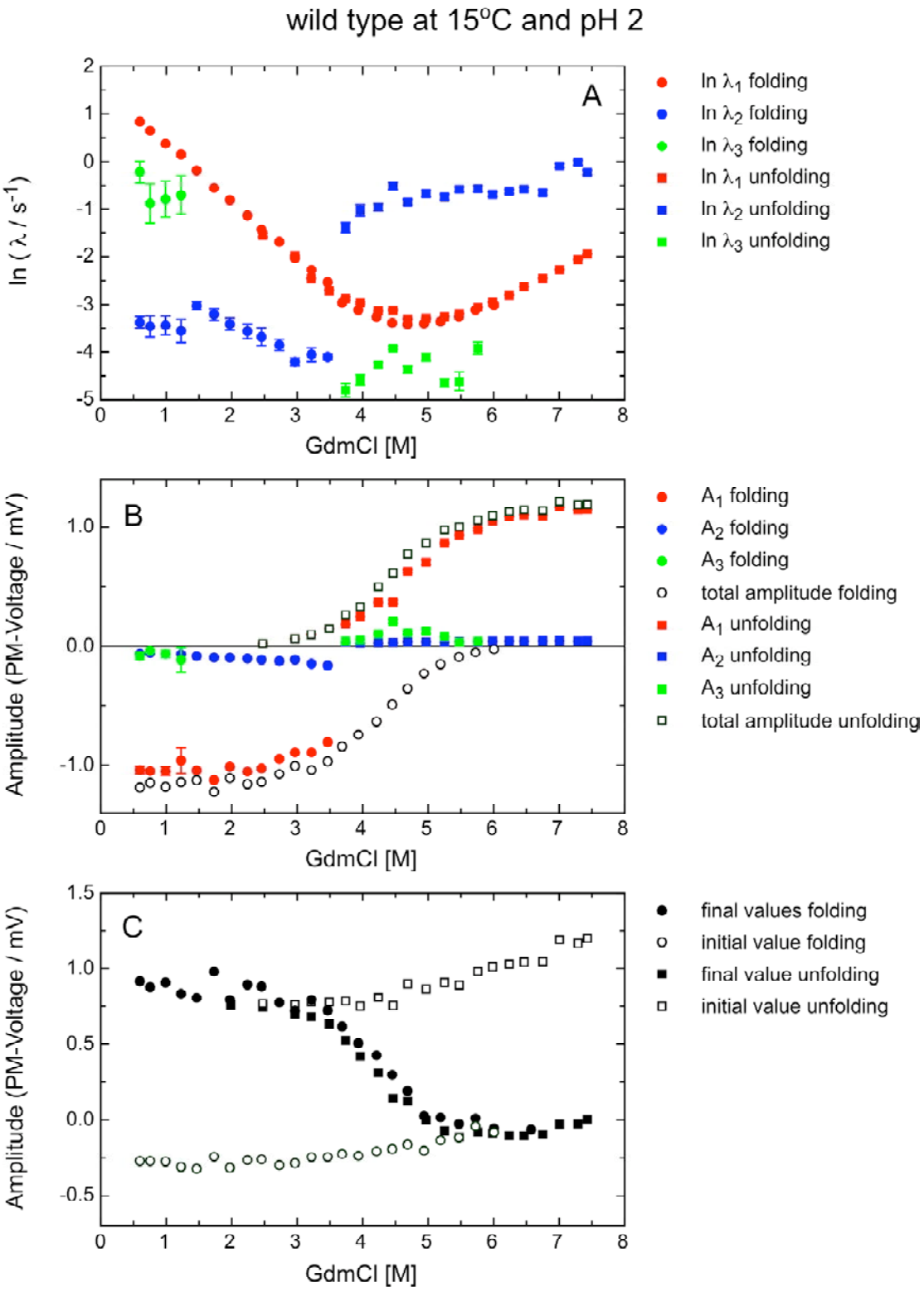
wild type at 15°C and pH 2
A
ln (λ / s-1)
GdmCl [M]
ln λ1 folding
ln λ2 folding
ln λ3 folding
ln λ1 unfolding
ln λ2 unfolding
ln λ3 unfolding
B
Amplitude (PM-Voltage / mV)
GdmCl [M]
A1 folding
A2 folding
A3 folding
total amplitude folding
A1 unfolding
A2 unfolding
A3 unfolding
total amplitude unfolding
C
Amplitude (PM-Voltage / mV)
GdmCl [M]
final values folding
initial value folding
final value unfolding
initial value unfolding

Figure 9-5

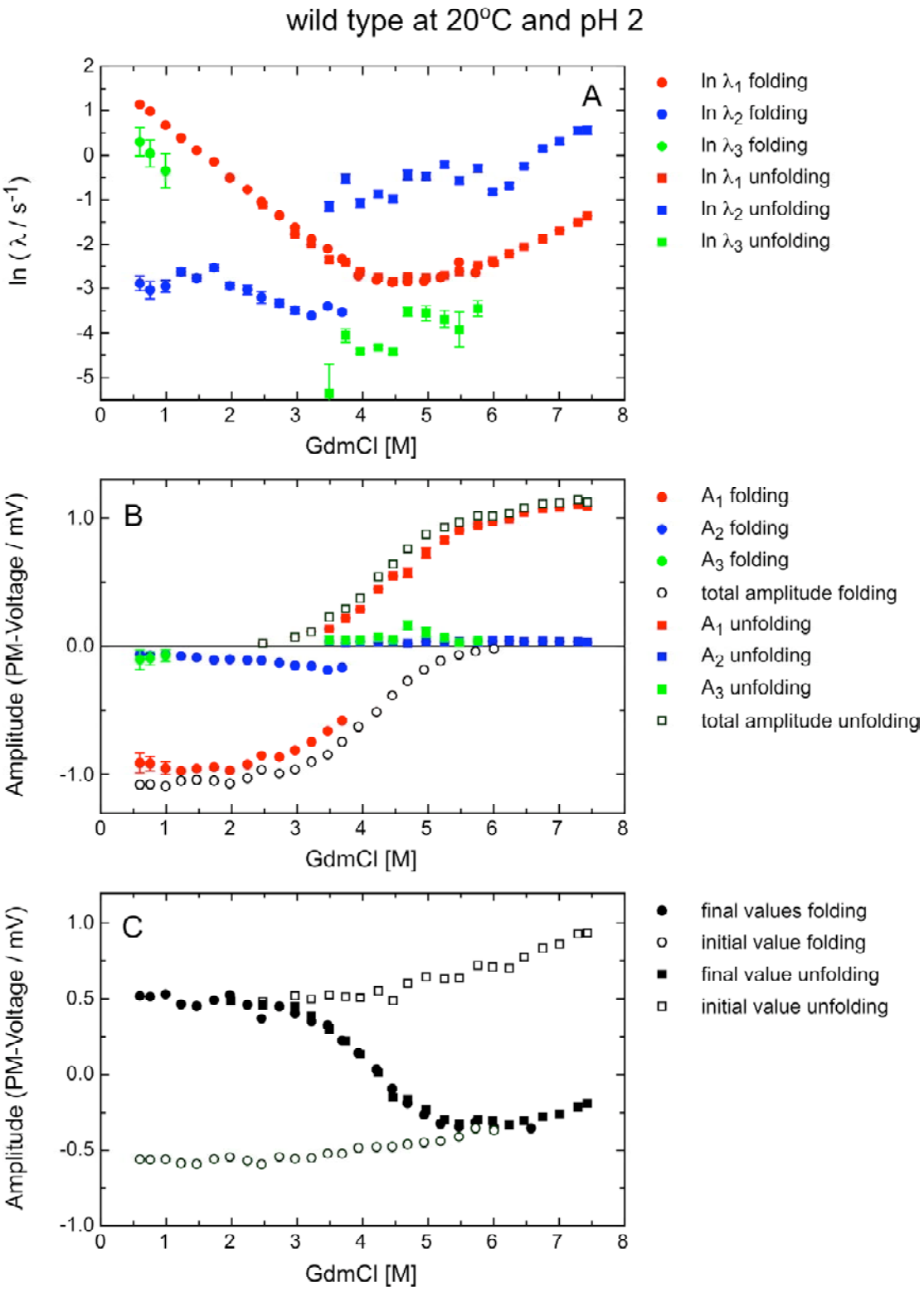
wild type at 20°C and pH 2
A
ln (λ / s-1)
GdmCl [M]
ln λ1 folding
ln λ2 folding
ln λ3 folding
ln λ1 unfolding
ln λ2 unfolding
ln λ3 unfolding
B
Amplitude (PM-Voltage / mV)
GdmCl [M]
A1 folding
A2 folding
A3 folding
total amplitude folding
A1 unfolding
A2 unfolding
A3 unfolding
total amplitude unfolding
C
Amplitude (PM-Voltage / mV)
GdmCl [M]
final values folding
initial value folding
final value unfolding
initial value unfolding

Figure 9-6

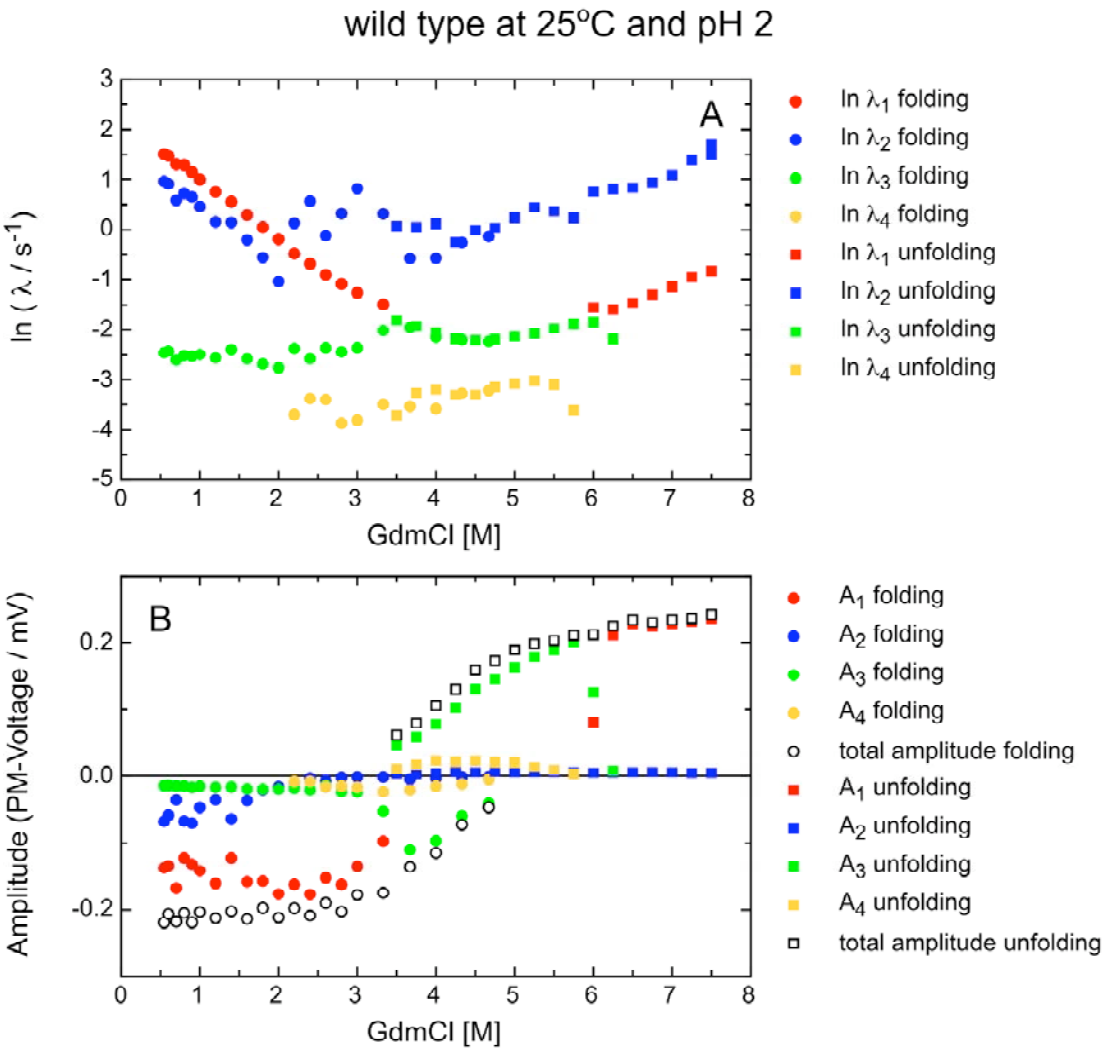
wild type at 25°C and pH 2
A
ln (λ / s-1)
GdmCl [M]
ln λ1 folding
ln λ2 folding
ln λ3 folding
ln λ4 folding
ln λ1 unfolding
ln λ2 unfolding
ln λ3 unfolding
ln λ4 unfolding
B
Amplitude (PM-Voltage / mV)
GdmCl [M]
A1 folding
A2 folding
A3 folding
A4 folding
total amplitude folding
A1 unfolding
A2 unfolding
A3 unfolding
A4 unfolding
total amplitude unfolding

Figure 9-7

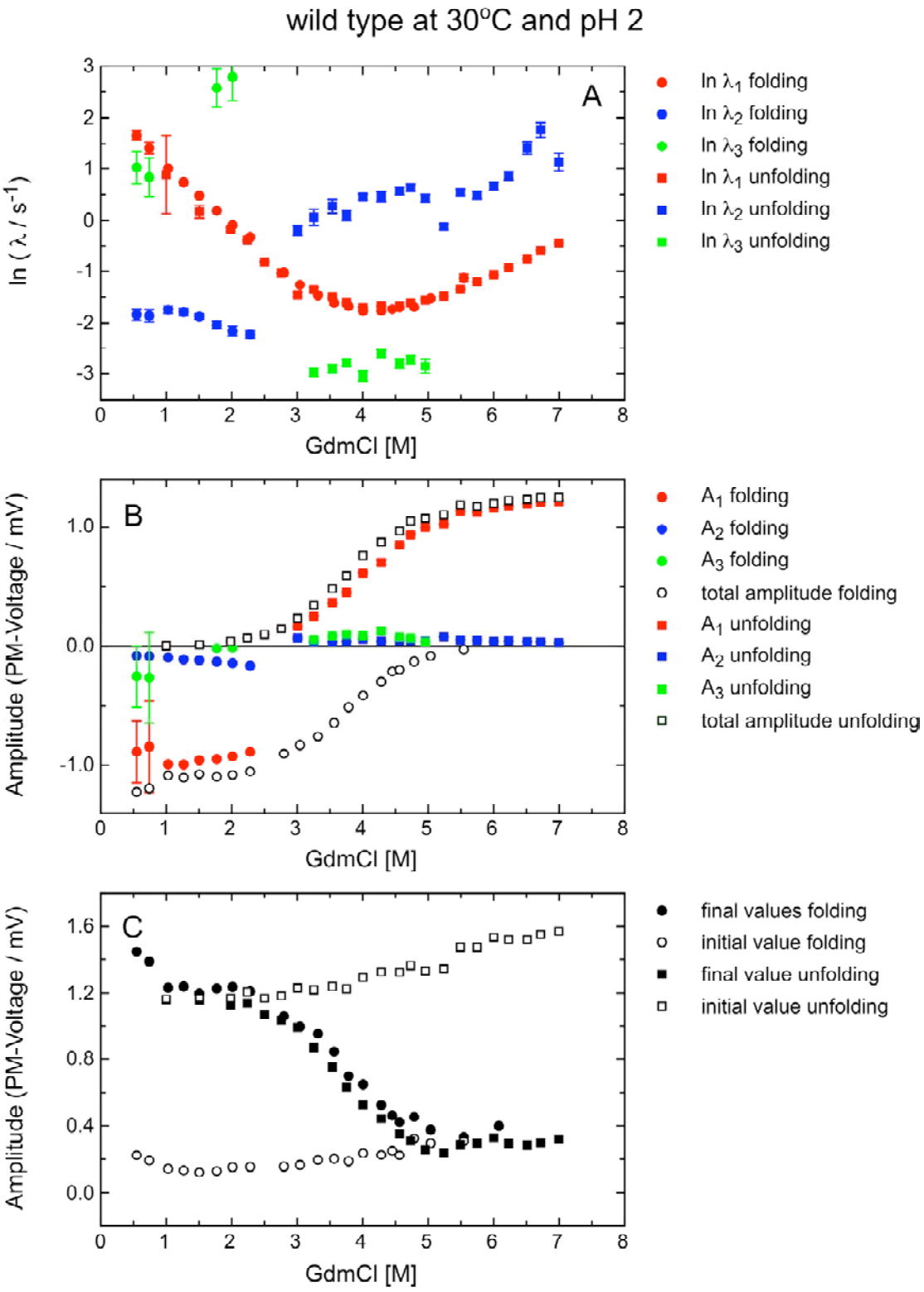
wild type at 30°C and pH 2
A
ln (λ / s-1)
GdmCl [M]
ln λ1 folding
ln λ2 folding
ln λ3 folding
ln λ1 unfolding
ln λ2 unfolding
ln λ3 unfolding
B
Amplitude (PM-Voltage / mV)
GdmCl [M]
A1 folding
A2 folding
A3 folding
total amplitude folding
A1 unfolding
A2 unfolding
A3 unfolding
total amplitude unfolding
C
Amplitude (PM-Voltage / mV)
GdmCl [M]
final values folding
initial value folding
final value unfolding
initial value unfolding

Figure 9-8

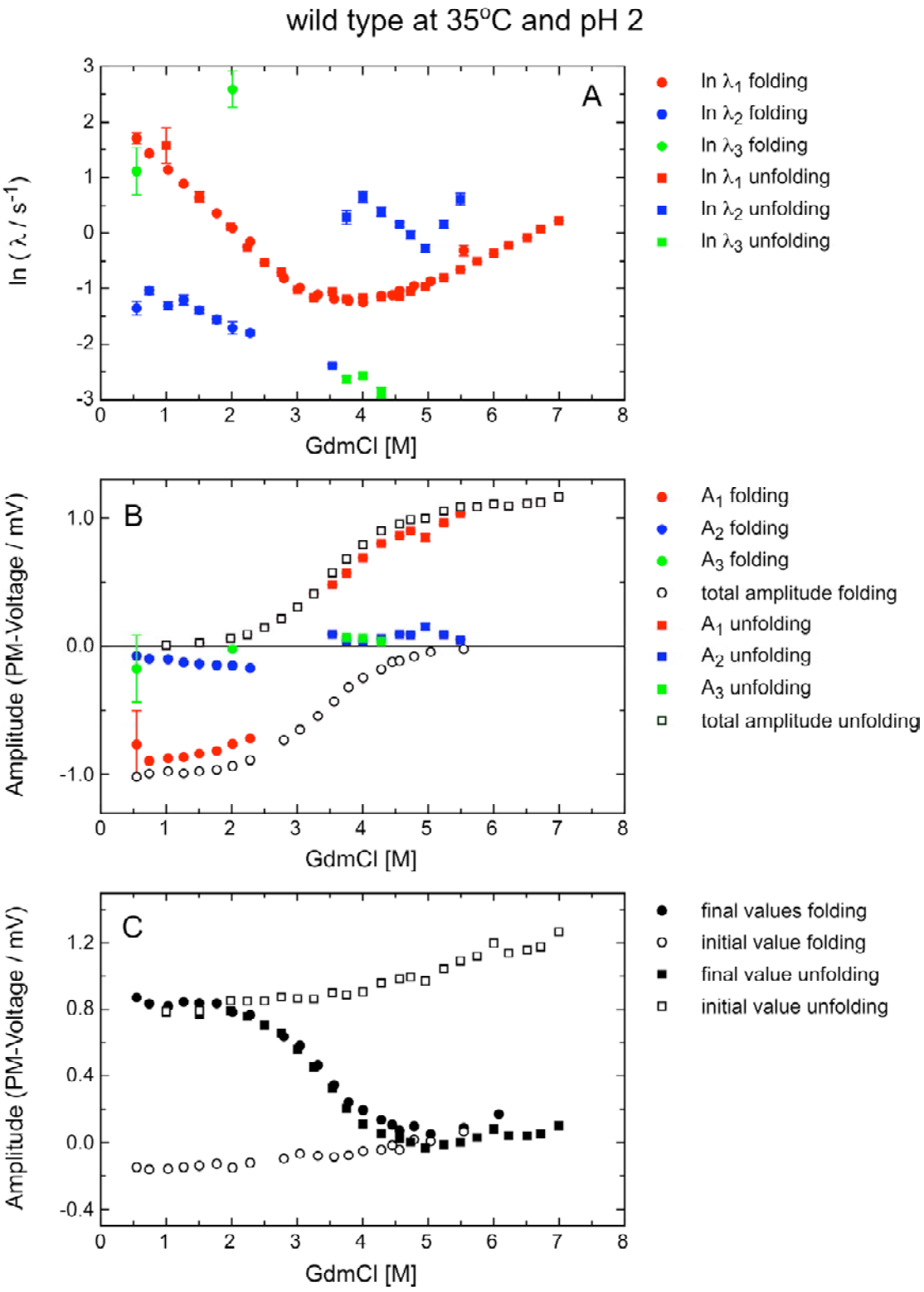
wild type at 35°C and pH 2
A
ln (λ / s-1)
GdmCl [M]
ln λ1 folding
ln λ2 folding
ln λ3 folding
ln λ1 unfolding
ln λ2 unfolding
ln λ3 unfolding
B
Amplitude (PM-Voltage / mV)
GdmCl [M]
A1 folding
A2 folding
A3 folding
total amplitude folding
A1 unfolding
A2 unfolding
A3 unfolding
total amplitude unfolding
C
Amplitude (PM-Voltage / mV)
GdmCl [M]
final values folding
initial value folding
final value unfolding
initial value unfolding

Figure 9-9

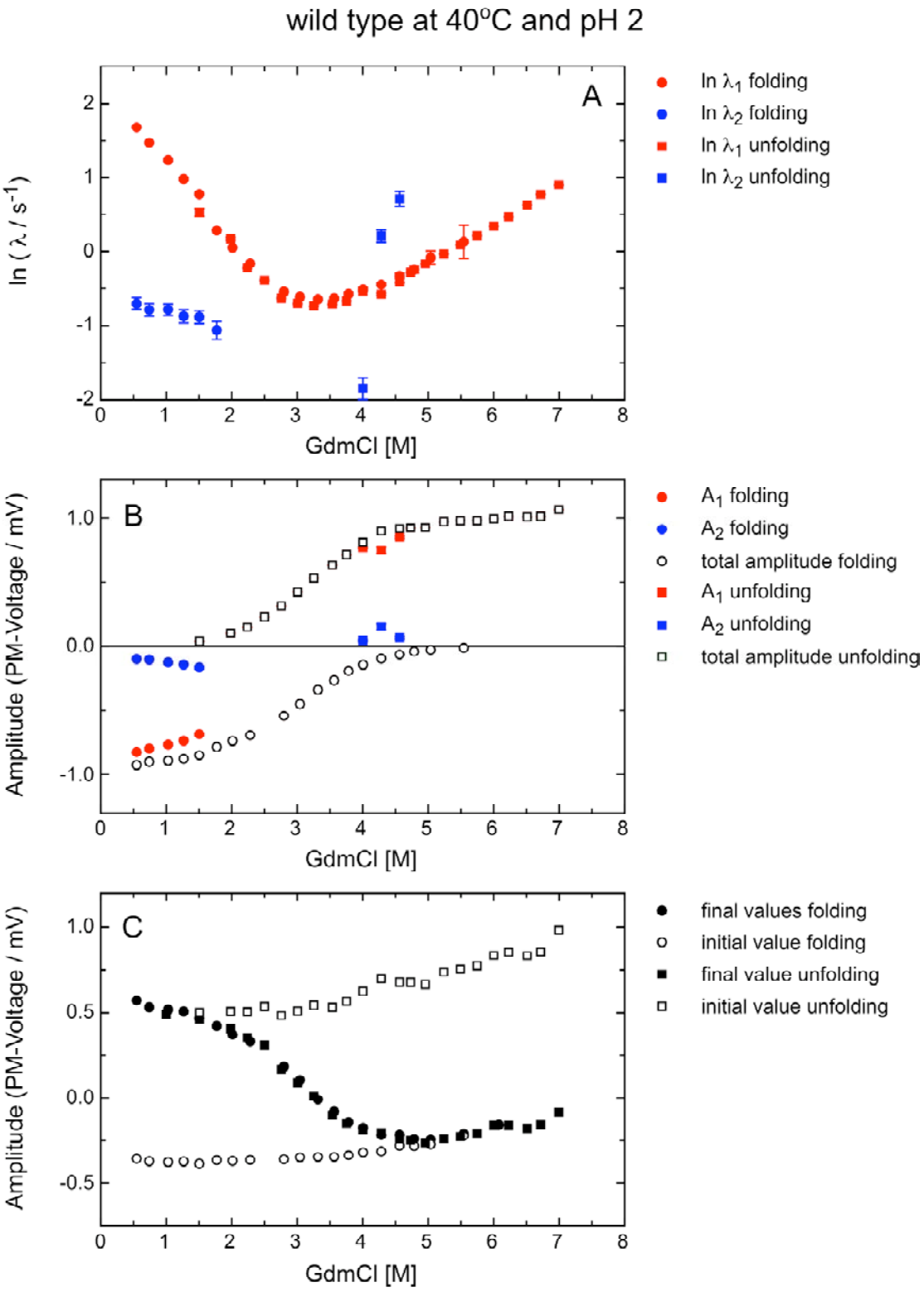
wild type at 40°C and pH 2
A
ln (λ / s-1)
GdmCl [M]
ln λ1 folding
ln λ2 folding
ln λ1 unfolding
ln λ2 unfolding
B
Amplitude (PM-Voltage / mV)
GdmCl [M]
A1 folding
A2 folding
total amplitude folding
A1 unfolding
A2 unfolding
total amplitude unfolding
C
Amplitude (PM-Voltage / mV)
GdmCl [M]
final values folding
initial value folding
final value unfolding
initial value unfolding

Figure 9-10

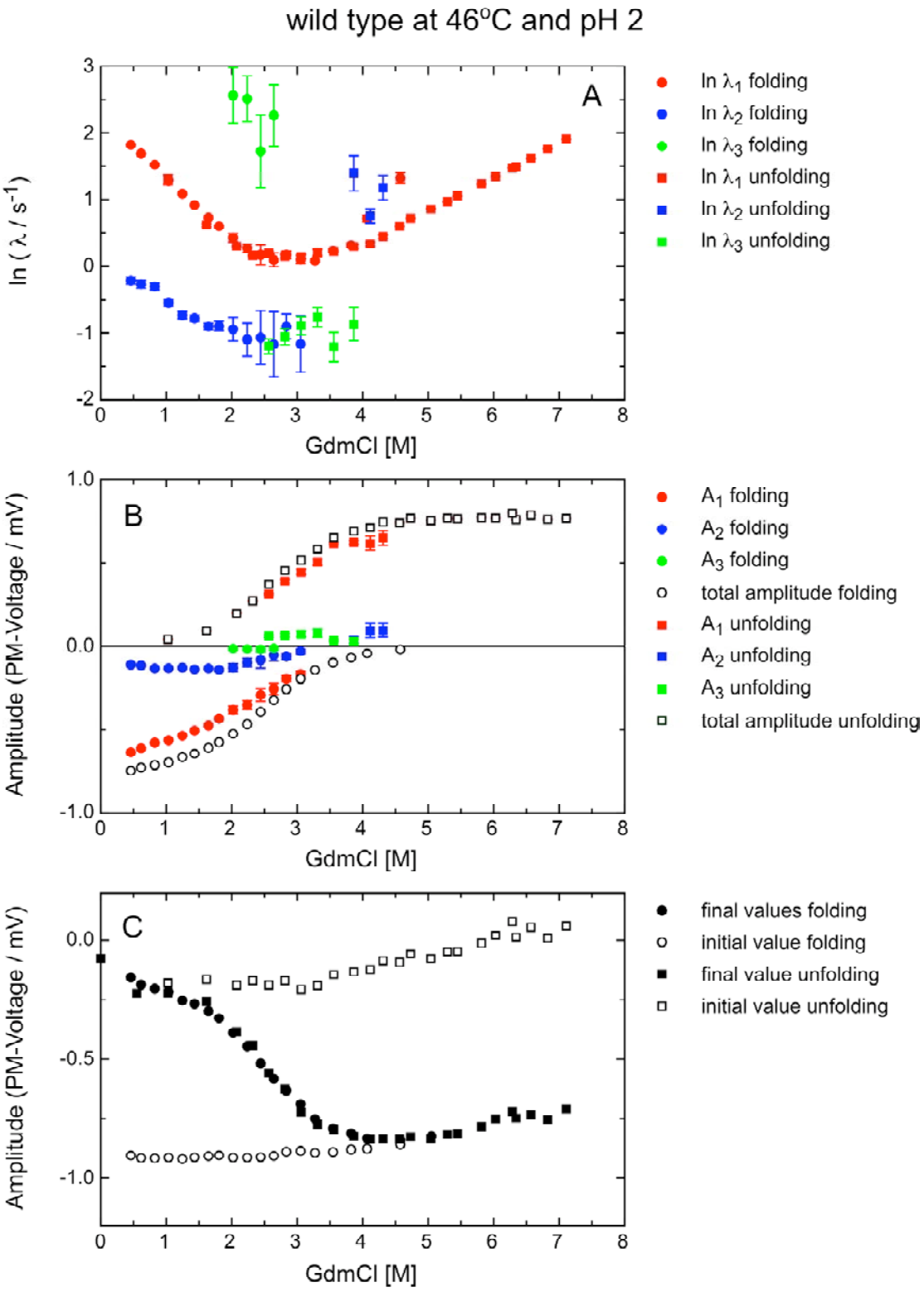
wild type at 46°C and pH 2
A
ln (λ / s-1)
GdmCl [M]
ln λ1 folding
ln λ2 folding
ln λ3 folding
ln λ1 unfolding
ln λ2 unfolding
ln λ3 unfolding
B
Amplitude (PM-Voltage / mV)
GdmCl [M]
A1 folding
A2 folding
A3 folding
total amplitude folding
A1 unfolding
A2 unfolding
A3 unfolding
total amplitude unfolding
C
Amplitude (PM-Voltage / mV)
GdmCl [M]
final values folding
initial value folding
final value unfolding
initial value unfolding

Figure 9-11

9.2 Temperature-dependence of the tendamistat disulfide variant C11A/C27S at pH 7

A detailed analysis of the data are described in "*Evidence for Parallel Pathways at the Early Stage of Tendamistat Folding*", Schätzle, M. & Kiefhaber, T., 2005, to be submitted. The results are summarized in chapter 3.1.

Kinetic data were measured for the tendamistat disulfide variant C11A/C27S at pH 7 at various temperatures. They were measured monitoring the change in fluorescence after initiation by 11-fold dilution of native and unfolded protein, respectively, into various denaturant concentration to a final concentration of 4 μM protein in 100 mM cacodylic acid, pH 7.

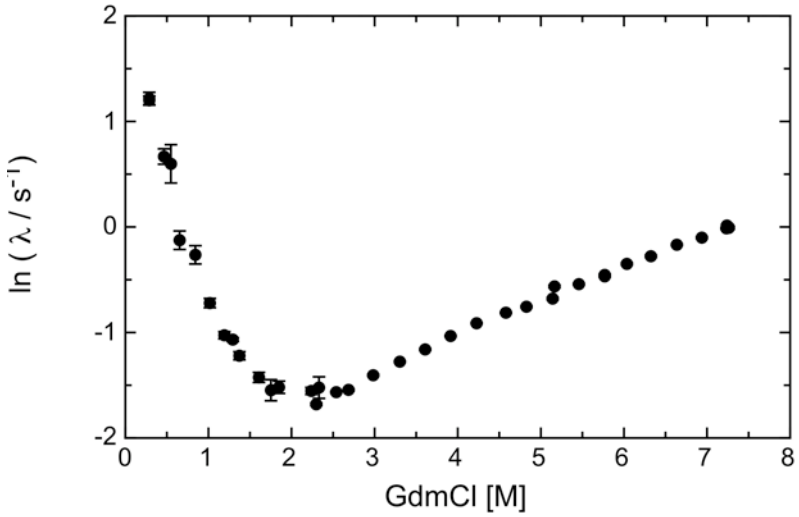

Figure 9-12: GdmCl-dependence of the apparent rate constant of refolding and unfolding of the tendamistat variant C11A/C27S at pH 7 and 20°C. Only the rate constant with the major amplitude is plotted. Data were measured from Annett Bachmann.

Figure 9-13 – Figure 9-18: (following pages): GdmCl-dependence of the apparent rate constants λ_i (A), the amplitudes A_i (B) and the final and initial values for the folding of the tendamistat variant C11A/C27S at pH 7 at different temperatures. The values for the refolding reaction are plotted as circles, for the unfolding reaction as squares.

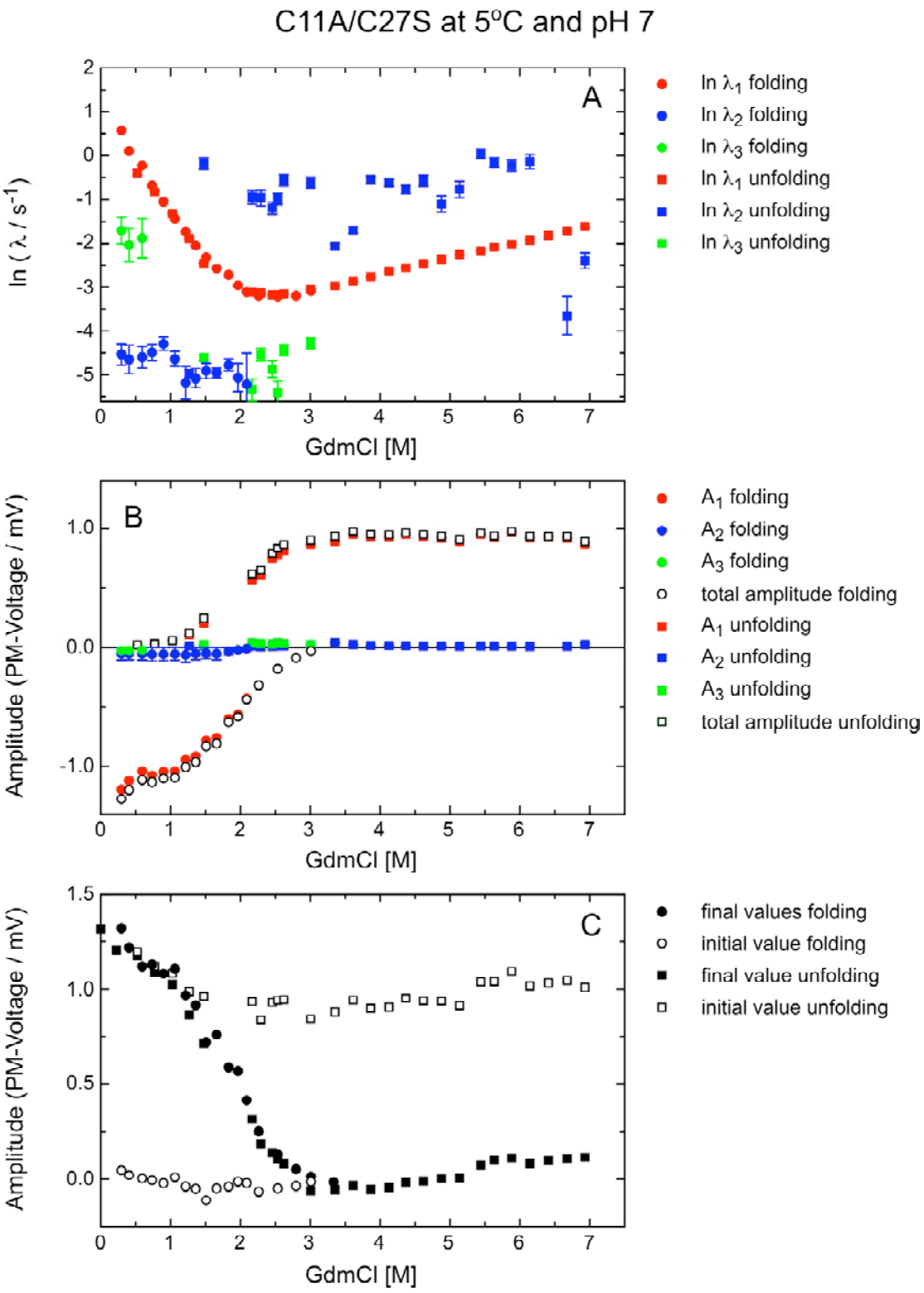
C11A/C27S at 5°C and pH 7
A
ln (λ / s-1)
GdmCl [M]
ln λ1 folding
ln λ2 folding
ln λ3 folding
ln λ1 unfolding
ln λ2 unfolding
ln λ3 unfolding
B
Amplitude (PM-Voltage / mV)
GdmCl [M]
A1 folding
A2 folding
A3 folding
total amplitude folding
A1 unfolding
A2 unfolding
A3 unfolding
total amplitude unfolding
C
Amplitude (PM-Voltage / mV)
GdmCl [M]
final values folding
initial value folding
final value unfolding
initial value unfolding

Figure 9-13

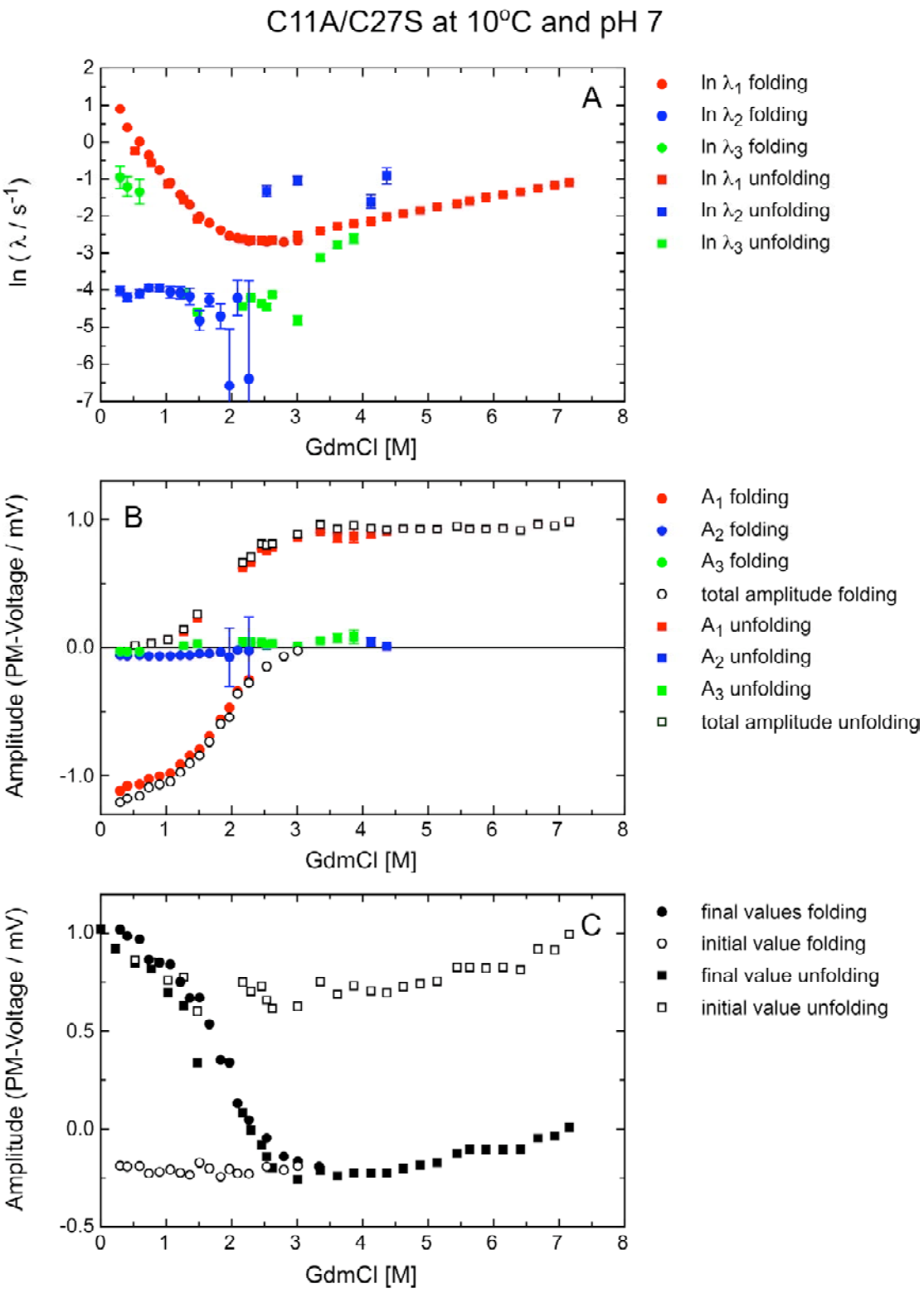
C11A/C27S at 10°C and pH 7
A
ln (λ / s-1)
GdmCl [M]
ln λ1 folding
ln λ2 folding
ln λ3 folding
ln λ1 unfolding
ln λ2 unfolding
ln λ3 unfolding
B
Amplitude (PM-Voltage / mV)
GdmCl [M]
A1 folding
A2 folding
A3 folding
total amplitude folding
A1 unfolding
A2 unfolding
A3 unfolding
total amplitude unfolding
C
Amplitude (PM-Voltage / mV)
GdmCl [M]
final values folding
initial value folding
final value unfolding
initial value unfolding

Figure 9-14

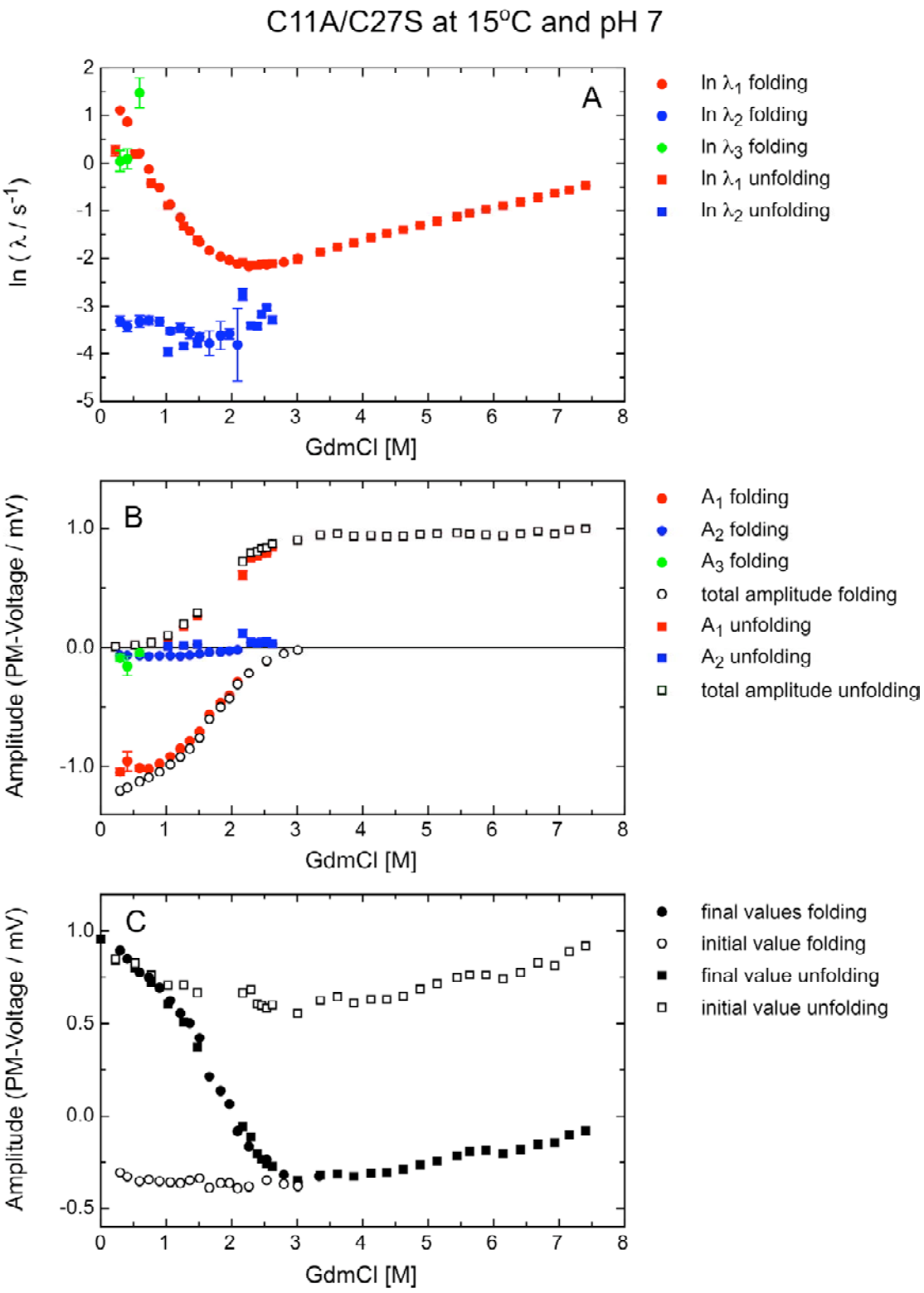
C11A/C27S at 15°C and pH 7
A
ln (λ / s-1)
GdmCl [M]
ln λ1 folding
ln λ2 folding
ln λ3 folding
ln λ1 unfolding
ln λ2 unfolding
B
Amplitude (PM-Voltage / mV)
GdmCl [M]
A1 folding
A2 folding
A3 folding
total amplitude folding
A1 unfolding
A2 unfolding
total amplitude unfolding
C
Amplitude (PM-Voltage / mV)
GdmCl [M]
final values folding
initial value folding
final value unfolding
initial value unfolding

Figure 9-15

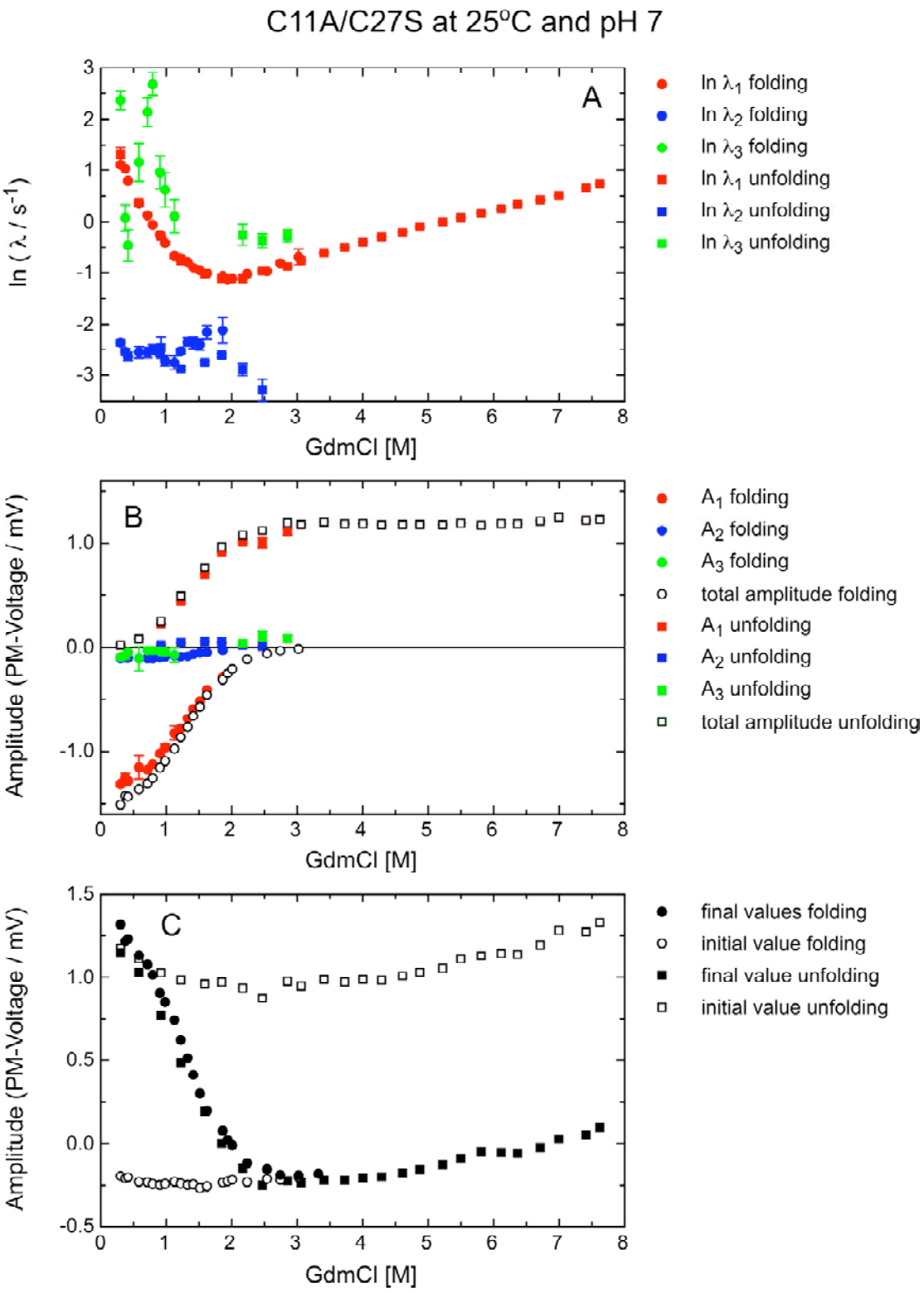
C11A/C25S at 25°C and pH 7
A
ln (λ / s-1)
GdmCl [M]
ln λ1 folding
ln λ2 folding
ln λ3 folding
ln λ1 unfolding
ln λ2 unfolding
ln λ3 unfolding
B
Amplitude (PM-Voltage / mV)
GdmCl [M]
A1 folding
A2 folding
A3 folding
total amplitude folding
A1 unfolding
A2 unfolding
A3 unfolding
total amplitude unfolding
C
Amplitude (PM-Voltage / mV)
GdmCl [M]
final values folding
initial value folding
final value unfolding
initial value unfolding

Figure 9-16

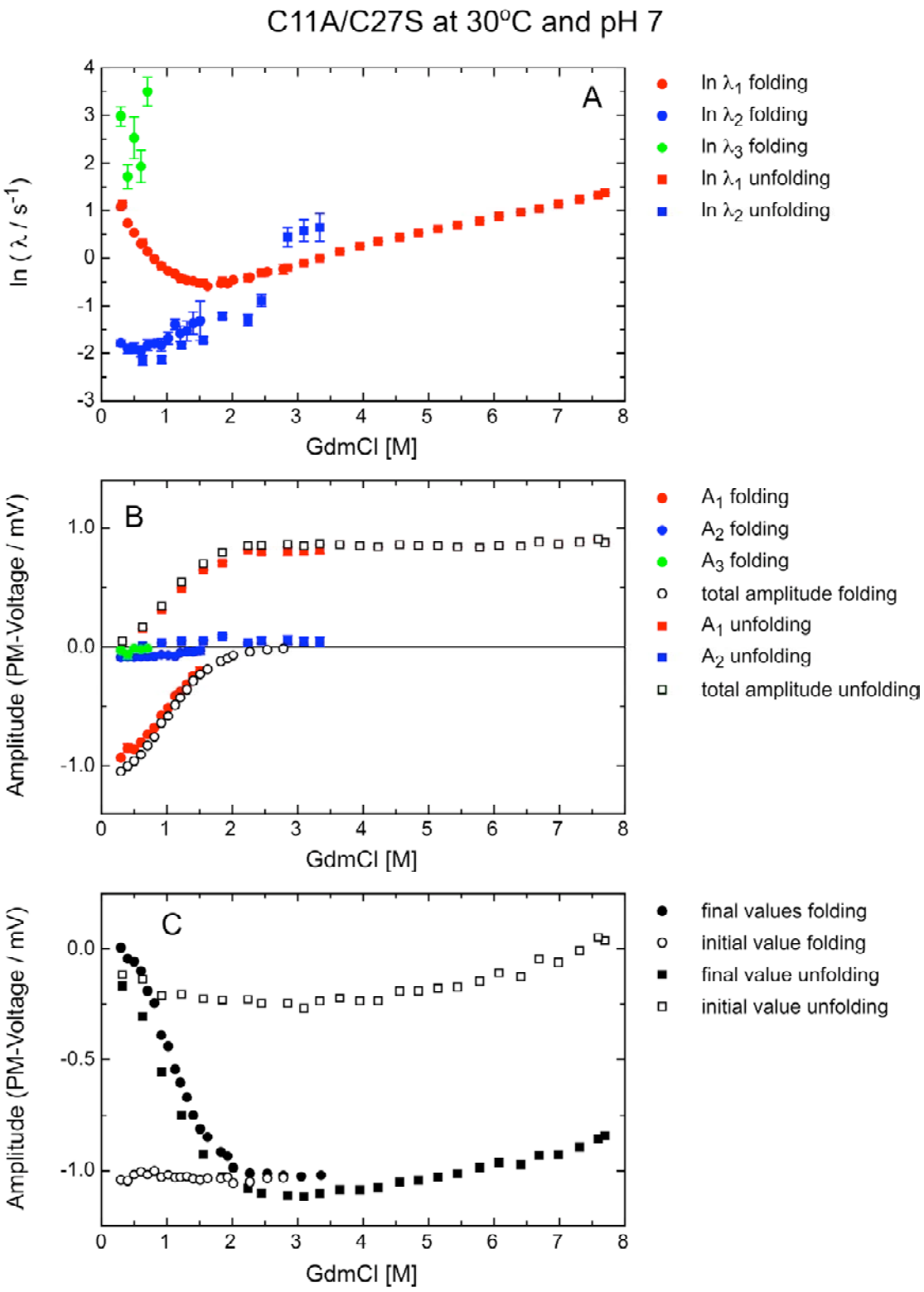
C11A/C27S at 30°C and pH 7
A
ln (λ / s-1)
GdmCl [M]
ln λ1 folding
ln λ2 folding
ln λ3 folding
ln λ1 unfolding
ln λ2 unfolding
B
Amplitude (PM-Voltage / mV)
GdmCl [M]
A1 folding
A2 folding
A3 folding
total amplitude folding
A1 unfolding
A2 unfolding
total amplitude unfolding
C
Amplitude (PM-Voltage / mV)
GdmCl [M]
final values folding
initial value folding
final value unfolding
initial value unfolding

Figure 9-17

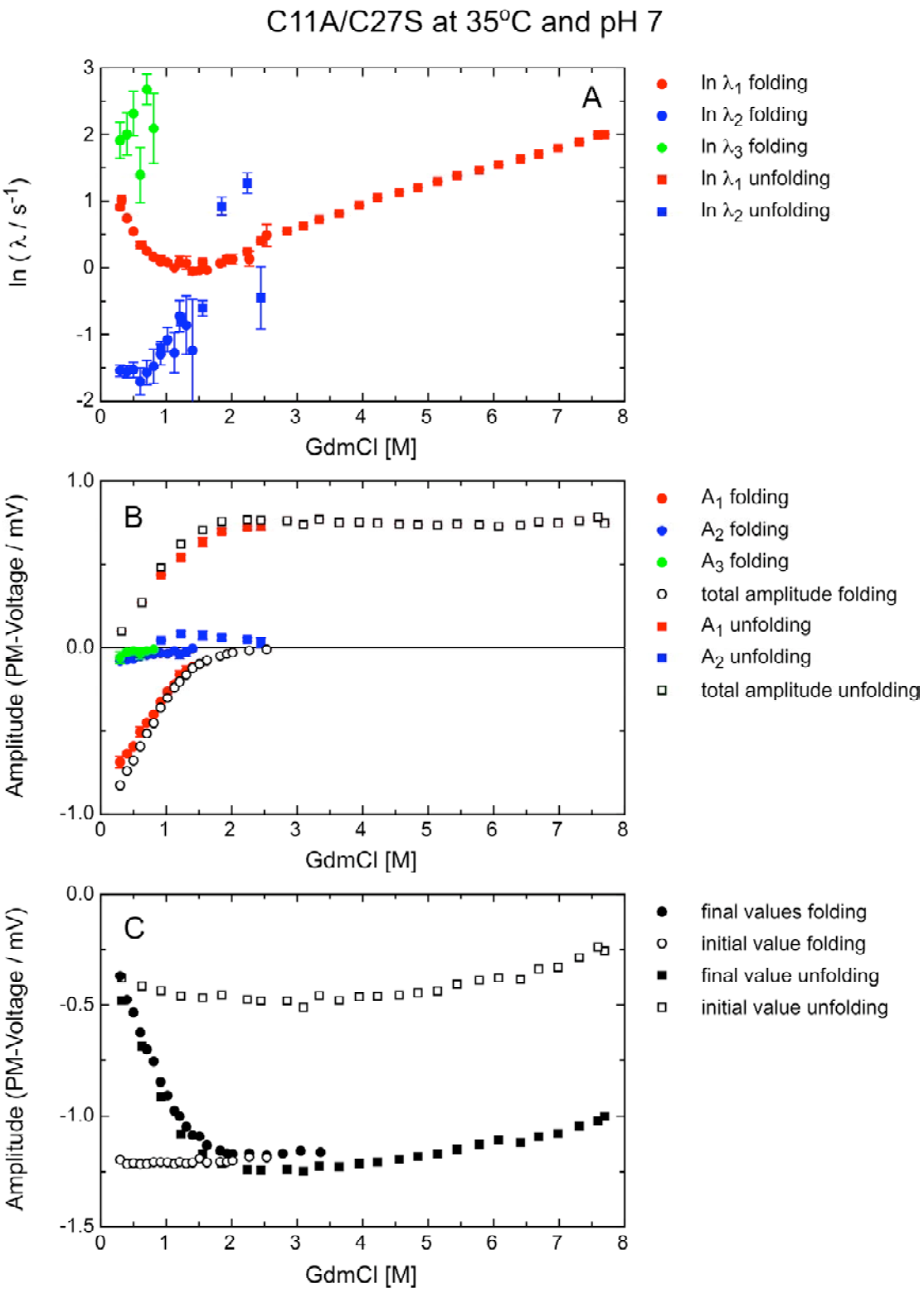
C11A/C27S at 35°C and pH 7
A
ln (λ / s-1)
GdmCl [M]
ln λ1 folding
ln λ2 folding
ln λ3 folding
ln λ1 unfolding
ln λ2 unfolding
B
Amplitude (PM-Voltage / mV)
GdmCl [M]
A1 folding
A2 folding
A3 folding
total amplitude folding
A1 unfolding
A2 unfolding
total amplitude unfolding
C
Amplitude (PM-Voltage / mV)
GdmCl [M]
final values folding
initial value folding
final value unfolding
initial value unfolding

Figure 9-18

9.3 Variants with the early transition state rate-limiting

(a) Tendamistat variants with stability as wild type

Analysis and results of the data are described in detail in chapter 4.2.

Equilibrium and kinetic data were measured for the tendamistat variants **S10M**, **R19L**, **S21A**, **L44A** and **I61M** at pH 7 and 25°C. Equilibrium data were obtained with 10 μM protein in 100 mM cacodylic acid, pH 7, by monitoring the ellipticity at 227 nm. The kinetics were measured monitoring the change in fluorescence after initiation by dilution of native and unfolded protein, respectively, into various denaturant concentration to a final concentration of 4 μM protein in 100 mM cacodylic acid, pH 7.

L44A

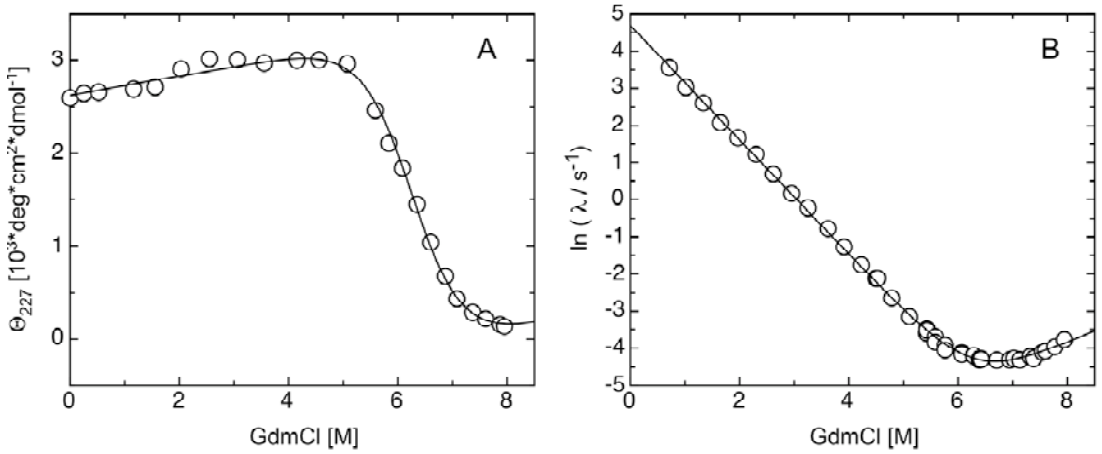

I61M

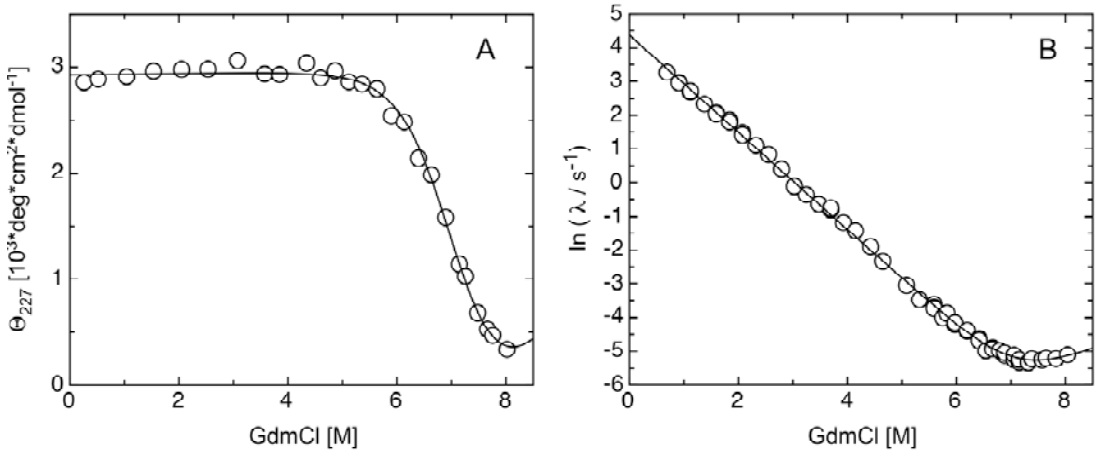

*Figure 9-19: GdmCl-induced unfolding transition (A) and the GdmCl-dependence of the apparent rate constant of refolding and unfolding (B) of **L44A** and **I61M** at pH 7 and 25°C. Only the rate constant with the major amplitude is plotted. The solid lines represent the results of the global fit. Data were measured from Daniel Poso.*

S10M

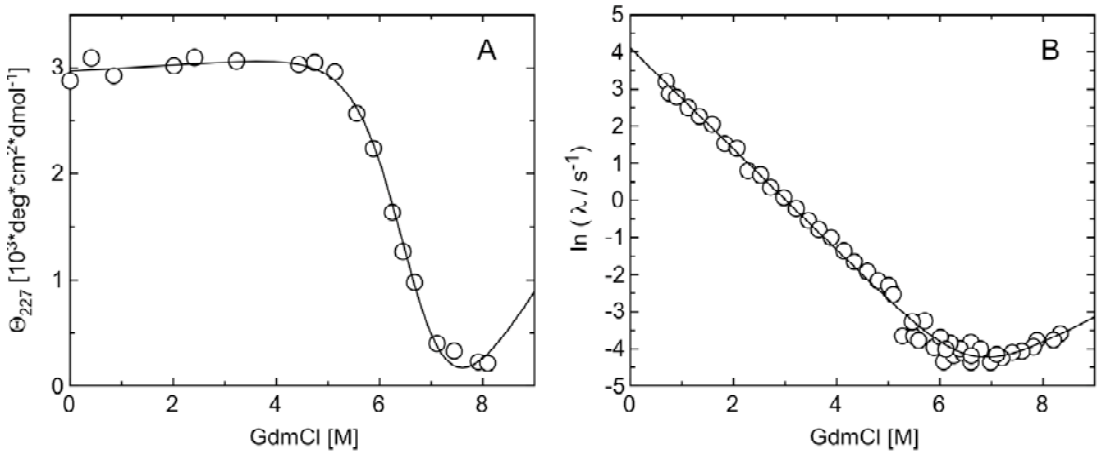

R19L

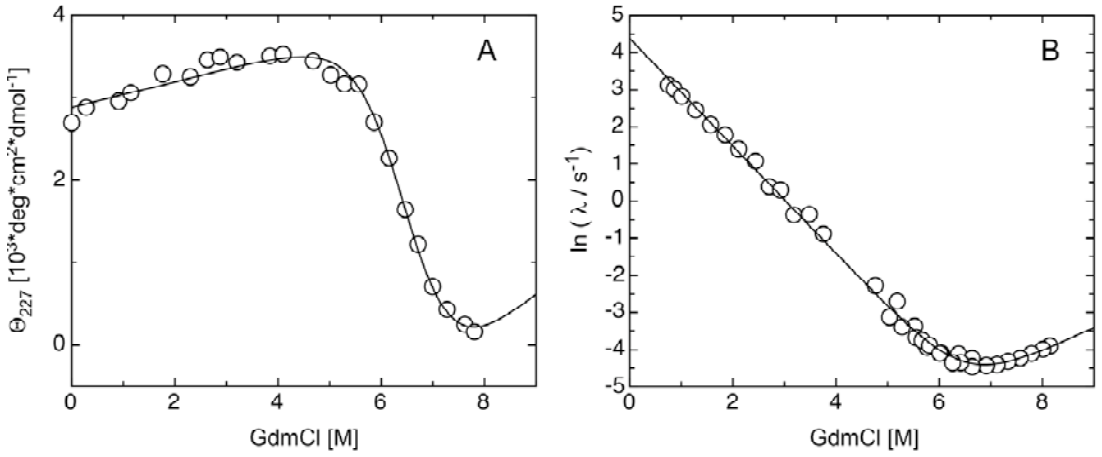

S21A

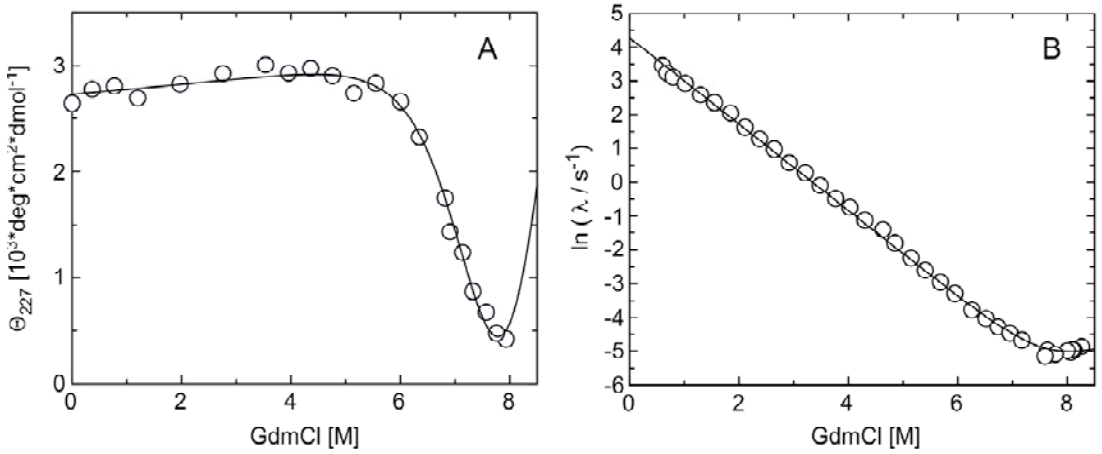

*Figure 9-20: GdmCl-induced unfolding transition (A) and the GdmCl-dependence of the apparent rate constant of refolding and unfolding (B) of **S10M, R19L** and **S21A** at pH 7 and 25°C. Only the rate constant with the major amplitude is plotted. The solid lines represent the results of the global fit.*

*Figure 9-21 - Figure 9-23 (following pages): GdmCl-dependence of the apparent rate constants λ_i (A), the amplitudes A_i (B, C) and the final and initial values (D, E) for folding of the tendamistat variants **S10M, R19L** and **S21A** at pH 7 and 25°C. The values for the refolding reaction are plotted as circles, for the unfolding reaction as squares. The kinetics were measured by stopped-flow mixing (B, D) and by manual-mixing (C, E).*

*Figure 9-21: Folding of the tendamistat variant **S10M**.*

*Figure 9-22: Folding of the tendamistat variant **R19L**.*

*Figure 9-23: Folding of the tendamistat variant **S21A**.*

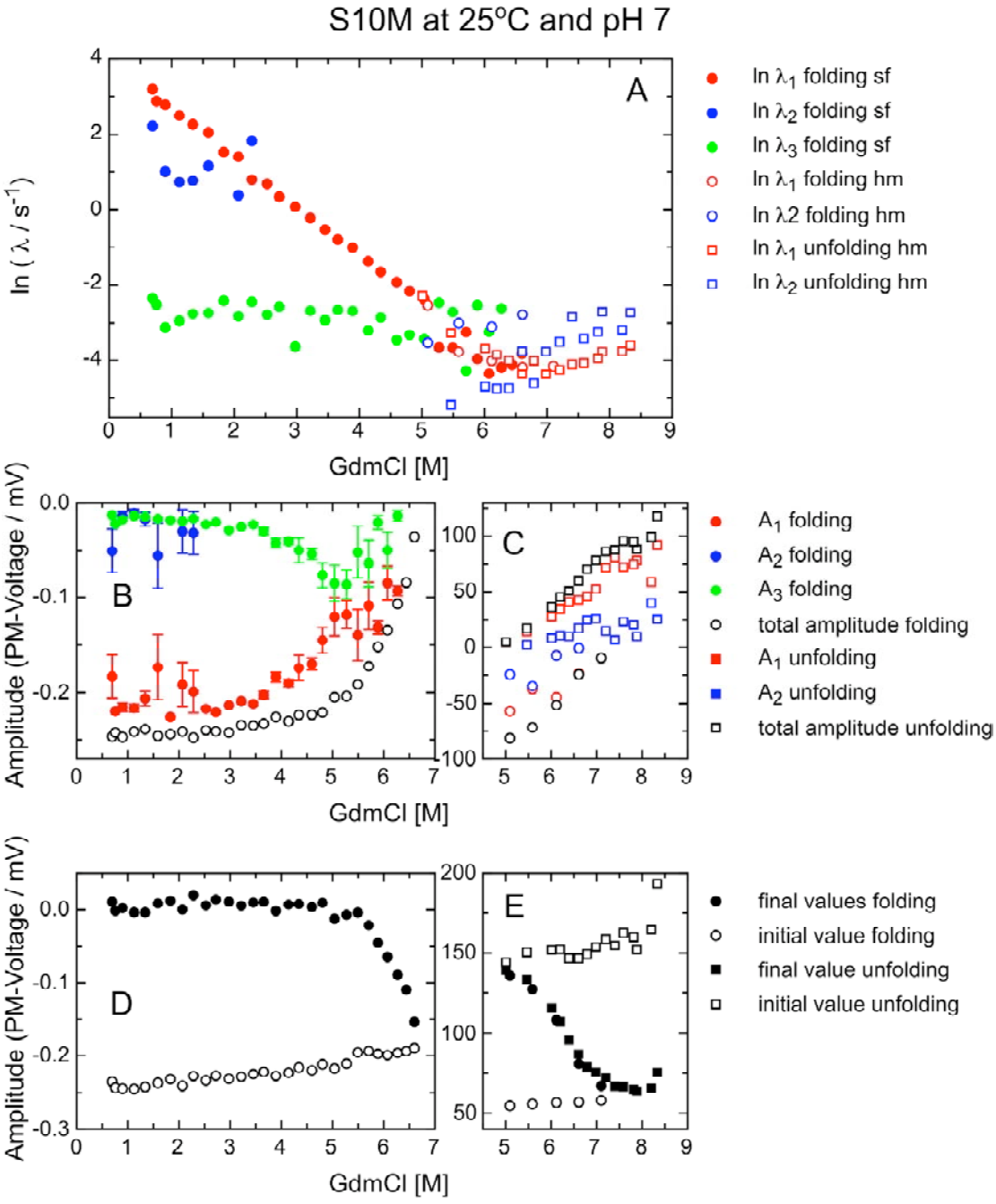

Figure 9-21

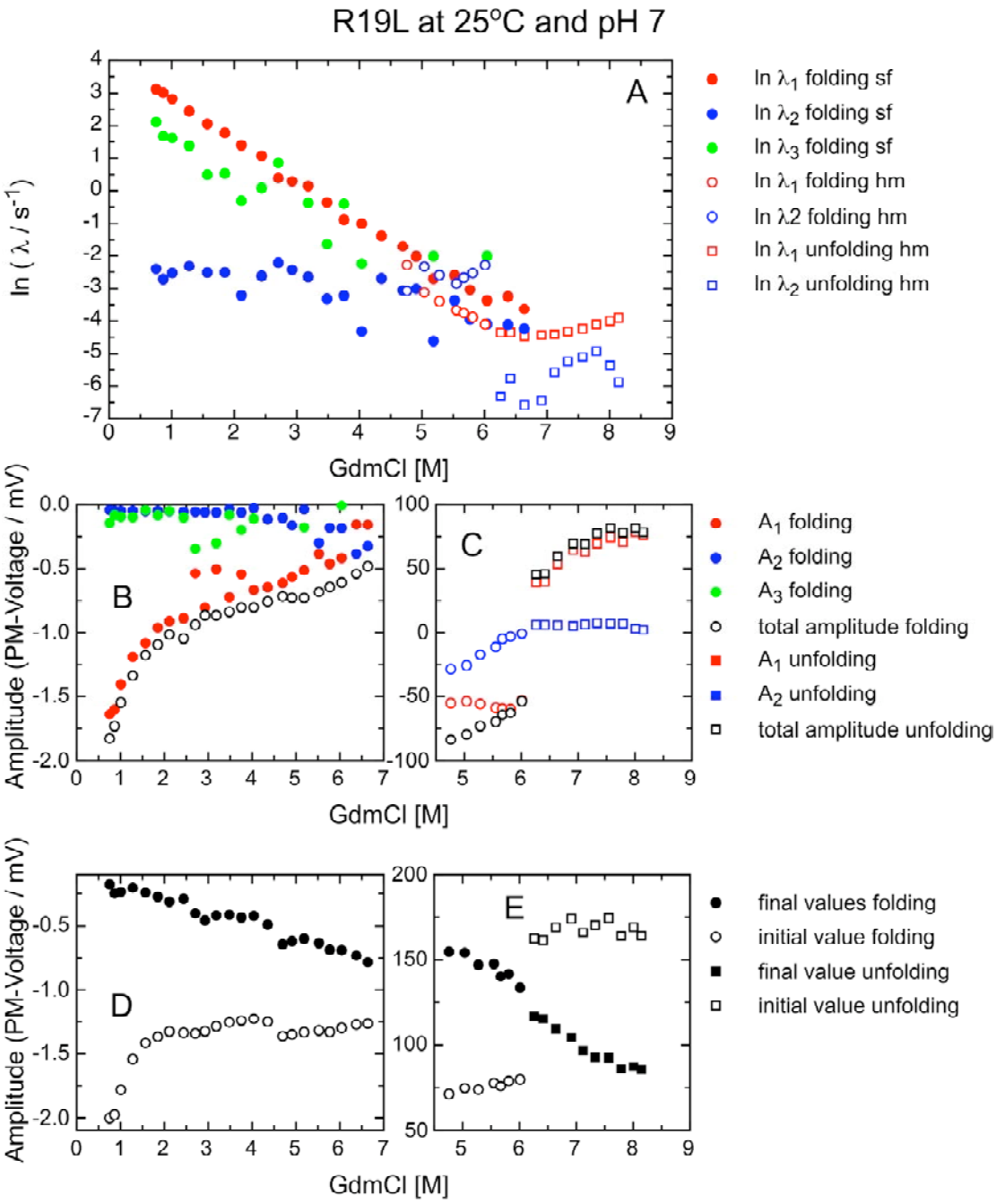
R19L at 25°C and pH 7
A
ln (λ / s^{-1})
GdmCl [M]
ln λ_1 folding sf
ln λ_2 folding sf
ln λ_3 folding sf
ln λ_1 folding hm
ln λ2 folding hm
ln λ_1 unfolding hm
ln λ_2 unfolding hm
B
C
Amplitude (PM-Voltage / mV)
GdmCl [M]
A_1 folding
A_2 folding
A_3 folding
total amplitude folding
A_1 unfolding
A_2 unfolding
total amplitude unfolding
D
E
Amplitude (PM-Voltage / mV)
GdmCl [M]
final values folding
initial value folding
final value unfolding
initial value unfolding

Figure 9-22

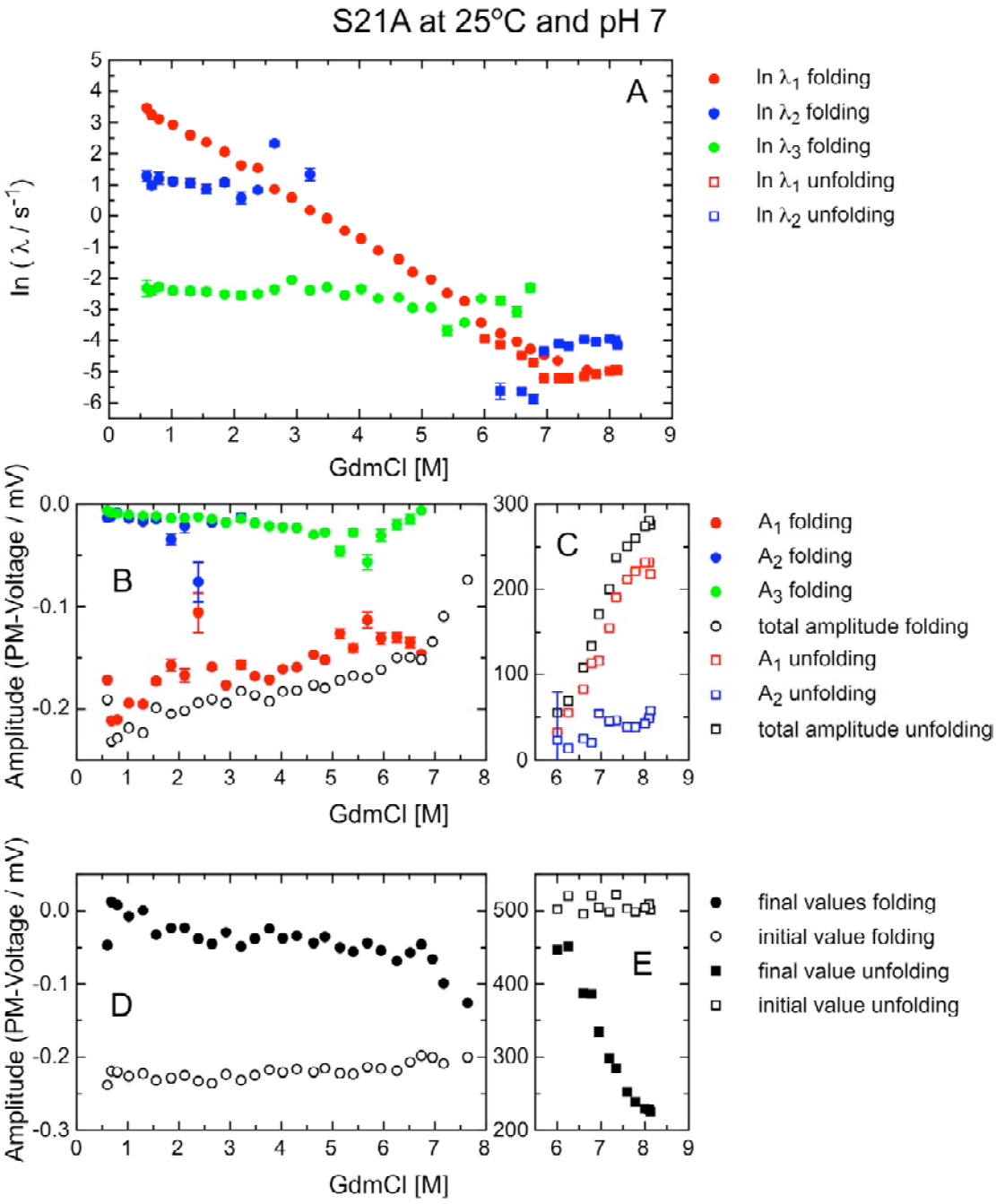
S21A at 25°C and pH 7
A
ln (λ / s⁻¹)
GdmCl [M]
ln λ1 folding
ln λ2 folding
ln λ3 folding
ln λ1 unfolding
ln λ2 unfolding
B
C
Amplitude (PM-Voltage / mV)
A1 folding
A2 folding
A3 folding
total amplitude folding
A1 unfolding
A2 unfolding
total amplitude unfolding
D
E
final values folding
initial value folding
final value unfolding
initial value unfolding

Figure 9-23

(b) Tendamistat variants with less stability as wild type

A detailed analysis of the temperature dependence of L14V are described in "*Shape of Free Energy Barrier for Tendamistat Folding*", Schätzle, M. & Kiefhaber, T., 2005, to be submitted, and "*Thermodynamic Properties of the Transition States in Tendamistat Folding*", Schätzle, M. & Kiefhaber, T., 2005, to be submitted. The results are summarized in chapter 3.1. Analysis and results of the other data are described in chapter 4.2.

Equilibrium and kinetic data were measured for the tendamistat variants **S21G, V31A** and **T32A** at pH 7 and 25°C and for the tendamistat variant **L14V** at pH 7 and various temperatures. Equilibrium data were obtained with 10 μM protein in 100 mM cacodylic acid, pH 7, by monitoring the ellipticity at 227 nm and for L14V at 233 nm. The kinetics were measured monitoring the change in fluorescence after initiation by dilution of native and unfolded protein, respectively, into various denaturant concentration to a final concentration of 4 μM protein in 100 mM cacodylic acid, pH 7.

T32A

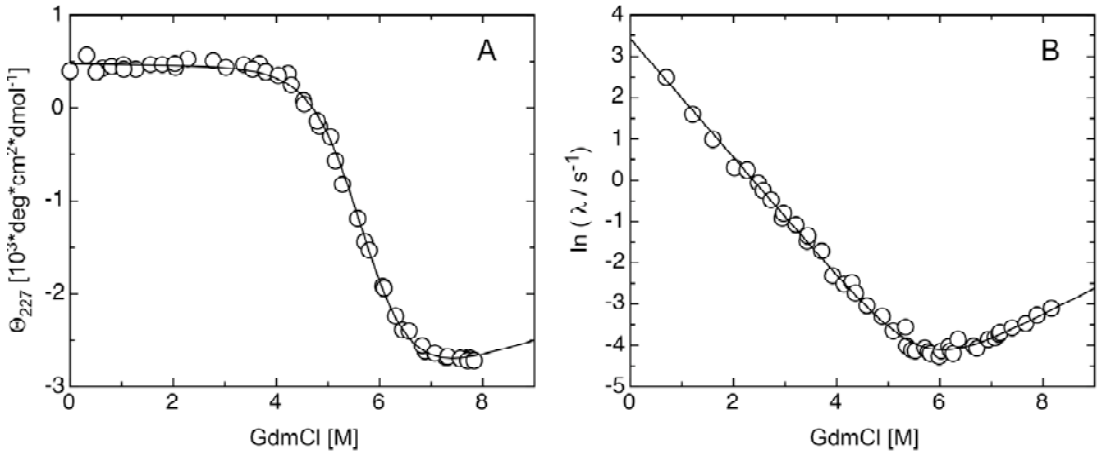

*Figure 9-24: GdmCl-induced unfolding transition (A) and the GdmCl-dependence of the apparent rate constant of refolding and unfolding (B) of **T32A** at pH 7 and 25°C. Only the rate constant with the major amplitude is plotted. The solid lines represent the results of the global fit. Data were measured from Daniel Poso.*

L14V

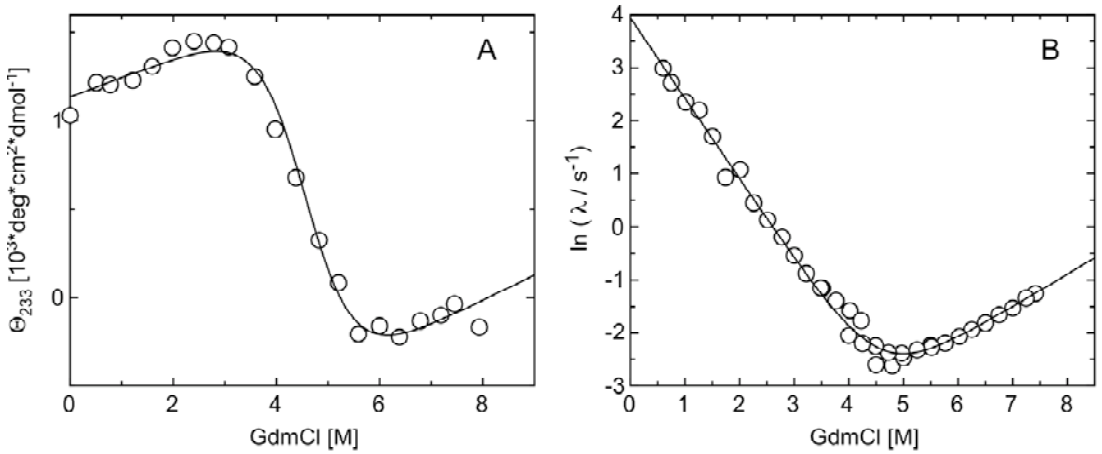

S21G

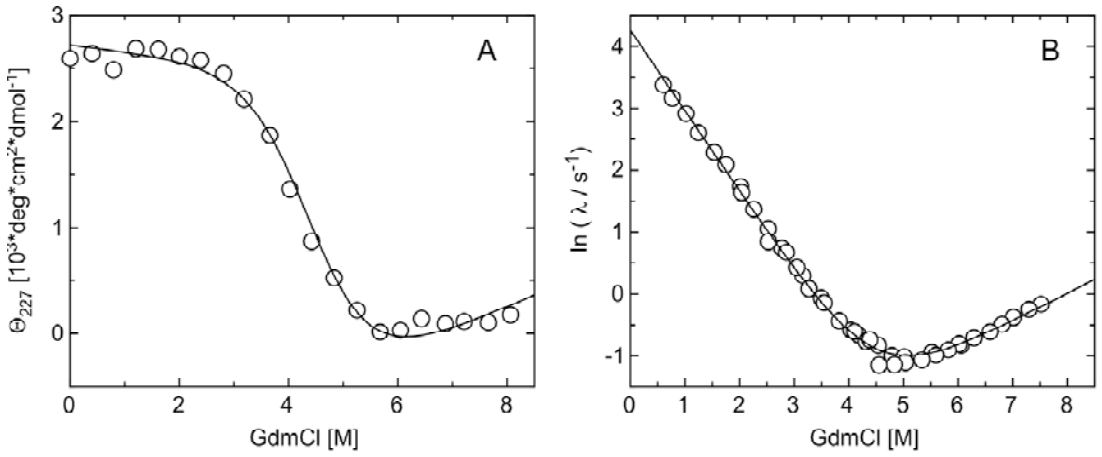

V31A

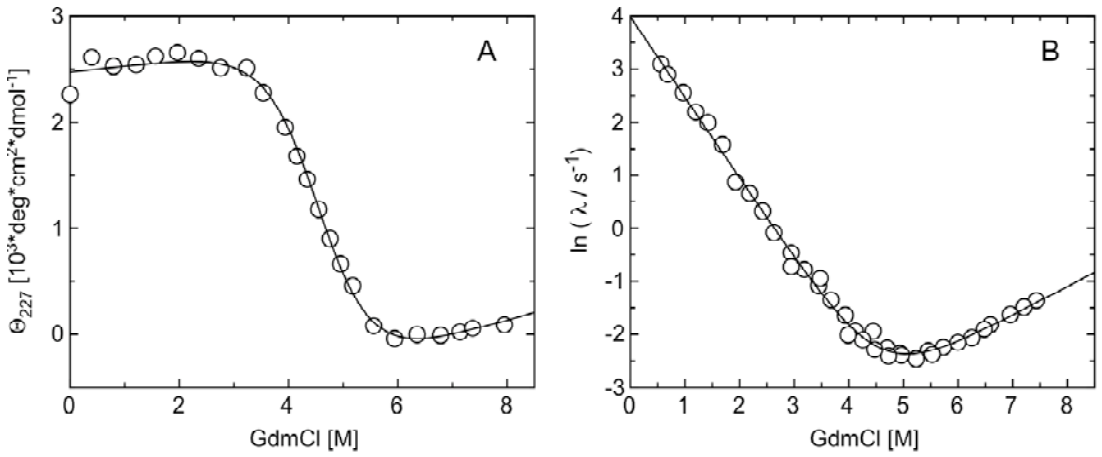

*Figure 9-25: GdmCl-induced unfolding transition (A) and the GdmCl-dependence of the apparent rate constant of refolding and unfolding (B) of **L14V**, **S21G** and **V31A** at pH 7 and 25°C. Only the rate constant with the major amplitude is plotted. The solid lines represent the results of the global fit.*

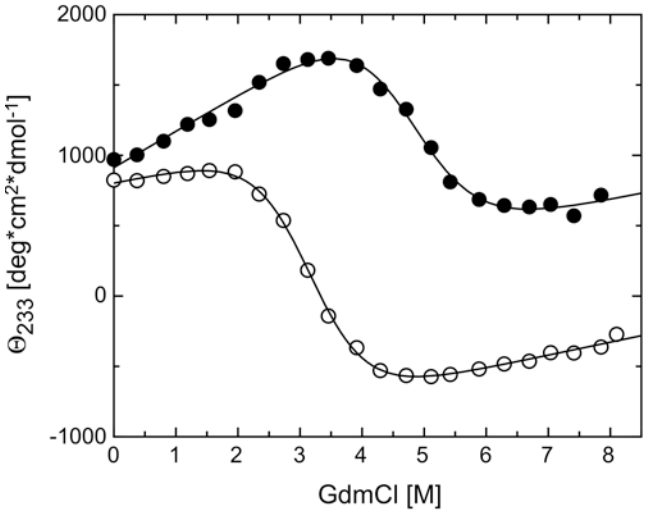

*Figure 9-26: GdmCl-induced unfolding transition of **L14V** at pH 7 at 5°C (●) and 45°C (○). The line represents the analysis assuming the two-state model.*

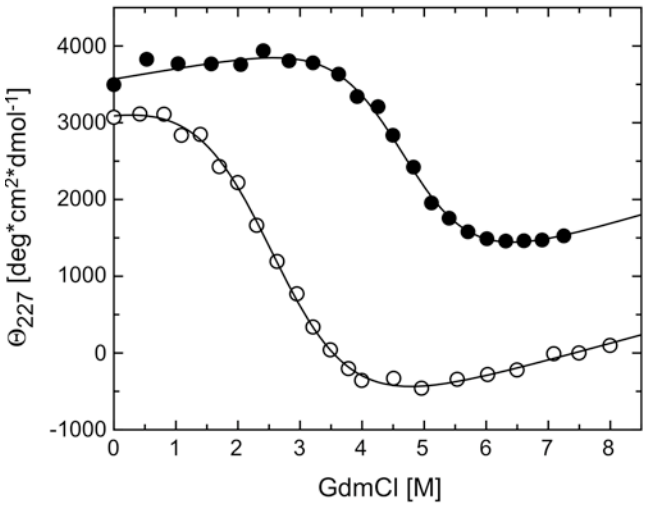

*Figure 9-27: GdmCl-induced unfolding transition of **S21G** at pH 7 at 5°C (●) and 45°C (○). The line represents the analysis assuming the two-state model.*

*Figure 9-28 – Figure 9-40 (following pages): GdmCl-dependence of the apparent rate constants λ_i (A), the amplitudes A_i (B) and the final and initial values (C) for folding of the tendamistat variants **L14V, S21G** and **V31A** at pH 7 at different temperatures. The values for the refolding reaction are plotted as circles, for the unfolding reaction as squares.*

*Figure 9-28 – Figure 9-36: Folding of the tendamistat variant **L14V** at different temperatures.*

*Figure 9-37 – Figure 9-39: Folding of the tendamistat variant **S21G** at different temperatures.*

*Figure 9-40: Folding of the tendamistat variant **V31A** at 25°C.*

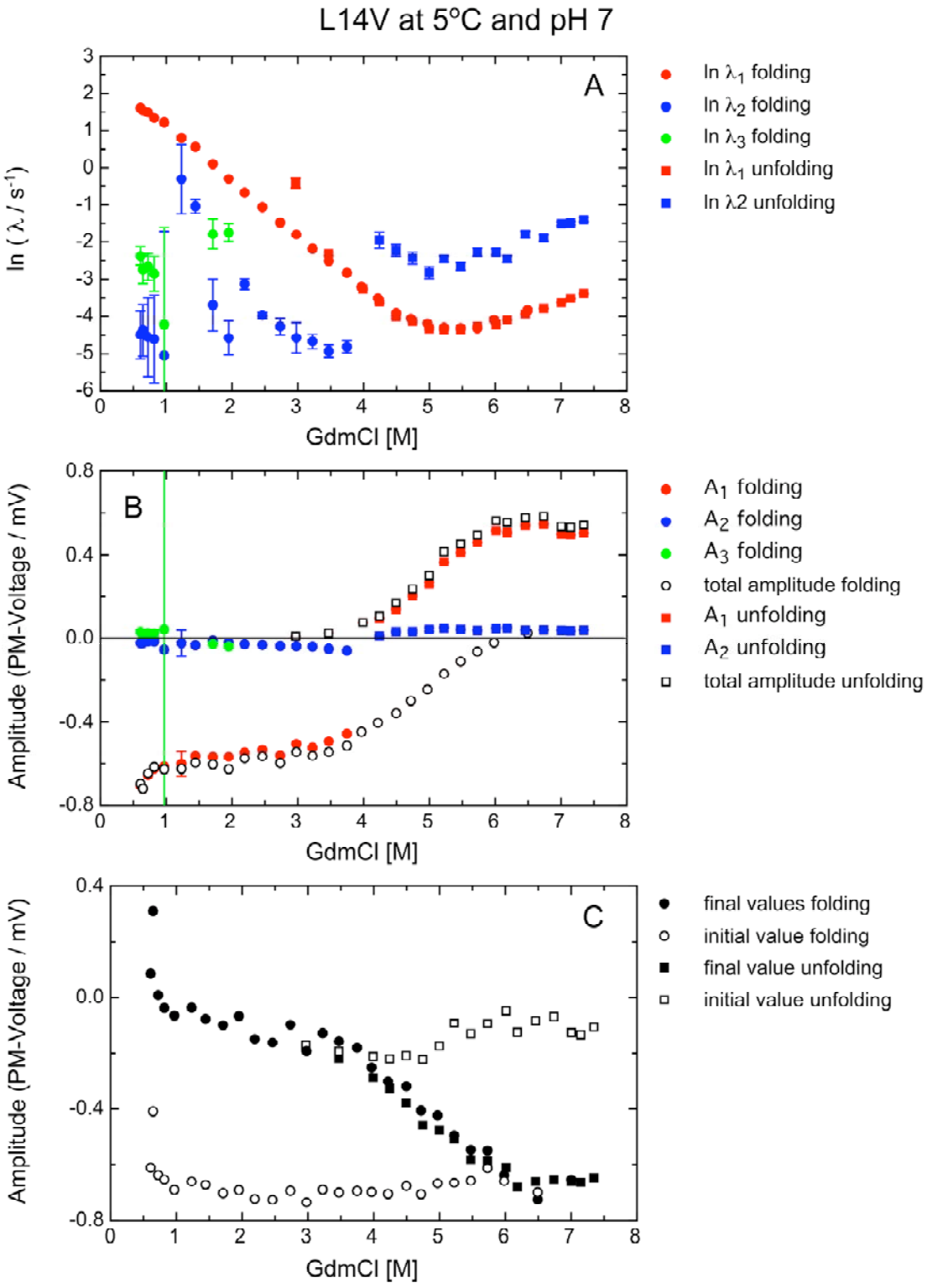
L14V at 5°C and pH 7
A
ln (λ / s-1)
GdmCl [M]
ln λ1 folding
ln λ2 folding
ln λ3 folding
ln λ1 unfolding
ln λ2 unfolding
B
Amplitude (PM-Voltage / mV)
GdmCl [M]
A1 folding
A2 folding
A3 folding
total amplitude folding
A1 unfolding
A2 unfolding
total amplitude unfolding
C
Amplitude (PM-Voltage / mV)
GdmCl [M]
final values folding
initial value folding
final value unfolding
initial value unfolding

Figure 9-28

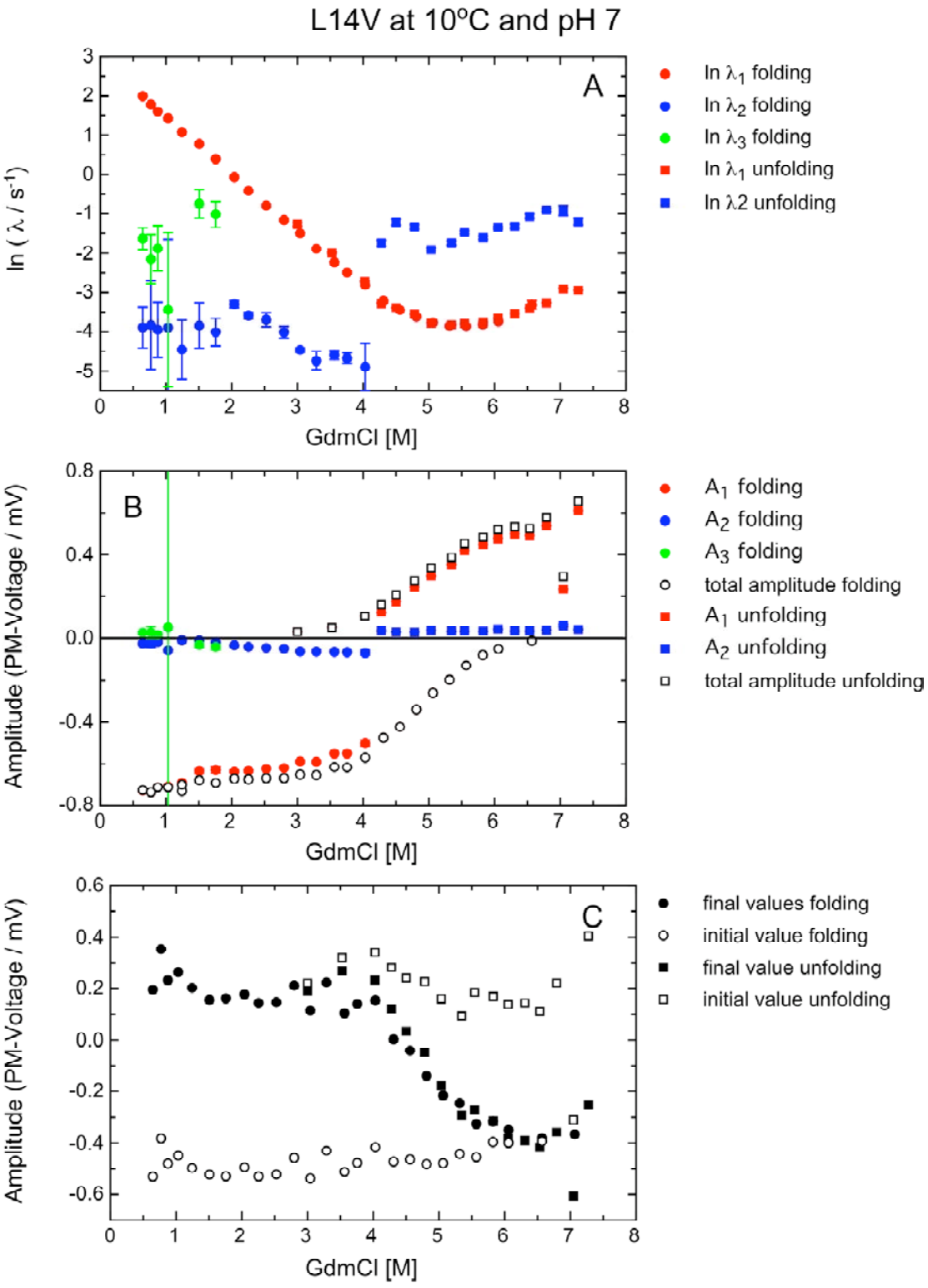
L14V at 10°C and pH 7
A
ln (λ / s-1)
GdmCl [M]
ln λ1 folding
ln λ2 folding
ln λ3 folding
ln λ1 unfolding
ln λ2 unfolding
B
Amplitude (PM-Voltage / mV)
GdmCl [M]
A1 folding
A2 folding
A3 folding
total amplitude folding
A1 unfolding
A2 unfolding
total amplitude unfolding
C
Amplitude (PM-Voltage / mV)
GdmCl [M]
final values folding
initial value folding
final value unfolding
initial value unfolding

Figure 9-29

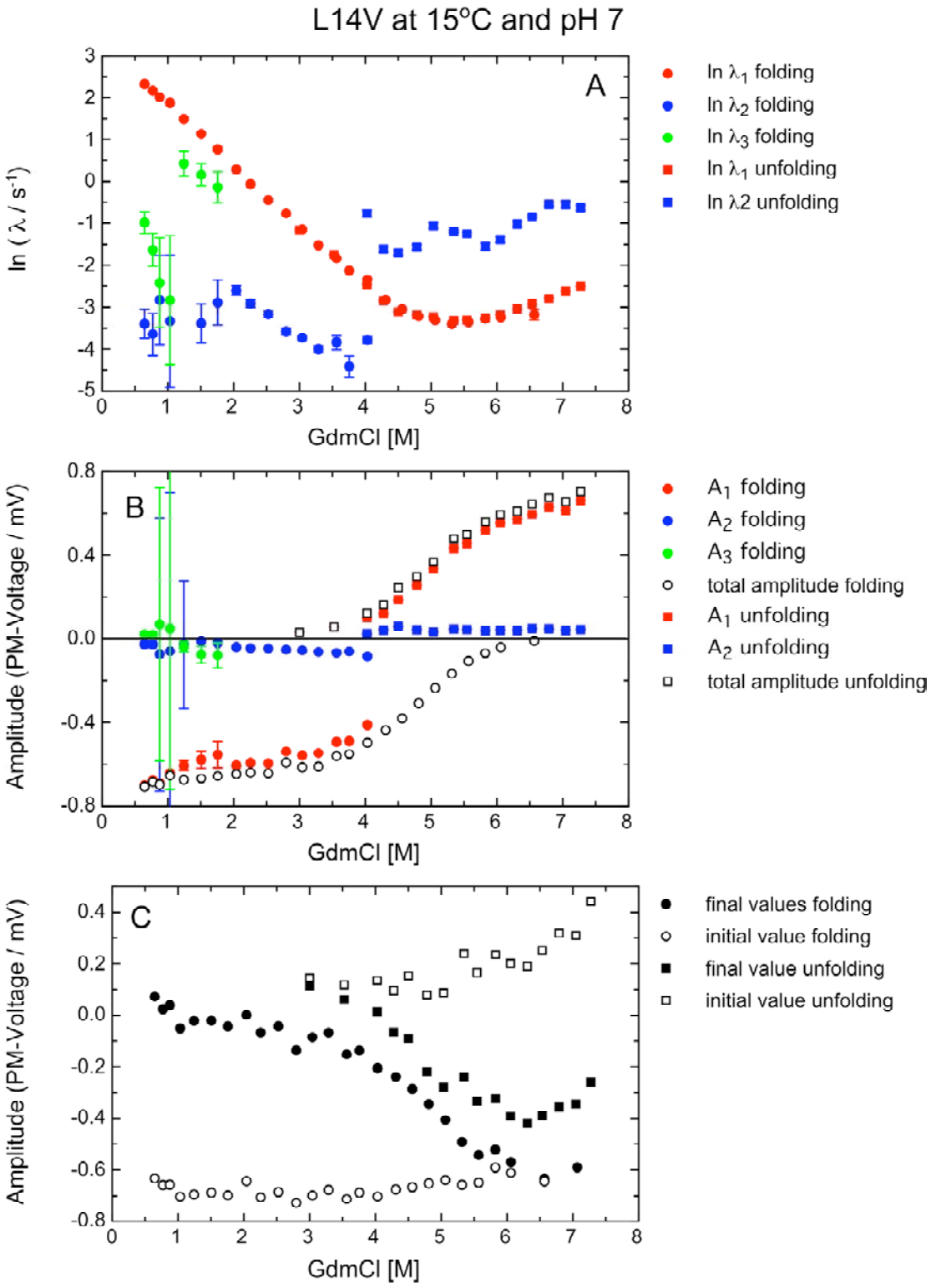
L14V at 15°C and pH 7
A
ln (λ / s-1)
GdmCl [M]
ln λ1 folding
ln λ2 folding
ln λ3 folding
ln λ1 unfolding
ln λ2 unfolding
B
Amplitude (PM-Voltage / mV)
GdmCl [M]
A1 folding
A2 folding
A3 folding
total amplitude folding
A1 unfolding
A2 unfolding
total amplitude unfolding
C
Amplitude (PM-Voltage / mV)
GdmCl [M]
final values folding
initial value folding
final value unfolding
initial value unfolding

Figure 9-30

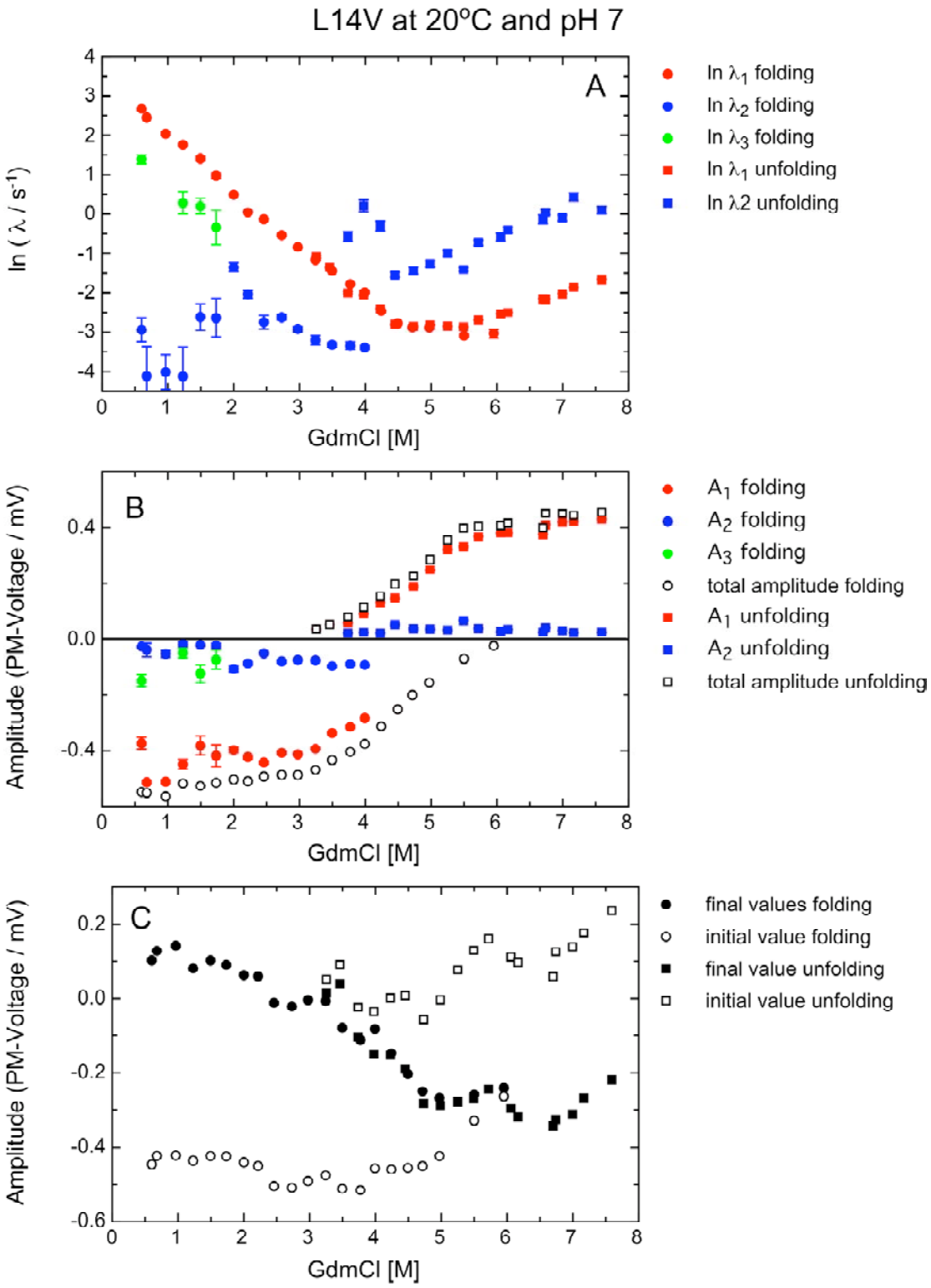
L14V at 20°C and pH 7
A
ln (λ / s-1)
GdmCl [M]
ln λ1 folding
ln λ2 folding
ln λ3 folding
ln λ1 unfolding
ln λ2 unfolding
B
Amplitude (PM-Voltage / mV)
GdmCl [M]
A1 folding
A2 folding
A3 folding
total amplitude folding
A1 unfolding
A2 unfolding
total amplitude unfolding
C
Amplitude (PM-Voltage / mV)
GdmCl [M]
final values folding
initial value folding
final value unfolding
initial value unfolding

Figure 9-31

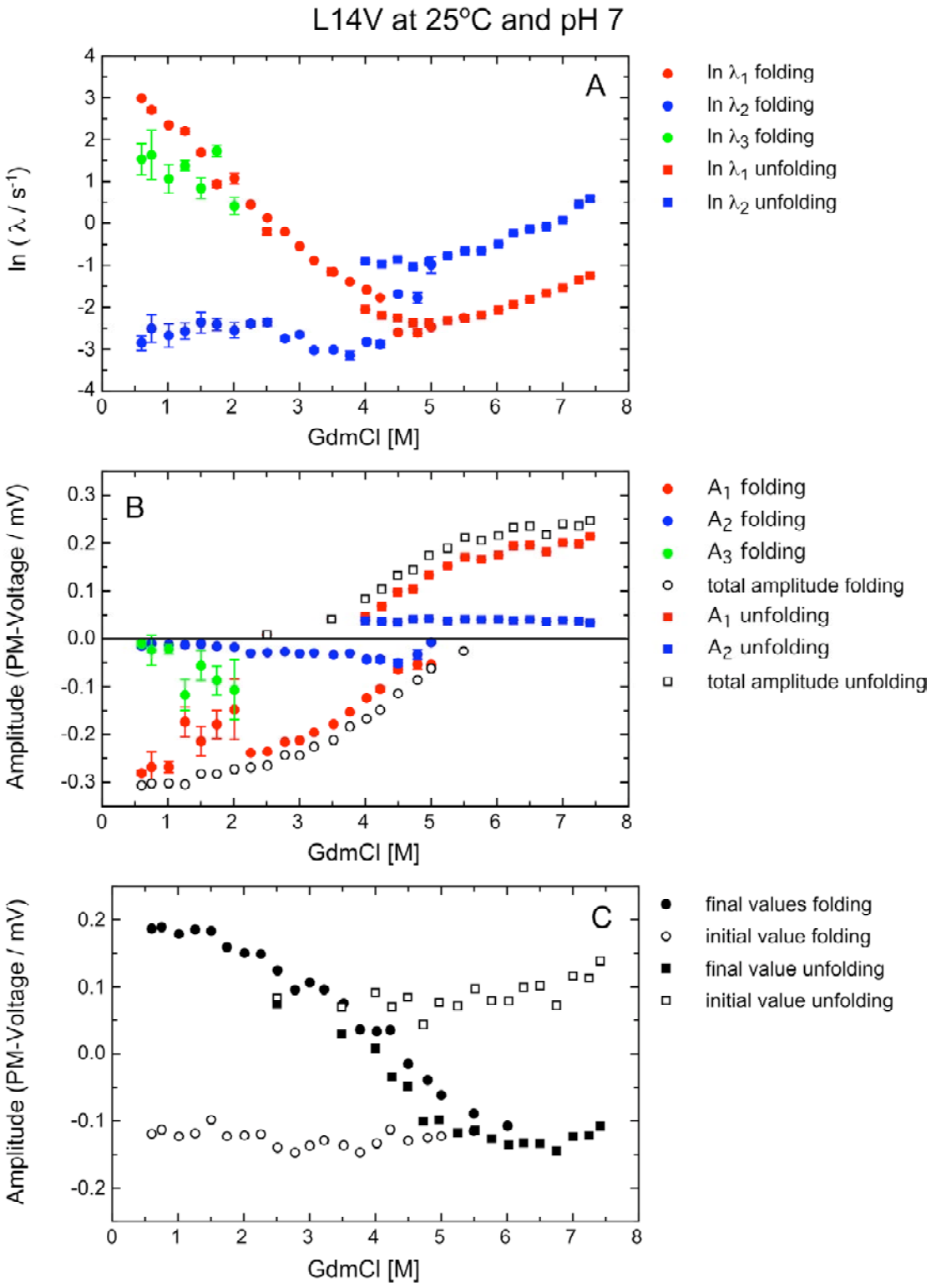
L14V at 25°C and pH 7
A
ln (λ / s-1)
GdmCl [M]
ln λ1 folding
ln λ2 folding
ln λ3 folding
ln λ1 unfolding
ln λ2 unfolding
B
Amplitude (PM-Voltage / mV)
GdmCl [M]
A1 folding
A2 folding
A3 folding
total amplitude folding
A1 unfolding
A2 unfolding
total amplitude unfolding
C
Amplitude (PM-Voltage / mV)
GdmCl [M]
final values folding
initial value folding
final value unfolding
initial value unfolding

Figure 9-32

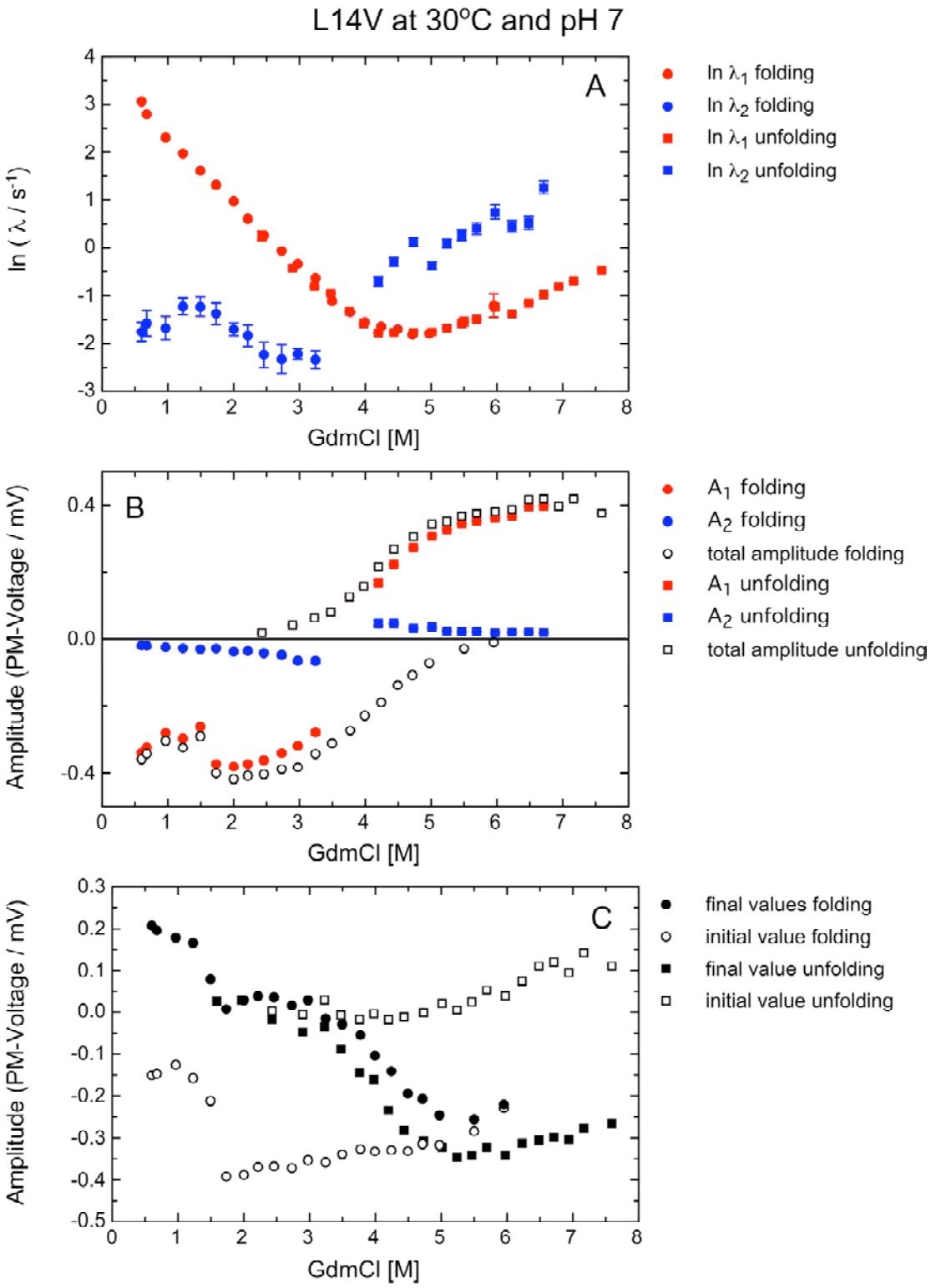
L14V at 30°C and pH 7
A
ln (λ / s-1)
GdmCl [M]
ln λ1 folding
ln λ2 folding
ln λ1 unfolding
ln λ2 unfolding
B
Amplitude (PM-Voltage / mV)
GdmCl [M]
A1 folding
A2 folding
total amplitude folding
A1 unfolding
A2 unfolding
total amplitude unfolding
C
Amplitude (PM-Voltage / mV)
GdmCl [M]
final values folding
initial value folding
final value unfolding
initial value unfolding

Figure 9-33

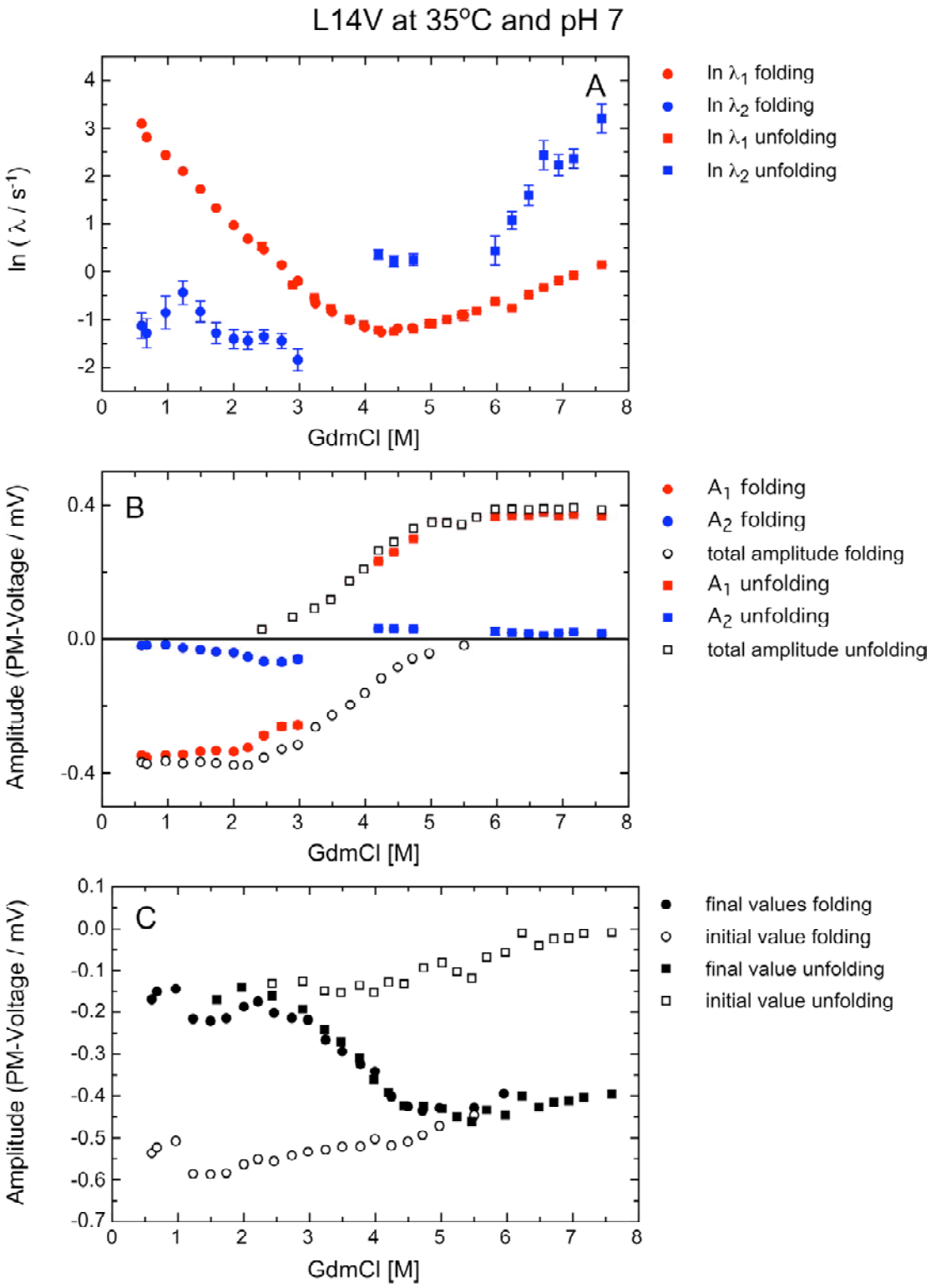
L14V at 35°C and pH 7
A
ln λ1 folding
ln λ2 folding
ln λ1 unfolding
ln λ2 unfolding
ln (λ / s-1)
GdmCl [M]
B
A1 folding
A2 folding
total amplitude folding
A1 unfolding
A2 unfolding
total amplitude unfolding
Amplitude (PM-Voltage / mV)
GdmCl [M]
C
final values folding
initial value folding
final value unfolding
initial value unfolding
Amplitude (PM-Voltage / mV)
GdmCl [M]

Figure 9-34

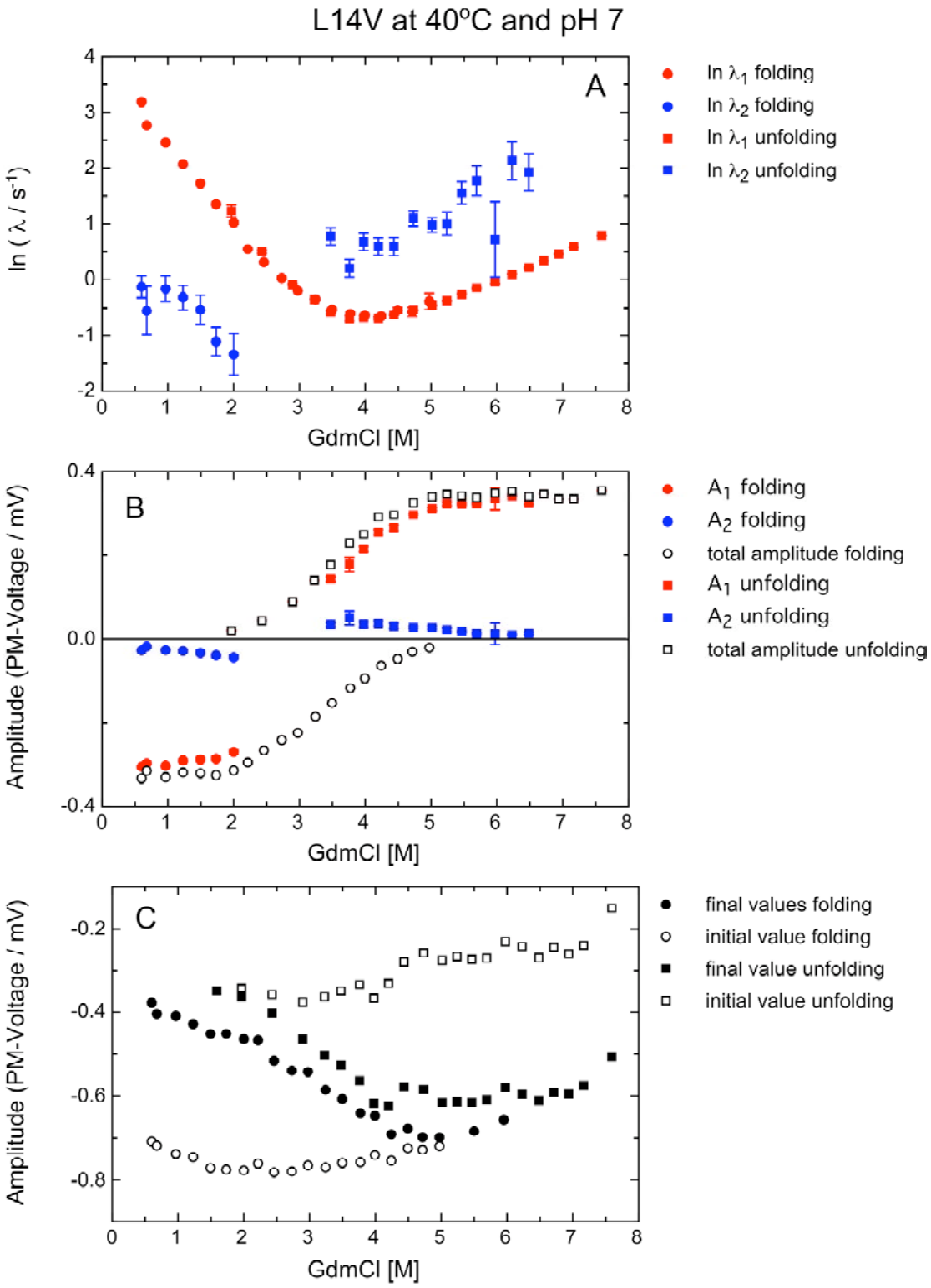
L14V at 40°C and pH 7
A
ln (λ / s-1)
GdmCl [M]
ln λ1 folding
ln λ2 folding
ln λ1 unfolding
ln λ2 unfolding
B
Amplitude (PM-Voltage / mV)
GdmCl [M]
A1 folding
A2 folding
total amplitude folding
A1 unfolding
A2 unfolding
total amplitude unfolding
C
Amplitude (PM-Voltage / mV)
GdmCl [M]
final values folding
initial value folding
final value unfolding
initial value unfolding

Figure 9-35

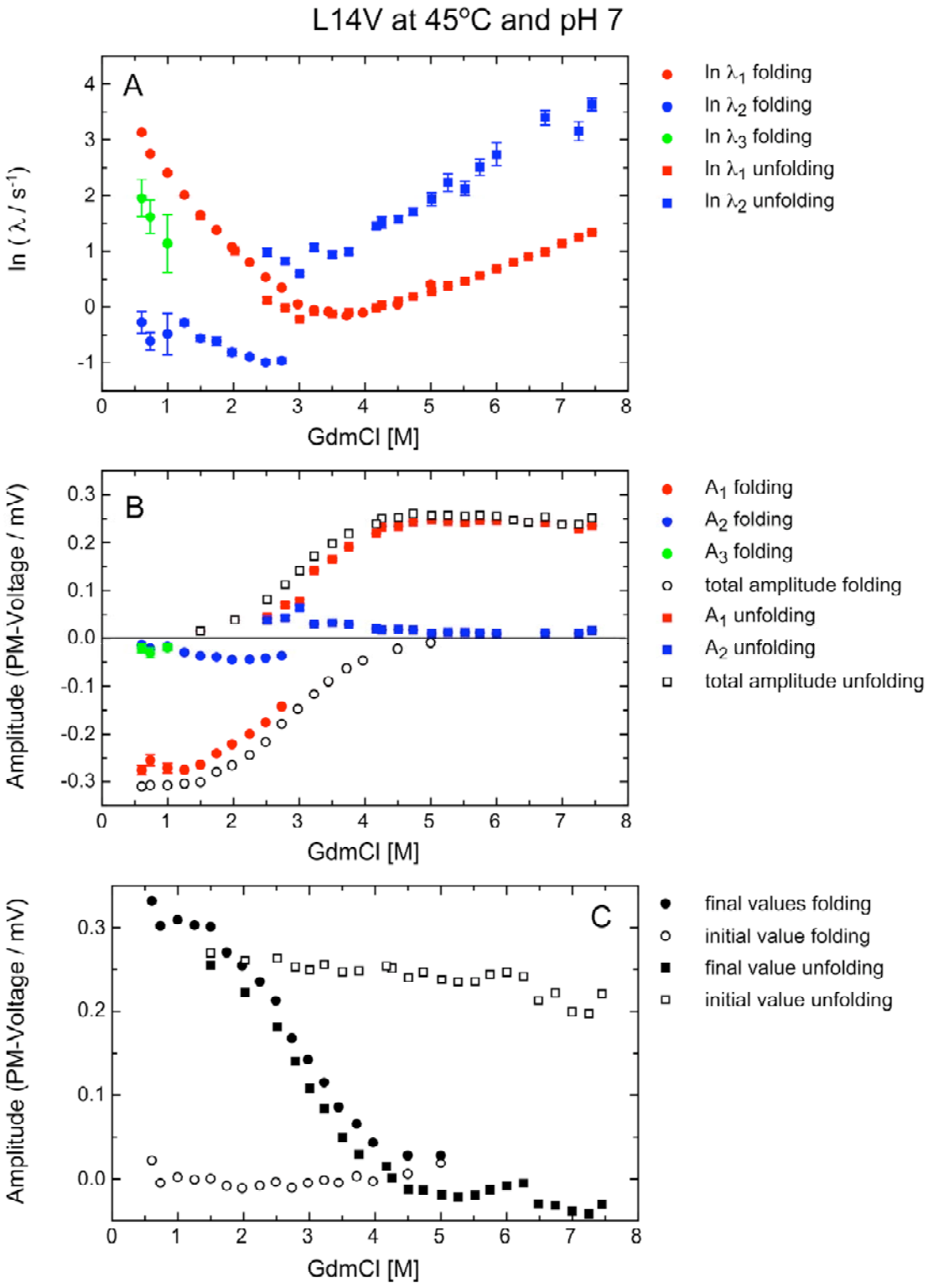
L14V at 45°C and pH 7
A
ln (λ / s-1)
GdmCl [M]
ln λ1 folding
ln λ2 folding
ln λ3 folding
ln λ1 unfolding
ln λ2 unfolding
B
Amplitude (PM-Voltage / mV)
GdmCl [M]
A1 folding
A2 folding
A3 folding
total amplitude folding
A1 unfolding
A2 unfolding
total amplitude unfolding
C
Amplitude (PM-Voltage / mV)
GdmCl [M]
final values folding
initial value folding
final value unfolding
initial value unfolding

Figure 9-36

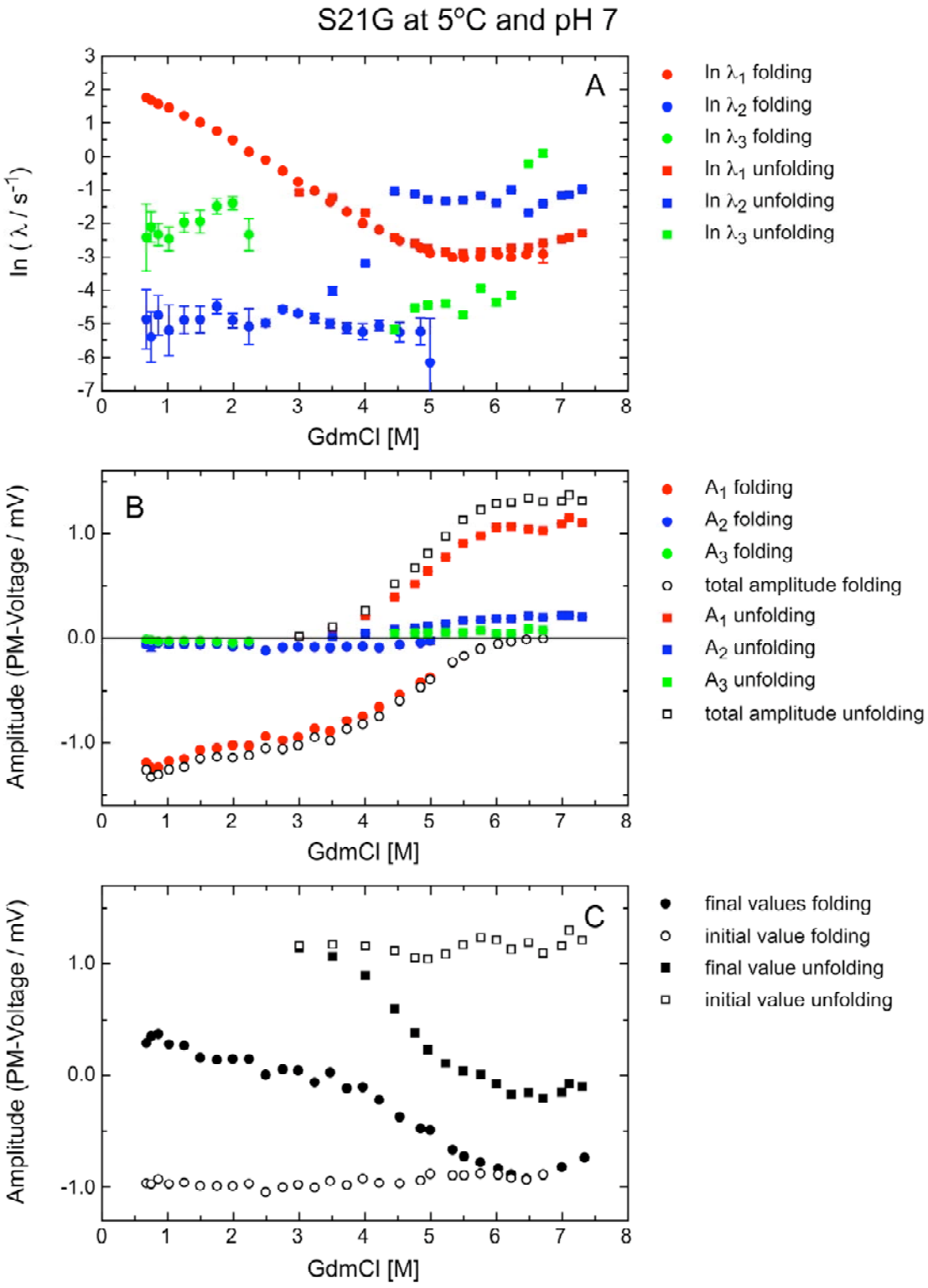
S21G at 5°C and pH 7
A
ln (λ / s^{-1})
GdmCl [M]
ln λ_1 folding
ln λ_2 folding
ln λ_3 folding
ln λ_1 unfolding
ln λ_2 unfolding
ln λ_3 unfolding
B
Amplitude (PM-Voltage / mV)
GdmCl [M]
A_1 folding
A_2 folding
A_3 folding
total amplitude folding
A_1 unfolding
A_2 unfolding
A_3 unfolding
total amplitude unfolding
C
Amplitude (PM-Voltage / mV)
GdmCl [M]
final values folding
initial value folding
final value unfolding
initial value unfolding

Figure 9-37

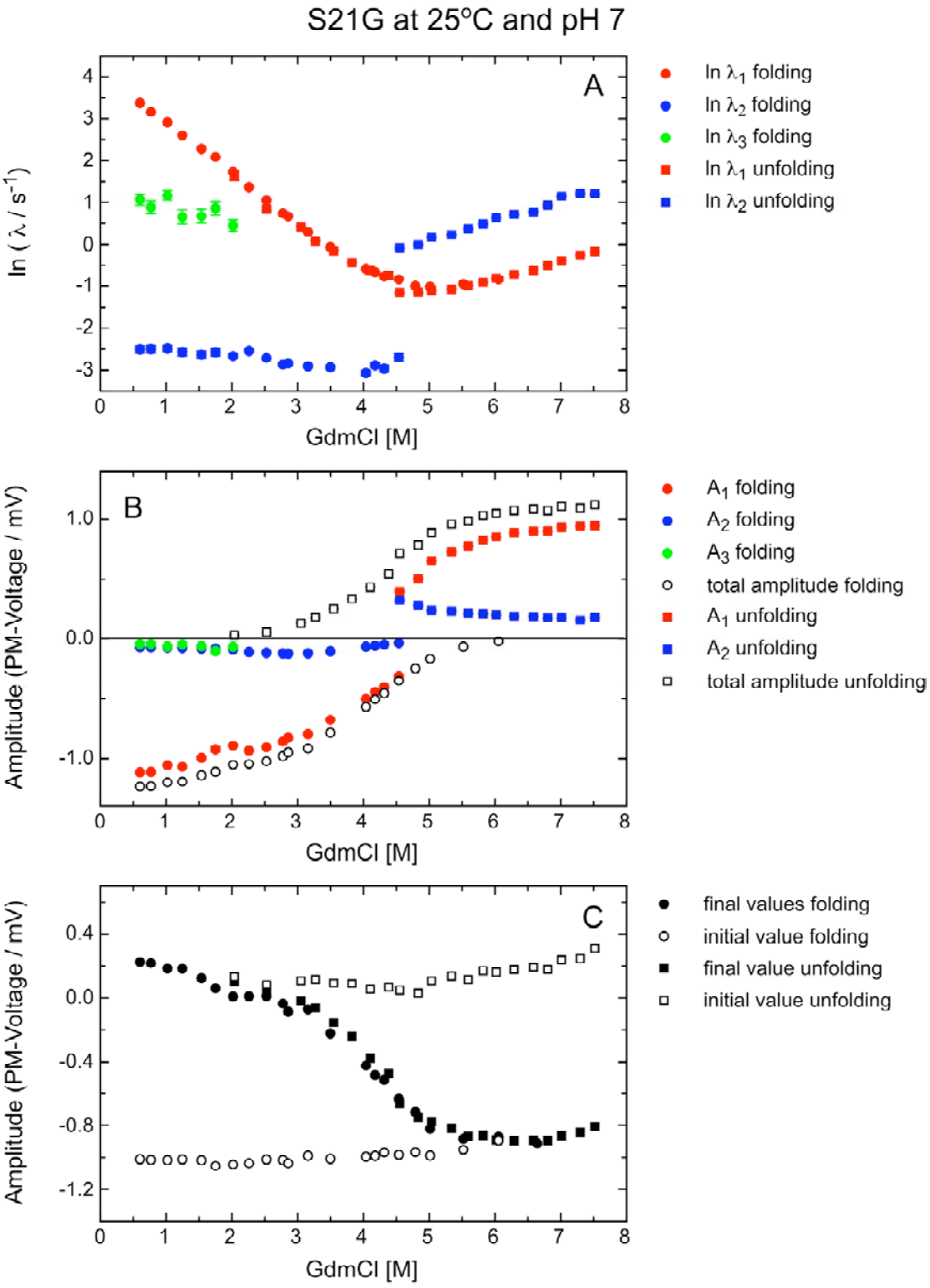
S21G at 25°C and pH 7
A
ln (λ / s^{-1})
GdmCl [M]
ln λ_1 folding
ln λ_2 folding
ln λ_3 folding
ln λ_1 unfolding
ln λ_2 unfolding
B
Amplitude (PM-Voltage / mV)
GdmCl [M]
A_1 folding
A_2 folding
A_3 folding
total amplitude folding
A_1 unfolding
A_2 unfolding
total amplitude unfolding
C
Amplitude (PM-Voltage / mV)
GdmCl [M]
final values folding
initial value folding
final value unfolding
initial value unfolding

Figure 9-38

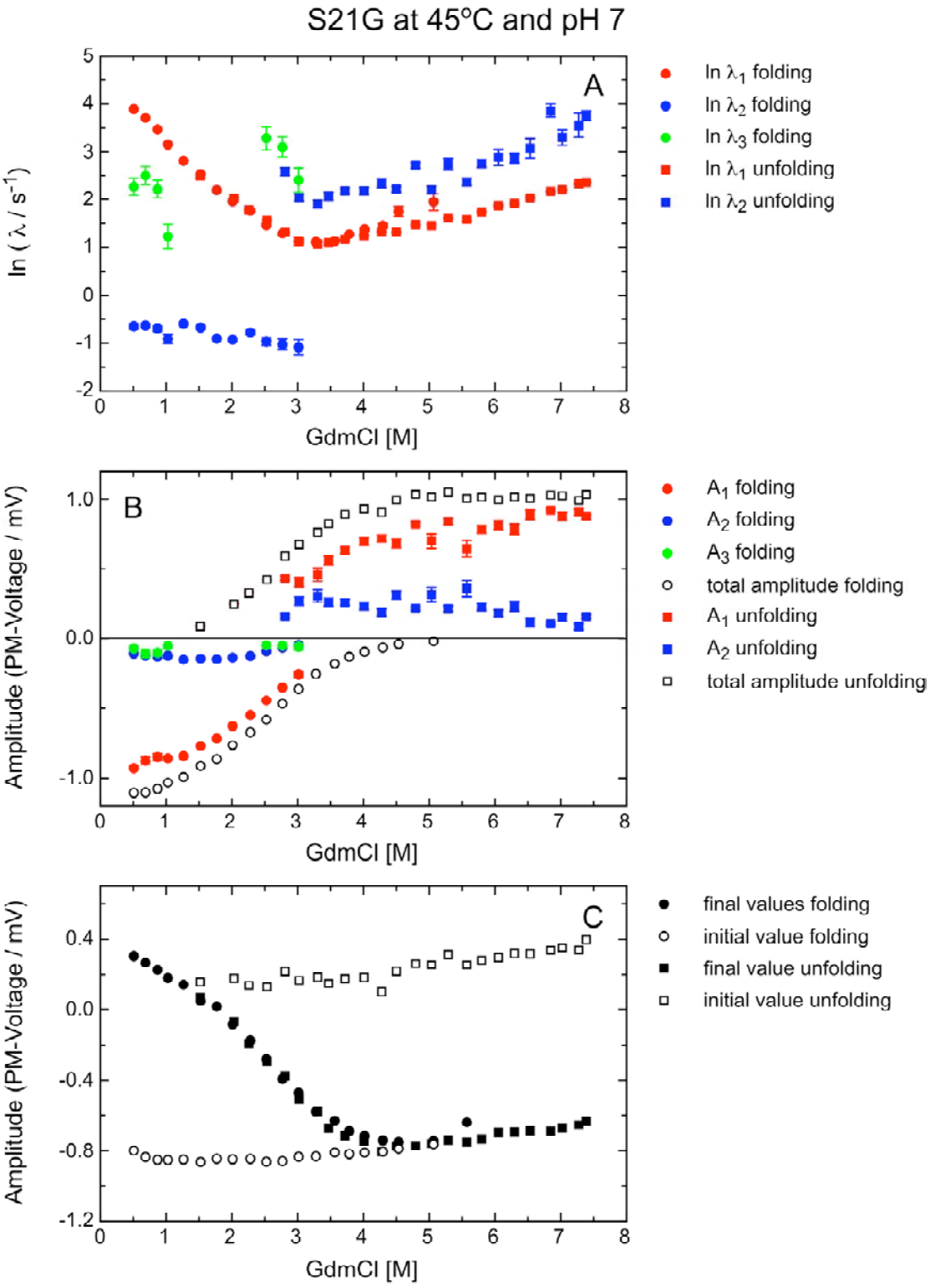
S21G at 45°C and pH 7
A
ln (λ / s^{-1})
GdmCl [M]
ln λ_1 folding
ln λ_2 folding
ln λ_3 folding
ln λ_1 unfolding
ln λ_2 unfolding
B
Amplitude (PM-Voltage / mV)
GdmCl [M]
A_1 folding
A_2 folding
A_3 folding
total amplitude folding
A_1 unfolding
A_2 unfolding
total amplitude unfolding
C
Amplitude (PM-Voltage / mV)
GdmCl [M]
final values folding
initial value folding
final value unfolding
initial value unfolding

Figure 9-39

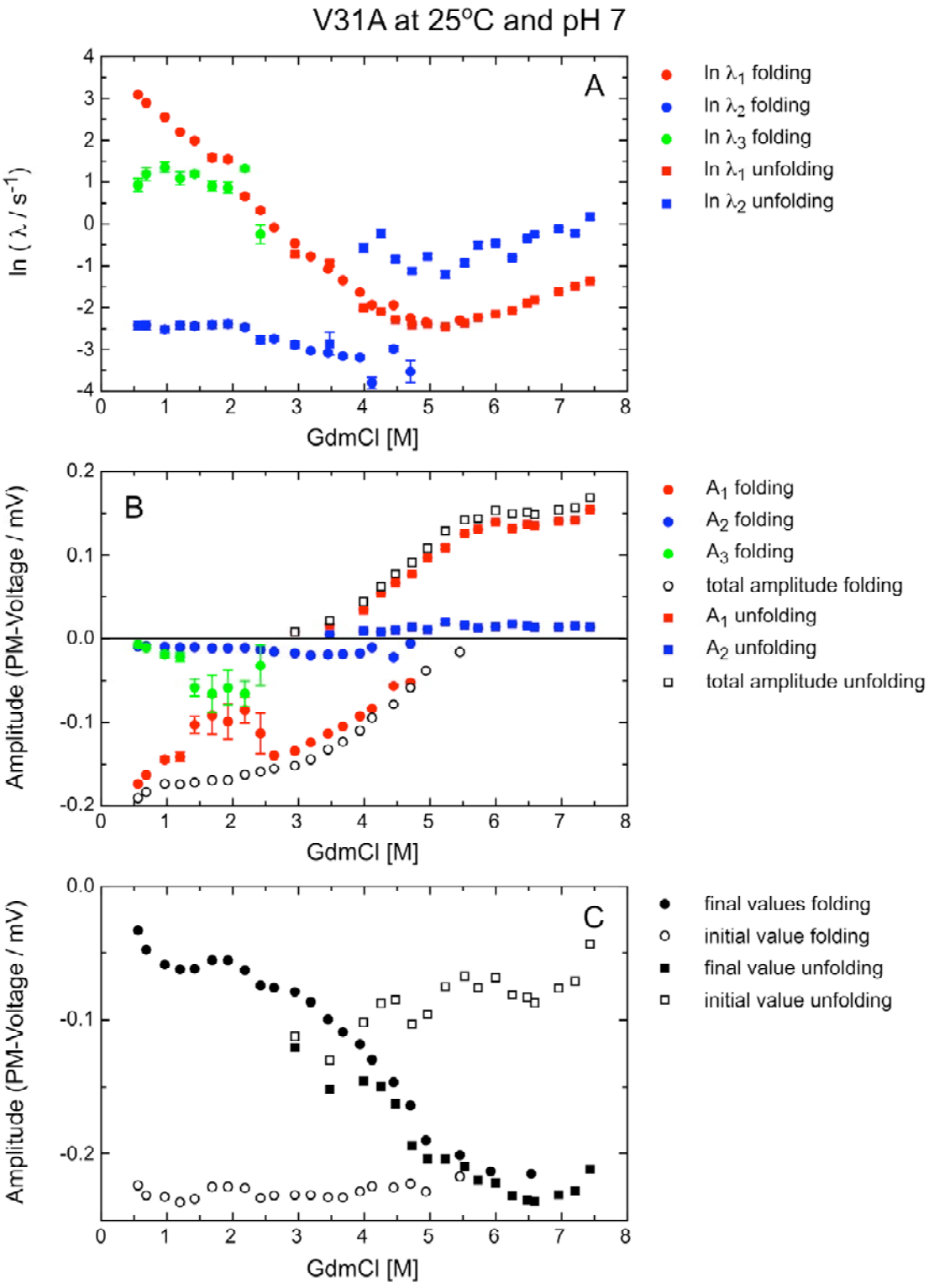
V31A at 25°C and pH 7
A
ln (λ / s-1)
GdmCl [M]
ln λ1 folding
ln λ2 folding
ln λ3 folding
ln λ1 unfolding
ln λ2 unfolding
B
Amplitude (PM-Voltage / mV)
GdmCl [M]
A1 folding
A2 folding
A3 folding
total amplitude folding
A1 unfolding
A2 unfolding
total amplitude unfolding
C
Amplitude (PM-Voltage / mV)
GdmCl [M]
final values folding
initial value folding
final value unfolding
initial value unfolding

Figure 9-40

9.4 Variants with the late transition state rate-limiting

A detailed analysis of the temperature dependence of N25A are described in "*Shape of Free Energy Barrier for Tendamistat Folding*", Schätzle, M. & Kiefhaber, T., 2005, to be submitted, and "*Thermodynamic Properties of the Transition States in Tendamistat Folding*", Schätzle, M. & Kiefhaber, T., 2005, to be submitted. The results are summarized in chapter 3.1. Analysis and results of the other data are described in chapter 4.2.

Equilibrium and kinetic data were measured for the tendamistat variants **L14A** and **N25A** at pH 7 at various temperatures and salt concentrations. Equilibrium data were obtained with 10 μM protein in 100 mM cacodylic acid, pH 7, by monitoring the ellipticity at 227 nm. The kinetics were measured monitoring the change in fluorescence after initiation by dilution of native and unfolded protein, respectively, into various denaturant concentration to a final concentration of 4 μM protein in 100 mM cacodylic acid, pH 7.

L14A

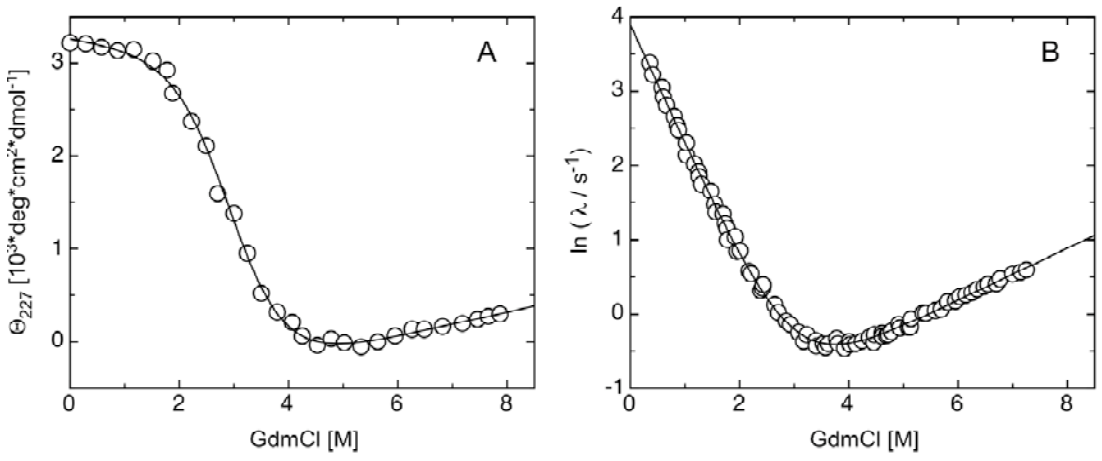

*Figure 9-41: GdmCl-induced unfolding transition (A) and the GdmCl-dependence of the apparent rate constant of refolding and unfolding (B) of **L14A** at pH 7 and 25°C. Only the rate constant with the major amplitude is plotted. The solid lines represent the results of the global fit. Data were measured from Daniel Poso.*

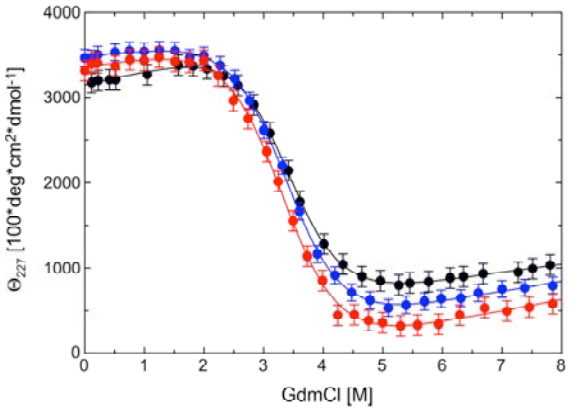

*Figure 9-42: GdmCl-induced unfolding transition of **L14A** at pH 7 at 5°C (●) 10°C (●) and 15°C (●). The line represents the analysis assuming the two-state model. Data were measured from Daniel Poso.*

*Figure 9-43 (following page): GdmCl-dependence of the apparent rate constant of refolding and unfolding of **L14A** at pH 7 and various temperatures. Only the rate constant with the major amplitude is plotted. The solid lines represent the results of the single fits assuming the two-state model. Data were measured from Daniel Poso.*

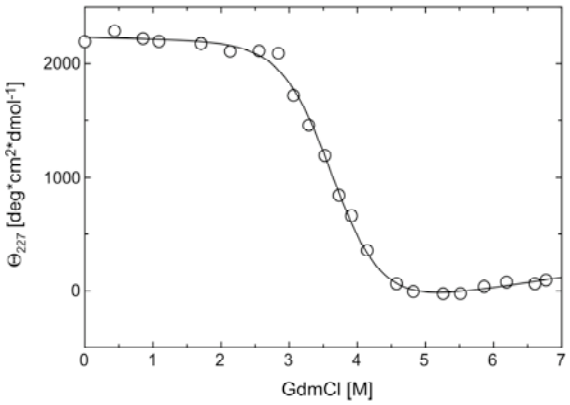

*Figure 9-44: GdmCl-induced unfolding transition of **L14A** at pH 7 at 25°C and 0.5 M Na_2SO_4. The line represents the analysis assuming the two-state model.*

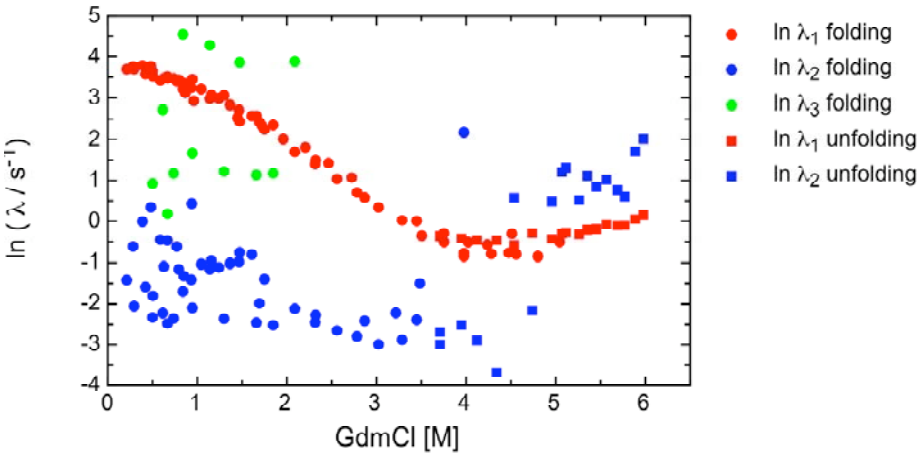

*Figure 9-45: GdmCl-dependence of the apparent rate constant λ_i of refolding and unfolding of **L14A** at pH 7 at 25°C and 0.5 M Na_2SO_4. The values for the refolding reaction are plotted as circles, for the unfolding reaction as squares.*

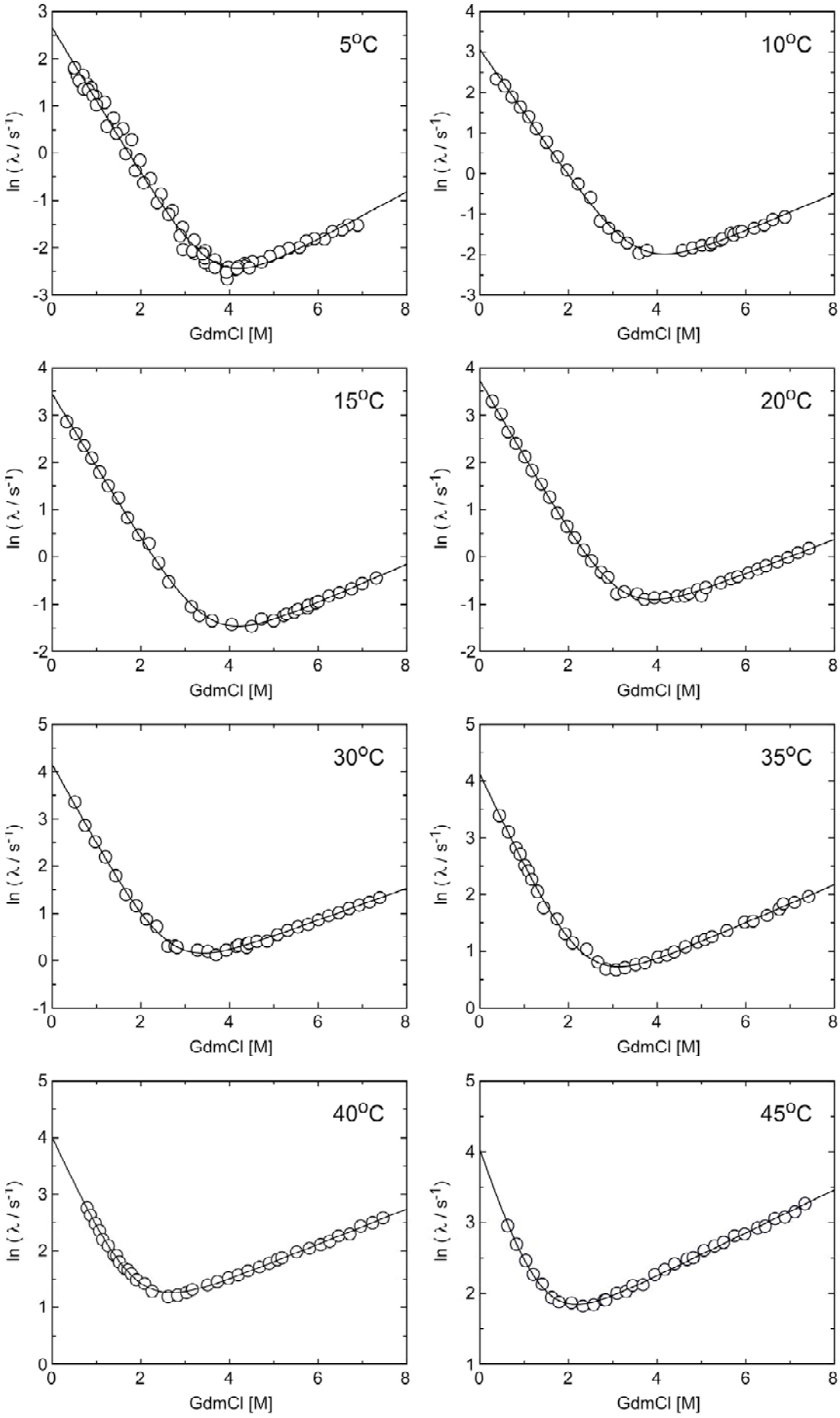
5°C
10°C
15°C
20°C
30°C
35°C
40°C
45°C
ln (λ / s⁻¹)
GdmCl [M]

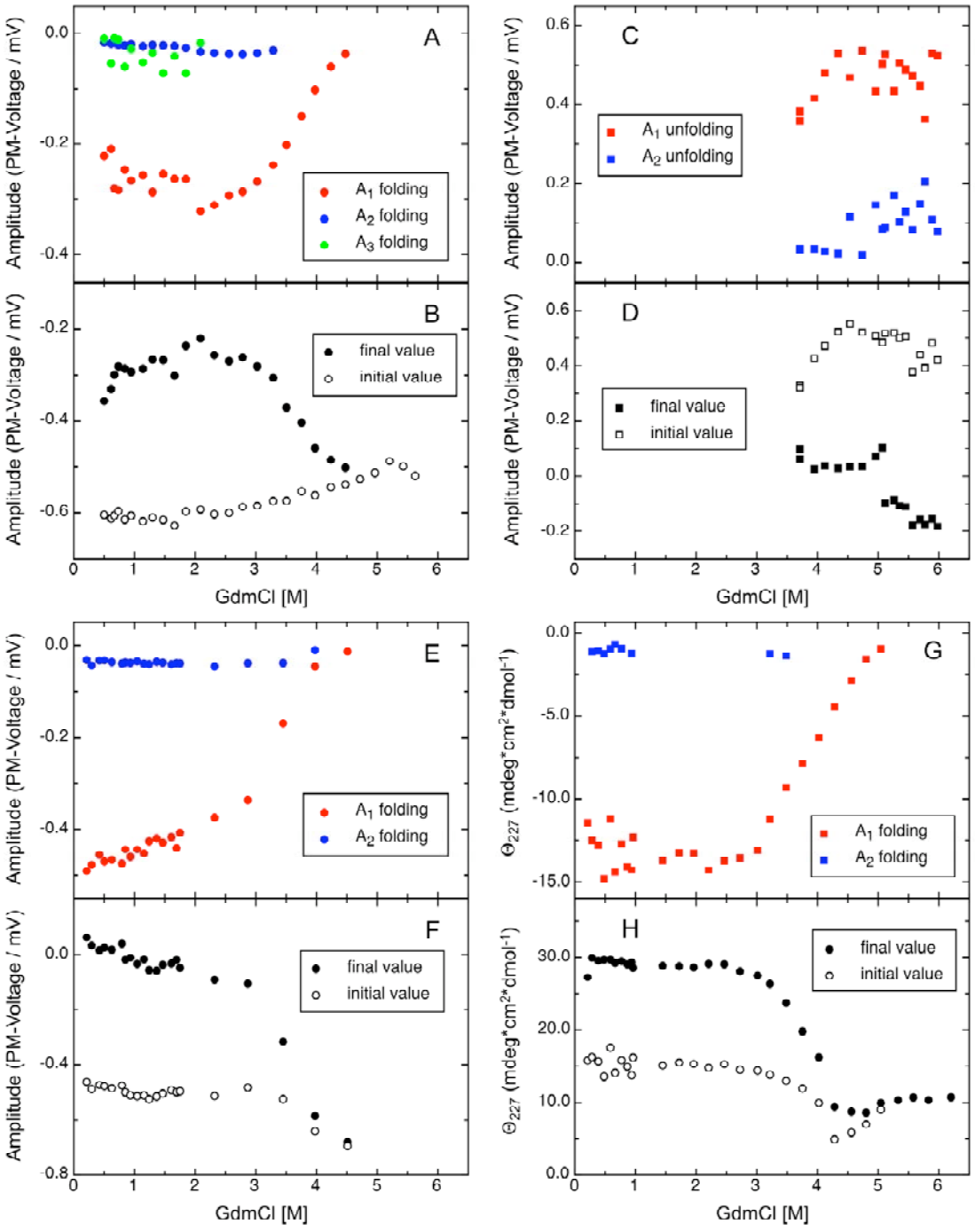

*Figure 9-46: GdmCl-dependence of the amplitudes A_i (A, C, E, G) and the final and initial values (B, C, F, H) for folding of the tendamistat variant **L14A** at pH 7 and 25°C at 0.5 M Na_2SO_4. Kinetics were measured monitoring the change in ellipticity (G, H) and the change in fluorescence after initiation by 11-fold (A-D) and 26-fold (E, F) dilution of protein into various denaturant concentrations.*

N25A

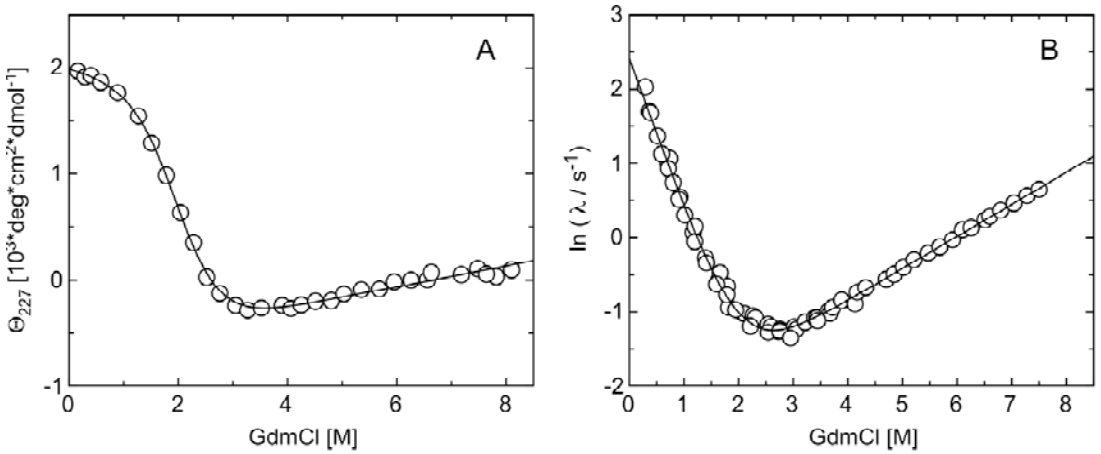

*Figure 9-47: GdmCl-induced unfolding transition (A) and the GdmCl-dependence of the apparent rate constant of refolding and unfolding (B) of **N25A** at pH 7 and 25°C. Only the rate constant with the major amplitude is plotted. The solid lines represent the results of the global fit. Data were measured from Daniel Poso.*

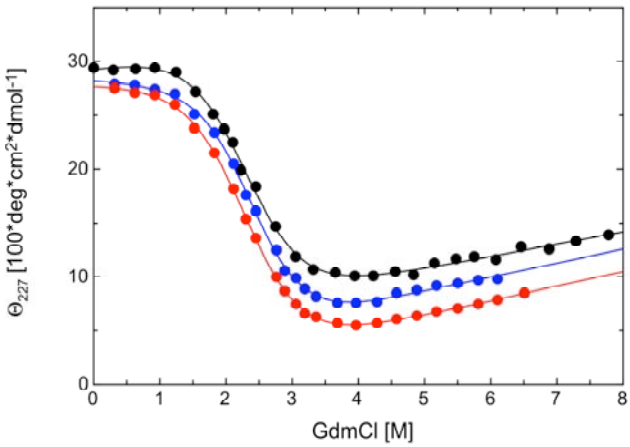

*Figure 9-48: GdmCl-induced unfolding transition of **N25A** at pH 7 at 5°C (●) 10°C (●) and 15°C (●). The line represents the analysis assuming the two-state model. Data were measured from Daniel Poso.*

*Figure 9-49 (following page): GdmCl-dependence of the apparent rate constant of refolding and unfolding of **N25A** at pH 7 and various temperatures. Only the rate constant with the major amplitude is plotted. The solid lines represent the results of the single fits assuming the two-state model. Data were measured from Daniel Poso.*

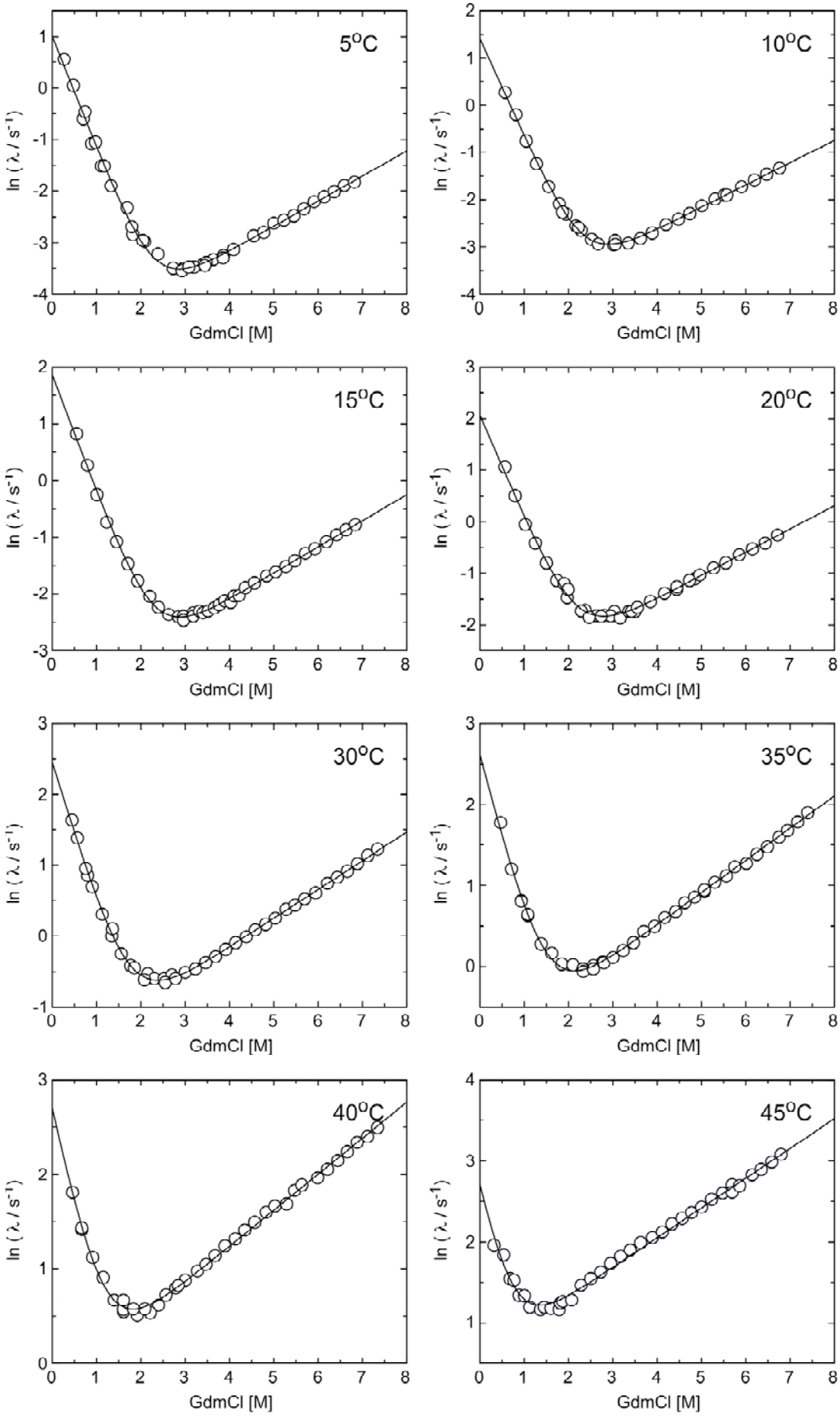
5°C
10°C
15°C
20°C
30°C
35°C
40°C
45°C
ln (λ / s-1)
GdmCl [M]

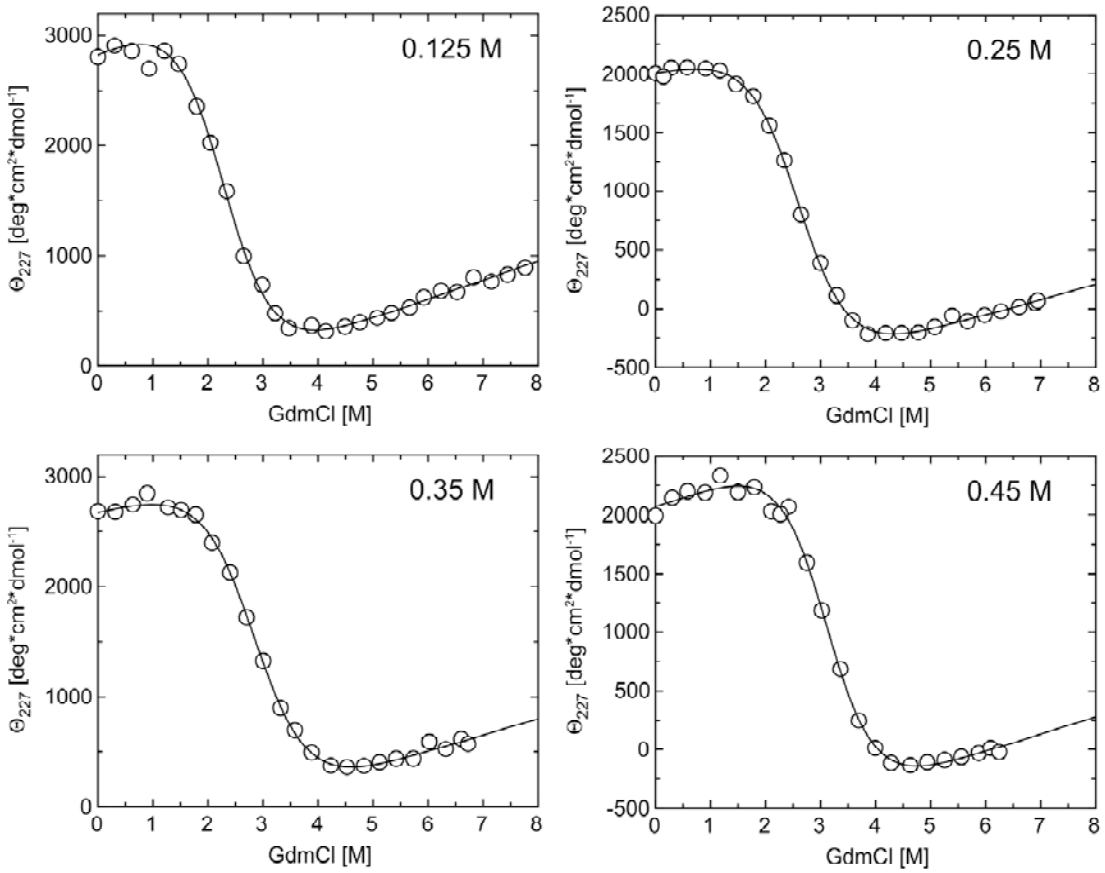

*Figure 9-50: GdmCl-induced unfolding transition of **N25A** at pH 7 and 25°C at different sodium sulfate concentrations. The line represents the analysis assuming the two-state model.*

*Figure 9-51 – Figure 9-54 (following pages): GdmCl-dependence of the apparent rate constants λ_i (A), the amplitudes A_i (B) and the final and initial values (C) for the folding of the tendamistat variant **N25A** at pH 7 and 25°C at different sodium sulfate concentrations. The values for the refolding reaction are plotted as circles, for the unfolding reaction as squares.*

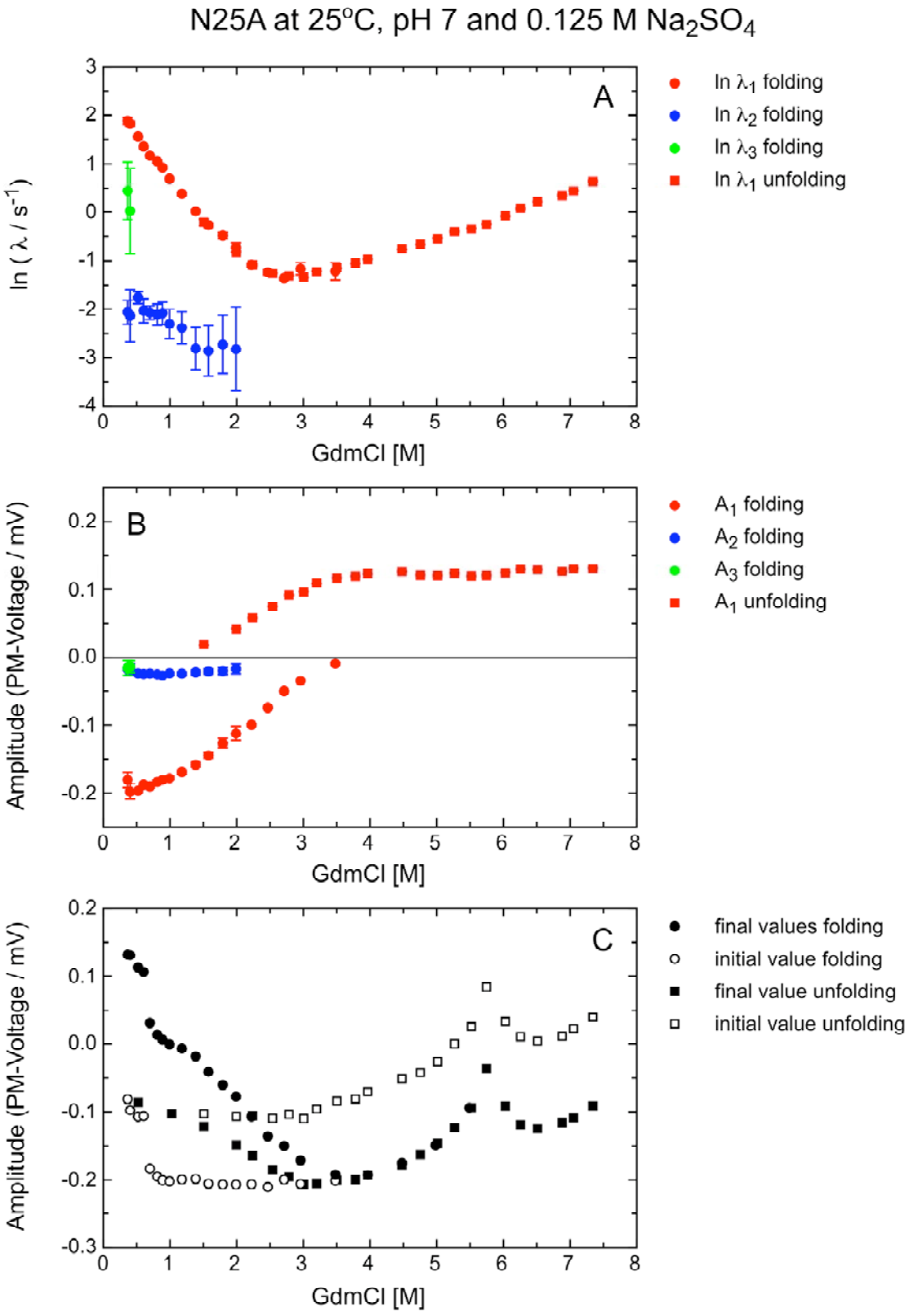
N25A at 25°C, pH 7 and 0.125 M Na2SO4
A
ln (λ / s-1)
GdmCl [M]
ln λ1 folding
ln λ2 folding
ln λ3 folding
ln λ1 unfolding
B
Amplitude (PM-Voltage / mV)
GdmCl [M]
A1 folding
A2 folding
A3 folding
A1 unfolding
C
Amplitude (PM-Voltage / mV)
GdmCl [M]
final values folding
initial value folding
final value unfolding
initial value unfolding

Figure 9-51

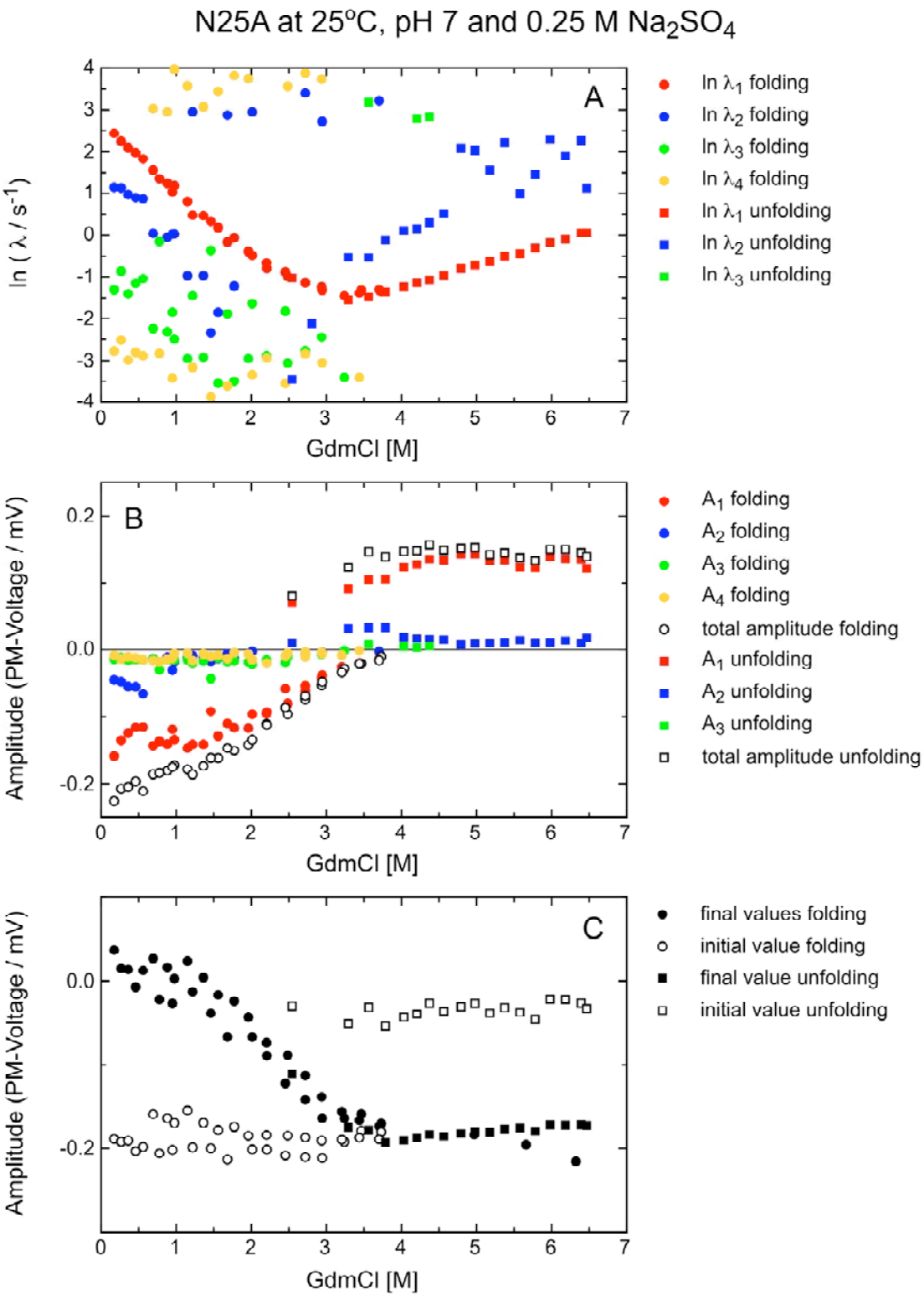
N25A at 25°C, pH 7 and 0.25 M Na2SO4
A
ln (λ / s-1)
GdmCl [M]
ln λ1 folding
ln λ2 folding
ln λ3 folding
ln λ4 folding
ln λ1 unfolding
ln λ2 unfolding
ln λ3 unfolding
B
Amplitude (PM-Voltage / mV)
GdmCl [M]
A1 folding
A2 folding
A3 folding
A4 folding
total amplitude folding
A1 unfolding
A2 unfolding
A3 unfolding
total amplitude unfolding
C
Amplitude (PM-Voltage / mV)
GdmCl [M]
final values folding
initial value folding
final value unfolding
initial value unfolding

Figure 9-52

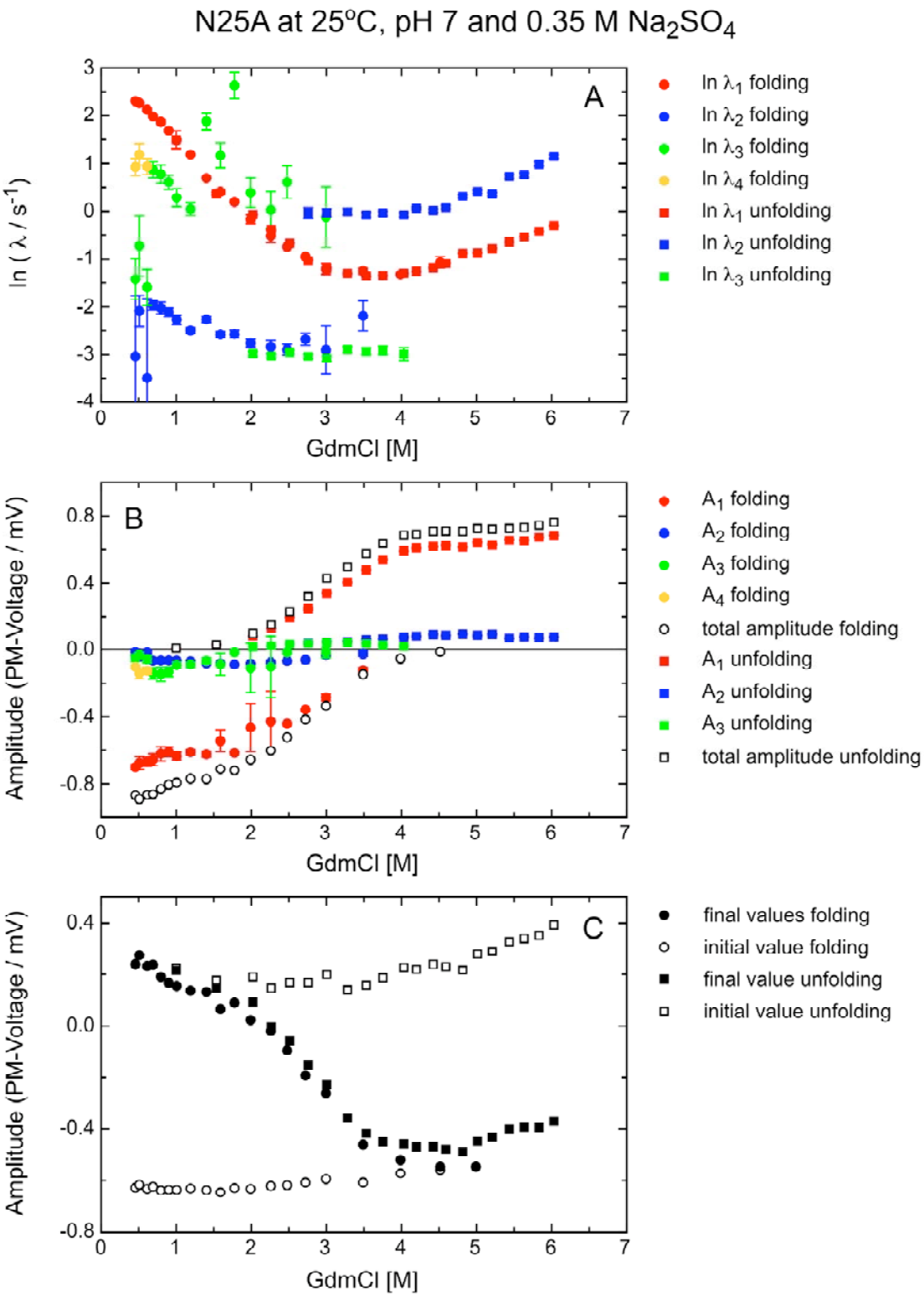
N25A at 25°C, pH 7 and 0.35 M Na2SO4
A
ln (λ / s-1)
GdmCl [M]
ln λ1 folding
ln λ2 folding
ln λ3 folding
ln λ4 folding
ln λ1 unfolding
ln λ2 unfolding
ln λ3 unfolding
B
Amplitude (PM-Voltage / mV)
GdmCl [M]
A1 folding
A2 folding
A3 folding
A4 folding
total amplitude folding
A1 unfolding
A2 unfolding
A3 unfolding
total amplitude unfolding
C
Amplitude (PM-Voltage / mV)
GdmCl [M]
final values folding
initial value folding
final value unfolding
initial value unfolding

Figure 9-53

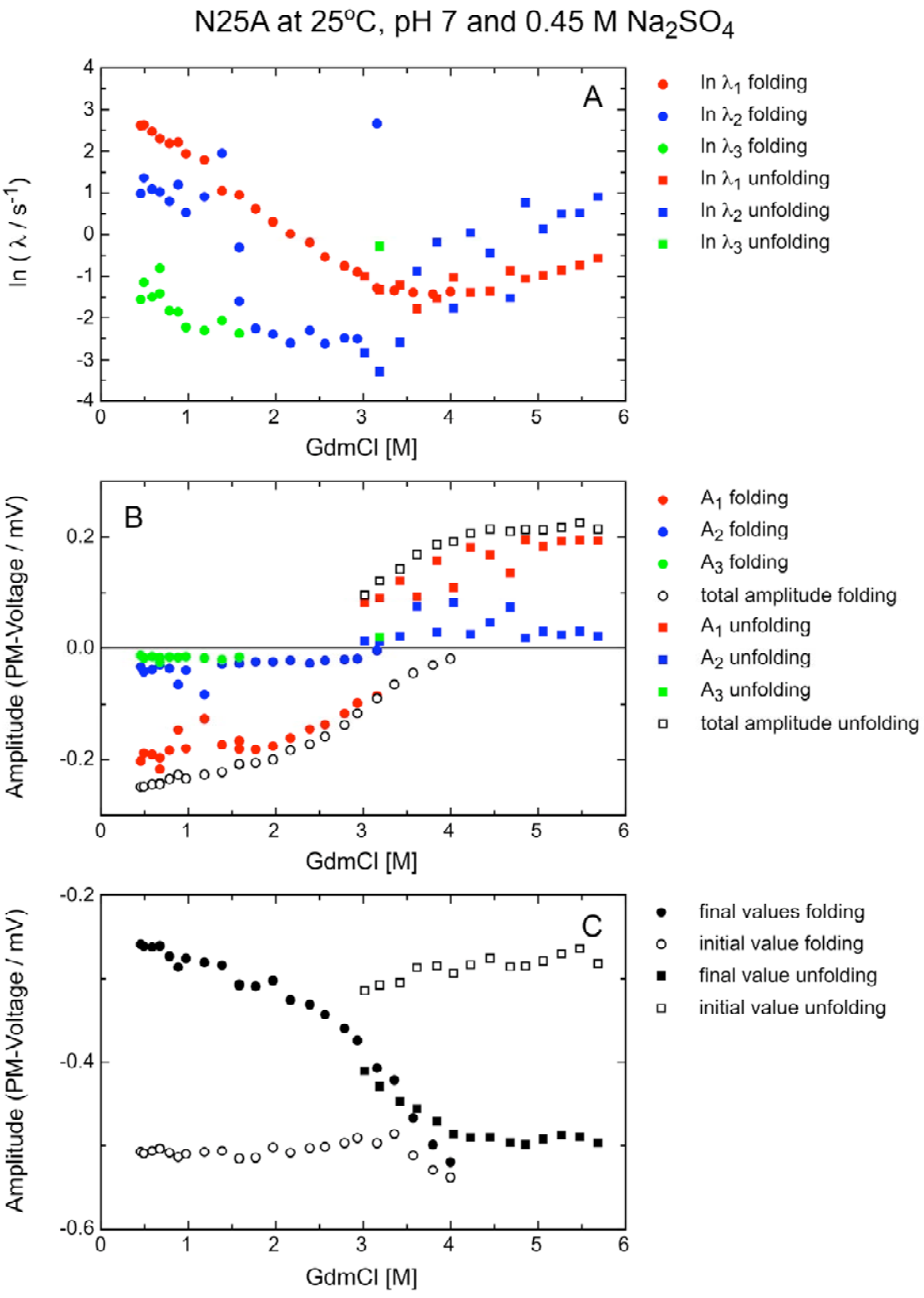
N25A at 25°C, pH 7 and 0.45 M Na2SO4
A
ln (λ / s-1)
GdmCl [M]
ln λ1 folding
ln λ2 folding
ln λ3 folding
ln λ1 unfolding
ln λ2 unfolding
ln λ3 unfolding
B
Amplitude (PM-Voltage / mV)
GdmCl [M]
A1 folding
A2 folding
A3 folding
total amplitude folding
A1 unfolding
A2 unfolding
A3 unfolding
total amplitude unfolding
C
Amplitude (PM-Voltage / mV)
GdmCl [M]
final values folding
initial value folding
final value unfolding
initial value unfolding

Figure 9-54

9.5 Variants with complex unfolding kinetics

Analysis and results of the data are described in detail in chapter 4.2.

Equilibrium and kinetic data were measured for the tendamistat variants **V36A**, **V36G**, **E38Q** and **D39A** at pH 7 and 25°C. Equilibrium data were obtained with 10 μM protein in 100 mM cacodylic acid, pH 7, by monitoring the ellipticity at 227 nm. The kinetics were measured monitoring the change in fluorescence after initiation by 11-fold dilution of native and unfolded protein, respectively, into various denaturant concentration to a final concentration of 4 μM protein in 100 mM cacodylic acid, pH 7.

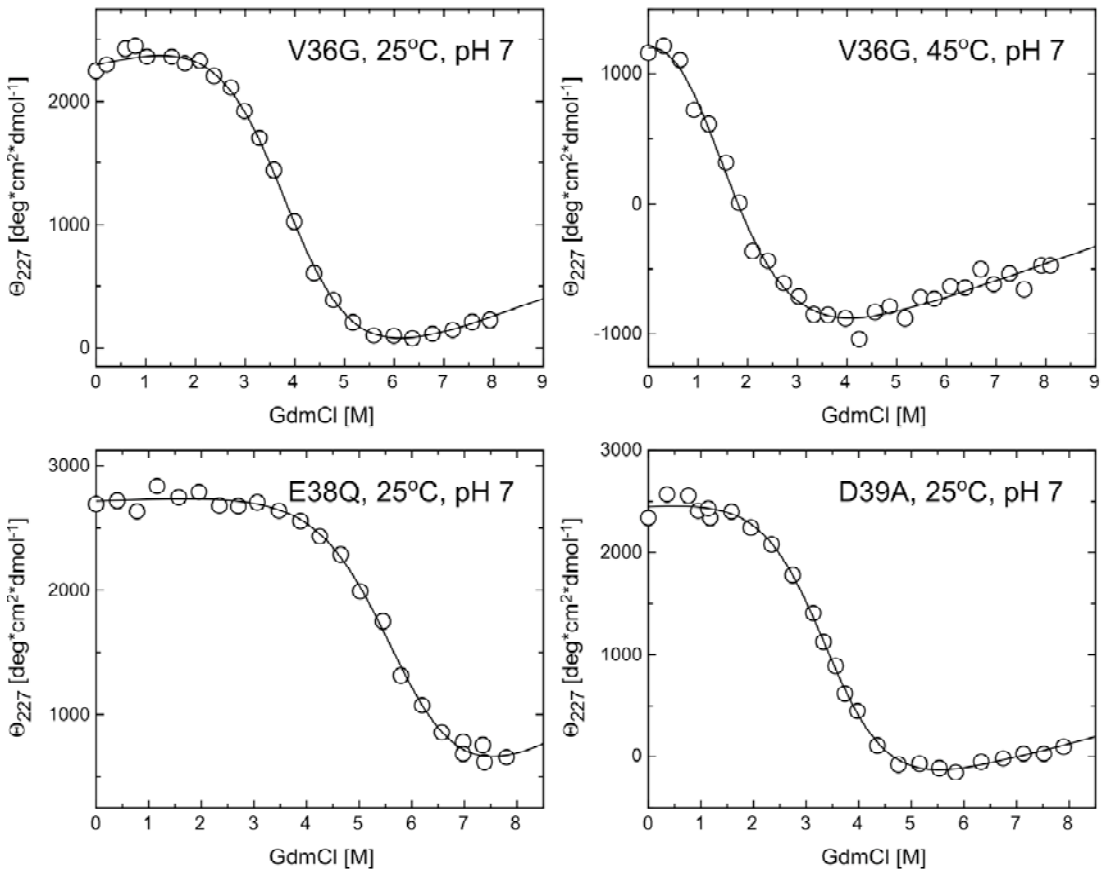

*Figure 9-55: GdmCl-induced unfolding transition of **V36G**, **E38Q** and **D39A** at pH 7 and 25°C and **V36G** at 45°C. The line represents the analysis assuming the two-state model.*

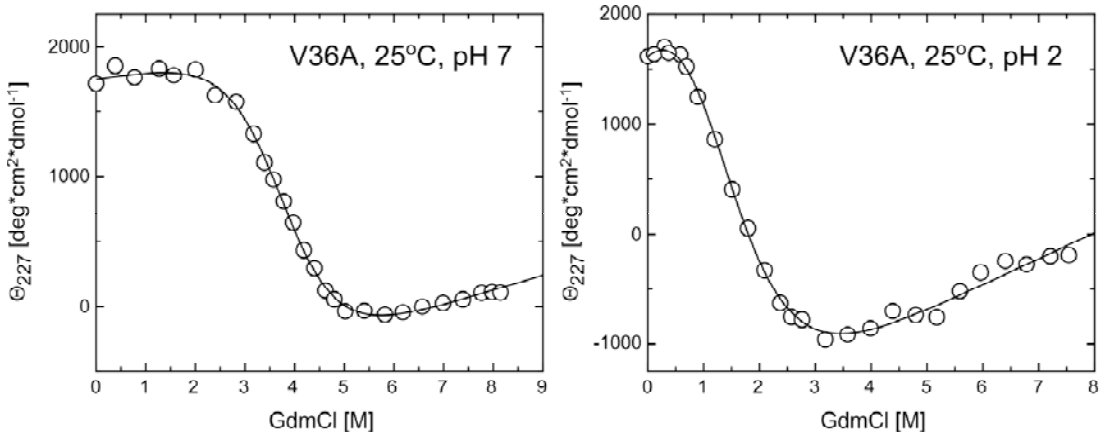

*Figure 9-56: GdmCl-induced unfolding transition of **V36A** at pH 7, pH 2 and 25°C. The line represents the analysis assuming the two-state model.*

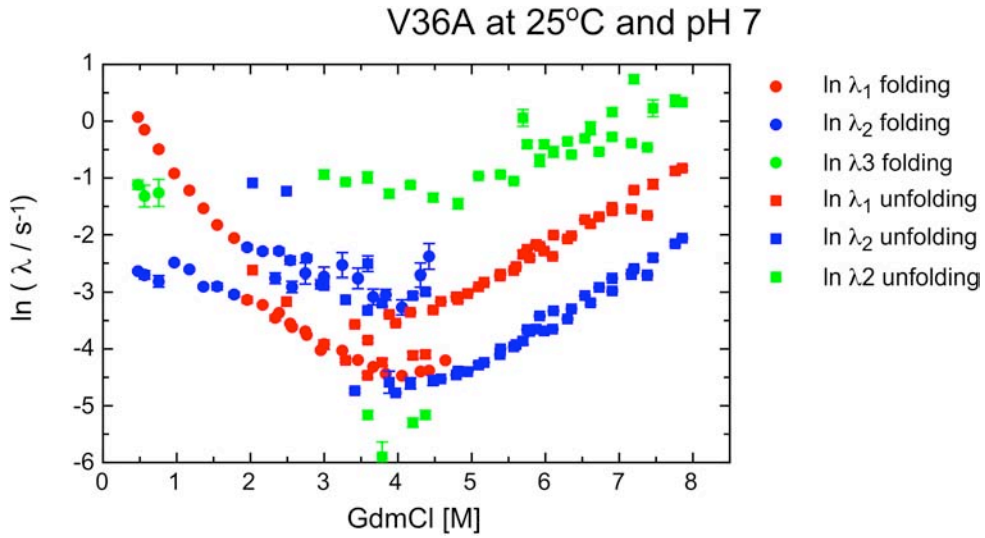

*Figure 9-57: GdmCl-dependence of the apparent rate constant λ_i of refolding and unfolding of **V31A** at pH 7 at 25°C. The values for the refolding reaction are plotted as circles, for the unfolding reaction as squares.*

Figure 9-58 (following page): *GdmCl-dependence of the amplitudes A_i (A, B, C) and the final and initial values (D, E, F) for folding of the tendamistat variant V36A at pH 7 and 25°C.*

*Figure 9-59, Figure 9-61 - Figure 9-63 (following pages): GdmCl-dependence of the apparent rate constants λ_i (A), the amplitudes A_i (B) and the final and initial values (C) for the folding of the tendamistat variants **V36A** (pH 2, 25°C), **V36G** (pH 7, 45°C), **E38Q** (pH 7, 25°C) and **D39A** (pH 7, 25°C). The values for the refolding reaction are plotted as circles, for the unfolding reaction as squares.*

*Figure 9-59: Folding of the tendamistat variant **V36A** at pH 2.*

*Figure 9-60: (following pages): GdmCl-dependence of the apparent rate constants λ_i (A), the amplitudes A_i (B, C) and the final and initial values (D, E) for folding of the tendamistat variant **V36G** at pH 7 and 25°C. The values for the refolding reaction are plotted as circles, for the unfolding reaction as squares. The kinetics were measured by stopped-flow mixing (B, D) and by manual-mixing (C, E).*

*Figure 9-61: Folding of the tendamistat variant **V36G** at 45°C.*

*Figure 9-62: Folding of the tendamistat variant **E38Q**.*

*Figure 9-63: Folding of the tendamistat variant **D39A**.*

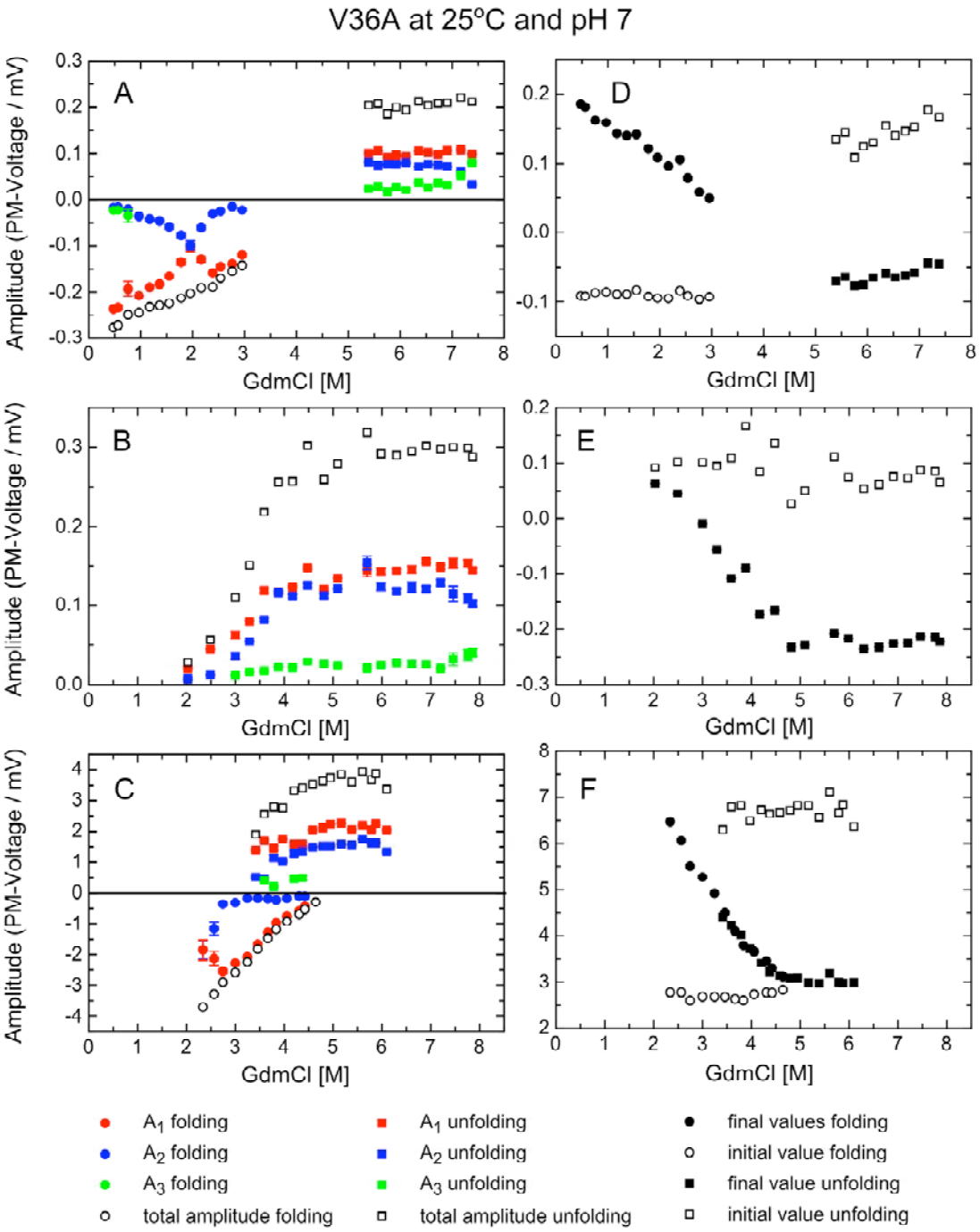
V36A at 25°C and pH 7
A
B
C
D
E
F
Amplitude (PM-Voltage / mV)
GdmCl [M]
A1 folding
A2 folding
A3 folding
total amplitude folding
A1 unfolding
A2 unfolding
A3 unfolding
total amplitude unfolding
final values folding
initial value folding
final value unfolding
initial value unfolding

Figure 9-58

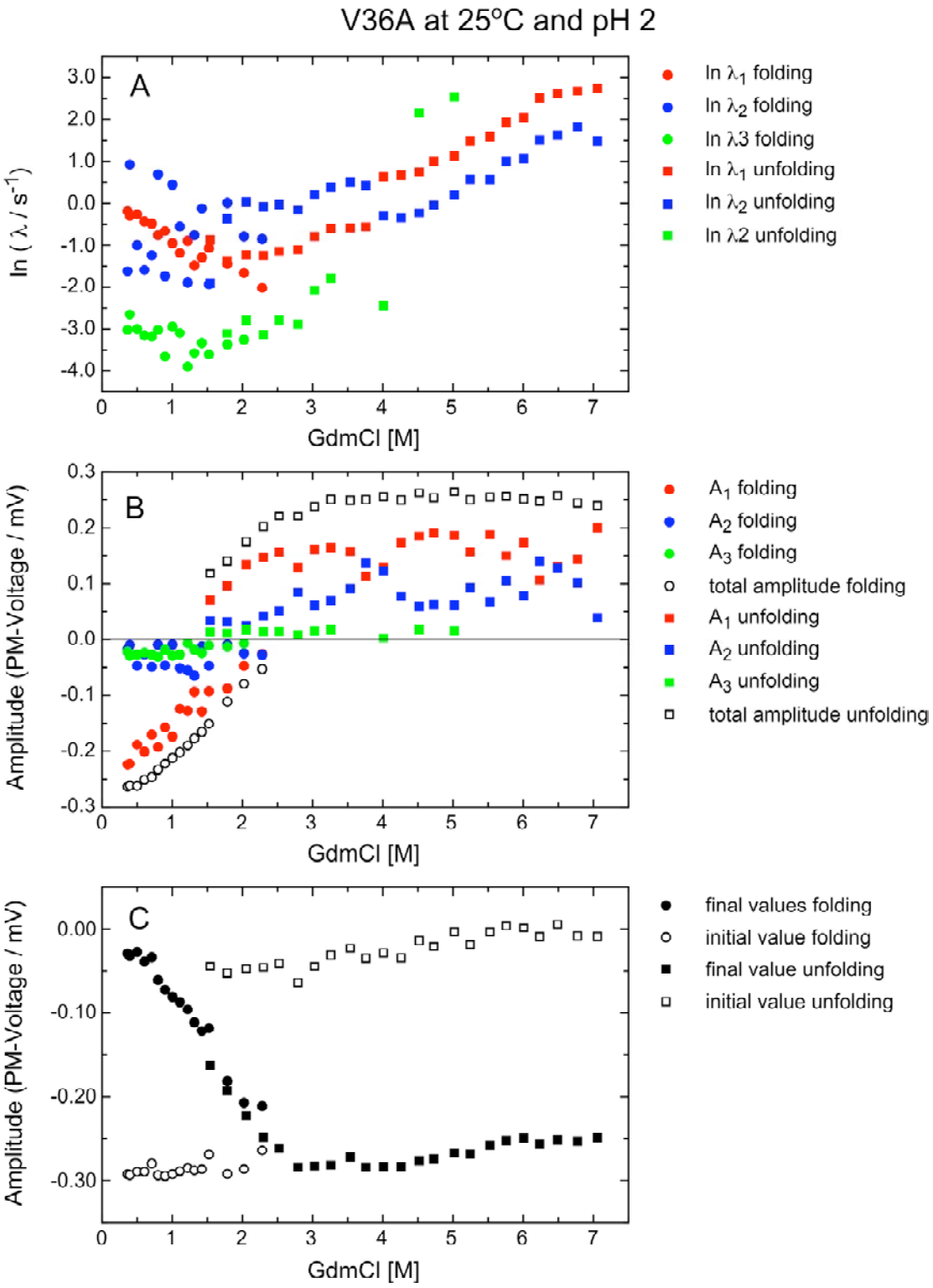
V36A at 25°C and pH 2
A
ln (λ / s-1)
GdmCl [M]
ln λ1 folding
ln λ2 folding
ln λ3 folding
ln λ1 unfolding
ln λ2 unfolding
ln λ2 unfolding
B
Amplitude (PM-Voltage / mV)
GdmCl [M]
A1 folding
A2 folding
A3 folding
total amplitude folding
A1 unfolding
A2 unfolding
A3 unfolding
total amplitude unfolding
C
Amplitude (PM-Voltage / mV)
GdmCl [M]
final values folding
initial value folding
final value unfolding
initial value unfolding

Figure 9-59

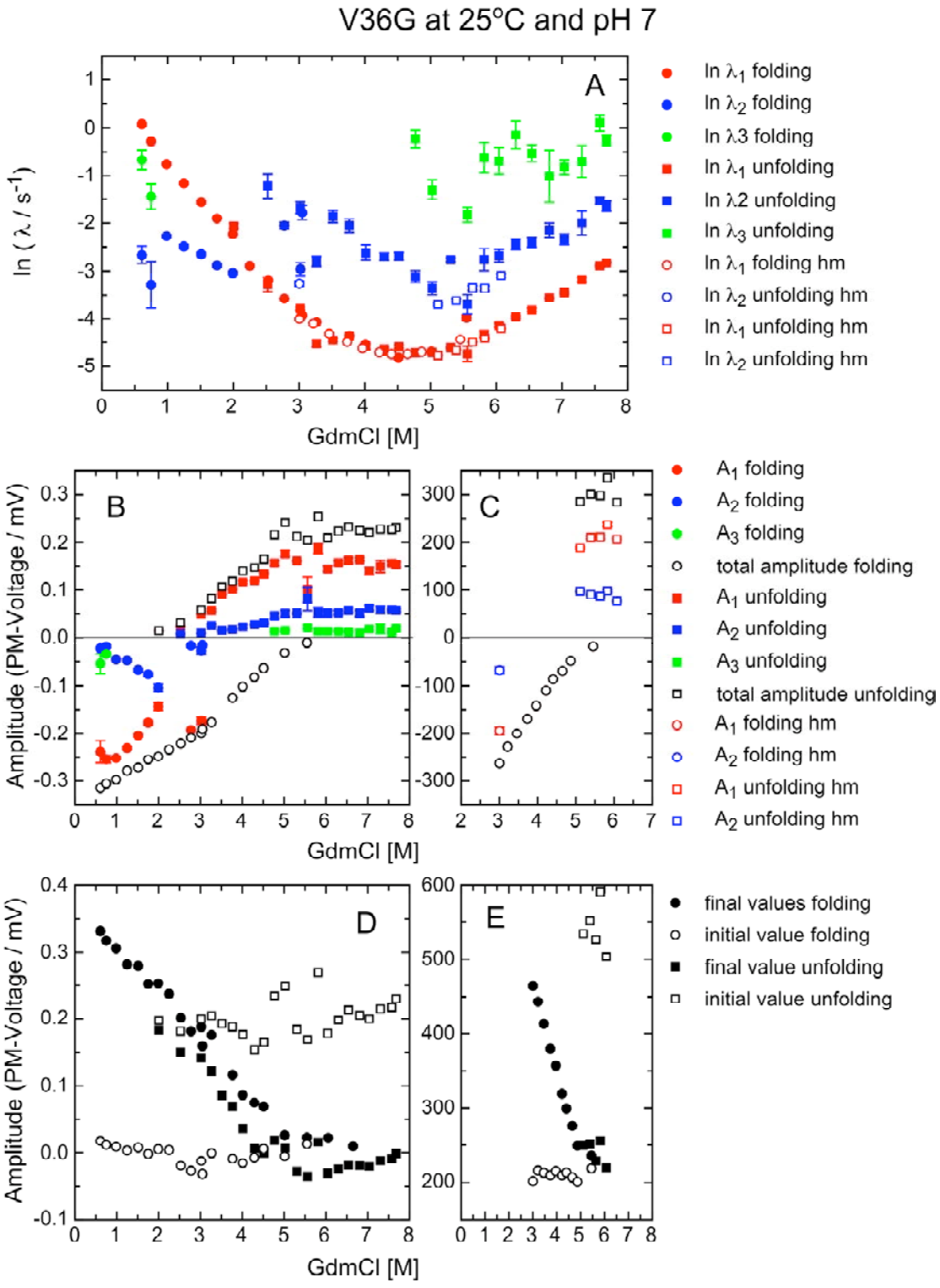
V36G at 25°C and pH 7
A
ln (λ / s-1)
GdmCl [M]
ln λ1 folding
ln λ2 folding
ln λ3 folding
ln λ1 unfolding
ln λ2 unfolding
ln λ3 unfolding
ln λ1 folding hm
ln λ2 unfolding hm
ln λ1 unfolding hm
ln λ2 unfolding hm
B
C
Amplitude (PM-Voltage / mV)
GdmCl [M]
A1 folding
A2 folding
A3 folding
total amplitude folding
A1 unfolding
A2 unfolding
A3 unfolding
total amplitude unfolding
A1 folding hm
A2 folding hm
A1 unfolding hm
A2 unfolding hm
D
E
Amplitude (PM-Voltage / mV)
GdmCl [M]
final values folding
initial value folding
final value unfolding
initial value unfolding

Figure 9-60

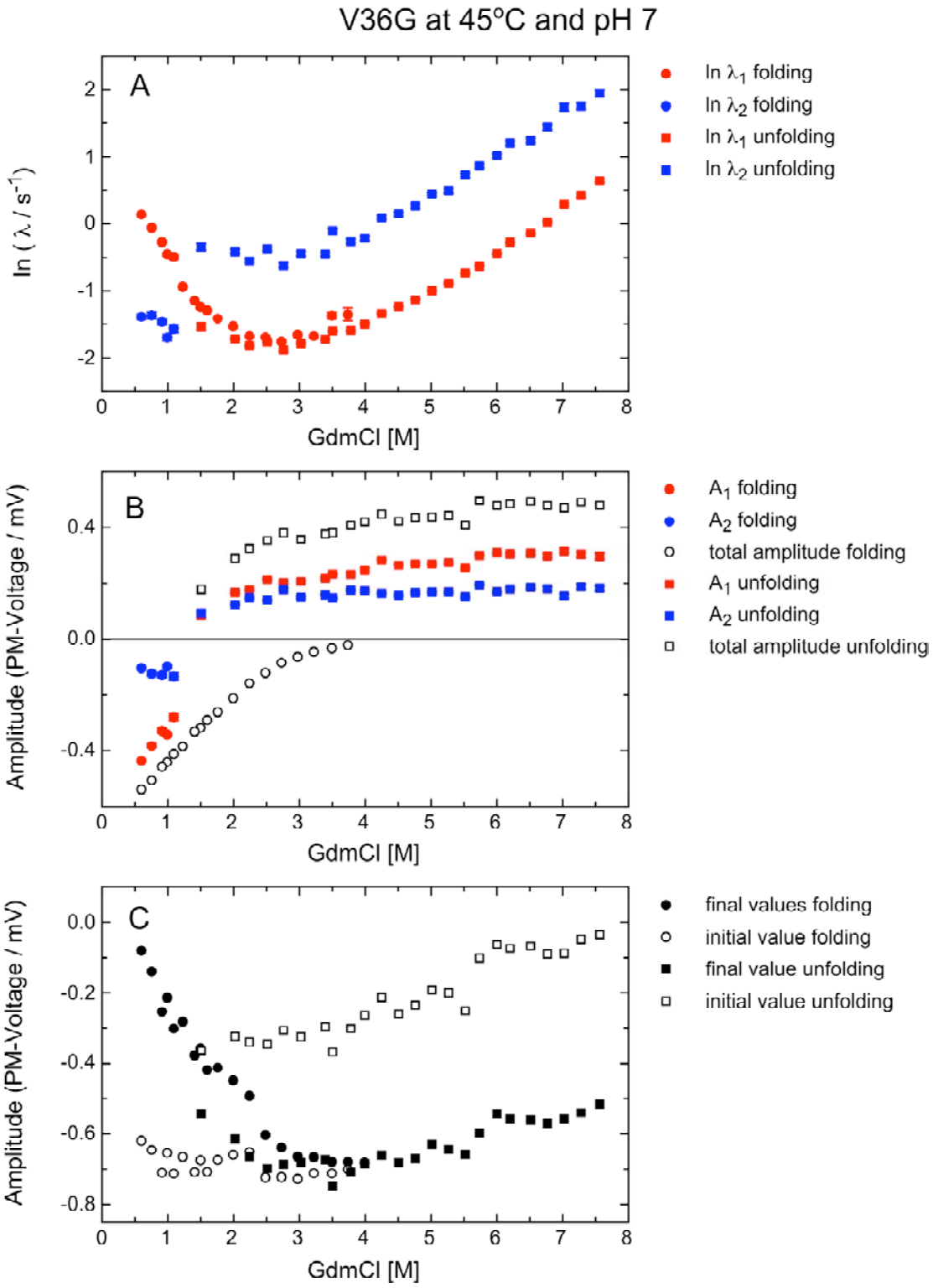
V36G at 45°C and pH 7
A
ln (λ / s-1)
GdmCl [M]
ln λ1 folding
ln λ2 folding
ln λ1 unfolding
ln λ2 unfolding
B
Amplitude (PM-Voltage / mV)
GdmCl [M]
A1 folding
A2 folding
total amplitude folding
A1 unfolding
A2 unfolding
total amplitude unfolding
C
Amplitude (PM-Voltage / mV)
GdmCl [M]
final values folding
initial value folding
final value unfolding
initial value unfolding

Figure 9-61

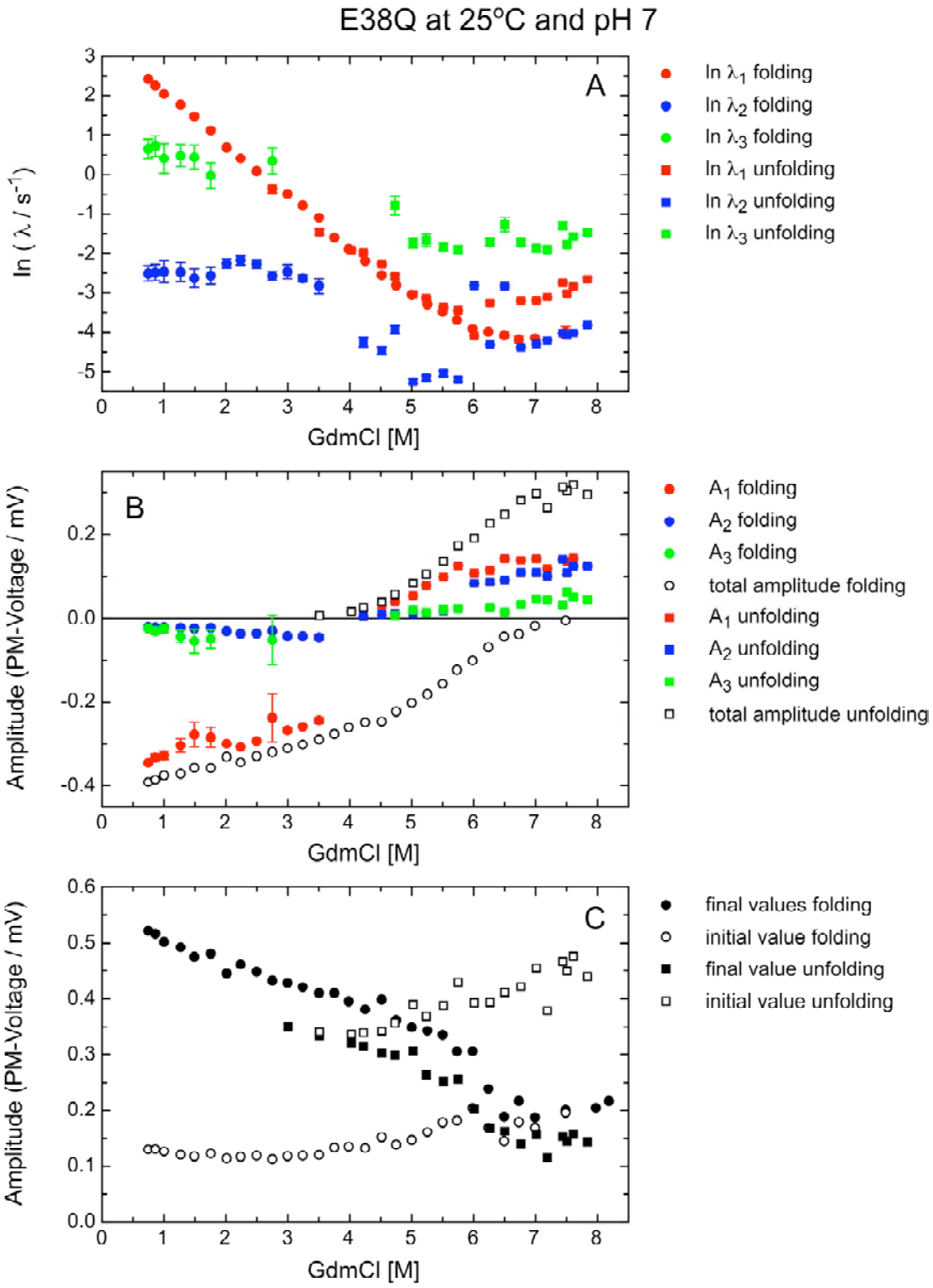
E38Q at 25°C and pH 7
A
ln (λ / s-1)
GdmCl [M]
ln λ1 folding
ln λ2 folding
ln λ3 folding
ln λ1 unfolding
ln λ2 unfolding
ln λ3 unfolding
B
Amplitude (PM-Voltage / mV)
GdmCl [M]
A1 folding
A2 folding
A3 folding
total amplitude folding
A1 unfolding
A2 unfolding
A3 unfolding
total amplitude unfolding
C
Amplitude (PM-Voltage / mV)
GdmCl [M]
final values folding
initial value folding
final value unfolding
initial value unfolding

Figure 9-62

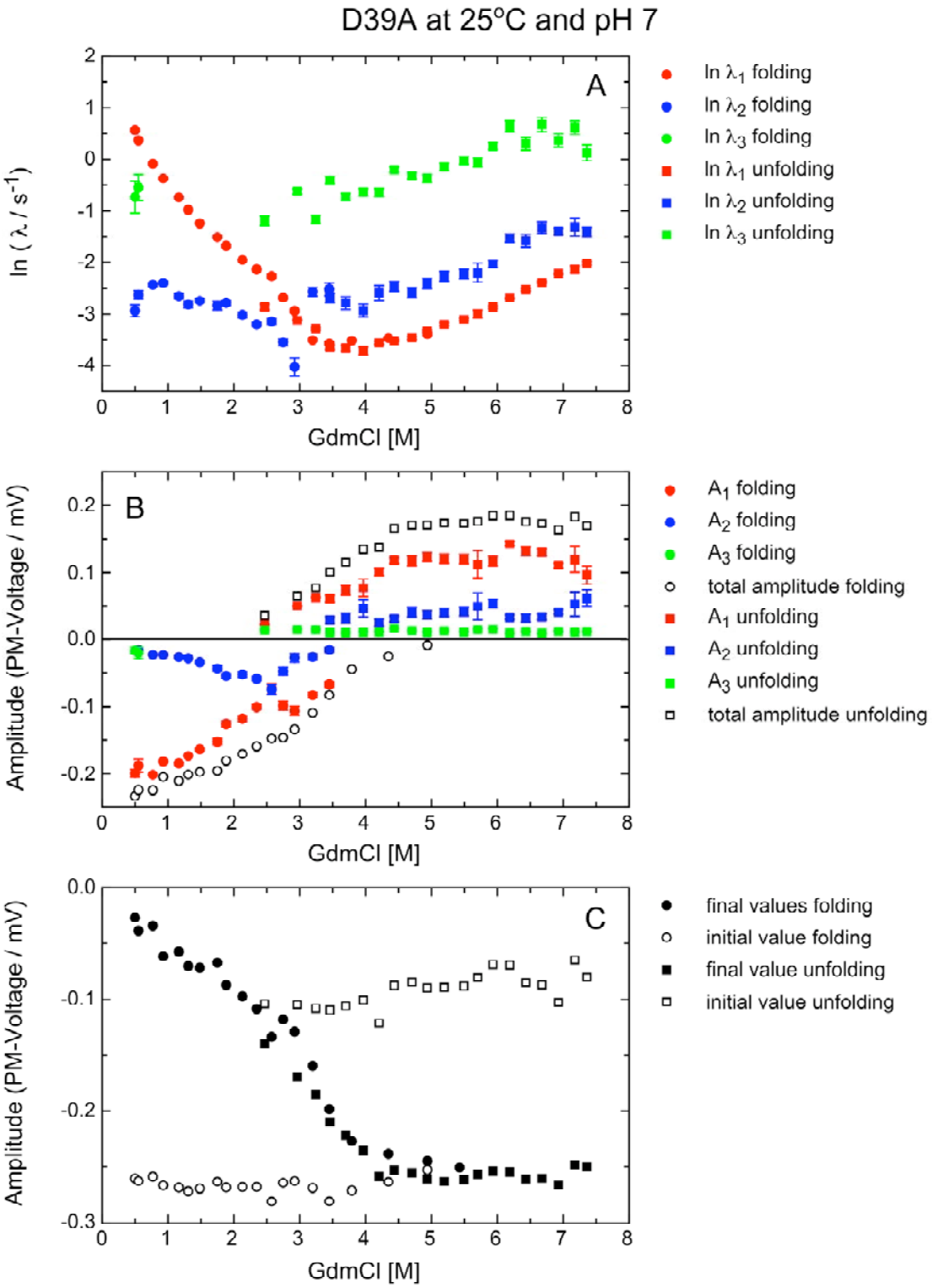
D39A at 25°C and pH 7
A
ln (λ / s-1)
GdmCl [M]
ln λ1 folding
ln λ2 folding
ln λ3 folding
ln λ1 unfolding
ln λ2 unfolding
ln λ3 unfolding
B
Amplitude (PM-Voltage / mV)
GdmCl [M]
A1 folding
A2 folding
A3 folding
total amplitude folding
A1 unfolding
A2 unfolding
A3 unfolding
total amplitude unfolding
C
Amplitude (PM-Voltage / mV)
GdmCl [M]
final values folding
initial value folding
final value unfolding
initial value unfolding

Figure 9-63